ASSESSMENT OF COSEISMIC LANDSLIDING FROM AN ALPINE FAULT EARTHQUAKE SCENARIO, NEW ZEALAND

A thesis submitted in partial fulfilment of the requirements

for the Degree of *Doctor of Philosophy (PhD)*

in Hazard and Disaster Management

in the University of Canterbury

Thomas R. Robinson

Department of Geological Sciences
University of Canterbury

2014

'*Kia Kaha* Christchurch' - A red-zoned family home in the eastern Christchurch suburb of Bexley following the 2010-11 Canterbury earthquake sequence. Poor pre-event land-use planning led to extensive residential development on land known to be highly prone to liquefaction. Following the earthquake sequence, large swathes of residential land in the eastern suburbs has had to be permanently retired at huge financial and social cost.

"Civilisation exists by geological consent, subject to change without notice."
— Will Durant, Philosopher/Historian

"Preparation through education is less costly than learning through tragedy."
— Max Mayfield, Director National Hurricane Center

"There's no harm in hoping for the best as long as you're prepared for the worst."
— Steven King, *Different Seasons*

"... we cannot underestimate the importance of emergency planning, nor can we assume we'll have ample warning time ... we won't necessarily have advanced alerts to double- and triple-check our plans."
- Ellen Tauscher, United States House Representative, California

Abstract

Disasters can occur without warning and severely test society's capacity to cope, significantly altering the relationship between society and the built and natural environments. The scale of a disaster is a direct function of the pre-event actions and decisions taken by society. Poor pre-event planning is a major contributor to disaster, while effective pre-event planning can substantially reduce, and perhaps even avoid, the disaster. Developing and undertaking effective planning is therefore a vital component of disaster risk management in order to achieve meaningful societal resilience. Disaster scenarios present arguably the best and most effective basis to plan an effective emergency response to future disasters.

For effective emergency response planning, disaster scenarios must be as realistic as possible. Yet for disasters resulting from natural hazards, intricately linked secondary hazards and effects make development of realistic scenarios difficult. This is especially true for large earthquakes in mountainous terrain. The primary aim of this thesis is therefore to establish a detailed and realistic disaster scenario for a M_w8.0 earthquake on the plate boundary Alpine fault in the South Island of New Zealand with specific emphasis on secondary effects. Geologic evidence of pre-historic earthquakes on this fault suggest widespread and large-scale landsliding has resulted throughout the Southern Alps, yet, currently, no attempts to quantitatively model this landsliding have been undertaken. This thesis therefore provides a first attempt at quantitative assessments of the likely scale and impacts of landsliding from a future M_w8.0 Alpine fault earthquake.

Modelling coseismic landsliding in regions lacking historic inventories and geotechnical data (e.g. New Zealand) is challenging. The regional factors that control the spatial distribution of landsliding however, are shown herein to be similar across different environments. Observations from the 1994 Northridge, 1999 Chi-Chi, and 2008 Wenchuan earthquakes identified MM intensity, slope angle and position, and distance from active faults and streams as factors controlling the spatial distribution of landsliding. Using fuzzy logic in GIS, these factors are able to successfully model the spatial distribution of coseismic landsliding from both the 2003 and 2009 Fiordland earthquakes in New Zealand. This method can therefore

be applied to estimate the scale of landsliding from scenario earthquakes such as an Alpine fault event.

Applied to an M_w8.0 Alpine fault earthquake, this suggests that coseismic landsliding could affect an area >50,000 km^2 with likely between 40,000 and 110,000 landslides occurring. Between 1,400 and 4,000 of these are expected to present a major hazard. The environmental impacts from this landsliding would be severe, particularly in west-draining river catchments, and sediment supply to rivers in some catchments may exceed 50 years of background rates. Up to 2 km^3 of total landslide debris is expected, and this will have serious and long-term consequences. Fluvial remobilisation of this material could result in average aggradation depths on active alluvial fans and floodplains of 1 m, with maximum depths substantially larger. This is of particular concern to the agriculture industry, which relies on the fertile soils on many of the active alluvial fans affected.

This thesis also investigated the potential impacts from such landsliding on critical infrastructure. The State Highway and electrical transmission networks are shown to be particularly exposed. Up to 2,000 wooden pole and 30 steel pylon supports for the transmission network are highly exposed, resulting in >23,000 people in the West Coast region being exposed to power loss. At least 240 km of road also has high exposure, primarily on SH6 between Hokitika and Haast, and on Arthur's and Lewis Passes. More than 2,750 local residents in Westland District are exposed to isolation by road as a result. The Grey River valley region is identified as the most critical section of the State Highway network and pre-event mitigation is strongly recommended to ensure the road and bridges here can withstand strong shaking and liquefaction hazards. If this section of the network can remain functional post-earthquake, the emergency response could be based out of Wellington using Nelson as a forward operating base with direct road access to some of the worst-affected locations. However, loss of functionality of this section of road will result in >24,000 people becoming isolated across almost the entire West Coast region.

This thesis demonstrates the importance and potential value of pre-event emergency response planning, both for the South Island community for an Alpine fault earthquake, and globally for all such hazards. The case study presented demonstrates that realistic estimates of potential coseismic landsliding and its impacts are possible, and the methods developed herein can be applied to other large mountainous earthquakes. A model for developing disaster scenarios in collaboration with a wide range of societal groups is presented and shown to be an effective method for emergency response planning, and is applicable to any hazard and location globally. This thesis is therefore a significant contribution towards understanding mountainous earthquake hazards and emergency response planning.

Acknowledgements

This thesis and the last three years would not have been possible without the generous support, encouragement, and expertise of many numerous people. There are far too many to name individually, but I am eternally grateful to all those who have so very kindly given me their time, assistance, and encouragement.

Firstly, I must give my gratitude to Huw Llewellyn, who so sadly passed away just a few months before this research was finished. Huw was the first to peak my interest in this field with his marvellous teaching style and ability. The obvious fervour and enjoyment Huw had for this subject was infectious and remains with me today. Had it not been for those few years being taught by Huw, I suspect I would have taken a different path through academia and, as such, I owe him my deepest gratitude. It is with great regret that Huw is no longer with us to see this work completed and I can only hope that he would have enjoyed reading it. Huw: you will be sadly missed, but never forgotten.

I must also say a huge thank you to my supervisors throughout this process: Prof. Tim Davies, Dr. Tom Wilson, and Dr. Caroline Orchiston. Firstly, my senior supervisor: Tim. From the moment I first contacted Tim about coming to Christchurch he has been nothing but supportive and passionate about this project. It has taken a much different path to that which we initially envisioned, but most certainly for the better. Tim has been unwavering in his support and encouragement, going above and beyond anything I could have expected throughout the last three years. It has been a utter joy to work with Tim and I am eternally grateful for the opportunity. Hopefully this is just the start of a far longer collaboration: Tim, you cannot retire yet, there is more work to do.

Secondly, I owe a great deal to Tom. It was he who first introduced me to the CDEM and started us down the path that eventually resulted in this thesis. Tom has been immensely supportive, both professionally and personally, throughout this whole process and it has been incredibly enjoyable to work alongside him. Tom's enthusiasm for the subject of disaster science has been infectious and I have learnt a great deal from him. His thoughts and comments have always been immensely helpful, not least of which relate to the structuring and framing

of a paper or a thought.

Finally, to Caroline. She joined this research early in it's undertaking and has been an integral part of it. Her thoughts and knowledge on community engagement and the communication and preparation of results have been gratefully appreciated. She has also acted as a tiebreaker in many a (friendly) disagreement between Tim and Tom, and I cannot understate the importance of this. Further, despite being in Dunedin, Caroline has always been readily available to provide her thoughts and opinions and has been a huge support both professionally and personally.

Thanks must also be given to all those at Canterbury CDEM, not least James Thompson, who I worked so closely with during the development of *Te Ripahapa*. It was a pleasure to work with them all and I hope it continues beyond this research. Susanna Jenkins graciously gave up some of her time to help with the numerous statistics contained within this thesis which turned out to be pivotal. Also to all those who I had the pleasure of sharing office 412 with over the years. They have all become some of my closest friends, and their ability to act as a living, breathing thesaurus is outstanding. It has been a pleasure sharing an office with each of you.

I would also like to thank my partner, Fritha. She has been the most understanding, helpful, and caring person anyone could wish for, especially during the final few crazy months of writing up. She has put up with countless long nights despite having to wake early herself, and has even encouraged my working weekends, which she so despises. She has believed in my abilities and encouraged me throughout, even during the most stressful of times. She has always listened to my ramblings and entertained my ideas no matter how outlandish, and has developed an uncanny ability to cut straight to the point, in true Kiwi fashion.

Finally, and most importantly, my family back in London, without whom none of this would have been possible. Their love and dedication has been unwavering. They have fully supported and encouraged me in the face of my moving very far from home, a feat I am certain not many would accept with such understanding. It has been their love, encouragement, kindness, support, and advice that has got me to where I am now. I will always be indebted to them. I am incredibly lucky to be part of such an amazing family, and hopefully my achievements here can go someway to demonstrating the incredible job they have done. Mum, Dad, Simon, thank you so very much.

Statement of co-authorship

The body chapters (2-6) of this thesis comprise a series of co-authored manuscripts published, submitted, or intended for submission in international scientific journals. As well as these, Appendix A has been published in an international scientific journal, Appendix B has been published as a GNS Science Miscellaneous Report, and Appendix C has been submitted to a New Zealand scientific journal. Signed co-authorship forms are provided for each co-authored manuscript. This co-authorship statement briefly summarises the various publications and the level of input for each of the co-authors.

A version of Chapter 2 was published in 2013 in ***Natural Hazards and Earth System Sciences*** (Vol. 13, pp. 2279-2299, doi: 10.5194/nhess-13-2279-2013), entitled 'Review Article: Potential geomorphic consequences of a future great (M_w8.0+) Alpine fault earthquake, South Island, New Zealand'. Mr. Robinson is the first author and Prof. Tim Davies is a co-author. Mr. Robinson wrote the majority of the manuscript and Prof. Davies contributed significantly to its refinement as well as providing considerable knowledge with regards to the pertinent literature. The version included in this thesis has been expanded upon to include information and literature made available since its original publication.

A version of Chapter 3 has been prepared for submission to ***Natural Hazards***. Mr. Robinson is the first author and Dr. Tom Wilson, Prof. Tim Davies, Dr. Caroline Orchiston, and Mr. James Thompson are co-authors. The concept of the paper was devised during discussions between Mr. Robinson and Dr. Wilson following the Canterbury CDEM emergency planning exercise for which Mr. Robinson, Dr. Wilson, Prof. Davies, and Dr. Orchiston worked in conjunction with Mr. Thompson. Mr. Robinson wrote the manuscript and produced the conceptual model included. Dr. Wilson, Prof. Davies, and Dr. Orchiston contributed significantly to the structure and scope of the study and provided detailed reviews and suggestions. Mr. Thompson added useful discussion as to the needs and requirements of emergency managers.

A version of Chapter 4 has been submitted to ***Journal of Geophysical Research: Earth Surface*** and is currently in review. This paper was equally joint written by Dr. Theo Kritikos

and Mr. Robinson. Dr. Kritikos is the first author, Mr. Robinson is the second author, and Prof. Tim Davies is a final co-author. The modelling technique introduced in the paper was developed by both Dr. Kritikos and Mr. Robinson, based on Dr. Kritikos' previous research of GIS-based landslide susceptibility modelling. Mr. Robinson collected and compiled the required data, and carried out seismic hazard modelling. Dr. Kritikos provided knowledge of the capabilities of GIS for such a modelling method, undertook data preparation, DEM processing and introduced Mr. Robinson to the evaluation techniques used. Mr. Robinson provided critical input to the interpretation of the results for the derivation of the user-defined memberships. The manuscript was written equally by Dr. Kritikos and Mr. Robinson. Prof. Davies provided useful discussion and review of both the manuscript and model throughout its development. The version included in this thesis has been entirely re-written in Mr. Robinson's own words, and sections of the original manuscript that were wholly Dr. Kritikos' own work have not been included.

Chapter 5 has been prepared for submission to ***Geomorphology***. Mr. Robinson is the first author and Prof. Tim Davies, Dr. Tom Wilson, and Dr. Caroline Orchiston are co-authors. Mr. Robinson conceived the research, undertook the modelling, interpreted the results, and wrote the manuscript. Prof. Davies provided detailed input and discussion on the modelling of total landslide volumes and the bedload carrying capacity of rivers. Dr. Wilson and Dr. Orchiston provided detailed and helpful reviews of the manuscript and its results.

Chapter 6 has been prepared for submission to ***Risk Analysis***. Mr. Robinson is the first author and Dr. Tom Wilson, Prof. Tim Davies, and Dr. Caroline Orchiston are co-authors. Mr. Robinson devised the research aims and the modelling technique, interpreted the results, and wrote the manuscript. Dr. Wilson, Prof. Davies, and Dr. Orchiston contributed significantly to the structure and conceptual framing of the manuscript, suggested the inclusion of the use of the model as a planning tool, and provided detailed and helpful reviews of both the modelling process and the manuscript.

Appendix A was published in 2014 in ***Landslides*** (doi: 10.1007/s10346-014-0492-y, available online from 30 April 2014) entitled 'The extremely long-runout Komansu rock avalanche in the Trans Alai range, Pamir Mountains, southern Kyrgyzstan'. Mr. Robinson is the first author and Prof. Tim Davies, Dr. Natasha Reznichenko, and Dr. Greg De Pascale are co-authors. The research was first conceived through discussions between Dr. Reznichenko and Prof. Davies. Field investigations were jointly undertaken by Mr. Robinson, Dr. Reznichenko, and Dr. De Pascale. The concept, interpretations, and figure are all that of Mr. Robinson who wrote the manuscript. Prof. Davies provided significant discussion on the framing of the manuscript as well as the comparison to volcanic debris avalanches. Both

Dr. Reznichenko and Dr. De Pascale were involved in field research, providing a substantial contribution to the research. As well as this both provided substantial reviews and discussion of the results and their interpretation.

Appendix B was published in 2014 in ***GNS Science Miscellaneous Series*** (Vol. 69, 113 p.) entitled 'Design and development of realistic exercise scenarios: a case study of the 2013 Civil Defence Exercise Te Ripahapa'. Mr. Robinson is the first author and Dr. Tom Wilson, Prof. Tim Daves, Dr. Caroline Orchiston, and Mr. James Thompson are co-authors. The paper was conceived through discussions between Mr. Robinson and Dr. Wilson following work undertaken with Canterbury CDEM and Mr. Thompson. Mr. Robinson wrote the manuscript and Dr. Wilson, Prof. Davies, Dr. Orchiston, and Mr. Thompson provided detailed reviews and discussion.

Appendix C has been submitted to ***Bulletin of the New Zealand Society of Earthquake Engineering*** and is currently in review. Mr. Robinson is the first author and Dr. Tom Wilson, Prof. Tim Daves, Dr. Caroline Orchiston, and Mr. James Thompson are co-authors. The model, results, and manuscript was established and developed by Mr. Robinson following work undertaken in partnership with Canterbury CDEM and Mr. Thompson. Dr. Wilson provided detailed discussion on the manuscript and suggested the inclusion of the discussion on the Darfield earthquake results. Prof. Davies and Dr. Orchiston provided helpful reviews and discussion of the manuscript and its results.

Deputy Vice-Chancellor's Office
Postgraduate Office

UNIVERSITY OF CANTERBURY
Te Whare Wānanga o Waitaha
CHRISTCHURCH NEW ZEALAND

Co-Authorship Form

This form is to accompany the submission of any thesis that contains research reported in co-authored work that has been published, accepted for publication, or submitted for publication. A copy of this form should be included for each co-authored work that is included in the thesis. Completed forms should be included at the front (after the thesis abstract) of each copy of the thesis submitted for examination and library deposit.

Chapter 2 *– Review Article: Potential geomorphic consequences of a future great (Mw=8.0+) Alpine Fault earthquake, South Island, New Zealand*

Published in *– Natural Hazards and Earth System Sciences (Volume 13, Pages 2279-2299)*
Published: 23 Septmber 2013

The published manuscript was compiled and written by Mr Robinson. Additions to the manuscript included in the thesis version were also written by Mr Robinson. Prof Tim Davies contributed significantly to the structure of the manuscript as well as refining it.

Certification by Co-authors:
If there is more than one co-author then a single co-author can sign on behalf of all
The undersigned certifys that:

- The above statement correctly reflects the nature and extent of the PhD candidate's contribution to this co-authored work
- In cases where the candidate was the lead author of the co-authored work he or she wrote the text

Name: *Tim Davies* Signature: Date: *18 September 2014*

Deputy Vice-Chancellor's Office
Postgraduate Office

UNIVERSITY OF CANTERBURY
Te Whare Wānanga o Waitaha
CHRISTCHURCH NEW ZEALAND

Co-Authorship Form

This form is to accompany the submission of any thesis that contains research reported in co-authored work that has been published, accepted for publication, or submitted for publication. A copy of this form should be included for each co-authored work that is included in the thesis. Completed forms should be included at the front (after the thesis abstract) of each copy of the thesis submitted for examination and library deposit.

Chapter 3 *– Developing effective disaster sceanrios for local- and regional-scale emergency management exercises: a case study of an Alpine fault earthquake scenario*

Prepared for submission to *– Natural Hazards*

The published manuscript and conceptual model was concieved, compiled, and written by Mr Robinson. Dr Tom Wilson, Prof Tim Davies,& Dr Caroline Orchiston contributed significantly to the structure and scope of the manuscript and provided detailed reviews and suggestions as to its contents. Mr James Thompson added useful discussion and review of the manuscript and the role of CDEM and emergency management in New Zealand.

Certification by Co-authors:
If there is more than one co-author then a single co-author can sign on behalf of all
The undersigned certifys that:

- The above statement correctly reflects the nature and extent of the PhD candidate's contribution to this co-authored work
- In cases where the candidate was the lead author of the co-authored work he or she wrote the text

Name: *Tim Davies* Signature: Date: *18 September 2014*

Deputy Vice-Chancellor's Office
Postgraduate Office

UNIVERSITY OF CANTERBURY
Te Whare Wānanga o Waitaha
CHRISTCHURCH NEW ZEALAND

Co-Authorship Form

This form is to accompany the submission of any thesis that contains research reported in co-authored work that has been published, accepted for publication, or submitted for publication. A copy of this form should be included for each co-authored work that is included in the thesis. Completed forms should be included at the front (after the thesis abstract) of each copy of the thesis submitted for examination and library deposit.

Chapter 4 *– A new GIS-based approach for assessment of regional coseismic landslide susceptibility: the effects of ground shaking and topography on the spatial distribution of coseismic slope failures*

Submitted to *– Journal of Geophysical Research - Earth Surface*
Submitted: 27 May 2014

The submitted manuscript was the equally joint work of Mr Robinson and Dr Theodosios Kritikos. The modelling technique was developed by both Dr Kritikos and Mr Robinson, based on Dr Kritikos' previous work. Mr Robinson collected and compiled the required data, and carried out seismic hazard modelling. Dr Kritikos provided knowledge of the capabilities of GIS, undertook DEM processing, and introduced Mr Robinson to the evaluation techniques used. Mr Robinson provided critical input to the interpretation of the results for derivation of the user-defined memberships. The submitted manuscript was equally written by Dr Kitikos (50%) and Mr Robinson (50%). Prof Tim Davies provided useful discussion and review of the manuscript and the modelling technique throughout its development. The submitted manuscript has been re-edited into Mr Robinson's own words for the thesis version; sections of the submitted manuscript written solely by Dr Kritikos have not been included in the thesis version.

Certification by Co-authors:
If there is more than one co-author then a single co-author can sign on behalf of all
The undersigned certifys that:

- The above statement correctly reflects the nature and extent of the PhD candidate's contribution to this co-authored work
- In cases where the candidate was the lead author of the co-authored work he or she wrote the text

Name: *Tim Davies* Signature: Date: *18 September 2014*

Deputy Vice-Chancellor's Office
Postgraduate Office

UNIVERSITY OF CANTERBURY
Te Whare Wānanga o Waitaha
CHRISTCHURCH NEW ZEALAND

Co-Authorship Form

This form is to accompany the submission of any thesis that contains research reported in co-authored work that has been published, accepted for publication, or submitted for publication. A copy of this form should be included for each co-authored work that is included in the thesis. Completed forms should be included at the front (after the thesis abstract) of each copy of the thesis submitted for examination and library deposit.

Chapter 5 *– Coseismic landsliding estimates for an Alpine fault earthquake and its effects on erosion and aggradation in major river catchments*

Intended for Submission to *– Geomorphology*

The manuscript and modelling was conceived, compiled, and undertaken by Mr Robinson following the work of Mr Robinson and Dr Theodosios Kritikos for Chapter 4. Prof Tim Davies provided substantial discussion around bedload rates for aggradation and the derivation of total landslide volume. Dr Susanna Jenkins introduced Mr Robinson to the SEM method for deriving landslide number. Dr Tom Wilson and Dr Caroline Orchiston provided useful discussion and review of the manuscript

Certification by Co-authors:
If there is more than one co-author then a single co-author can sign on behalf of all
The undersigned certifys that:

- The above statement correctly reflects the nature and extent of the PhD candidate's contribution to this co-authored work
- In cases where the candidate was the lead author of the co-authored work he or she wrote the text

Name: *Tim Davies* Signature: Date: *18 September 2014*

Deputy Vice-Chancellor's Office
Postgraduate Office

UNIVERSITY OF CANTERBURY
Te Whare Wānanga o Waitaha
CHRISTCHURCH NEW ZEALAND

Co-Authorship Form

This form is to accompany the submission of any thesis that contains research reported in co-authored work that has been published, accepted for publication, or submitted for publication. A copy of this form should be included for each co-authored work that is included in the thesis. Completed forms should be included at the front (after the thesis abstract) of each copy of the thesis submitted for examination and library deposit.

Chapter 6 *– Modelling critical infrastructure exposure to coseismic landsliding from an Alpine fault earthquake*

Intended for Submission to *– Risk Analysis*

The manuscript and modelling was concieved, developed, and written by Mr Robinson. Dr Tom Wilson provided a valuable contribution to the structure and conceptual framing of the paper. Prof Tim Davies and Dr Caroline Orchiston provided major reviews and discussions of the results as well as suggesting the application of the model for planning purposes.

Certification by Co-authors:
If there is more than one co-author then a single co-author can sign on behalf of all
The undersigned certifys that:

- The above statement correctly reflects the nature and extent of the PhD candidate's contribution to this co-authored work
- In cases where the candidate was the lead author of the co-authored work he or she wrote the text

Name: *Tim Davies* Signature:  Date: *18 September 2014*

Deputy Vice-Chancellor's Office
Postgraduate Office

UNIVERSITY OF CANTERBURY
Te Whare Wānanga o Waitaha
CHRISTCHURCH NEW ZEALAND

Co-Authorship Form

This form is to accompany the submission of any thesis that contains research reported in co-authored work that has been published, accepted for publication, or submitted for publication. A copy of this form should be included for each co-authored work that is included in the thesis. Completed forms should be included at the front (after the thesis abstract) of each copy of the thesis submitted for examination and library deposit.

Appendix A *– The extremely long-runout Komansu rock avalanche in the Trans Alai range, Pamir Mountains, southern Kyrgyzstan*

Published in *– Landslides*

Published online: 30 April 2014

The initial field investigation was concieved by Dr Natalya Reznichenko through discussions with Prof Tim Davies. The concept and writing of the manuscript was undertaken by Mr Robinson. The data, figures, concepts, and results discussed in the paper are those of Mr Robinson. Prof Tim Davies provided significant discussion and framing of the manuscript as well as suggesting the comparison to volcanic debris avalanches such as Socompa. Dr Reznichenko and Dr Greg De Pascale were both involved in field investigations and provided substantial reviews and discussions on the manuscript results and contents.

Certification by Co-authors:

If there is more than one co-author then a single co-author can sign on behalf of all

The undersigned certifys that:

- The above statement correctly reflects the nature and extent of the PhD candidate's contribution to this co-authored work
- In cases where the candidate was the lead author of the co-authored work he or she wrote the text

Name: *Tim Davies* Signature: Date: *18 September 2014*

Deputy Vice-Chancellor's Office
Postgraduate Office

UNIVERSITY OF CANTERBURY
Te Whare Wānanga o Waitaha
CHRISTCHURCH NEW ZEALAND

Co-Authorship Form

This form is to accompany the submission of any thesis that contains research reported in co-authored work that has been published, accepted for publication, or submitted for publication. A copy of this form should be included for each co-authored work that is included in the thesis. Completed forms should be included at the front (after the thesis abstract) of each copy of the thesis submitted for examination and library deposit.

Appendix B *– Design and development of realistic exercise scenarios: a case study of the 2013 Civil Defence Exercise* Te Ripahapa

Published in *– GNS Science Miscellaneous Series 69*
Published: 17 February 2014

The manuscript was devised and written by Mr Robinson. The framing and outline of the paper was developed through detailed discussions between Mr Robinson and Dr Tom Wilson. Prof Tim Davies, Dr Caroline Orchiston and Mr James Thompson provided detailed reviews and discussions of the manuscript.

Certification by Co-authors:
If there is more than one co-author then a single co-author can sign on behalf of all
The undersigned certifys that:

- The above statement correctly reflects the nature and extent of the PhD candidate's contribution to this co-authored work
- In cases where the candidate was the lead author of the co-authored work he or she wrote the text

Name: *Tim Davies* Signature: Date: *18 September 2014*

Deputy Vice-Chancellor's Office
Postgraduate Office

UNIVERSITY OF CANTERBURY
Te Whare Wānanga o Waitaha
CHRISTCHURCH NEW ZEALAND

Co-Authorship Form

This form is to accompany the submission of any thesis that contains research reported in co-authored work that has been published, accepted for publication, or submitted for publication. A copy of this form should be included for each co-authored work that is included in the thesis. Completed forms should be included at the front (after the thesis abstract) of each copy of the thesis submitted for examination and library deposit.

Appendix C *– A rapid method for estimating expected fatalities from future strong earthquakes*
Submitted to *– Bulletin of the New Zealand Society for Earthquake Engineering*
Submitted: 24 August 2014

The model, results, and manuscript were established and developed by Mr Robinson in conjunction with Mr James Thompson as part of the CDEM emergency planning Exercise Te Ripahapa. *Dr Tom Wilson provided detailed discussion of the manuscript and suggested the included discussion of the 4 September 2010 Darfield earthquake, which was written by Mr Robinson. Prof Tim Davies and Dr Caroline Orchiston provided helpful reviews of the manscript contents.*

Certification by Co-authors:
If there is more than one co-author then a single co-author can sign on behalf of all
The undersigned certifys that:

- The above statement correctly reflects the nature and extent of the PhD candidate's contribution to this co-authored work
- In cases where the candidate was the lead author of the co-authored work he or she wrote the text

Name: *Tim Davies* Signature: Date: *18 September 2014*

Contents

List of Figures

List of Tables

Nomenclature and formula variables

γ	User-defined variable for *fuzzy Gamma* operator; typically $\sim$0.9
ρ	Density
σ_s	Sample standard deviation
$\chi_A(x)$	Set theory function
$\mu_A(x)$	Fuzzy logic membership value
$tan\alpha$	Coefficient of friction
A	Total area affected by landsliding[1]
A_C	River catchment area
A_{Lmax}	Largest landslide area
A_{LT}	Total landslide area
Aoraki/Mt Cook	New Zealand's tallest peak; known by both its Māori and European names
AUC	Area under the curve
CDEM	Civil Defence and Emergency Management
D	Difference between mainshock magnitude and largest aftershock magnitude
DEM	Digital Elevation Model
E	Exposure
EM	Emergency Management
EOC	Emergency Operations Centre
F	Frequency
FEMA	Federal Emergency Management Agency
Fr	Frequency Ratio
GIS	Geographical Information System(s)
GNS	GNS Science; New Zealand crown research institute
H	Landslide fall height
HEP	Hydroelectric Power
IDT	Integrated Design Team(s)

[1] Also used to represent a 'set' in fuzzy logic (Chapter 4).

k	Landslide volume coefficient
L	Landslide runout distance
L_d	Landslide deposit length
M_a	Largest aftershock magnitude
M_L	Landslide magnitude
M_m	Mainshock magnitude
M_w	Moment Magnitude
MCDEM	Ministry of Civil Defence and Emergency Management
MM	Modified Mercalli shaking intensity
N_C	Number of landslides in river catchment
N_i	Point on network
N_{LT}	Total number of landslides
N_t	Number of trials
NCMC	National Crisis Management Centre
NIWA	National Institute of Water and Atmospheric Research
NZTA	New Zealand Transport Agency
$p(V_L)$	Landslide volume probability density
PGA	Peak Ground Acceleration
Q1/Q2/Q3	First, second (median), and third quartiles
QMap	1:250,000 New Zealand Geologic maps
R^2	Coefficient of determination
$RAND$	Random number
REC	River Environment Classification
S_V	Sediment volume
SEM	Standard error of the mean
SH	State Highway
SSY	Suspended Sediment Yield
$\overline{T}$	Average time between mainshock and largest aftershock
TPI	Topographic Position Index
ULR	Unformed Legal Road
USGS	United States Geological Survey
V	Landslide volume
V'	Landslide exceedance volume
V_{Lmax}	Largest landslide volume
V_{LT}	Total landslide volume

Chapter 1

Introduction

1.1 Preparing for disasters

Disasters can occur at any time and have countless potential causes, ranging from geophysical to meteorological to technological and beyond (**Fig. 1.1**). Regardless of their cause, disasters significantly and negatively alter the relationship between a community and its built and natural environments (Kroll-Smith and Couch, 1991). The defining feature of a disaster is that it severely tests, and often exceeds, the ability of community's to respond to the unfolding crisis (Quarantelli, 1985, 1987). Disasters are directly related to pre-event decisions and actions regarding land-use, building structures, emergency response planning, public education and many others (Kroll-Smith and Couch, 1991). This is clearly apparent in the recent experience in Christchurch, New Zealand, following the devastating 2010-11 Canterbury earthquake sequence (Gledhill et al., 2011; Kaiser et al., 2012). Prior to the earthquake, the potential for widespread liquefaction throughout the eastern suburbs and rockfall and cliff collapse in the Port Hills had been well established (Brown et al., 1995; Clough, 2006), yet poor land-use planning decisions allowed these areas to be developed and inhabited. Consequently, following the earthquake sequence, large swathes of residential land has been retired as a result of irreparable ground damage from liquefaction and substantial rockfall risks (see Rogers et al., 2014).

Effective pre-event planning for potential disasters is therefore vital to developing community preparedness and resilience. This pre-event planning can take a number of different forms and involve the full spectrum of society. Freeman et al. (2003) showed in their disaster risk management framework that pre-event planning requires the combined efforts of disaster scientists (i.e. physical or social researchers directly involved in the study of disasters), engineers, emergency managers, local, regional and national governance, insurance and re-

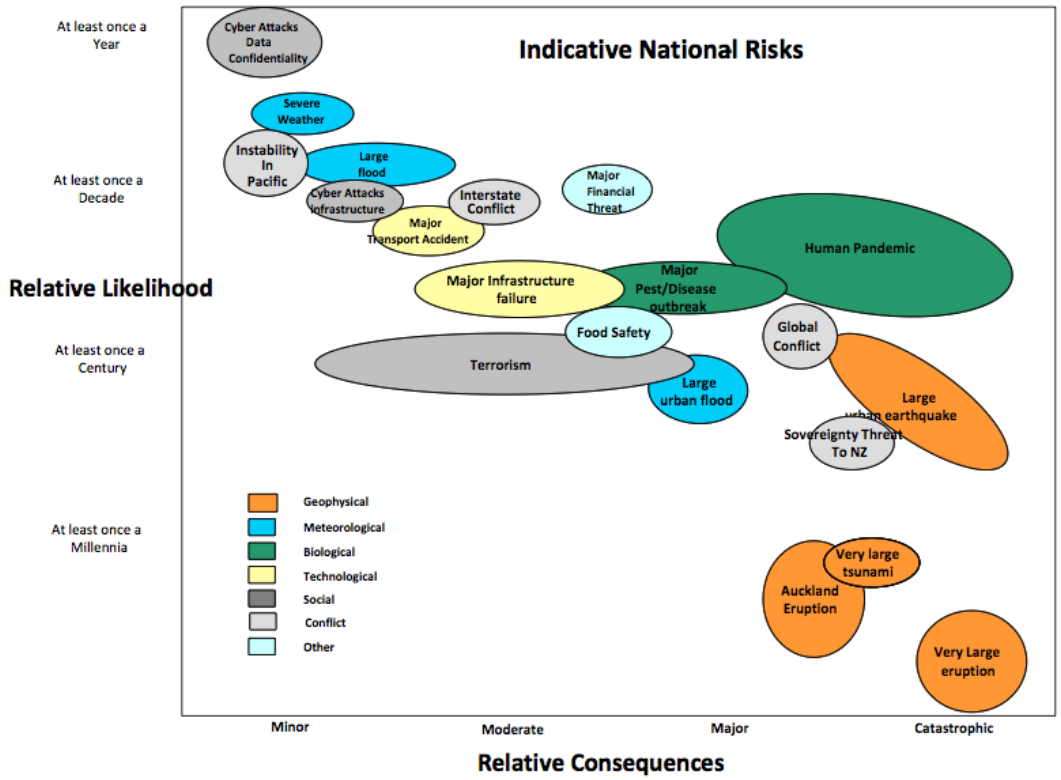

Figure 1.1: Frequency and severity of potential disasters in New Zealand. From DPMC, 2011.

insurance, and local communities. Key pre-event actions include hazard and risk assessments (Nirupama, 2013), preparedness through emergency response plans and management capabilities (Freeman et al., 2003), risk transfer through insurance, re-insurance, and calamity funds (Andersen, 2001; Freeman and Kunreuther, 1997), and a combination of hard and soft mitigation (Lichterman, 2000). Underpinning all of this is the need for knowledge and understanding of the hazards that communities face. Developing an understanding of future hazards and their consequent disasters can take a number of different approaches, which can be broadly categorised into probabilistic and deterministic techniques (see Bommer, 2002).

Probabilistic approaches attempt to identify all the possible occurrences of a hazard that may affect a site and to characterise the frequency of occurrence of different event magnitudes through recurrence relationships (Abrahamson, 2000; Bommer, 2002). They effectively identify the most likely hazards over long-time periods by assigning probabilities to each hazard. Probabilistic Seismic Hazard Analysis (PSHA) for instance, details the expected peak ground acceleration (PGA) with various exceedance probabilities over timescales of hundreds-to-thousands of years (e.g. Stirling et al., 2002). As such they are especially useful for insurance purposes and for informing engineering design codes as both require information on the

most likely hazards (Bommer, 2002). Conversely, deterministic approaches develop hazard or disaster scenarios that explicitly describe the location, magnitude, and intensity of specific hazard events and their consequent effects (Kramer, 1996; Reiter, 1990). Deterministic approaches are widely applied to emergency management exercises, personnel training, risk communication, contingency planning etc. as these require detailed and precise scenarios. While both approaches are clearly important for pre-event disaster planning, probabilistic approaches are more suited to a longer-term view based primarily around insurance, financial security and life safety, by assessing the most probable hazards over hundreds-to-thousands of years. This is not useful, however, for emergency response planning for the immediate aftermath of a disaster or for planning short-to-medium term post-disaster recovery strategies. Thus, in terms of emergency management and emergency response planning, developing deterministic disaster scenarios is vital.

1.2 Emergency management and disaster scenarios

Emergency management can be defined in a variety of different ways (see Blanchard, 2008), however perhaps the most encompassing definition is: '*the coordination and integration of all activities necessary to build, sustain, and improve the capabilities to prepare for, respond to, recover from, or mitigate against threatened or actual disasters or emergencies, regardless of cause*' (DHS, 2007). Emergency management therefore plays a pivotal role before, during, and after any disaster. Following a series of damaging hurricanes affecting Florida in 2004, Kapucu (2008) demonstrated that effective pre-event planning by emergency management groups actively increased the preparedness and thus resilience of affected communities. Freeman et al. (2003) suggested that undertaking emergency management exercises was a key component of disaster risk management pre-event planning, and consequently such emergency management exercises are mandated by legislation in most industrialised nations (Selvarajah 1993; CDEM Act, 2002).

Exercises have been shown to increase safety, decrease errors and improve judgement, and are useful for teaching and evaluating specific skills amongst participants (Bearnson and Wiker, 2005). Further, participants who undertake exercises typically score higher in self-confidence and perceived-confidence in their ability to manage situations than those not participating (Scherer et al., 2007). In highly stressful occupations like emergency management, such increases in self-confidence can be critical as they determine whether coping strategies are initiated, how much effort is applied, and how long this effort is sustained when experiencing difficulties (Harder, 2010). Consequently, it is important that exercises invoke and

teach the processes and behaviours required in responding to an emergency (Holling, 2004; Park et al., 2013). The disaster scenarios must therefore be as detailed and realistic as possible (Alexander, 2000). Given the large number and complexity of potential hazards that can threaten a community (**Fig. 1.1**), Preuss and Godfrey (2006) note that complete and accurate disaster scenarios must be co-produced using knowledge and expertise from a wide variety of social groups. To date, however, the processes involved in developing disaster scenarios have not been adequately described.

1.2.1 Hazard and emergency management in New Zealand

New Zealand is susceptible to a wide range of hazards (**Fig. 1.1**) and as a result, has a highly active emergency management sector. The sector is broken down into three levels:

1. National - the Ministry for Civil Defence and Emergency Management (MCDEM), the National Crisis Management Centre (NCMC), and central government;
2. Group - the regional Civil Defence and Emergency Management (CDEM) Groups, and the Regional and Environment Councils (**Fig. 1.2**); and
3. Local - the local City and District Councils (**Fig. 1.2**).

This structure allows for dispersed accountability where the lower levels respond to any emergency and upper levels provide support. The CDEM sector takes a disaster risk management approach to all hazards as defined in the 2002 CDEM Act (CDEM Act, 2002). There is a focus on risk and resilience with key objectives being to enable local communities to achieve acceptable levels of risk, and to promote the sustainable management of hazards. The CDEM Act also recognises that emergencies are often multi-agency events and therefore encourages collaboration across a range of agencies including critical infrastructure stakeholders and emergency services.

Despite the large number of potential hazards in New Zealand (**Fig. 1.1**), McLean et al. (2012) noted that even at a regional level emergencies were relatively uncommon, making it difficult for emergency managers to maintain their response skills and efficiency. To combat this and in order to evaluate the level of emergency management sector preparedness, New Zealand undertakes a number of emergency planning exercises of varying scale each year. These are most often based around the occurrence of a natural hazard given New Zealand's propensity for and diversity of natural hazards (**Fig. 1.1**). Exercises vary in scale denoted by a tier number, with higher numbers describing larger-scale exercises:

- *Tier 1* - Local exercise (individual City or District Council)

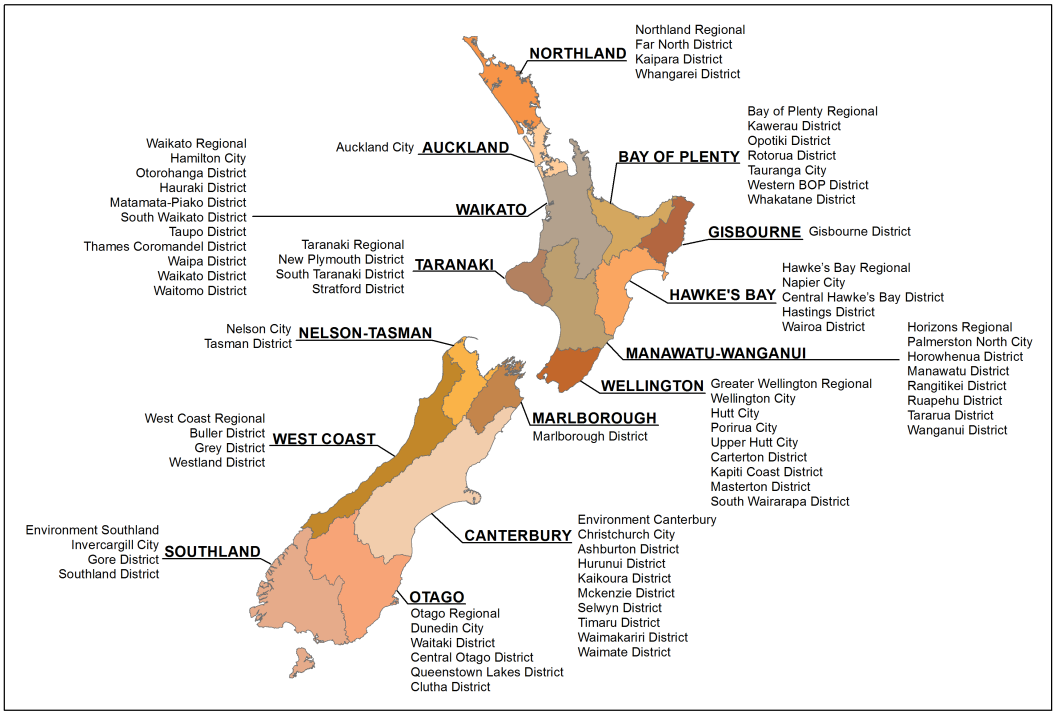

Figure 1.2: New Zealand's Civil Defence and Emergency Management Groups and their associated local and regional councils (www.civildefence.govt.nz).

- *Tier 2* - Group exercise (individual CDEM Group and associated partner agencies/councils)
- *Tier 3* - Inter-Group exercise (multiple CDEM Groups and associated partner agencies/councils)
- *Tier 4* - National exercise (All CDEM Groups and central government)

Typically more than 10 of these exercises are undertaken each year, with the majority being Tier 2-3, while Tier 4 exercises occur every two to three years (www.civildefence.govt.nz). These exercises are highly adaptable and the range of exercise types are described in **Table 1.1**. Nevertheless, regardless of the tier or exercise type, all New Zealand CDEM exercises require a detailed and realistic disaster scenario. Establishing explicit processes for the design and development of disaster scenarios, as well as increasing the knowledge and understanding of the hazards facing New Zealand, is therefore vital for developing a prepared and resilient community.

Table 1.1: Different emergency management exercise types. From www.civildefence.govt.nz.

Exercise Type	Description
Orientation Exercise	Also known as a 'walk-through', this is generally used as a method to familiarise participants with the roles and activities they are required to perform
Drill Exercise	A short exercise whose focus is on participants physically using specific equipment or performing specific procedures
Tabletop Exercise	Also known as a 'discussion exercise', participants are required to discuss the scenario in order to formulate an appropriate response or solution
Functional Exercise	Also known as an 'operational' or 'tactical exercise', this takes place in a fully simulated operational environment requiring participants to actually perform their assigned functions and roles
Full-scale Exercise	Also known as a 'practical exercise', this is a fully simulated exercise similar to a *functional exercise* but including the deployment of field teams

One of the most significant hazards facing New Zealand is that of a large earthquake. New Zealand is situated on a major plate boundary between the Australian and Pacific plates resulting in one of the highest seismicity rates in the world (**Fig. 1.3**). In the South Island, at least 20 large, damaging earthquakes have occurred since 1848; an average rate of more than one a decade (see Chapter 2). Qualitative assessments of New Zealand's national risks by the Department of the Prime Minister and Cabinet (DPMC) placed large earthquakes alongside human pandemic as the highest national risk, both being potentially catastrophic and relatively common (**Fig. 1.1**). The 2010-11 Canterbury earthquake sequence has vividly demonstrated the earthquake hazard in New Zealand and has resulted in a strong drive by the public and government at all levels to increase earthquake resilience throughout New Zealand. One of the major factors of the Canterbury earthquake sequence involved the devastating secondary effects that occurred in the form of liquefaction, rockfall, and cliff collapse, which caused a substantial portion of Christchurch's eastern residential suburbs to be abandoned. Historically, widespread and damaging secondary effects have been witnessed in a large proportion of New Zealand earthquakes, with landsliding being the most common occurrence (see Chapter 2). Understanding the full complement of hazards likely to result from large earthquakes

is therefore vital for hazard assessments and emergency response planning. Finding ways to better understand and include such geomorphic hazards into emergency management exercises is therefore an important research topic.

1.3 Earthquakes and associated hazards

1.3.1 Earthquake hazard in New Zealand

One of the most significant seismic hazards currently facing New Zealand is posed by the Alpine fault in the South Island. This fault runs >400 km along the western edge of the Southern Alps forming the primary onshore segment of the Australian-Pacific plate boundary (**Fig. 1.3**). During the last 7-10 Ma the fault has accommodated ∼480 km of lateral displacement (Wellman, 1955) and 21-25 km of uplift (Cooper, 1990; Kamp et al., 1989). Present-day displacement rates are some of the fastest in the world with strike-slip rates averaging 27±5 mm/a and dip-slip rates reaching a maximum of ∼12 mm/a (Norris and Cooper, 2001). Evidence suggests that the Alpine fault has historically produced M∼8 or larger earthquakes and is currently late in its seismic cycle (Adams, 1980b; Beavan et al., 1999; Berryman et al., 2012a; Cooper and Norris, 1990; De Pascale and Langridge, 2012; Yetton, 1998). Such earthquakes almost certainly result in very strong shaking intensities in the vicinity of the western range-front of the Southern Alps along strike of the fault, and throughout the range as a result of topographic amplification along ridgelines (Buech et al., 2010). In addition, there is substantial palaeoseismic evidence to suggest previous events have caused widespread secondary effects (Bull, 1996; De Pascale et al., 2014; Yetton, 1998).

Deep-seated, large volume ($>10^6$ m^3) landslides have been identified throughout the Southern Alps (Whitehouse and Griffiths, 1983), and a large number have been attributed to previous ruptures of the Alpine fault (although large earthquakes on other faults may also be responsible). Some of these are among the largest in the world, particularly the 27 km^3 Green Lake (see Hancox and Perrin, 1994, 2009), 1 km^3 John O'Groats, and 0.75 km^3 Cascade (see Barth, 2014) landslides. Also of note is the Round Top landslide deposit thought to have resulted from an Alpine fault earthquake around 930 CE, which has an anomalously long (∼4 km) runout length (Wright, 1998). As well as individual landslides, Davies and Korup (2007) and Berryman et al. (2001) identified evidence of widespread landsliding throughout the central Southern Alps. They observed buried soils at depths of several metres in at least four alluvial outwash surfaces west of the Southern Alps, all of which were buried contemporaneously post-1600 CE. They inferred that this demonstrated that widespread landsliding had occurred in the mountains sometime during the 1600s; subsequently landslide debris had

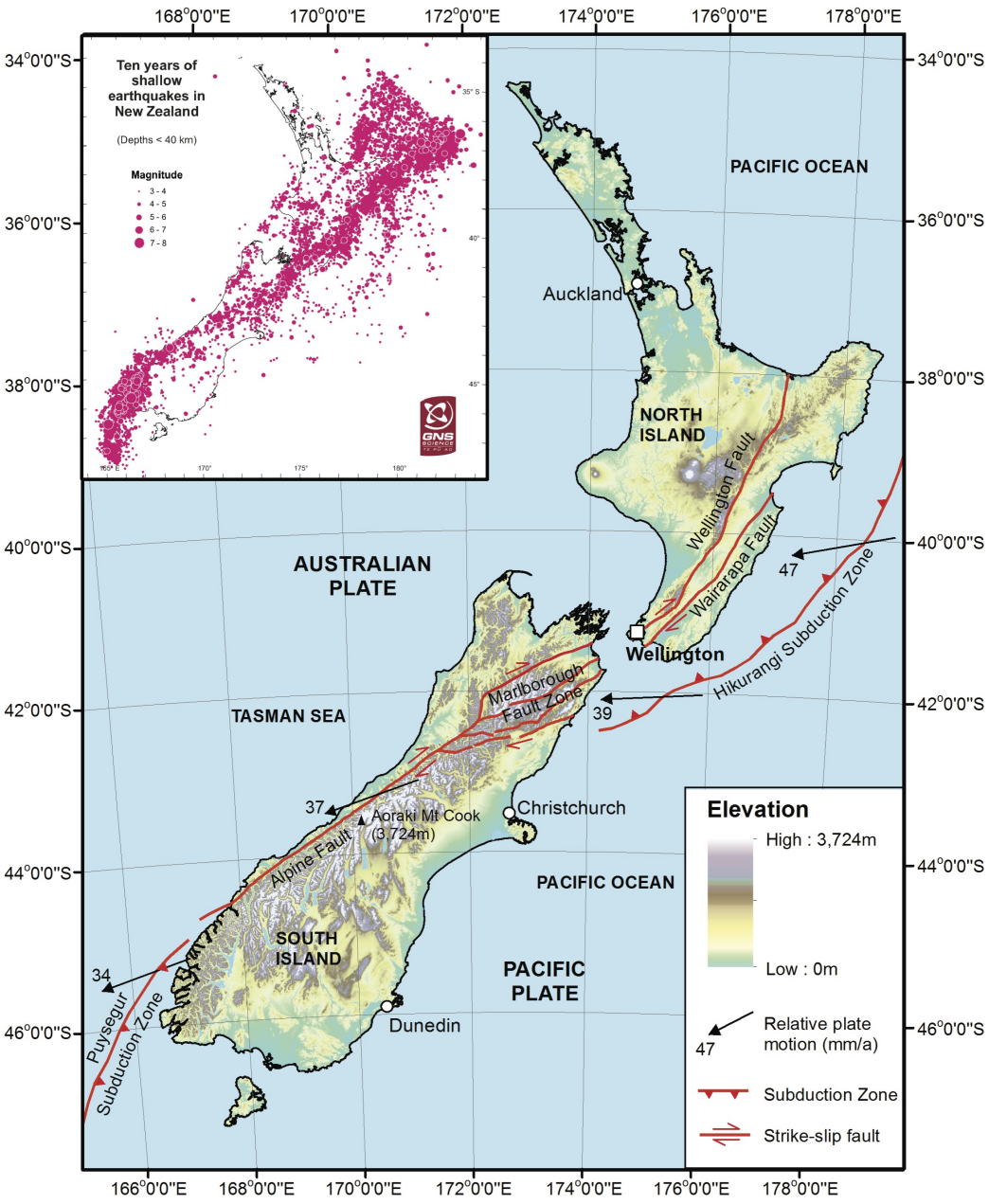

Figure 1.3: Tectonic setting of New Zealand showing the major fault systems associated with the Pacific-Australian plate boundary and the relative plate motion vectors. Inset: Ten years of shallow (<40 km) seismicity throughout New Zealand (from www.info.geonet.org.nz/display/quake/Earthquake)

been remobilised and deposited on alluvial fans, burying the soils. They concluded the most likely cause was an Alpine fault earthquake. Nevertheless, an Alpine fault earthquake has not occurred historically, and thus understanding of its potential geomorphic effects are limited to just a few sites where geologic evidence has been identified. Observations of historic earthquakes globally may provide insights into the full scale of potential geomorphic effects from a future Alpine fault earthquake.

1.3.2 Historic earthquake events

Since 1900, earthquakes have affected >180 million people, resulting in >2.5 million deaths and >US$760 billion in damage (CRED, 2013). In recent years, catastrophic secondary consequences have most notably been demonstrated by the 2004 Indonesian and 2011 Japanese tsunamis, caused by offshore mega-thrust earthquakes. Consequently, tsunamis are perhaps the most widely modelled secondary earthquake hazard (see Annaka et al., 2007; Ng et al., 1990; Power et al., 2007). However, of all the earthquakes to have killed >1,000 people since 1900, only 15% involved tsunamis; in comparison, >30% involved landsliding (**Fig. 1.4**). Recent events such as the 1999 Chi-Chi (Taiwan), 2005 Kashmir (Pakistan), and 2008 Wenchuan (China) earthquakes have demonstrated that coseismic landsliding can be just as catastrophic as earthquake-generated tsunamis. This was most evident in the Wenchuan earthquake that triggered ∼60,000 landslides (Gorum et al., 2011; Li et al., 2014; Parker et al., 2011) which accounted for up to a third of the estimated >60,000 fatalities (Yin et al., 2009). The >250 landslide dams that formed as a result presented a substantial emergency response issue alone; the largest threatened a total of 1.2 million people with a potentially catastrophic outburst flood (Peng and Zhang, 2012; Xu et al., 2009).

Like tsunami, landslides resulting from earthquakes have the potential to affect very large areas and can substantially increase the total area severely affected by the initial earthquake. In the Chi-Chi, Kashmir, and Wenchuan earthquakes, it was not simply individual landslides that exacerbated the disaster, but the magnitude of landsliding as a whole. Landslides from the Chi-Chi earthquake affected a total area in excess of 11,000 km^2 (Hung, 2000), those in Kashmir affected an area of at least 7,500 km^2 (Owen et al., 2008), while landslides in Wenchuan affected >100,000 km^2 (Huang et al., 2010) with a total debris volume >2 km^3 (Li et al., 2014; Parker et al., 2011). In each event the scale of landsliding dramatically impacted the emergency response, blocking key routes into devastated regions and in some instances destroying entire towns.

Coseismic landsliding also contributes to far longer term geomorphic consequences. In the years following an earthquake, long duration, heavy rainstorms can remobilise landslide

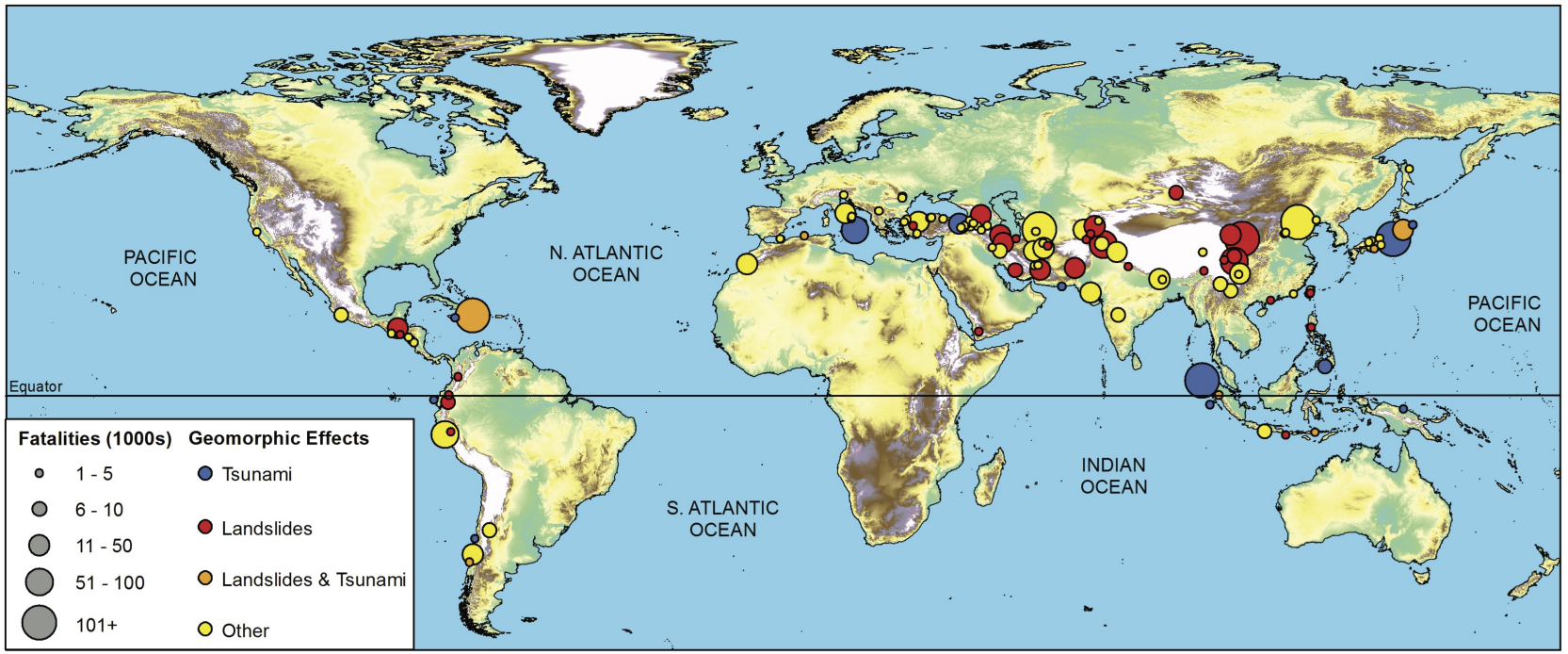

Figure 1.4: All known earthquakes causing >1,000 deaths since 1900 and their associated geomorphic effects. Data from USGS, 2014.

material as debris flows, which have the potential to cause additional fatalities and destruction (Lin et al., 2003; Xu et al., 2012). Storms also remobilise landslide material in a more gradual but equally devastating process known as aggradation, which notably raised river beds by up to tens of metres in Wenchuan and resulted in the infilling of several reservoirs in Taiwan (**Fig. 1.5**). The latter can have devastating effects for water supply or hydroelectric power. Furthermore, landslide dams present a continuing outburst flood hazard to downstream populations as well as forming upstream lakes which can submerge vital access routes and towns. Following the Wenchuan earthquake, 15 million people were evacuated from their homes (USGS, 2014), many due to the continued threat of landsliding and outburst floods. Earthquakes in mountainous environments therefore pose both an immediate, local hazard and a long-term, more widespread hazard.

1.4 Previous Alpine fault earthquake scenarios

To-date, the only publicly available disaster scenario studies undertaken for an Alpine fault earthquake are the West Coast Engineering Lifeline Group (WCELG) reports completed in 2006 (see McCahon et al., 2006a,b,c). These were a series of reports for each of the three West Coast District Councils and the West Coast Regional Council that investigated the potential effects of an Alpine fault earthquake on critical infrastructure throughout the region. The precise scenario was derived qualitatively from a collaboration of information on previous earthquakes in New Zealand and globally, but no new research was carried out (McCahon et al., 2006a,b,c). Until recently (see Chapter 3) this was the most detailed Alpine fault disaster scenario available. The scenario identified the likely scale of ground shaking as well as locations susceptible to liquefaction, and was able to draw conclusions about the likely affects for transport, drainage, water supply, sewerage, power supply, and telecommunications networks. Detailed estimates of landsliding were not undertaken with only qualitative statements of the potential hazard included. While the reports did provide estimates of the potential impacts and recovery times on a qualitative basis for landslide affected infrastructure, a robust and accurate assessment cannot be completed without a quantitative evaluation of the coseismic landsliding likely to occur.

Since the 1950s many methods have been proposed to assess the stability of slopes during earthquakes (see Lee et al., 2008; Miles and Keefer, 2000; Newmark, 1965; Stewart et al., 2003), however to date this remains challenging, particularly in regions with no historic events (Wasowski et al., 2011). Advancing understanding of coseismic landsliding is a critical research priority, and is vital to increasing the resilience of society in general to

Figure 1.5: Time series of the infilling of the Wushe Resevoir as a result of heavy rainstorms following the 1999 Chi-Chi earthquake. Image from: http://www2.ce.ntu.edu.tw/∼mh/TaiwanPostcards/Wushe-Resevoir.html.

future earthquakes. One of the primary research needs is for a quantitative method to model coseismic landsliding from scenario earthquakes in regions where no historic events have occurred and no geotechnical data is available. Developing such a method will allow the creation of a more detailed Alpine fault earthquake scenario that includes detailed estimates of the potential scale of landsliding. The difficulties associated with modelling coseismic landsliding, particularly in terms of landslide occurrence, location, volume, and runout distance, make detailed risk assessments for critical infrastructure complex. Recent attempts by Catani et al. (2005) and Pellicani et al. (2013) have made significant strides forward, however these primarily focus on the potential financial losses. Emergency response planning requires a detailed account of infrastructure functionality, as it is a significant factor in determining the response (Whitman et al., 1997). Developing a means to assess critical infrastructure exposure to coseismic landsliding specifically for emergency response planning purposes is therefore a further important research gap.

1.5 Thesis aims and objectives

The primary aim of this research is to develop a detailed and realistic disaster scenario for an Alpine fault earthquake that includes quantitative estimates of coseismic landsliding for use in emergency response planning. Given the widespread use and importance of disaster scenarios for such purposes, this research will also address the process of developing disaster scenarios for any hazard for emergency management. Disaster scenarios have been addressed by several previous authors (e.g. Alexander, 2000; Borodzicz and van Haperen, 2002; Faccioli, 2006; Preuss and Godfrey, 2006) yet specific frameworks or models for their development are still currently lacking. Similarly, modelling coseismic landsliding has been addressed by several authors (e.g. Lee et al., 2008; Miles and Keefer, 2000; Newmark, 1965), yet each of these models requires either detailed geotechnical data or accurate historic inventories from the study area. No method currently exists for assessing landslide susceptibility in regions without this information (e.g. New Zealand), and thus understanding coseismic landslide hazards remains a critical research priority (Freeman et al., 2003; Wasowski et al., 2011). This research will provide information that will enable greater preparedness and yield better community resilience within New Zealand to an Alpine fault earthquake, and enable similar work to be undertaken elsewhere.

The primary aim of this research will be addressed in the following objectives:

1. Identify, describe, and review the various geomorphic hazards that result from large earthquakes in mountainous environments.

2. Establish a general framework/model for the development of disaster scenarios for emergency management with application to other hazards.

3. Establish a method for modelling coseismic landslide susceptibility for regions with no historic inventories or geotechnical data.

4. Quantify the magnitude of coseismic landsliding likely to arise from a maximum-credible Alpine fault earthquake scenario.

5. Establish a method for assessing the exposure of critical infrastructure networks to landslide susceptibility scenarios and apply this to an Alpine fault earthquake scenario.

1.6 Thesis structure

The body of this thesis consists of five chapters comprising either published, submitted, or prepared-for-submission manuscripts for scientific journals. Chapter 2 reviews published material on the various geomorphic effects of large mountainous earthquakes and the evidence for such effects in the South Island. Chapter 3 establishes a method for developing detailed and realistic disaster scenarios and applies the method to a New Zealand CDEM exercise for an Alpine fault earthquake. Chapter 4 utilises data from historic coseismic landslide inventories to derive a statistically-based method for establishing coseismic landslide susceptibility from scenario earthquakes. This method is applied in Chapter 5 to the Alpine fault earthquake scenario described in Chapter 3, and analysed to provide estimates of the scale of landsliding expected. Finally, Chapter 6 develops a method for assessing the exposure of critical infrastructure to coseismic landsliding and applies the method to the Alpine fault earthquake scenario. Chapter 7 concludes the thesis with a general summation and discussion of the main results, and highlights potential avenues for further research. The Appendices describe additional research undertaken by the author which supports, but is not directly relevant to, the main aim of the thesis. Appendix A demonstrates an extreme example of coseismic landsliding hazard from Kyrgyzstan. Appendix B describes in further detail the processes undertaken to develop the CDEM Exercise described in Chapter 3. Appendix C details a method for rapid evaluation of fatalities from scenario earthquakes, and provides fatality estimates for the Alpine fault earthquake scenario described in Chapter 3 and Appendix B.

All of the methodologies, applications, and results described herein are the direct outcomes of the author's own research; however, several co-authors have made invaluable contributions to some of the chapters. Their specific inputs have been detailed in the signed co-authorship statements at the beginning of this thesis.

Chapter 2

Geomorphic consequences of large earthquakes in mountainous environments

2.1 Introduction

New Zealand is especially susceptible to large earthquakes, being situated at the boundary between the Pacific and Australian tectonic plates. The South Island, in particular, has an extremely high seismic hazard with numerous active faults distributed throughout the island (**Fig. 2.1**; GNS, 2014). However, because of New Zealand's relatively short recorded history (European settlement only began around the mid-1800s), historic rupture has only been recorded on a small number of these faults (**Fig. 2.1**). Of these ruptures, only two have occurred on major faults with the other ruptures occurring on subsidiary, and usually previously unknown faults. The hazard from most of the subsidiary faults is relatively poorly known, with most having long or unknown recurrence intervals (**Fig. 2.1**; GNS, 2014). Research has therefore focussed primarily on the larger-scale fault systems which are thought capable of producing large ($>M_w 7.0$) earthquakes (Pettinga et al., 2001; Stirling et al., 2002) and are therefore thought to present the most significant hazard. Of these larger-scale faults, the plate-boundary Alpine fault at the western edge of the Southern Alps presents the most significant hazard.

The Alpine fault has a $\sim$400 km long onshore surface expression and is a segment of one of the most active tectonic plate boundaries on earth (**Fig. 1.3**). The well-defined 200 km long central segment accommodates ⅔ of the $\sim$38.5 mm/a relative plate motion as a combination of dextral slip (70%) and uplift (30%) (Cooper and Norris, 1994). Recognised as

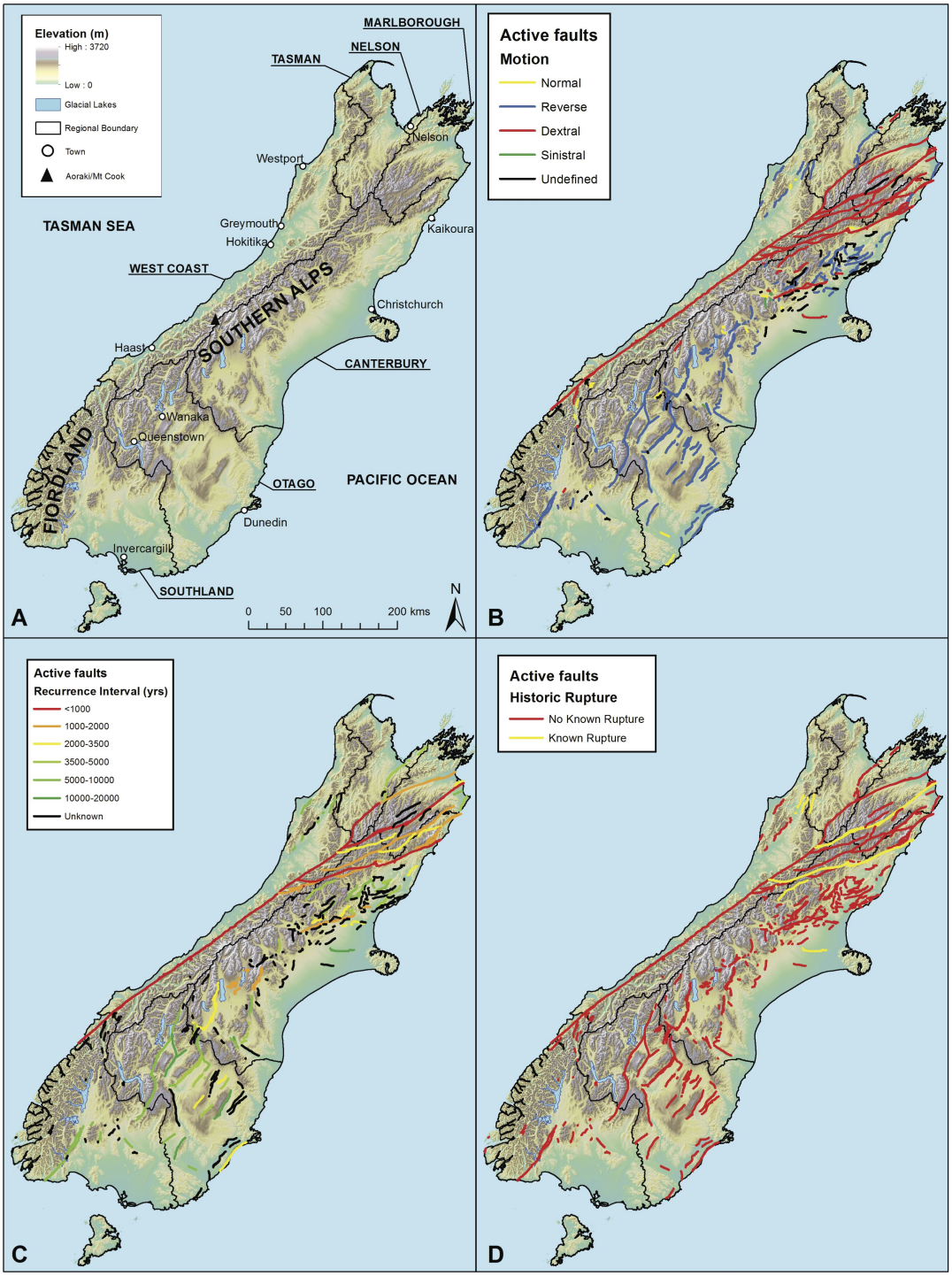

Figure 2.1: South Island active faults: a) location map; b) faulting motion; c) recurrence interval; d) known historic rupture. Adapted from GNS, 2014.

the source of large displacements of lithologic units in the 1940s (Wellman and Willett, 1942) and generally accepted as being seismogenic in the 1990s (Norris and Cooper, 1995; Yetton, 1998), the Alpine fault is thought capable of generating M_w8+ earthquakes with a recurrence interval of ~200-400 years (Berryman et al., 2012b; De Pascale et al., 2014; Sutherland et al., 2007). The most-recent event occurred in c. 1717 CE and involved a 380 km long segment of the fault (Wells et al., 1999; Yetton, 1998). Thus, currently there is an estimated 1-2% annual likelihood of rupture (Rhoades and Van Dissen, 2003) and at least a 30% probability in the next 50 years.

Geological evidence of previous Alpine fault earthquakes suggests the next rupture could have potentially devastating consequences for the entire South Island. This corresponds with observations from recent historic earthquakes elsewhere in the world which generated widespread geomorphic consequences (see Chapter 1). The subsequent geomorphic effects from an Alpine fault event may include landslides, landslide dams, outburst floods, river aggradation and avulsion, lake tsunami, liquefaction, debris flows, and glacier advance, amongst others. Many of these will occur immediately, during the initial ground shaking; however some may persist for many decades after the initial earthquake (see Hewitt et al., 2008). This chapter therefore reviews published material on the consequential geomorphic effects of historic earthquakes around the globe as well as the evidence for such effects from previous Alpine fault events. It serves as a baseline compilation of likely processes with order-of-magnitude estimates of their scale from the available data, from which more detailed work can develop.

2.2 South Island tectonic setting

2.2.1 Plate motion

The Alpine fault marks the onshore boundary between the Australian and Pacific plates and accommodates the change from east-dipping subduction in the south to west-dipping subduction in the north (**Fig. 1.3**). The rate of displacement across the boundary averaged over the last 3 million years is 37 $\pm$ 2 mm/a on a bearing of 071 $\pm$ 2° (DeMets et al., 1994). Along the central segment of the fault this motion is partitioned 35.5 $\pm$ 1.5 mm/a parallel and 10 $\pm$ 1.5 mm/a perpendicular to the fault, forming a transpressional boundary with right-lateral oblique motion (Norris and Cooper, 2001). Strike-slip displacement rates along the fault consistently average 27 $\pm$ 5 mm/a while dip-slip rates vary widely from a maximum of ~12 mm/a in the Aoraki/Mt Cook region to almost zero south of Haast (Norris and Cooper, 2001).

2.2.2 The Alpine fault

At a broad scale, the Alpine fault appears as a simple linear feature striking southwest-northeast; however in detail the fault is more complex (**Fig. 2.2**). The central and northern segments of the fault are segmented at a scale of kilometres, consisting of north-striking oblique-reverse sections and east-striking dextral strike-slip sections (Norris and Cooper, 1995); however the southern segment appears to simplify to a linear structure with little to no reverse motion (Berryman et al., 1992; Norris and Cooper, 2001; Sutherland and Norris, 1995). Seismic reflection imaging in the Aoraki/Mt Cook region suggests that the fault dips $\sim 40 \pm 5°$ southeast and continues to depths of ~25 km (Davey et al., 1995).

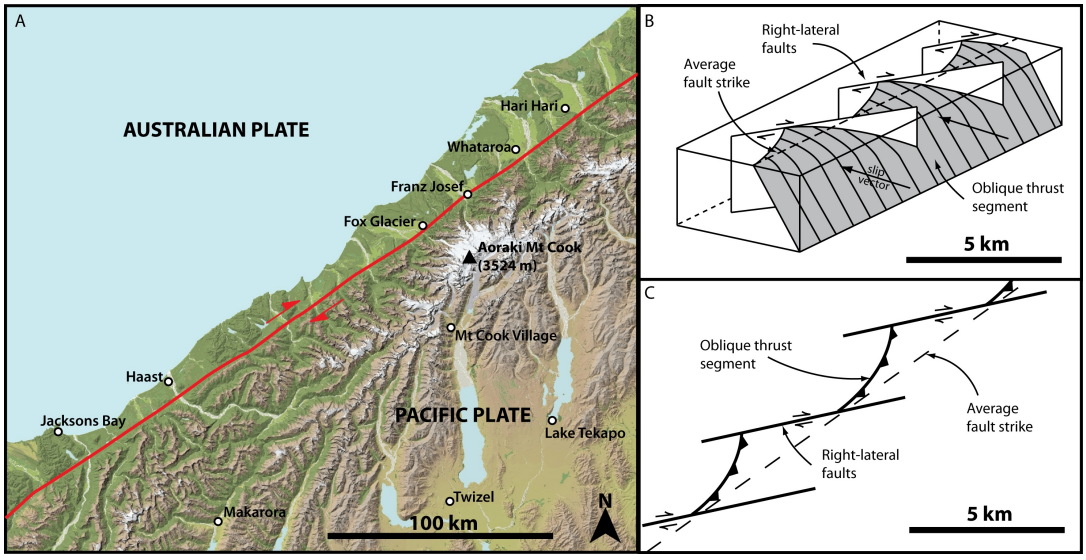

Figure 2.2: Structure of the Alpine fault: a) Overview of the central segment of the Alpine fault which appears as a simple linear feature; b) simplified 3D model showing complex segmentation (adapted from Norris and Cooper 1995); c) birds-eye view of b.

Uplift on the hanging wall, which has formed the Southern Alps, is estimated to have begun between 10 Ma (Cooper, 1990; Kamp and Tippett, 1993) and 7 Ma (Kamp et al., 1989). Total uplift estimates are between 21.5 km (Kamp et al., 1989) and 25 km (Cooper, 1990) and total lateral offset is ~480 km (Berryman et al., 1992; Wellman, 1955). Beavan et al. (1999) found little to no aseismic slip anywhere along the fault suggesting this offset has accumulated purely coseismically. Recent work has identified and dated the last 24 ruptures of the fault deriving an average recurrence interval of 329 ± 66 years between events with the most recent event occurring in c. 1717 (Berryman et al., 2012a). Combined with measured slip-rates this suggests individual ruptures involve ~9 m horizontal and up to ~3 m vertical motion which matches identified individual rupture displacements of 8-9 m lateral and 2-3 m

vertical (Adams, 1980b; Berryman et al., 2012a; Cooper and Norris, 1990; De Pascale and Langridge, 2012; De Pascale et al., 2014; Hull and Berryman, 1986; Sutherland et al., 2007; Sutherland and Norris, 1995). This suggests previous magnitudes of ∼M8 and confirms that all motion along the fault is accommodated coseismically.

2.2.3 The Southern Alps

The Southern Alps have formed on the hanging wall of the Alpine fault as a result of the Australian-Pacific plate collision. They have an average elevation of ∼1,000-1,500 m, currently reaching a maximum of 3,724 m at Aoraki/Mt Cook. The mountains are relatively young, forming in the last 7-10 Ma (Kamp et al., 1989; Kamp and Tippett, 1993) and present-day uplift rates along the Alpine fault make them some of the fastest rising mountains on earth. For this reason, west-draining rivers are relatively short and steep, reaching the Tasman sea in <30 km, while east-draining rivers have a much gentler gradient, travelling for >100 km to reach the Pacific ocean and building extensive alluvial fans. As a result of the rapid uplift, the Southern Alps are also some of the fastest-eroding mountains on earth, with regional erosion rates matching uplift, suggesting they are in an overall dynamic equilibrium (Adams, 1980a; Wellman, 1979). Consequently, South Island rivers carry large sediment loads resulting in extensive alluvial fans and braided gravel-bed river systems.

The central and northern Southern Alps are composed primarily of Mesozoic greywacke and schist which alters to mylonite and ultramylonite close to the Alpine fault. To the west of the fault, the underlying bedrock is primarily granitic, however on the west coast this is generally covered by thick quaternary deposits and thus only visible in isolated outcrops. This granite has been sheared and displaced to the north by the Alpine fault from its emplaced location west of Fiordland. As a result, the central and northern Southern Alps form tall, steep mountains with deeply incised river valleys, while Fiordland consists of lower mountains with high vertical cliff faces and obviously glaciated valley systems.

During the Last Glacial Maximum (LGM) ∼22,000 years before present (yrs BP), the Southern Alps were extensively glaciated as evidenced by the large, well-preserved lateral moraines along the west coast, the numerous large glacial lakes within the ranges south of Aoraki/Mt Cook, and the extensive cirques and fiord systems in Fiordland. Presently, there are >3,100 glaciers in the South Island covering a total area of >245 km^2 with a total ice volume of ∼53.3 km^3 (Chinn, 1989, 2001). Despite the large number of glaciers, most are very small with just seven covering >0.1 km^2, the longest of which is Tasman Glacier at 27 km. The six largest glaciers (Tasman, Murchison (18 km), Fox (13 km), Mueller (13 km), Franz Josef (12 km), and Hooker (11 km)) are all located in the central-Southern Alps within

15 km of Aoraki/Mt Cook, and the two west-flowing glaciers (Fox and Franz Josef) reach their termini at just $\sim$ 300 m above sea level (asl).

The prevailing winds blow from the west bringing heavy rainfall to the western ranges averaging $>$11 m/a, and forming a rain-shadow east of the main divide (annual rainfall in Christchurch is as little as 600 mm (Hicks et al., 1996)). Rainfall is evenly distributed throughout the year with no defined wet and dry seasons (Chinn, 2001). Consequently, the western ranges are covered in a thick temperate rainforest which extends to $\sim$1,500 m asl while east of the divide are semi-arid tussock grasslands, much of which have been cultivated for farming. Intensive agriculture has also developed on most west coast alluvial fans, however the region is particularly remote and difficult to access, especially south of Fox Glacier, and thus it remains sparsely inhabited. The ranges themselves are also largely uninhabited and remote with only a few townships. Most are small with populations of up to several hundred, however the major tourist towns of Wanaka and Queenstown exist in the lower ranges of inland Otago (**Fig 2.1a**) and have permanent populations of 10,000 and 30,000 respectively.

2.3 Historical Earthquakes

Since European settlement of New Zealand in the mid 1800s, the South Island has sustained at least 20 damaging earthquakes (**Table 2.1**). Almost all of these earthquakes are known to have generated widespread, and in some instances catastrophic, secondary geomorphic consequences. Unsurprisingly, virtually all have resulted in some degree of landsliding within the Southern Alps; however liquefaction is also a common occurrence (**Table 2.1**). Nonetheless, very few of these earthquakes are likely to be representative of an Alpine fault event. The Puysegur trench earthquakes recorded between 1988 and 2009, for instance, primarily affected the Fiordland region which is markedly different from the central and northern Southern Alps most likely to be affected by an Alpine fault event (see above). Both of the 1929 events as well as the 1968 Inangahua earthquake may be representative of an Alpine fault event but on a smaller scale as these each generated very strong shaking within the central Southern Alps. However, it is the 1855 Wairarapa earthquake which is likely to be most representative of an Alpine fault event. Despite occurring in the lower North Island this event caused widespread landsliding in the Southern Alps in Marlborough and northern Canterbury, as well as the Rimutaka mountains in the North Island (Downes, 2005; Grapes and Downes, 1997; Hancox, 2005). These are similar to the Southern Alps in that they are comprised of sheared greywacke with steep slopes reaching heights $\sim$1,000 m, and are bounded by, and on the upthrown side of, the Wairarapa fault.

Table 2.1: Damaging earthquakes and their known geomorphic effects for the South Island since European settlement.

Year	Location	Region	Fault	M_w	Geomorphic effects	References
1848	Blenheim	Marlborough	Awatere	7.4-7.5	Landsliding	Grapes et al. (1998)
1855	Wairarapa	Wellington	Wairarapa	8.0-8.2	Landsliding; landslide dams; outburst floods; liquefaction; tsunami; seiche	Grapes and Downes (1997); Downes (2005); Hancox (2005)
1868	Farewell Spit	Tasman	Wakamarama	7.2-7.6	Unknown	Anderson et al. (1994)
1869	Christchurch	Canterbury	Unknown	$\sim$6	Unknown	Pettinga et al. (2001)
1870	Christchurch	Canterbury	Unknown	5.5-6.0	Rockfall	Pettinga et al. (2001)
1881	Castle Hill	Canterbury	Castle Hill?	6.0-6.8	Liquefaction	Pettinga et al. (2001)
1888	Lewis Pass	Canterbury	Hope	7.0-7.3	Unknown	Smith and Berryman (1986); Cowan (1990)
1901	Cheviot	Canterbury	Unknown	6.9	Landsliding; liquefaction	Berril et al. (1994)
1922	Motunau	Canterbury	Unknown	6.4	Landsliding; liquefaction	Pettinga et al. (2001); Bull (2003)
1929	Arthur's Pass	Canterbury	Poulter	7.0-7.1	Landsliding; landslide dams	Berryman and Villamor (2004)
1929	Murchison	West Coast	White Creek	7.3	Landsliding; landslide dams	Dowrick (1994)
1968	Inangahua	West Coast	Inangahua? Lyell?	7.1	Landsliding; landslide dams	Adams (1981); Anderson et al. (1994)
1988	Te Anau	Southland	Puysegur trench	6.7	Landsliding	Reyners et al. (1991)
1993	Secretary Island	Southland	Puysegur trench	6.8	Landsliding; tsunami	Reyners and Webb (2002)
1994	Arthur's Pass	Canterbury	Unknown	6.7	Landsliding; avalanches (snow)	Robinson et al. (1995)
2003	Secretary Island	Southland	Puysegur trench	7.2	Landsliding; tsunami	Power et al. (2005)

Table 2.1 – continued from previous page

Year	Location	Region	Fault	M_w	Geomorphic effects	References
2007	George Sound	Southland	Puysegur trench	6.7	Landsliding	Peterson et al. (2009)
2009	Dusky Sound	Southland	Puysegur trench	7.8	Landsliding	Beavan et al. (2010b)
2010	Darfield	Canterbury	Greendale	7.1	Rockfall; liquefaction	Quigley et al. (2010); Gledhill et al. (2011)
2011	Christchurch	Canterbury	Lyttelton	6.3	Rockfall; liquefaction	Beavan et al. (2011); Holden (2011)

2.3.1 The 1855 Wairarapa earthquake

This earthquake occurred on the Wairarapa fault near Wellington and is thought to have been M_w8.1-8.4, making it the largest recorded earthquake in New Zealand (Grapes and Downes, 1997; Little and Rodgers, 2004). Surface rupture was measured over >140 km with lateral displacements reaching 18.7 m, the largest ever measured anywhere in the world (Little and Rodgers, 2004; Ongley, 1943). It is known to have generated widespread landsliding, affecting an area of at least 52,000 km^2 possibly extending to 135,000 km^2 (Grapes and Downes, 1997; Hancox, 2005). Some of these landslides were noted by Hancox (2005) to be reactivated by a severe rainstorm in 2005, exactly 150 years after the initial earthquake.

The largest reported landslide was $\sim 11 \times 10^6$ m^3 (Hancox, 2005), however at the time of the earthquake much of the affected area was uninhabited and larger landslides may have occurred without being identified. Nevertheless, this landslide blocked the Ruamahanga River forming several landslide dams, one of which subsequently partially failed causing an outburst flood which destroyed a Māori Pā (village) downstream (Grapes, 1988). Some of these lakes still remain intact as of 2014 and therefore pose a continued downstream hazard.

As well as landsliding this event is known to have caused substantial liquefaction, seiches, and tsunami. Liquefaction is reported to have occurred in numerous susceptible locations in the lower North Island and upper South Island (Grapes and Downes, 1997; Hancox, 2005). Seiches, which are the oscillation of confined or semi-confined water bodies, are reported to have occurred at many locations across the entire country, most distantly in Dunedin, >600 km from the epicentre (Downes, 2005). Submarine landsliding in Cook Strait, which separates the North and South Islands, was also recorded and potentially resulted in a 10 m tsunami wave recorded along the southern coast of the North Island, although offshore rupture has also been attributed as the cause (Grapes and Downes, 1997).

2.4 An Alpine fault earthquake

Despite no historically recorded Alpine fault earthquake having occurred, geological evidence of the consequences of previous ruptures has been identified. Combined with observations of historic New Zealand earthquakes, such as the Wairarapa earthquake, as well as other large earthquakes in mountainous environments globally, it is possible to infer the likely magnitude of geomorphic effects resulting from a future Alpine fault earthquake.

2.4.1 Seismic effects

Mainshock

Using a variety of different methods, including fault trenching, tree coring, landscape offset features etc., various authors have concluded that the Alpine fault produces characteristic (i.e. unimodal) earthquakes (see Berryman et al., 2012b; De Pascale and Langridge, 2012; Leitner et al., 2001; Wells and Goff, 2007; Wells et al., 1999). Of the last nine dated ruptures, eight appear to have involved rupture of >380 km of the fault, virtually its entire length from Milford Sound to its junction with the Awatere and Waiau faults (**Fig. 2.3**). Such a rupture length likely corresponds to $\sim$M$_w$8.0 earthquakes, confirmed by measured individual offsets (Adams, 1980b; Berryman et al., 2012a; Cooper and Norris, 1990; De Pascale and Langridge, 2012; De Pascale et al., 2014; Hull and Berryman, 1986; Sutherland et al., 2007; Sutherland and Norris, 1995).

Nevertheless, De Pascale et al. (2014) suggested that the Alpine fault may accommodate bimodal behaviour, with smaller (M6-7) earthquakes occurring between major, full-length, M8 events. They showed direct evidence for partial rupture of the Alpine fault around 1600 CE and indirect evidence of rupture around 1826 CE, either side of the well-defined, full-length rupture in 1717 CE. However, evidence for the event in 1826 is primarily Tasman sea tsunami deposits found in Fiordland and along the west coast. It seems unlikely that a predominately onshore, strike-slip fault would generate a large-scale ocean tsunami and no evidence of Tasman sea tsunami has been identified from other confirmed Alpine fault events. The 1826 earthquake may therefore actually represent a large earthquake on the Puysegur trench offshore of Fiordland, where large earthquakes and tsunamis have occurred historically (**Table 2.1**). Thus, no rupture of the Alpine fault has likely occurred since 1717 (297 years in 2014), which, combined with slip-rate estimates, suggest the next earthquake has the potential to result in displacements of at least 8 m laterally and 3.5 m vertically. This matches measured rupture offsets corresponding to M8 earthquakes and thus, regardless of whether the fault is unimodal or bimodal, it seems most likely that the next Alpine fault earthquake will involve its full length and be $\sim$M$_w$8.

Presently, the Alpine fault is estimated to be locked to a depth of at least 10 km (Beavan et al., 2010a, 1999) suggesting any future earthquake is likely to initiate at a relatively shallow depth, possibly around 8-12 km. Combining this with the above knowledge, the likely extent of MM shaking intensity can be modelled using OpenSHA modelling software. OpenSHA is an open-source Seismic Hazard Analysis (SHA) tool which calculates the probability that an Intensity Measure Type (IMT) will exceed some Intensity Measure Level (IML) (Field et al.,

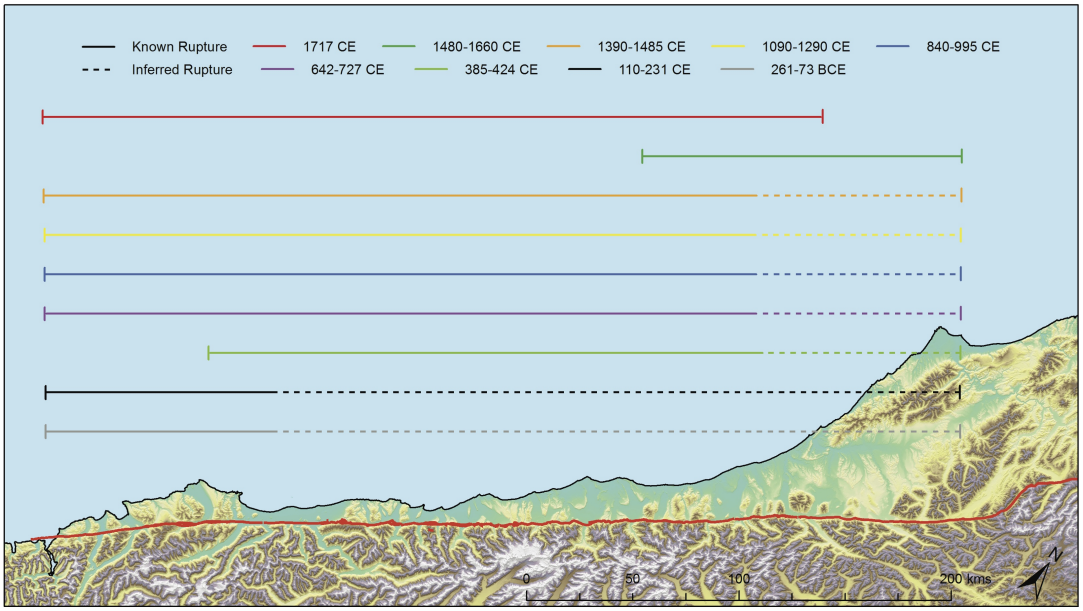

Figure 2.3: Known and inferred rupture lengths of the last nine identified ruptures of the Alpine fault. Dates from Berryman et al. (2012a) and De Pascale et al. (2014).

2003). For example, one can calculate the probability of Peak Ground Acceleration (PGA) exceeding 0.7g or, alternatively, the MM intensity that will occur 50% of the time. Thus it is an excellent tool for modelling potential earthquake scenarios. The results of this modelling for an M_w8.0 Alpine fault earthquake with a randomly assigned epicentre location are shown in **Figure 2.4**, which demonstrates that a maximum intensity of MM 9 is expected in isolated locations along the fault, with MM 7+ expected across most of the western range-front of the Southern Alps. While OpenSHA utilises a crude global shear wave velocity model for estimating shaking intensity attenuation as a result of lithology (Field et al., 2003) it does not account for topographic amplification (see Buech et al., 2010) and therefore higher shaking intensities are possible within the Southern Alps.

The duration of shaking is also an important concept, as mountain slopes exposed to longer periods of intense shaking experience more dynamic fatigue and are therefore more likely to result in failure during the earthquake. Shaking duration is closely related to duration of fault rupture which in turn is dependent on rupture length and rupture speed. Rupture speed during the 1906 M_w7.8 San Francisco earthquake has been estimated to have averaged $\sim$3.2 km/s and peaked at $\sim$3.7 km/s (USGS, 2014) while that of the 2001 M_w7.8 Kunlun earthquake varied between 2.4 km/s and 5 km/s (Bouchon and Vallèe, 2003; Robinson et al., 2006). Both faults accommodate predominantly lateral motion, with rupture lengths in excess of 350 km and maximum displacements of $>$7 m, as well as being similar magnitudes to an

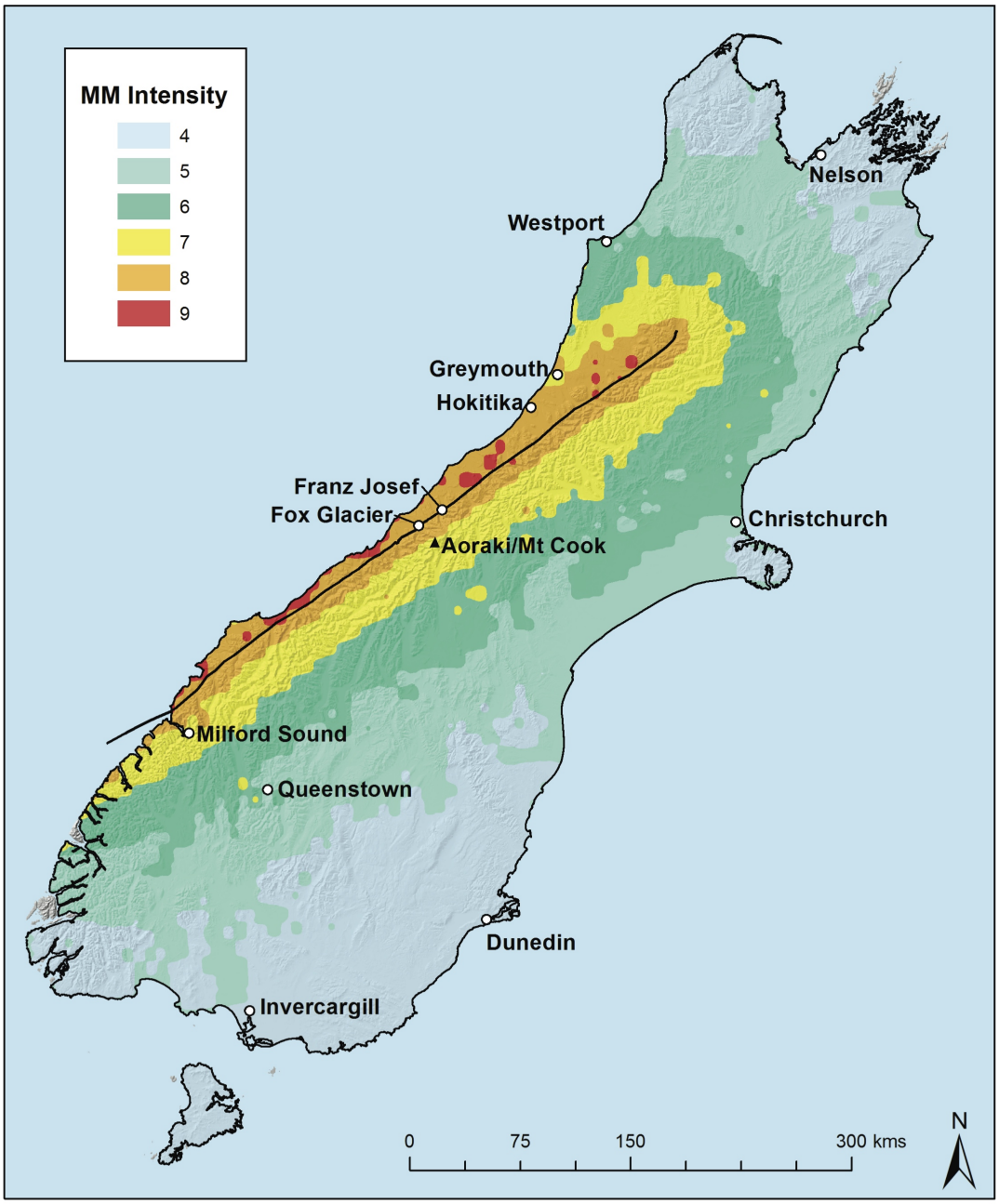

Figure 2.4: Modelled isoseismals for a M_w8.0 earthquake involving full-length rupture of the Alpine fault (black line).

expected Alpine fault earthquake. Bi-directional rupture of the Alpine fault initiating from a central epicentre would include rupture length of ∼200 km in either direction while uni-directional rupture from one end would have a full ∼400 km of rupture. Thus, assuming similar rupture speeds, shaking could last between ∼40 seconds (200 km at 5 km/s) and 160 seconds (400 km at 2.5 km/s), and will most likely last at least a minute or more close to the fault. This agrees with much of the published work on the duration of strong ground motion from various different earthquake magnitudes (see Bommer and Martínez-Pereira, 1999). As distance from the fault rupture increases so will the duration of shaking as the seismic waves spread out, however intensity will also decrease due to attenuation. Thus, regions west of the Southern Alps main divide can expect to experience strong (MM 7+) shaking for possibly up to a minute while locations east of the mountains will experience less severe shaking (<MM 6) lasting for possibly several minutes.

Aftershocks

All aftershock sequences are unique, but it is possible to make general statements about the expected maximum magnitude aftershock and its possible timing, as well as estimating general aftershock decay patterns. For instance, Utsu (1970) showed that the difference, D between the mainshock magnitude, M_m and the maximum aftershock magnitude, M_a could be roughly determined by

$$D \approx 5.0 - 0.5M_m \qquad (\text{for } M_m > 6.0) \tag{2.1}$$

Thus M_a for an Alpine fault earthquake is expected to be $\sim$ 7.0 which agrees with Hainzl et al. (2000) who showed that typically the largest aftershock is one magnitude smaller than the mainshock. The average time, $\overline{T}$, between M_m and M_a in days was empirically shown by Utsu (1970) to be

$$log\overline{T} \approx 0.5M_m - 3.5 \tag{2.2}$$

suggesting on average M_a will occur $\sim$ 3 days after the initial mainshock. However, Utsu (1970) noted that there was a large degree of scatter between $\overline{T}$ and M_m, such that the former varied between $0.01\overline{T}$ and $100\overline{T}$. Thus, M_a could feasibly occur anytime between 40 mins and 1 year after the initial mainshock.

A more appropriate method for analysing aftershock sequences is the modified Ohmori formula which effectively measures the decay of an aftershock sequence over time (Utsu et al., 1995) such that

$$n(t) = k(t+c)^{-p} \tag{2.3}$$

where $n(t)$ is the number of aftershocks above a given magnitude per time, t, and k, c, and p are constants to be calculated, with c and p dependent on the aftershock magnitude being considered. Following the 1993 M_w7.8 Nansei-Oki earthquake, Utsu et al. (1995) showed that 100 days after the mainshock, aftershocks $> M_w$4.0 were still occurring at a rate of one every 10 days, while those $> M_w$3.2 (considered the smallest 'noticeable' magnitude) were still occurring at a rate of almost three per day. Following the 2010 M_w7.1 Darfield earthquake in central Canterbury, three major ($> M_w$6.0) aftershocks occurred five, nine, and 15 months after the initial mainshock (Bannister and Gledhill, 2012). These were each preceded by a decrease in aftershock rates and, unsurprisingly, immediately followed by a large increase in aftershock rates. Furthermore, the spatial distribution of aftershocks was unusual, in that aftershock locations did not cluster around the mainshock-generating Greendale fault, instead gradually moving eastwards, first beneath the city of Christchurch and then offshore (**Fig. 2.5**; Bannister and Gledhill 2012).

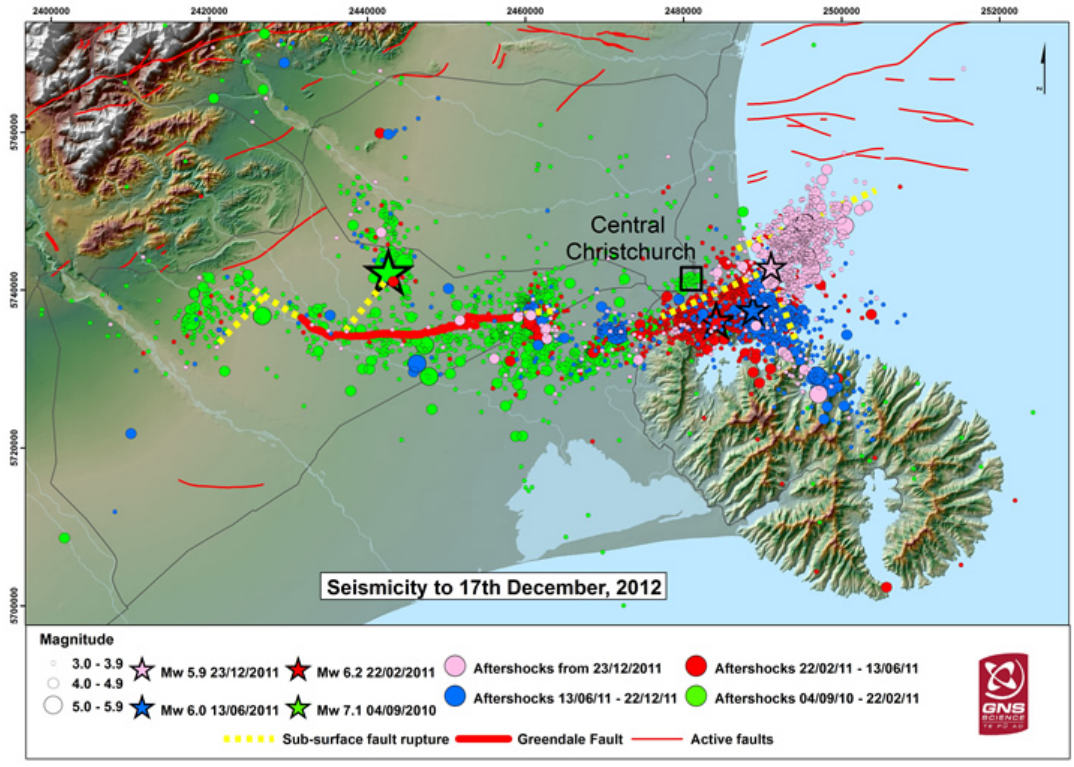

Figure 2.5: Location of all earthquakes during the Canterbury earthquake sequence from 4 September 2010 to 17 December 2012. From GNS.

Thus, there is much difficulty in estimating an aftershock sequence following an Alpine fault earthquake; however it will most likely involve several aftershocks $> M_w$6 and possi-

bly up to M_w7, with the largest most likely occurring sometime within the first year. The whole sequence will last for several years and will most probably focus around the epicentre and along the length of the Alpine fault and other proximal faults, although the Canterbury sequence demonstrates the possibility of aftershocks affecting a much larger area. Further, (Toda et al., 2008) demonstrated that following the 2008 M_w8.0 Wenchuan earthquake, the probability of earthquakes on active faults >400 km away from the mainshock fault more than doubled. Thus it is prudent to anticipate aftershocks of all sizes on other active South Island faults (see **Fig. 2.1**).

2.4.2 Geomorphic effects

The resulting geomorphic effects of earthquakes are intricately linked in a cascading sequence of effects over various timescales (see Hewitt et al., 2008). From available data on historic earthquakes in mountains it is possible to derive the interlinkages between these various cascading effects and delimit broad timings for their occurrence and duration (**Fig. 2.6**). Below is a detailed discussion of each effect including evidence for previous occurrences during Alpine fault earthquakes if present.

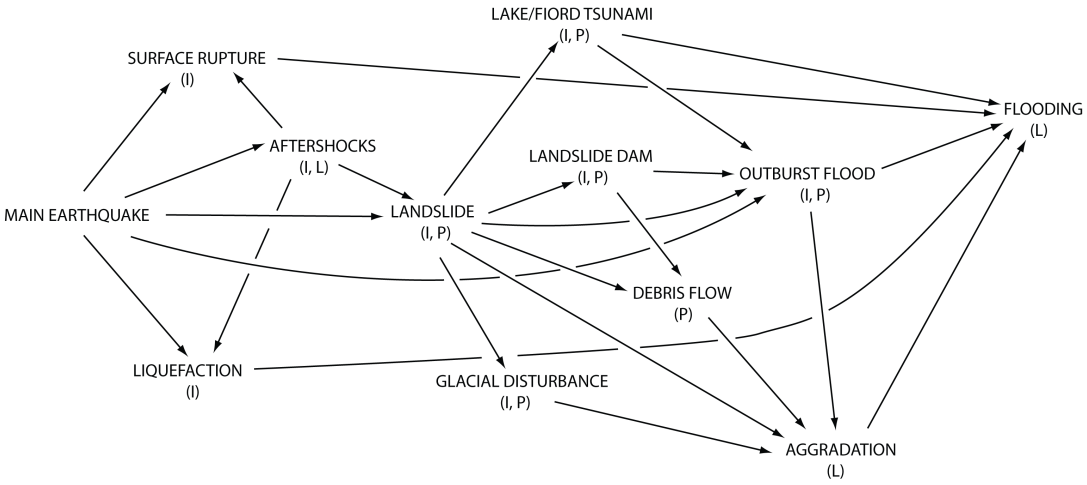

Figure 2.6: Flow chart of geomorphic consequences resulting from earthquakes in mountainous terrain. I - immediate: lasting for or occurring within one week of the mainshock; P - prolonged: lasting or occurring within one year of the mainshock; L - long-term: lasting or occurring for more than one year after the mainshock.

Landslides

Landslides are always a major hazard in the Southern Alps due to the steep, heavily eroded topography, high annual rainfall, and high seismicity on numerous active faults. Globally, the majority of rapid, large ($> 10^6$ m^3, also referred to as rock avalanches), deep-seated landslides result from high-intensity shaking, and a large number of these have been identified throughout the Southern Alps and Fiordland (**Fig. 2.7**). Several of these are very large ($> 10^8$ m^3) including Green Lake (27 km^3), John O'Groats (1 km^3), Adelaide (0.75 km^3), and Cascade (0.75 km^3) all of which are thought to have resulted from Alpine fault earthquakes (Barth, 2014; Hancox and Perrin, 2009). The Green Lake rock avalanche, one of the largest globally, is thought to have required MM 9-10 shaking intensity to initiate failure (Hancox and Perrin, 2009); yet at >100 km distance from the Alpine fault (**Fig. 2.7**) it seems unlikely any earthquake on the Alpine fault could generate such strong shaking at such a large distance (see **Fig. 2.4**). It seems much more likely that the Green Lake rock avalanche initiated from a large earthquake on the nearby Hauroko fault (Hall et al., 2014). Thus, the largest identified landslide likely to have formed from an Alpine fault earthquake is the 1 km^3 John O'Groats landslide, which demonstrates the large size of individual landslides possible in the Southern Alps.

Maximum run-out distances for landslides have been related to total fall height by Hsü (1975) who showed that:

$$L = \frac{H}{tan\alpha} \tag{2.4}$$

where H is total fall height in metres, L is runout distance in metres, and $tan\alpha$ is the apparent coefficient of friction. The coefficient of friction for rock-on-rock is approximately 0.6 (Byerlee, 1978), and fall heights in the Southern Alps are likely to be at least several hundred metres suggesting runout distances of up to 1 km are possible. Nevertheless, Davies (1982) showed that for large volume events, a process of mechanical fluidisation occurred within the moving rock debris which substantially increased runout distance. He showed that

$$L_d \sim 10(V)^{\frac{1}{3}} \tag{2.5}$$

where V is the landslide volume and L_d is deposit length. Thus for a 1 km^3 rock avalanche a deposit length of 10 km is possible. Numerous other factors have also been identified as influencing runout distance including runout over glacial ice (Eisbacher, 1979; Evans and Clague, 1988; McSaveney, 1978) and valley morphology (Nicoletti and Sorriso-Valvo, 1991). Furthermore, an earthquake-generated landslide in Kyrgyzstan, central Asia, has recently been identified with a runout length of ~28 km from an initial failure volume of just 4 km^3 as a result of a high water content and large-scale entrainment during runout (see Appendix

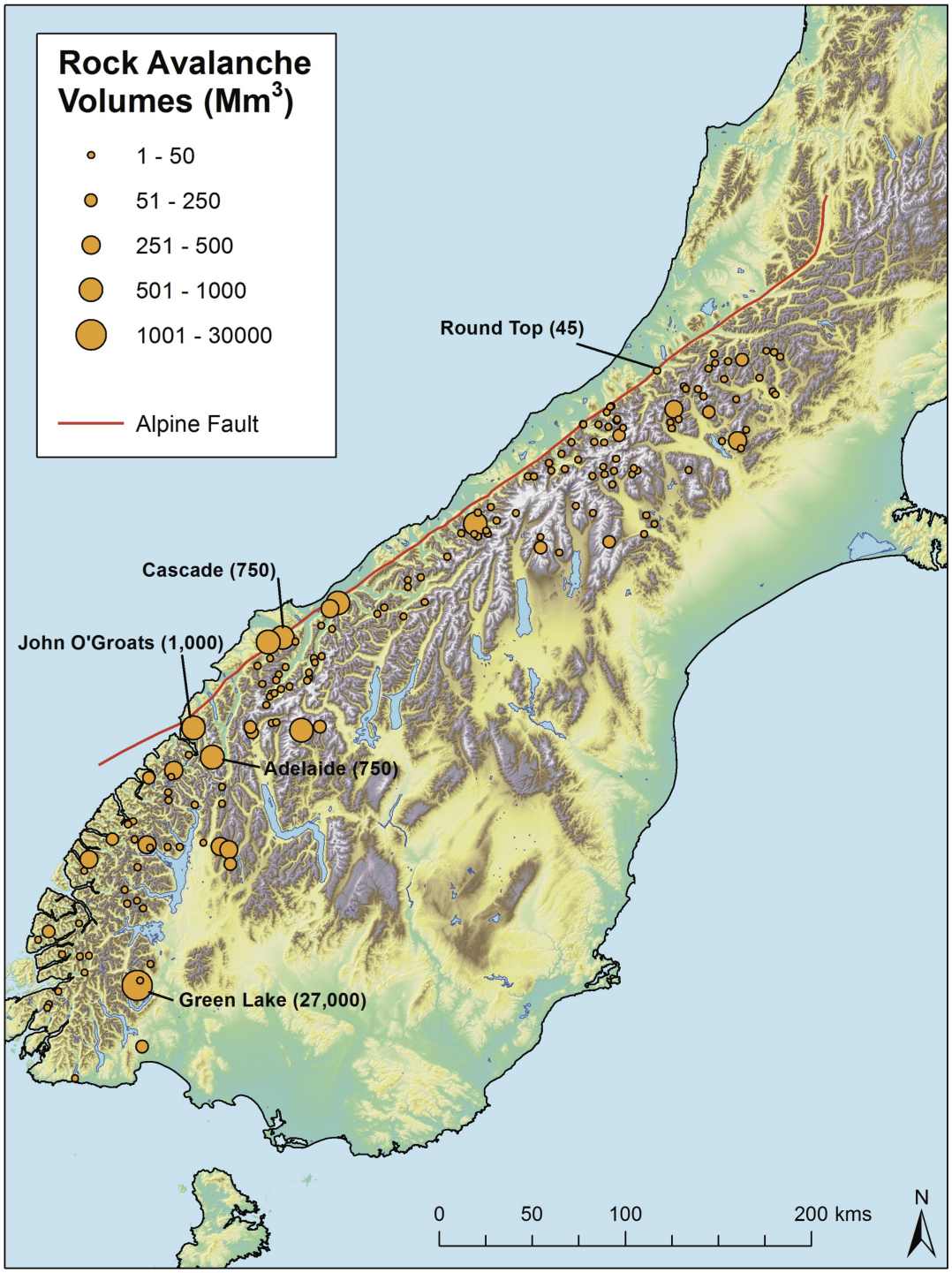

Figure 2.7: Landslide deposits larger than 1 million cubic metres throughout the Southern Alps and Fiordland. The proximity to the Alpine fault has led many authors to assume an Alpine fault earthquake origin for the majority of these deposits

A). The longest-runout landslide deposit identified in the Southern Alps is the $\sim 45 \times 10^6$ m^3 Round Top landslide which ran out for a total of 4 km (Dufresne et al., 2009; Wright, 1998). This landslide has been dated to c. 930 CE around the same time as a major Alpine fault earthquake, although other dates have been reported suggesting it may represent multiple events (Dufresne et al., 2009). The potential for large volume, long runout landslides in the event of an Alpine fault earthquake is therefore evident, especially along the western range-front where there are very few obstacles (such as steep valley walls) to hinder runout. Despite the substantial evidence for major, individual landslides from Alpine fault earthquakes, the total scale of coseismic landsliding is still poorly-known.

Keefer (1984) and Malamud et al. (2004) attempted to relate earthquake magnitude to total scale of landsliding using numerous historical earthquakes. Using data from Keefer (1984) along with data from the 1994 Northridge earthquake, Malamud et al. (2004) showed that

$$logN_{LT} = 1.27M_w - 5.45(\pm 0.46) \tag{2.6}$$

where N_{LT} is the total number of landslides generated and M_w is the moment magnitude of the earthquake. Despite achieving a good statistical fit, this formula does not consider the topography that the earthquake occurs in (i.e. flat plains vs. mountains) and thus there is a wide degree of variation. For instance, the M_w6.9 Kobe earthquake in Japan affected a primarily flat, urban environment and thus generated just 700 landslides, while the M_w6.7 Northridge earthquake in California affected a largely mountainous area and thus caused $>$11,000 landslides. Malamud et al. (2004) were also able to relate M_w to total landslide area (sum of all individual landslide areas, not affected area), A_{LT} (km^2), total landslide volume, V_{LT} (km^3), largest landslide area, A_{Lmax} (km^2), and largest landslide volume, V_{Lmax} (km^3) by

$$logA_{LT} = 1.27M_w - 7.96(\pm 0.46) \tag{2.7}$$

$$logV_{LT} = 1.42M_w - 11.26(\pm 0.52) \tag{2.8}$$

$$logA_{Lmax} = 0.91M_w - 6.85(\pm 0.33) \tag{2.9}$$

$$logV_{Lmax} = 1.36M_w - 11.58(\pm 0.49) \tag{2.10}$$

while Keefer and Wilson (1989) were able to show that the affected area (area within which all landslides are encapsulated), A (km^2) could also be estimated from earthquake magnitude by

$$logA = M_w - 3.46(\pm 0.47) \qquad (5.5 < M_w \leq 9.2) \tag{2.11}$$

Again however, despite achieving a good statistical fit there is a wide degree of variability in the observed data. For instance, the M_w7.6 Buller earthquake in New Zealand generated

Table 2.2: Landslide variables for a future M_w8.0 Alpine fault earthquake as calculated from the equations of Keefer and Wilson (1989) and Malamud et al. (2004).

Variable	Mean Value	Range
Total number	51,286	17,782 - 147,910
Affected area (km^2)	34,673	11,749 - 102,329
Total landslide area (km^2)	158	55 - 457
Largest landslide area (km^2)	2.7	1.3 - 5.8
Total landslide volume (km^3)	1.3	0.4 - 4.2
Largest landslide volume (km^3)	0.2	0.07 - 0.6

1.3 km^3 of landslide debris while the larger M_w7.9 Torricelli Mountains earthquake in Papua New Guinea generated just 0.2 km^3. Furthermore, these equations are unable to anticipate extreme events. For instance, according to equation 2.10 the Green Lake rock avalanche required a M_w9.5 earthquake, an event for which there is no evidence on any faults around the southern South Island. The Daguangbao landslide, the largest formed during the 2008 M_w8.0 Wenchuan earthquake, had an area of $\sim$7.8 km^2, almost 2 km^2 larger than suggested by equation 2.9. These formulae are therefore useful to gauge an order of magnitude of landsliding likely from a given earthquake but not for a detailed hazard assessment.

Applied to a M_w8.0 Alpine fault event (**Table 2.2**) this suggests that between $\sim$20,000 and 150,000 landslides could occur, affecting an area between $\sim$12,000 and 100,000 km^2. However, the largest landslide expected is between 0.07 and 0.6 km^3, smaller than the John O'Groats, Adelaide, and Cascade landslides which are all inferred to have resulted from Alpine fault earthquakes. Furthermore, the total expected landslide volume has a mean value similar to the size of each of these landslides with a maximum range only four times larger. Given the volume of the largest known events, and the number of landslides expected (**Table 2.2**), this value may be substantially underestimated. Nevertheless, this shows that landsliding from an Alpine fault earthquake is likely to affect a very large area with a substantial number of landslides, some of which are likely to be large volume. Howarth et al. (2012) appear to have confirmed this by showing that in some instances during the $\sim$50 years immediately post-earthquake, as much sediment is deposited in Lake Paringa on the west coast as during the entire intervening period before the next earthquake. This suggests that Alpine fault earthquakes provide a substantial contribution to the overall erosion of the Southern Alps (Davies and Korup, 2007).

Landslide Dams

Landslides falling into river valleys often form landslide dams and landslide-dammed lakes. These have a number of associated up- and downstream hazards, the most significant of which is a catastrophic collapse of the dam resulting in an outburst flood. At least 232 landslide dams have been recorded in New Zealand since c. 1846 including 140 with currently intact lakes (Korup, 2004b, 2005a). Statistically, New Zealand has some of the largest landslide dams in the world in terms of dam volume and lake volume (Korup, 2004b). In the Southern Alps the majority are situated between 400 m asl and 1,000 m asl although in Fiordland most appear to form at, or close to, sea-level. Of all New Zealand landslide dams, most (88%) have very small contributing catchment areas, often $<$100 km^2; of those with catchment areas $<$10 km^2, 79% have yet to fail while a further 5% have had lakes infilled without failure (Korup, 2004b). In fact, only 37% of all landslide dams in New Zealand appear to have failed, far below the global average; however this is likely to be a result of under-reporting due to the short historical records and relatively unpopulated mountainous terrain.

Costa and Schuster (1988) showed that globally 27% of landslide dams failed within a day of formation, and $\sim$50% failed within the first 10 days; only 15% survived for longer than one year. Korup (2004b) showed similar results, but highlighted that there was a large degree of variation between failure times, ranging from several minutes after formation up to $>$15 years. Some landslide dams appear to become permanent landscape features, such as Lake Waikaremoana in the North Island of New Zealand which has survived for two millennia (Read et al., 1992). Nevertheless, their stability is purely a statistical concept (Nash et al., 2008) and all landslide dams which form from an Alpine fault earthquake should be considered able to fail, with failure most likely within a few days of the event.

Costa and Schuster (1988) demonstrated six different types of landslide dams, of which most require steep-sided, narrow valleys to form although this is not always the case. In the central Southern Alps, up to 22 sites have been identified where the risk of large landslides falling into a river gorge was high (Arshad et al., 2004). A more regional study found that 15 west-draining rivers along the entire Southern Alps had the potential for landslide dam following an Alpine fault earthquake (**Fig. 2.8**; McCahon et al. 2006a,b,c) several of which are known to have been blocked by both historic and pre-historic earthquakes in the region (Adams, 1981). Very little work has been undertaken as to the potential of east-draining rivers to form landslide dams in an Alpine fault earthquake; however these rivers have very different morphology to west-draining rivers with far larger catchment areas and wider tributary valleys and thus may have a smaller potential for damming. Nevertheless, the major Waimakariri River which flows just north of the city of Christchurch has previously been

identified as a potential source of landslide dam with at least eight active landslides identified in the Waimakariri Gorge (Yetton and McMorran, 2004). Thus, there is the potential for several, primarily west-draining rivers to become blocked following an Alpine fault event with Davies et al. (2005) estimating somewhere between three and 30. Given the number of landslides expected (**Table 2.2**) this seems reasonable, however following the Wenchuan earthquake, >250 landslide dams formed (Xu et al., 2009) across a landslide affected area >100,000 km^2 with an estimated ∼60,000 landslides (Gorum et al., 2011; Li et al., 2014; Parker et al., 2011). It is possible therefore for several hundred landslide dams to form, possibly with multiple dams on a single river.

Outburst Floods

Outburst floods or dam-break floods are the most obvious hazard resulting from landslide dams. They occur as the result of complete or partial dam failure releasing the impounded water to cause major, rapid-onset downstream flooding, and occasionally debris flows as the dam material mixes with the water. Following the initial flood wave sediment stored in the dam and the dammed lake is progressively deposited downstream on the active alluvial fan often resulting in widespread aggradation. Landslide dams can fail from a number of different processes as shown by Costa and Schuster (1988) including overtopping, piping, and slope failure. Overtopping is by far the most common and occurs when the impounded lake level exceeds the dam height, resulting in water spilling over and eroding the dam crest creating a positive feedback loop which typically results in catastrophic failure. Since landslide dams do not undergo compaction as with engineered dams, they are often porous allowing internal erosion (piping) to occur, causing failure. While this is rare, at least three historic cases are known (see Costa and Schuster, 1988). Occasionally the landslide dam itself will be unstable after formation and can experience secondary slope failure resulting in outburst. Another potential source of failure is further landsliding, either impacting the dam itself, or into the impounded lake causing an overtopping wave. This is of particular concern following a large earthquake as subsequent aftershocks will continue to shake the region for some time after the mainshock (see above) increasing the likelihood of further landsliding. Any older dams existing at the time of the mainshock are also at risk (see **Fig. 2.6**).

The best-studied example of a landslide outburst flood in New Zealand is that from the 1999 Mt Adams rock avalanche, which blocked the Poerua River. The initial landslide had a volume of 10-15 $\times 10^6$ m^3 and blocked the river to a depth of ∼120 m, forming a lake with an estimated volume of 5-7 $\times 10^6$ m^3 (Becker et al., 2007; Hancox et al., 2005). It took 48 hours for the lake to completely fill and overtop the dam, however it did not fail until heavy

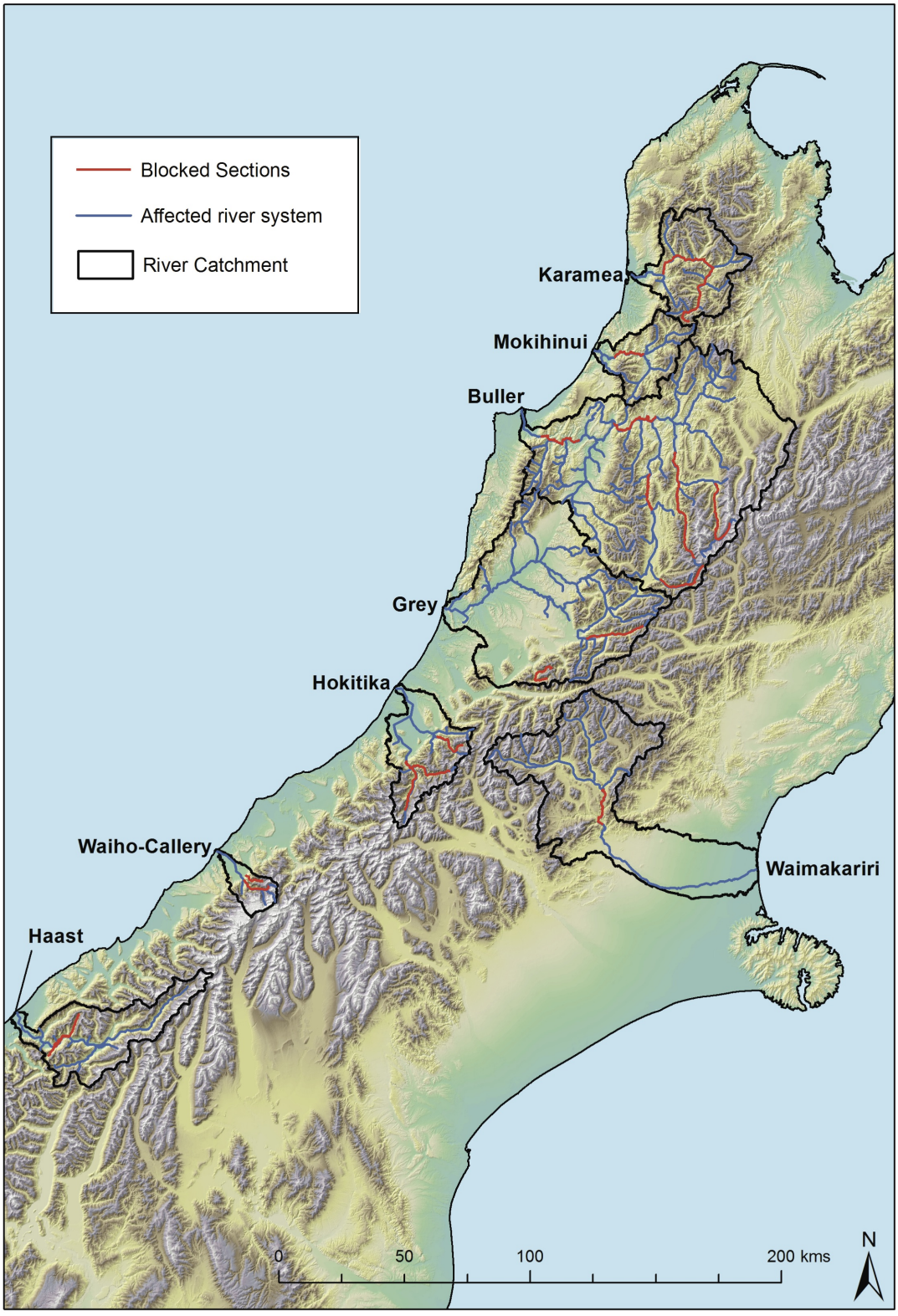

Figure 2.8: Major South Island river catchments with identified landslide dam potential from an Alpine fault earthquake.

rainfall five days after formation (Hancox et al., 2005). The dam failure was catastrophic with ∼75% of the lake being rapidly drained resulting in a peak flow of ∼3000 cumecs (cubic metres per second) (Davies, 2002; Davies et al., 2007; Hancox et al., 2005). In the gorge immediately downstream of the dam, the flood peak is inferred to have reached ∼5 m in height, travelling at up to 5 m/s while in the Poerua valley flood heights peaked at 2 m (Davies, 2002). Fortunately, the downstream valley was only very sparsely populated, and nobody was injured, however the farmland immediately below the gorge was substantially affected in both the short- and long-term (see below). Had the event occurred in a river with a large downstream population, the results could have been catastrophic. Following the Wenchuan earthquake, the Tangjiashan landslide dam, which was the largest of the >250 that formed, posed an immediate threat of outburst flood to >1.2 million people living downstream, some as far as 30 km away (Peng and Zhang, 2012; Xu et al., 2009). This dam posed such a high risk that the Chinese government elected to artificially control breach the dam using a spillway (Xu et al., 2009). The low population of the South Island, and particularly the West Coast region, mean landslide dams will likely pose a threat to several hundred people at most; however this will still require a rapid response from authorities in order to mitigate the hazard before dam failure occurs.

Aggradation

Aggradation is the process of rivers building up their alluvial fan(s) when sediment is deposited from upstream. Under normal circumstances this can be a very gradual process, however following massive sediment inputs into river catchments (e.g. following a large earthquake) it can be relatively rapid and devastating. Davies and Korup (2007) investigated a number of alluvial fans on the west coast in the central Southern Alps and identified buried soils and massive gravel deposits at depths of several metres on all the studied fans. Furthermore, they found that these deposits appeared to be contemporaneous, dating to between 1616 and 1682 CE, matching results found by Berryman et al. (2001) on the Whataroa fan north of Davies and Korup (2007)'s study area. It was inferred that at some time in the 1600s a massive landsliding event had occurred in the Southern Alps which had subsequently resulted in large-scale aggradation on many, if not all, alluvial fans on the west coast. The most likely cause of this landsliding was a large earthquake, corresponding with other external evidence of a possible Alpine fault earthquake in the early 1600s (see De Pascale et al., 2014).

No such evidence was found on any of these fans dating to post-1717 CE, the date of the last Alpine fault earthquake. This suggests that either very little landsliding occurred in the mountains or the evidence for it has not been identified. The former may be explained

by the short time interval between the ∼1600 and 1717 events (<100 years) not providing enough time for the slopes to re-stabilise in order to sustain massive landsliding. However, Howarth et al. (2012, 2014) showed that following the 1717 earthquake, thick hyperpycnal deposits formed in Lake Paringa and Lake Mapourika over a period ∼50 years suggesting that large sediment inputs had occurred within the mountains. Thus it seems most likely that evidence of such landsliding has not been identified, perhaps because the short time between the last two events did not allow soil to develop on the re-surfaced alluvial fans, allowing the later aggradation deposits to be deposited contiguously on top of the early deposits. Delineating the boundary between these deposits would be particularly difficult. The Lake Paringa evidence suggests alluvial fans may have had <50 years to develop soils before the 1717 earthquake, which may be insufficient for soils to develop. Alternatively, had soils developed they could have been removed by erosive flow prior to deposition of landslide debris.

Following the 1999 Poerua outburst flood, it is estimated that ∼1-1.5 $\times 10^6$ m^3 of sediment was deposited along a 5 km stretch of the Poerua alluvial fan in just six years (Davies et al., 2005). By 2001 aggradation had caused the flow of the river to shift ∼800 m to the east, actively eroding a channel across farmland and a tributary rivers alluvial fan (**Fig. 2.9**). By 2003, alluvium deposited in the river channel had raised that tributary 25 m above its 1992 level (Hancox et al., 2005). This resulted in widespread gravel deposition through rainforest-covered terraces, destroying much of the vegetation. Aggradation of >10 m elevated the main river bed so that the river flowed across the fan surface into which it was previously incised, resulting in severe damage (Davies et al., 2005; Hancox et al., 2005). The aggradation is thought to have reached its peak ∼10 years after the initial outburst flood. In total the event is estimated to have added the equivalent of 500 years of normal supply of sediment to the fanhead (Davies et al., 2005) with sediment delivery only beginning to return to normal in 2014.

Following a large sediment input, most of the sediment carried by rivers will be transported offshore as suspended load. The aggradation will therefore primarily result from the sediment carried as bedload, although suspended load may be deposited as overbank deposits for which there is evidence in the Whataroa Gorge >15 km from the range-front (Davies and Korup, 2007). The proportion of bedload to total sediment load is estimated to be between 10% (Griffiths, 1979) and 50% (Davies and McSaveney, 2006) suggesting between 0.04 km^3 and 2.1 km^3 (see **Table 2.2**) could be deposited across all active South Island alluvial fans. The total area of active fans in the South Island (calculated from QMap; see Rattenbury and Isaac 2012) is ∼13,351 km^2 suggesting an average depth of between 3 mm and 16 cm. However, sediment will not be evenly distributed across the whole fan, with most being deposited

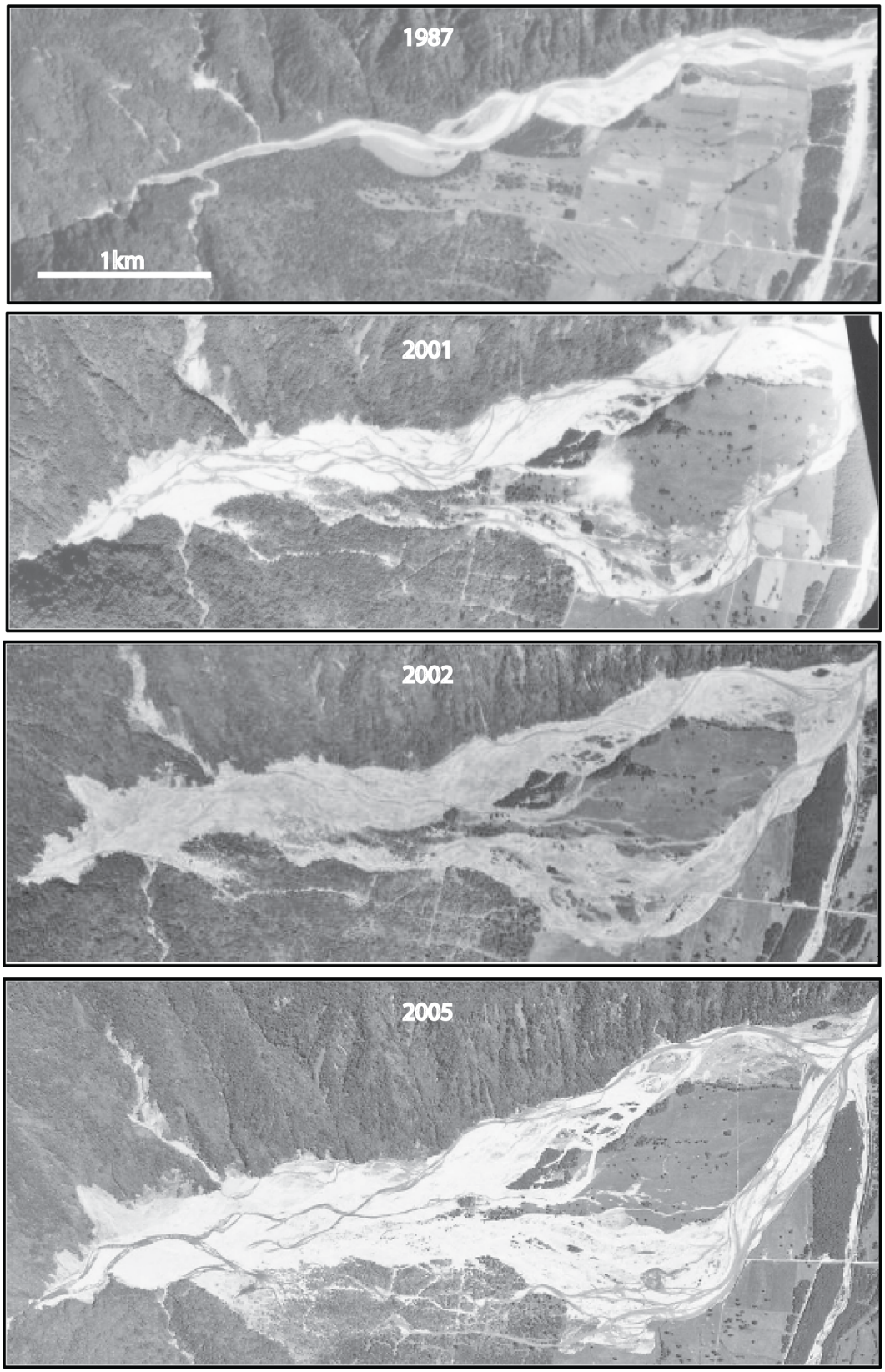

Figure 2.9: Aerial photos of the Poerua River from 1987 to 2005 showing the change in channel flow and active aggradation across the alluvial fan. After Davies et al. (2005).

in the sections proximal to the range-front, suggesting substantially greater average depths will occur. Furthermore, not all alluvial fans in the South Island will sustain aggradation because not all catchments will have upstream landslides. Landsliding is expected to be focussed primarily on the western range-front of the central Southern Alps meaning aggradation will likely be most prevalent on west coast fans. These fans cover an area of just $\sim$2,200 km^2 suggesting average aggradation depths (if material is deposited evenly across the entire fan) could reach up to 1 m, with local depths being much greater in places.

Debris Flows

Debris flows occur when sufficient available loose sediment is (re)mobilised by heavy or long-duration rainfall. Catchments which are particularly small and steep are especially susceptible (Welsh and Davies, 2011). In the central Southern Alps, at least 77 catchments have been identified has having potential for debris flows to form (O. Korup, University of Potsdam, pers. comm., 2011). Many west-draining catchments are small and steep and thus the potential for debris flows across much of the West Coast is high.

More than two years after the 2008 Wenchuan earthquake, long-duration rainfall resulted in a series of debris flows forming in the vicinity of Qingping town and Yingxiu city (Tang et al., 2011; Xu et al., 2012). In Qingping, 95 mm of rain fell over a 12 hour period with reports suggesting larger amounts fell in the mountains. As a result, debris flows formed simultaneously in 11 different river catchments, burying Qingping town, killing 14, and destroying $>$370 buildings (Xu et al., 2012). In Yingxiu 162 mm fell over a 33 hour period resulting in 21 separate debris flows which combined and became a hyperconcentrated flow, blocking the Minjiang River which subsequently flooded Yingxiu city (Tang et al., 2011). In both instances, the amount of rain that fell was not unusual for the region; however the duration was. Rainfall along the western Southern Alps is especially high, with rainfall intensities often exceeding 50 mm/hr and storms lasting for several days at a time. Given widespread landsliding following a major earthquake, debris flows should therefore be anticipated in many of the short, steep catchments during subsequent rainstorms.

From available data on the Qingping events (see Xu et al., 2012), approximately 20% of the initial landslide volume was remobilised in the debris flows. This suggests that between 0.08 km^3 and 0.8 km^3 (see **Table 2.2**) of sediment could be mobilised in debris flows following an Alpine fault earthquake. The Qingping events did not occur until $>$2 years after the initial earthquake, meaning rivers had time to rework and remove some of the original landslide deposit. However, on the South Island west coast, long-duration heavy rainstorms can occur several times per year. Thus the time between the earthquake and the next long-

duration rainstorm is likely to be very much less than two years. Rivers will therefore have very little time to rework and remove landslide debris meaning any resulting debris flows could potentially involve a larger percentage of the initial debris volume. Consequently, a very large number of debris flows could occur with many containing very large volumes.

Tsunami

As the 2004 Sumatran and 2011 Japanese disasters vividly demonstrated, large near-field tsunami can be catastrophic, resulting in tens-to-hundreds of thousands of deaths and widespread devastating damage. Tsunami most typically result from large, offshore subduction earthquakes which vertically displace the seabed, although both large submarine and subaerial landslides can also cause tsunami. Despite the Alpine fault being neither an offshore, or (primarily) reverse fault, instances of tsunami in the Tasman Sea have been identified and related to Alpine fault events. De Pascale et al. (2014) identified several tsunami deposits along the west coast and in Fiordland which all dated to $\sim$1826. Fault trenching did not identify rupture of the Alpine fault at this date, despite identifying ruptures in 1717 and $\sim$1600 CE. Furthermore, all other off-fault evidence was concentrated in the southernmost region of the Southern Alps and Fiordland. It therefore seems unlikely that the $\sim$1826 event was an Alpine fault earthquake; more likely it was an earthquake on the Puysegur trench for which tsunami are expected and have been witnessed historically. Nonetheless, Nichol et al. (2007) used trenching and coring techniques to identify tsunami deposits at Okarito Lagoon on the central west coast which they dated to the mid 1400s, matching a known rupture of the Alpine fault. However, Okarito Lagoon is comprised of very fine silty and sandy sediments which are especially susceptible to liquefaction (see below) during strong ground shaking. Thus, this tsunami deposit may be a local anomaly resulting from subsidence of the lagoon allowing the sea to move inland, mimicking a tsunami. There is therefore no conclusive evidence for large-scale, widespread ocean tsunami following Alpine fault earthquakes and thus it seems unlikely that one will occur with the next earthquake.

Regardless, the South Island, and especially the alpine region, has numerous large lakes and fiords surrounded by steep mountain slopes and is therefore susceptible to landslide-generated tsunami. Most of Fiordland's fiords are remote and unpopulated, however Milford Sound is relatively accessible by a main highway and is a popular tourist destination, attracting on average $>$1,000 visitors per day (Dykstra, 2012). The Alpine fault runs offshore at the mouth of Milford Sound, and thus the entire fiord is within 15 km of the fault. Analysis of swath bathymetry identified as many as 20 large ($> 10^7$ m^3) landslide deposits on the bed of Milford Sound, post-dating deglaciation of the fiord $\sim$16,000 yrs BP (Dykstra, 2012). Each

of these deposits are large enough to have generated a tsunami of several metres, and it was concluded there was a 25% chance of such a landslide occurring in the fiord in any given Alpine fault earthquake. Thus there is a substantial threat of landslide tsunami at Milford Sound in the next Alpine fault earthquake.

Globally, the best-known example of landslide-generated tsunami occurred at Lituya Bay, Alaska, following a M_w8.3 earthquake on the nearby Fairweather fault in 1958. This earthquake caused a landslide of $\sim 30 \times 10^6$ m^3 to fall into the bay generating a mega-tsunami with a maximum measured run-up of 524 m asl (**Fig. 2.10**); the largest ever recorded (Fritz et al., 2009; Miller, 1960; Tocher, 1960). In total this wave destroyed >10 km^2 of shoreline forest and sank two boats, killing two people onboard. While this is an extreme example, the possibility of a similar tsunami in one of the South Island's lakes cannot be discounted. Of particular concern are Lakes Wakatipu and Wanaka which have the major tourist townships of Queenstown and Wanaka immediately on their shoreline. These events are incredibly rapid, with the Lituya Bay wave estimated to have reached speeds of 150-200 km/hr. At such speeds, there will be little time to evacuate any exposed people with the wave potentially making landfall while shaking from the earthquake is still occurring.

Liquefaction

Liquefaction affects saturated, loose, sandy/silty soils which settle and compress under intense shaking causing fluids and silts within the soil to rise towards the surface. Hancox et al. (1997) found that throughout New Zealand the intensity threshold for liquefaction was MM 7 while lateral spreading requires MM 8; however it is possible for each to occur at one intensity lower for particularly susceptible material. During the 2011 Tohoku earthquake liquefaction occurred in Tokyo >400 km from the epicentre and is believed to have resulted from long-duration, low frequency, MM 6 shaking (Bhattacharya et al., 2011). Thus, any susceptible area within the South Island must be considered to have the potential to experience liquefaction during an Alpine fault earthquake.

During the Canterbury earthquake sequence, Christchurch experienced multiple liquefaction events following each $> M_w$6.0 earthquake, with some areas experiencing >1 m of total subsidence (Cubrinovski et al., 2011b). This was particularly devastating to the built environment and resulted in large swathes of the city's eastern suburbs being designated as no longer suitable for residential purposes. Subsequently, several recent heavy rainstorms in the city have resulted in widespread flooding throughout subsided areas, further exacerbating the effects of the earthquake sequence. Similarly, historic liquefaction has been recorded in multiple susceptible locations throughout Canterbury following major earthquakes (**Table 2.1**).

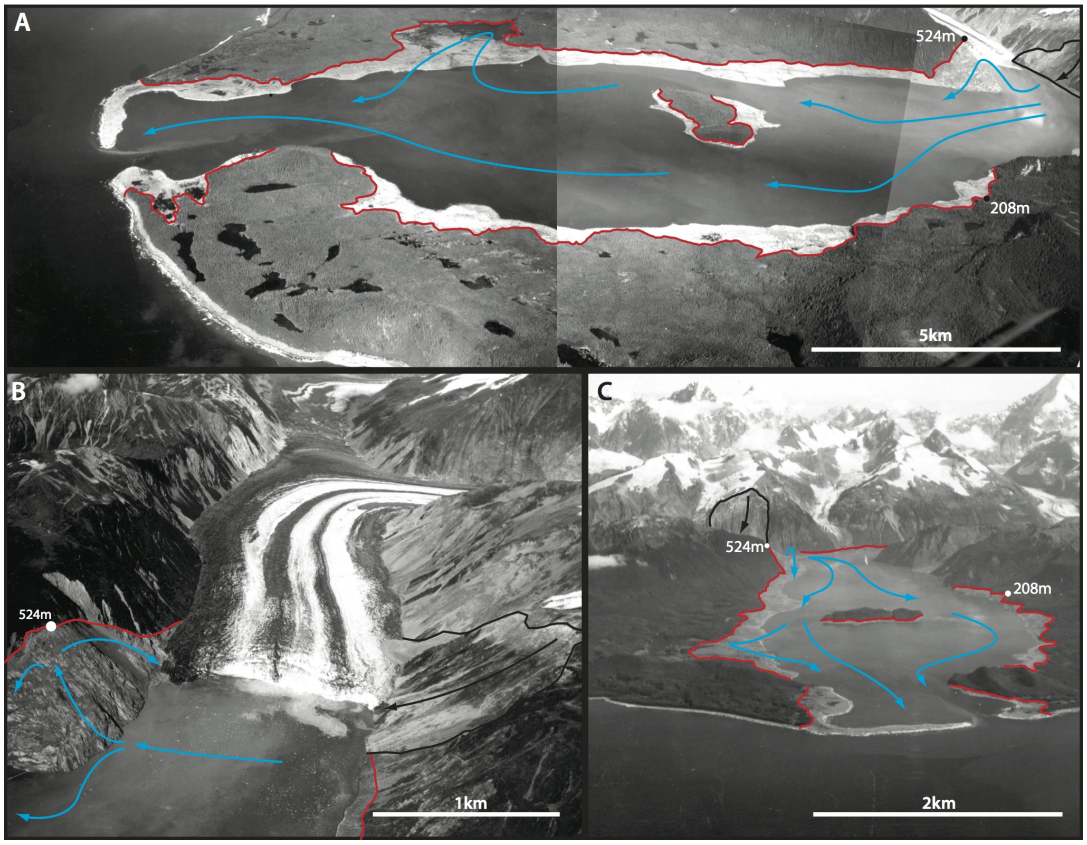

Figure 2.10: Lituya Bay following the 1958 mega-tsunami. a) panoramic view of Lituya Bay looking NW; b) NW view of Lituya Glacier and the landslide scar (right) showing maximum wave run-up on the spur opposite; c) overview of Liutya Bay looking NE. Photos from USGS.

These locations may therefore also be at threat of liquefaction following a large Alpine fault earthquake. McCahon et al. (2006a,b,c) also identified a number of potential liquefaction locations in the West Coast region and found that the major towns of Westport, Greymouth, and Hokitika were particularly susceptible being situated on the floodplains of the Buller, Grey, and Hokitika rivers respectively.

Glacial Response

Landslides that deposit supraglacially can significantly alter glacier behaviour by adding extra mass and by reducing ice-surface ablation. Debris covering $>$10% of a glacier's ablation zone suppresses ablation, causing glacial advance (Reznichenko et al., 2011; Shulmeister et al., 2009). This effect was first witnessed in Alaska following a series of large earthquakes in 1899 (Tarr and Martin, 1912) but was not properly studied until the 1964 Alaskan earthquake when $\sim$50% of the Sherman glacier ablation zone was covered by landslide deposits leading

to an 80% reduction in surface ablation (McSaveney, 1975). Prior to the earthquake the Sherman glacier was experiencing substantial retreat, however following the earthquake this changed to a slow advance which was still continuing 40 years later (Reznichenko et al., 2011). Another well-studied example is the Baultar glacier in the Karakoram Himalayas where 15-20% of the ablation zone was covered by a landslide, causing a two year glacial surge followed by a slower 2 km advance over the next 12 years (Hewitt, 2009).

Despite the South Island hosting >3,100 glaciers, most are very small (<0.1 km^2; Chinn 2001) and remote. Landslides falling onto such small glaciers are unlikely to have a significant effect. Nevertheless, landslides falling onto the major glaciers may have a substantial effect. These glaciers cover an area of ∼245 km^2 which accounts for ∼1% of the total area affected by landsliding (**Table 2.2**); however each glacier is situated in a steep-sided, heavily eroded valley <20 km from the Alpine fault and thus the chance of landsliding onto any of the glaciers is high. Reznichenko et al. (2011) estimated that an 80% reduction in ablation of the Franz Josef glacier was sufficient to cause the glacier to advance ∼6 km down valley towards Franz Josef township. Such a scenario was estimated to occur within 3-6 years of the ablation zone becoming covered (Shulmeister et al., 2009). The Waiho Loop, a large terminal moraine down-valley from Franz Josef Glacier, is thought to have formed as a result of a large landslide, possibly from an Alpine fault earthquake, covering much of the glaciers ablation zone causing a substantial glacial advance (Tovar et al., 2008). Previous advances of South Island glaciers have caused severe aggradation of proglacial rivers although it is not known how much aggradation might follow such a large-scale advance.

2.5 Discussion

2.5.1 Importance of landsliding

Other than liquefaction, the geomorphic effects described above are a direct result of coseismic landsliding. However the estimates provided for landsliding (**Table 2.2**) cover an extremely large range and provide no data on potential spatial distribution, which further exacerbates the difficulty of understanding the hazard presented by an Alpine fault earthquake. Despite the Southern Alps and West Coast region having only small populations, determining whether or not these populations are susceptible to coseismic landsliding and its associated geomorphic effects is vital in understanding the hazard posed. Many of the critical lifelines that make everyday life possible in the West Coast region pass through the Southern Alps. Impacts to these from geomorphic effects could have substantial consequences for the West Coast region including isolation and long-term power loss. Further, very little work has in-

vestigated the historical effects for regions east of the main divide, and the estimates outlined above do not offer any more substantial detail than is already available. Thus for these areas Alpine fault hazard remains very much a subject of conjecture.

Additionally, the coseismic landsliding estimates above are based upon empirical relationships for historic earthquakes globally. An Alpine fault earthquake is not included in this data having not occurred historically and therefore it is not possible to conclusively determine whether these relationships are appropriate. An Alpine fault earthquake could feasibly generate much smaller or larger values than those presented. It is prudent therefore, to assume the values presented are reasonable at least as order-of-magnitude estimates. This highlights the need for a more robust and detailed analysis of the coseismic landsliding likely to result from an Alpine fault earthquake.

2.5.2 The Wenchuan earthquake

Various references to geomorphic effects resulting from the Wenchuan earthquake have been discussed above, because it is one of the best-studied recent examples of large mountainous earthquakes and their associated geomorphic effects. This M_w8.0 earthquake occurred on a major dextral-oblique fault with >300 km of surface rupture and displacements of ∼6 m lateral and ∼1 m vertical (Gorum et al., 2011; Xu et al., 2009). It affected steep, heavily vegetated mountainous terrain which bears remarkable similarities to the central Southern Alps and therefore may represent a reasonable analogue for the next Alpine fault earthquake. The Wenchuan event was particularly devastating because of the widespread, catastrophic landsliding that occurred. Xu et al. (2013) suggested that as many as ∼200,000 landslides, however most agree the number was closer to ∼60,000 (Gorum et al., 2011; Li et al., 2014; Parker et al., 2011). As a result, it has been suggested the earthquake had a net negative effect on mountain building, with more material being eroded from mountains by landslides than was uplifted by the earthquake (Parker et al., 2011); more recently however, this has been shown to be incorrect, however landsliding was still substantial enough to offset uplift. (Li et al., 2014).

There are major differences in the lithology between Wenchuan and the Southern Alps; the former is comprised of carbonates overlying granitic basement, while the latter consists of schists and greywacke. This may influence the degree of landsliding, however it is not currently known what effect, if any, this may have. Regardless, the Wenchuan earthquake demonstrates that large earthquakes in mountainous terrain can be extremely devastating, resulting in substantial geomorphic consequences. It therefore serves as a warning of the potential effects of such events and the need for better understanding of these secondary

processes in mountainous regions with known earthquake hazard, such as the Southern Alps.

2.6 Conclusions

There is $\sim$30% probability that the Alpine fault will generate a large earthquake at some time in the next 50 years. Evidence from previous ruptures suggests that the fault typically produces rupture lengths in excess of 300 km resulting in M_w8.0 earthquakes. Such an event will result in MM 8+ shaking across the western range-front of the Southern Alps with the Southern Alps themselves experiencing MM 7+ shaking. Empirical observations of other large earthquakes globally suggests that such an event could generate between $\sim$20,000 and 150,000 landslides affecting an area of $\sim$12,000 to 100,000 square kilometres. Geologic evidence appears to support the inference that the earthquake will be followed by substantial landsliding throughout the mountains. As a result, many South Island rivers are expected to be blocked by landslide dams; most of these are west-draining although the east-draining Waimakariri River is also of concern. The threat of outburst flood from any landslide dams which form will require immediate assessment as to the potential threat to downstream populations, with most dams expected to survive for only a short time period. Those surviving longer-term will present a continued hazard which will require on-going monitoring. Post-event aggradation is anticipated to occur on most, if not all, west coast alluvial fans and could reach average depths of $>$1 m. There is the possible threat of landslide-generated tsunami in lakes and fiords, particularly in Milford Sound, although Lake Wakatipu and Lake Wanaka are also at risk. Nevertheless, without more detailed, robust assessment of the likely magnitude and spatial distribution of coseismic landslides it is difficult to fully quantify the hazard an Alpine fault earthquake poses to the South Island. This thesis aims to address this gap in existing knowledge by developing a detailed and realistic scenario for an Alpine fault earthquake, including estimates of coseismic landsliding.

Chapter 3

Developing effective disaster scenarios for local- and regional-scale emergency management exercises: a case study of an Alpine fault earthquake scenario

3.1 Introduction

Disasters are infrequent and unpredictable events in which a range of interactions between societal and environmental systems can lead to major losses (Burton and Hewitt, 1974; Fritz, 1961). When considering specific future disasters, there is therefore the need to focus on the integrated social-environmental system (Berkes et al., 2003; Berkes and Folke, 1998). Deterministic scenario approaches provide such an opportunity as these consider a hazard scenario and its consequent social impacts as one; a hazard that does not affect the social system cannot be a disaster. Freeman et al. (2003) therefore highlight that developing scenarios is a key stage in pre-disaster risk management. Scenarios also enable lessons learnt during and in the aftermath of historic disasters to be applied to potential future events in order to gauge whether or not social systems have adapted sufficiently to cope with future disasters. They therefore act as a means to invoke and to test the processes and behaviours involved in responding to a disaster, which is vital to achieving resilience (Holling, 2004; Park et al., 2013).

To be effective, disaster scenarios must be as realistic as possible in the hazards and impacts that they describe (Alexander, 2000). Accurate disaster scenarios can only be developed when experts from a wide variety of social groups, including disaster science, engineering, emergency management (EM), health operators, governance, and local communities amongst others, combine their knowledge and understanding (Preuss and Godfrey, 2006). Thus effective disaster scenarios act as *'boundary objects'* between the various groups involved in their development (Carlile, 2002; Star and Griesemer, 1989), requiring knowledge to be co-produced by all participants. Yet to be truly fit for purpose, a disaster scenario must force the players involved to respond to the unravelling emergency in the same way they would respond to the actual emergency when it occurs (Holling, 2004). Thus the scenario must describe realistic events, but it is the process of responding to these events that is more important than the precise scenario.

Disaster scenarios have a wide variety of potential applications, including EM exercises, commercial planning, contingency planning, community preparedness, personnel training, public education, and risk communication amongst others. The scale of the scenario (i.e. how large a disaster it represents) is entirely dependent on its desired application. In EM exercises, scenarios can involve large-scale disasters such as earthquakes, volcanic eruptions, and major terrorist attacks. They are used widely in health and nursing studies to simulate emergency medical requirements, as they provide efficient and effective means for training personnel (Bearnson and Wiker, 2005; Scherer et al., 2007). Similarly, they are becoming popular tools for teaching university level students, particular those in hazard and disaster management and emergency management courses, as they provide first hand experience in dealing with disasters without requiring an actual disaster (Harpp and Sweeney, 2002). Paton and Johnston (2001) showed that scenarios are also an effective method for promoting preparatory behaviour in exposed communities. Yet it is in EM where they are perhaps most widely and successfully used. Their value to EM has long been known and in most industrialised nations, the use of disaster scenarios for emergency response exercises is mandated by legislation (Selvarajah 1993; CDEM Act, 2002).

This chapter focuses on the development of effective disaster scenarios for EM exercises, using a recent example from a regional-scale New Zealand exercise around a large plate-boundary earthquake. This exercise was the first regional-scale exercise scenario to be developed in New Zealand via the co-production of knowledge between EM personnel, disaster scientists, and infrastructure operators. It follows a maximum-credible earthquake on the Alpine fault and involves all the South Island Civil Defence and Emergency Management (CDEM) Groups and their associated local councils (**Fig. 3.1**). This exercise (Exercise *Te*

Ripahapa) follows two similar exercises in 2004 (Exercise Pegasus) and 2007 (Exercise Pandora) which also used maximum-credible earthquakes on the Alpine fault. However the 2004 and 2007 scenarios, which were developed primarily by EM personnel with limited science input, considered only the seismic scenario and its consequent impacts on built infrastructure. Chapter 2 has demonstrated that a rupture of the Alpine fault is also likely to contain numerous geomorphic effects, widely distributed spatially and temporally. Thus, to be a realistic, and therefore effective exercise, the disaster scenario for Exercise *Te Ripahapa* required the inclusion of detailed geomorphic effects, as well as seismic effects, and the resulting impacts of both. This chapter outlines the development of disaster scenarios for EM exercises and presents the Exercise *Te Ripahapa* scenario as an example of its application. It identifies several key knowledge gaps which require further research in order to increase understanding of an Alpine fault event, and of earthquakes in mountainous environments in general.

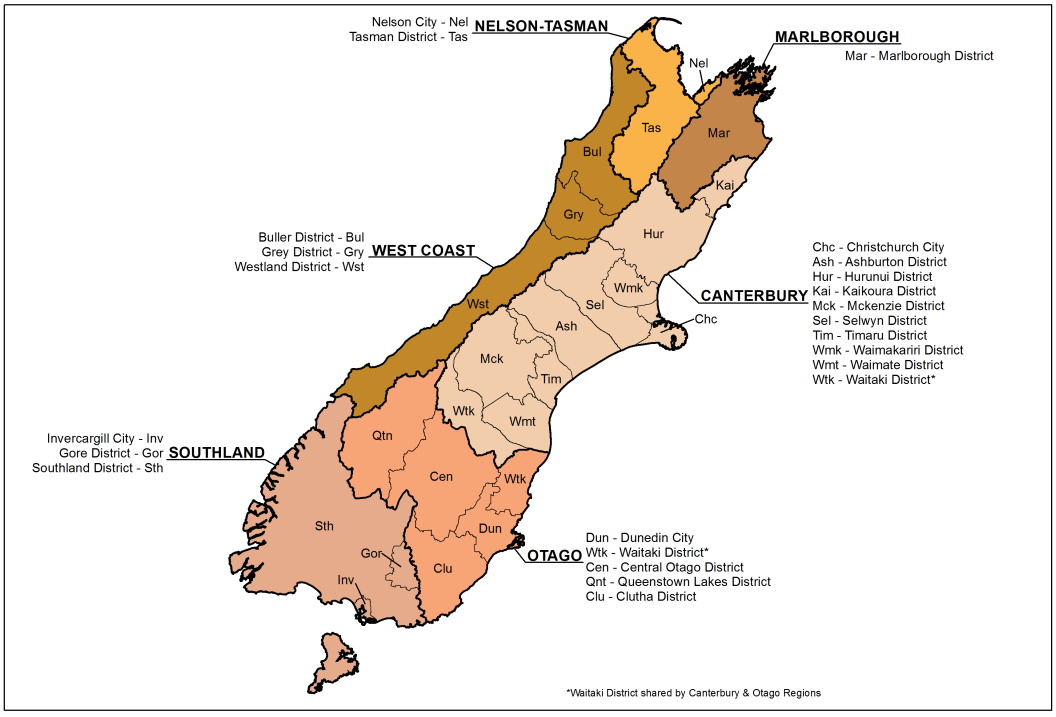

Figure 3.1: Location of the South Island, New Zealand, CDEM Groups and their associated local councils (www.civildefence.govt.nz).

3.2 Methodology

3.2.1 Disaster scenarios and their required elements

Developing resilience to future disasters from environmental hazards requires a focus on an integrated socio-environmental system (Berkes et al., 2003; Berkes and Folke, 1998) as, by definition, a disaster is the result of one or more natural hazards affecting the social system (Fritz, 1961). Learning from past events enables a better understanding of the ability of social systems to respond to future disastrous events and provides direct observations of previous successful and unsuccessful management processes (Alexander, 2000; Folke et al., 2005). Basing scenarios on previous events for which there is a substantial amount of information is common (Alexander, 2000; Faccioli, 2006). Nevertheless, simply re-enacting historical events is unwise as this can limit potential outcomes by allowing players to apply *de facto* solutions based upon their knowledge of the historic event (Alexander, 2000; Borodzicz and van Haperen, 2002). Using previous events as the basis for scenario design and altering various aspects of the disaster as well as including realistic but unexpected events is a better option (Alexander, 2000). Using available scientific literature on well-defined prehistoric events, particularly in an effort to establish the effects such an event would have had to society today, is also useful. Both these options allow realistic disaster scenarios to be developed without participants having pre-existing knowledge of the event and the processes required to respond.

Developing an effective scenario utilises both the implicit and explicit knowledge of those creating the scenario. Disasters affect the whole spectrum of society, so to produce a realistic scenario requires collaboration across all stakeholders. This includes disaster scientists (physical and social), emergency managers, governance (including politicians), engineers, local communities, commercial businesses etc. However communicating this knowledge between the different groups is often impeded by invisible boundaries (for instance terminology) between the groups that prevent the sharing of knowledge (Carlile, 2002). 'Boundary organisations' provide a conduit for sharing this knowledge, and for developing 'boundary objects' (e.g. a scenario; **Fig. 3.2**) which can be used by players from any of the associated groups without requiring the specific expertise of another group (Star and Griesemer, 1989). The key element for scenario development is therefore that they are co-produced by all associated social groups who effectively share their relevant knowledge.

To achieve realistic scenarios of disasters triggered by natural hazards it is important to include the full complement of hazards that are likely to arise. Natural hazards do not occur in isolation, as an initial (primary) hazard affects the surrounding environmental system

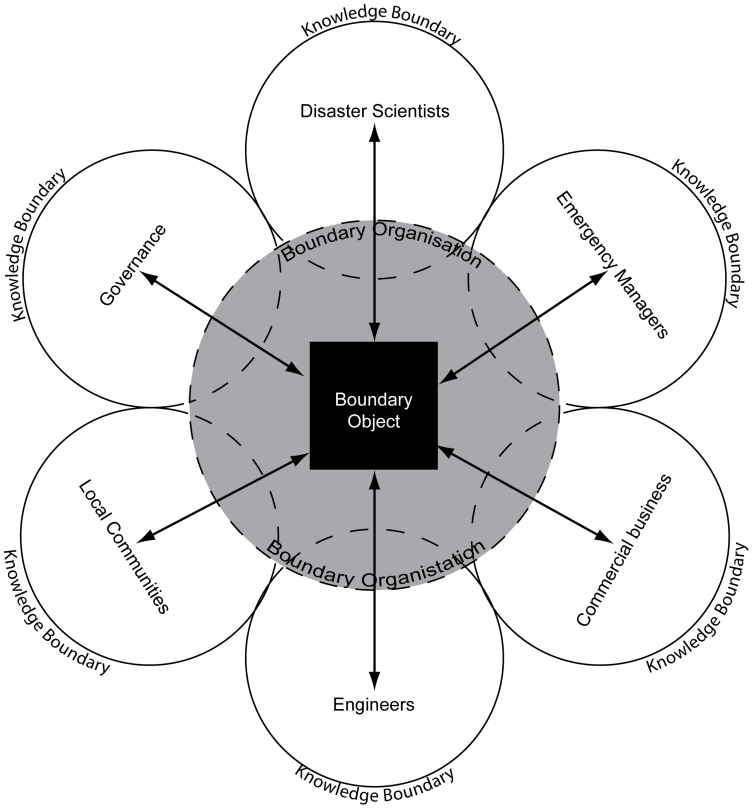

Figure 3.2: Schematic diagram of knowledge boundaries, boundary organisations, and boundary objects in the development of disaster scenarios (boundary objects).

as well as the social system, often resulting in a series of complexly interlinked cascading (secondary) hazards (Hewitt et al. 2008; Chapter 2). These can include storm surges and flooding from hurricanes and typhoons, jokulhaups (glacial outburst floods) from sub-glacial volcanic eruptions, landslides and debris flows from mountainous earthquakes, and landslide dams and outburst floods from landslides (see Chapter 2). Considering only the primary hazard in the disaster scenario therefore substantially underestimates the effects, both spatial and temporal, of the disaster. Recently, several large-scale EM exercises have successfully included secondary hazards in the associated disaster scenarios. These include *Hurricane Pam* (FEMA, 2004), the *Southern California ShakeOut* (Jones et al., 2008), and Exercise *Capital Quake* and Exercise *Ruamoko* in New Zealand (www.civildefence.govt.nz). However, these examples are exceptions as most disaster scenarios, particularly for smaller-scale exercises, typically only consider the primary hazard. This is especially true of earthquake scenarios (see Ansal et al., 2009; Faccioli, 2006; Fäh et al., 2001; Hok et al., 2011; Irikura and Miyake, 2011; Reichle, 1991; Slavov et al., 2004).

The inclusion of secondary hazards in recent large-scale exercises is primarily a result of wide collaboration between emergency managers, disaster scientists, engineers and critical infrastructure operators, local-, regional-, and national-governance, and communities (see Jones et al., 2008). In addition, perhaps their most notable advantage was their scale. All were large-scale (national-scale in the New Zealand cases) exercises which consequently had substantial development time, resources (data and funding), and personnel available (Jones et al. see 2008; FEMA, 2004). For instance the Southern California ShakeOut scenario involved >300 developers and used three different modelling teams each utilising different super-computers (Jones et al., 2008). For smaller-scale (local- and regional-scale) exercises this level of development is not possible due to timeframe, resource, and personnel constraints. Thus an alternative approach to co-producing disaster scenarios for these exercises is required.

As stated above, disaster scenarios must consider an integrated socio-environmental system. As well as including primary and secondary (and tertiary etc.) hazards, they must therefore also outline the impacts of these hazards on society. Particular societal elements are included depending on the intended application, and they can include multiple different elements or an individual element. For instance, a disaster scenario intended for risk identification for transportation and access can focus purely on the impacts on transport networks. Alternatively, a scenario intended for community preparedness should detail the impacts on a large number of different aspects including transport, power, sanitation, communications, welfare, business operations, and life safety. Understanding the intended application of the disaster scenario and the required impact needs are therefore crucial.

Finally, before a scenario can be applied, it must be independently verified (see Bielak et al., 2010) to ensure that it is both realistic and fit for purpose. This provides an added level of credibility which is typically desired by those participating in its application. Paton and Johnston (2001) suggested that for community preparedness applications, achieving consensus between the various participating groups is critical for maintaining empowerment within these individual groups. Undertaking a process of review and validation can cement such a consensus by demonstrating that the proposed disaster scenario is generally accepted, even beyond those involved in its creation and application. For multi-faceted scenarios involving multiple hazards and impacts on multiple aspects of society it is impractical to expect any single reviewer to have expertise on all included aspects. Including subject specific experts to review the relative particular elements as well as two (or more) traditional reviewers for the whole document is therefore more appropriate. This approach was successfully undertaken for the 2008 Southern California ShakeOut disaster scenario (Jones et al., 2008) with each

individual aspect of the scenario independently reviewed (e.g. Bielak et al., 2010), as well as the scenario as a whole.

3.2.2 Conceptual model

A generic conceptual model of the required contents for disaster scenarios is presented in **Fig. 3.3**. It has been developed through review of pertinent literature and from some experience of the author. First a description of the hazard events which initiate the disaster are required, based upon information on historic and/or pre-historic events. This information must include detailed descriptions of the primary and secondary (and tertiary etc.) hazards that occur. Including potentially unexpected hazards is possible as unpredictability is a defining characteristic of disasters (Quarantelli, 1998). The hazard scenario thus developed, forms the foundation of the disaster scenario as its spatial and temporal evolution is the basis of the resultant social impacts and thus of the disaster scenario as a whole.

Despite the hazards forming the foundation of the disaster scenario, it is their consequent impacts to society that are of the most interest, regardless of the desired application (Preuss and Godfrey, 2006). When considering the effects of the hazard scenario on the social system, the exposure of the elements required for the particular application need to be established first. The exposure of those elements to the hazard scenario will define the disaster. As stated above, a hazard which does not affect the social system cannot be a disaster; thus an element not directly exposed to a hazard cannot be directly affected. Nevertheless, an element can be indirectly affected as a result of direct (or other indirect) impacts on another element or elements (see Kameda, 2000). Thus it is important that the spatial and temporal distribution of all involved elements with respect to each other is also considered (see Preuss and Godfrey, 2006).

Combining the hazard and element exposure yields the vulnerability of individual elements, and also of society as a whole. The fragility and vulnerability of an element to the hazard(s) it is directly exposed to determines its consequent impacts. Consideration of any pre-existing mitigation is also important as this fundamentally alters elements' vulnerabilities. Finally, the interdependencies between the various elements are necessary to ascertain indirect losses. Preuss and Godfrey (2006) use the example of building damage to critical facilities such as hospitals, fire and police stations where collapse of these structures may result in direct fatalities, but will also have the potential to indirectly increase fatalities elsewhere through a lack of emergency response.

The disaster scenario thus derives from the vulnerability and the resultant impacts. An important factor in assessing the consequences of disasters is the remaining functionality of

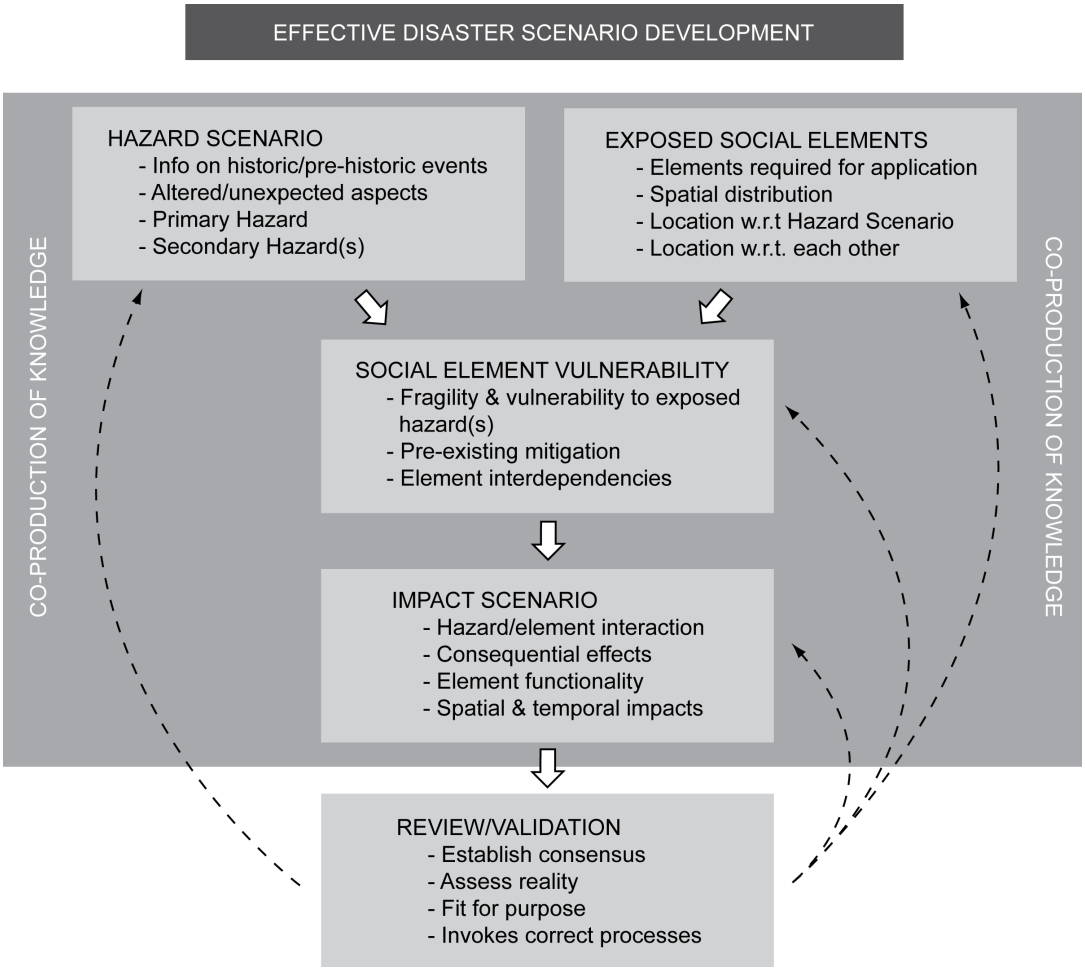

Figure 3.3: Conceptual model of the required elements for the design and development of disaster scenarios. Dashed arrows represent elements included only as required.

the various elements involved as this limits the response (Whitman et al., 1997). For instance, it is insufficient to know that a road has been damaged by landslides; what is required is a description of whether this damage is a complete or partial blockage of the road. As well as considering the spatial extent of impacts, it is necessary to consider their temporal extent (Alexander, 1995), both within the limits of the disaster scenario and beyond. Understanding how the effects progress throughout the scenario is evidently important, however participants must also consider how these effects will develop and perhaps continue after the scenario has ended, as this may influence their response during the scenario. For instance, following the 1991 Mt Pinatubo volcanic eruption, fluvial remobilisation of unconsolidated pyroclastic deposits over six years after the eruption meant lahars were still affecting exposed communities throughout central Luzon in the Philippines (Leone and Gaillard, 1999).

The review phase is vital to the credibility of the proposed scenario. An internal review process can be applied in the closing stages of development to ensure group consensus, which is vital for maintaining empowerment between all involved groups (Paton and Johnston, 2001). External review can also be used to check the reality of the proposed scenario and to ensure it is scientifically plausible (Alexander, 2000). This can be important for stakeholder (participants and governance) confidence in the scenario. Most importantly however, the review must ensure that the proposed scenario is sufficient to invoke the appropriate responses and behaviours during its application (Holling, 2004; Park et al., 2013). As long as the scenario contents are plausible and realistic, their precise details are unimportant as long as they are eliciting the correct processes to respond to such an event. Thus, the intended application and outcomes of the disaster scenario must be kept in mind throughout all stages of development, and should actively sculpt the development of the scenario.

3.3 Application: Exercise *Te Ripahapa*

In order to illustrate the use of this model, and its effectiveness for EM exercises, the 2013 New Zealand CDEM Exercise *Te Ripahapa* is briefly described below. For a full account of the methods undertaken and the complete scenario, see Appendix B. This example demonstrates the value of the model in local- and regional-scale exercise scenario development. The Exercise *Te Ripahapa* disaster scenario was the first regional-scale exercise in New Zealand to be fully co-developed and also the first to include detailed descriptions of secondary hazards. The scenario and exercise was judged to have been very successful and there is already evidence of up-take of the scenario beyond CDEM. Furthermore, the development of the scenario directly identified gaps in the current level of knowledge of earthquakes in mountainous environments, which the following chapters of this thesis address.

3.3.1 Exercise scope

Following the devastating 2010-11 Canterbury earthquake sequence (e.g. Gledhill et al., 2011; Kaiser et al., 2012), there has been a strong drive by the public and government at all levels to increase earthquake resilience throughout New Zealand. A country with already relatively high levels of earthquake mitigation and preparedness, the Canterbury earthquake sequence has provided an opportunity to instigate policy changes and embed lessons learned as a result of the disaster (MBIE, 2013). Consequently, Canterbury CDEM Group initiated proceedings for a regional South Island-wide exercise for an anticipated Alpine fault earthquake (*Te Ripahapa* is 'The Alpine fault' in the Māori language of New Zealand). The exercise aim was

to practise emergency response procedures resulting from a large-scale earthquake as well as to implement and test the lessons learned during the Canterbury earthquake sequence. The exercise was intended to simulate the first 18 hours following the occurrence of an Alpine fault earthquake, beginning six hours after the mainshock.

The specific requirements for the Exercise *Te Ripahapa* disaster scenario were to:

- represent a maximum-credible event from an Alpine fault rupture;
- be scientifically plausible;
- be extensive enough to generate regional effects;
- include consequences for critical infrastructure (State Highways, Hydroelectric Power, and Telecommunications)
- include an estimate of the number and spatial distribution of fatalities; and
- be of high enough probability that it cannot be criticised as an unusual or extreme event.

Previous Alpine fault scenarios (2004 Exercise Pegasus and 2007 Exercise Pandora) had successfully and accurately included the potential maximum-credible seismic effects of an Alpine fault earthquake, yet geomorphic effects were largely ignored. However, the geomorphic effects of the 2008 Wenchuan earthquake (see Gorum et al., 2011; Huang et al., 2010; Yin et al., 2009) and the widespread liquefaction and rockfall from the Canterbury earthquake sequence (Cubrinovski et al., 2011b; Khajavi et al., 2012) demonstrated to the CDEM Groups the need to include these effects in an Alpine fault scenario. Despite knowledge of the potential seismic effects within the CDEM and partner agencies being high (Exercises Pegasus and Pandora produced accurate earthquake effects with limited science input), knowledge of the potential geomorphic effects was significantly lacking. Consequently, Canterbury CDEM Group enlisted a group of disaster researchers from the University of Canterbury and the University of Otago to develop the scenario in conjunction with the South Island CDEM Groups and their associated partner agencies (**Table 3.1**). The disaster scientists were able to include their knowledge of geomorphic hazards and their cascading interactions following large earthquakes (see Chapter 2) to develop a scientifically plausible, maximum-credible and more complete event.

3.3.2 Scenario summary

The co-production of knowledge can take many different forms. One suggested approach to co-ordinating such multi-participant collaboration is that of an Integrated Design Team

Table 3.1: Exercise *Te Ripahapa* participants and their corresponding societal groups.

Discipline	Organisation
Disaster Scientists	University of Canterbury
	University of Otago
	GNS Science[a]
Emergency Management	Canterbury CDEM
	Marlborough CDEM
	Nelson-Tasman CDEM
	Otago CDEM
	Southland CDEM
	West Coast CDEM
	Ministry of Civil Defence and Emergency Management
	National Crisis Management Centre
Emergency Services	Coast Guard
	Defence Force (Military)
	Fire Service
	Police
Health Operators	Ministry of Health
	St Johns Ambulance Service
Critical Infrastructure Organisations	Christchurch International Airport
	Chorus (Telecommunications)
	Kiwi Rail
	Meridian Energy Ltd (Hydroelectric Power)
	NZ Transport Agency (NZTA; State Highways)
	Telecom (Telecommunications)
	Transpower Ltd (HEP Transmission)

[a]External reviewers

(IDT) as suggested by Reitman (1989). This involves a series of group-based discussions between the various participants in order to gather the best and most relevant data. It effectively deals with the issue of pragmatic knowledge (Reitman, 1989), whereby the desired output is actually a function of the various groups' knowledge and the specific requirements the team is attempting to achieve. Reitman (1989) applied this method to the development of expert systems processes; however it can be suitably adapted for EM exercises and thus a similar approach was suggested by Preuss and Godfrey (2006). An IDT allows participants to collaborate and share both knowledge and solution processes via a series of discussion groups. Mullin (1989) showed that for well-defined problems it is actually the experts' solution processes and judgements that are important rather than their underlying knowledge. Thus, including all of the participant groups in a round-table discussion can allow such solution processes to occur, as there is a need to explain systematically the reasoning behind the various conclusions rather than simply stating the conclusions themselves. Furthermore, Cooke and Goosens (2004) showed that expert elicitation resulted in no appreciable loss in detail or realism compared to other methods.

Such a process can expedite scenario development by effectively focussing the various participants on their own particular value (Reitman, 1989). However, it should be highlighted that it can require substantial development time which must be effectively managed with limited timeframes, and can also be subject to personality clashes between participants as well as professional pride (Reitman, 1989). Nevertheless, IDTs are a practical and easily applicable method for developing co-produced knowledge and thus were used in the design and development of the Exercise *Te Ripahapa* disaster scenario (**Fig. 3.4**).

These IDT-based discussion groups allowed the disaster scenario development teams to identify the most relevant information for the exercise. The results of these discussions, which took place over a four month period (**Fig. 3.4**), are summarised in **Table 3.2**. The evidence for these various conclusions is briefly described below.

Primary hazard

The CDEM were able to achieve detailed and accurate seismic scenarios for previous earthquakes by using the large repository of existing scientific literature that has established the seismic potential of the Alpine fault (e.g. Adams, 1980b; Beavan et al., 2010a; Berryman et al., 1992, 2012a,b; Bull, 1996; Cooper and Norris, 1990; De Pascale and Langridge, 2012; De Pascale et al., 2014; Norris and Cooper, 2001; Sutherland et al., 2007; Wells et al., 1999; Yetton, 1998). The current scientific consensus suggests that a maximum-credible event is likely to be a full length ($\sim$400 km) rupture, initiating at a shallow ($<$12 km) depth, resulting

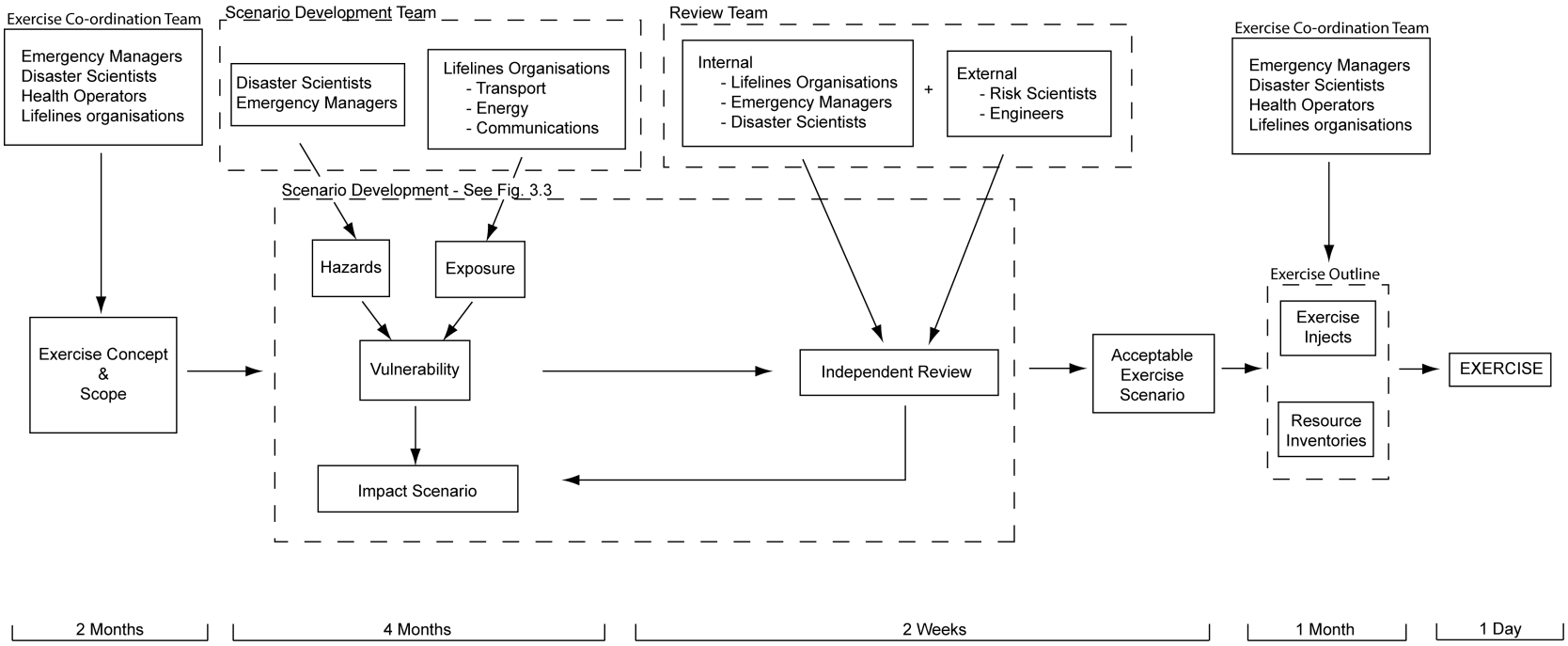

Figure 3.4: Indicative work-flow of the design and development of Exercise *Te Ripahapa* showing key inputs, integrated design teams, and timeframes.

Table 3.2: Summary of the key data for the Alpine fault earthquake disaster scenario for Exercise *Te Ripahapa*

		Summary
Hazards	Primary	M8.0 earthquake. Epicentre - Aoraki/Mt Cook region. 400 km bi-directional rupture. Maximum shaking intensity MM9; whole South Island >MM4 (**Fig. 2.4**). Shaking duration - ∼1 min near-field; >2 min far-field.
	Secondary	∼50,000 landslides in MM7+ zone. Landslide dams on 20 rivers. Debris flows in Aoraki/Mt Cook region. Outburst floods on 2 blocked rivers. 2 landslide generated tsunami in lake and fiord. No ocean tsunami. Liquefaction in all highly vulnerable soils (see McCahon et al., 2006c). See **Fig. 3.5**.
Impacts	Fatalities	293 total deaths; 224 in West Coast region. Greymouth worst affected (77); Hokitika (12) and Queenstown (10) also badly affected. Majority of fatalities in rural areas. See **Fig. 3.6** and Appendix C.
	Highways	>1,000 km of road impassable (1/5 of South Island network; **Fig. 3.7**). 10% of bridges in MM8+ zone catastrophically damaged. All alpine passes blocked by fault rupture, bridge collapse, and landslides/rockfalls. >20,000 people isolated by road; majority in West Coast region.
	Hydroelectric Power	No dams structurally damaged; temporary (<2 hours) shut-down of half generation sites. Inter-Island link remains functional. Transmission lines damaged by rockfall in alpine passes. Long-term power loss to >20,000 people in West Coast region and Queenstown (**Fig. 3.7**).
	Telecomms.	Short-term (1-2 hours) saturation-related loss nationwide (both islands). Power loss + tower damage-related long-term loss for West Coast region and Queenstown.

in an M_w8.0+ earthquake. Simple isoseismal modelling suggests a maximum shaking intensity of MM9 in isolated patches along the fault rupture (although MM10 cannot be discounted in some locations), MM8 along the entire rupture length, and MM5 shaking across ∼¾ of the South Island (see Chapter 2; **Fig. 2.4**).

Secondary hazards

There is substantial evidence of widespread, cascading, secondary geomorphic hazards occurring throughout the South Island dating to known ruptures of the Alpine fault (see Davies and Korup, 2007; Wright, 1998), and the likely scale and extent of these hazards has been broadly outlined in Chapter 2. Given the available timeframes and data, a rapid and basic empirical approach for establishing the scale of landsliding was undertaken. This followed the works of Keefer (1984) and Malamud et al. (2004) as outlined in Chapter 2. These empirical relationships suggest that for a M_w8.0 earthquake, ∼50,000 landslides are expected across an area of ∼34,000 km^2 (see Chapter 2). Further, Keefer (1984) showed that landsliding is typically most prominent in shaking intensities greater than MM6, although landslides have been observed at lower intensities under rare circumstances.

With such a large number of landslides it is clearly impractical to generate precise locations for each individual landslide. The alpine region of the South Island is sparsely inhabited (∼50,000 people), with only a few long, thin corridor links crossing the region and connecting the east and west coasts. Thus, the majority of landslides will have no direct impacts on population or infrastructure. Identifying the relatively small areas where landslides are likely to have direct impacts for population and/or infrastructure was therefore undertaken (**Fig. 3.5**). Of further interest, are those landslides that present an indirect threat to population and/or infrastructure in the form of landslide dams, outburst floods, and potential debris flows. For instance, the Aoraki/Mt Cook region in the central Southern Alps is known to be prone to debris flow hazard, while McCahon et al. (2006a,b,c) identified numerous west-draining river catchments likely to be blocked by landsliding in an Alpine fault earthquake (**Fig. 2.8**; **Fig. 3.5**).

The precise location of two landslides was included to form large landslide tsunamis as the potential hazard is considered high (Dykstra, 2012). The first of these was at Milford Sound in Southland region (**Fig. 3.5**). Dykstra (2012) investigated the threat of landslide tsunami at this location and found there had been multiple occurrences in the last ∼22 ka, concluding a 1 in 4 likelihood of occurrence during any given Alpine fault earthquake. The second occurred in Lake Brunner in West Coast region (**Fig. 3.5**) at the request of the West Coast CDEM Group to enable them to practise responding to a similar event. The original

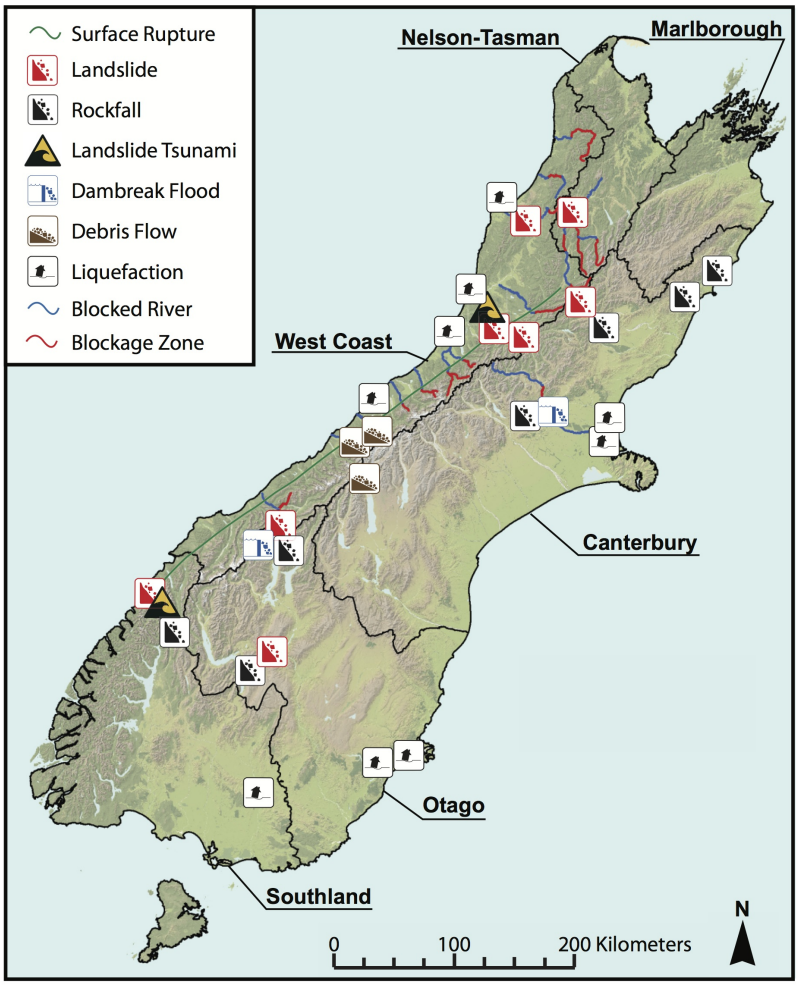

Figure 3.5: Regional-scale geomorphic scenario used in Exercise *Te Ripahapa*.

request was for a seiche, however during discussions this was considered unrealistic given Lake Brunner's close proximity to the Alpine fault.

Fatalities

Various models for estimating fatalities from strong earthquakes were available for the Exercise *Te Ripahapa*. However most of these require substantial data inputs and modelling time, which was not available, so a published empirical method was adapted for the rapid estimation of fatalities (see Appendix C). This method relied solely on global observations of the relation between fatality numbers, shaking intensity, and population density. The result was an estimated total 293 fatalities, 76% of which occurred in West Coast region, with 77 in Greymouth, West Coast region's largest town (**Fig. 3.6**).

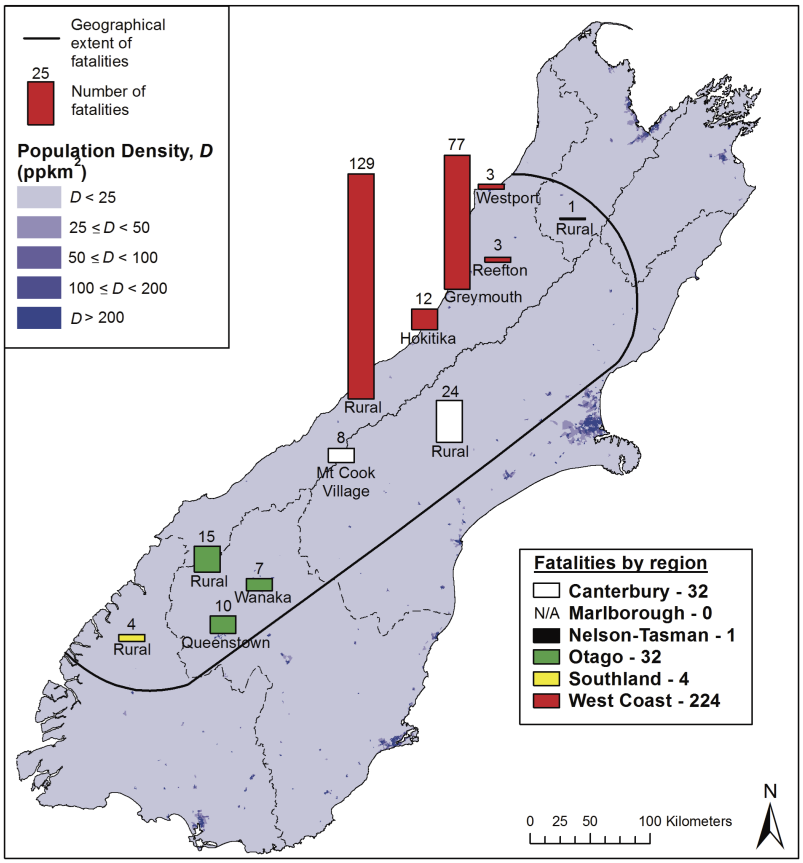

Figure 3.6: Estimated distribution of casualties resulting from an Alpine fault earthquake. Note: estimate only accounts for fatalities resulting from building collapse due to ground shaking and does not consider tourist numbers.

State Highways

The State Highway network has long, narrow corridor links with limited redundancy (**Fig. 3.7**). Only three routes traverse the Southern Alps connecting the east and west coasts, each of which crosses the known trace of the Alpine fault and passes through steep terrain prone to landslides. McCahon et al. (2006a,b,c) concluded that the alpine passes and SH6 in West Coast region were unlikely to be functional post-earthquake. The NZTA estimated that up to 10% of bridges experiencing MM8 or greater shaking would fail catastrophically (**Fig. 3.7**). The remaining bridges were likely to be damaged but useable for emergency vehicles only. Bridges experiencing MM7 or less were not anticipated to suffer any significant structural damage. Further, only short (<100 m) sections of one of the alpine passes has any rock-fall/landslide mitigation, so roads in landslide-prone areas were assumed to be highly vulnerable to landslide blockages.

Functionality of the South Island State Highway network following the earthquake was divided into three categories:

1. *Impassable*
   Road surface substantially displaced by fault rupture or cracking; bridges catastrophically damaged; fully blocked by landslide/rockfall

2. *Disrupted*
   Road surface damaged by cracking; bridges damaged but useable; partially blocked by landslide/rockfall

3. *Passable*
   Road surface generally undamaged; bridges intact; no landslides/rockfalls

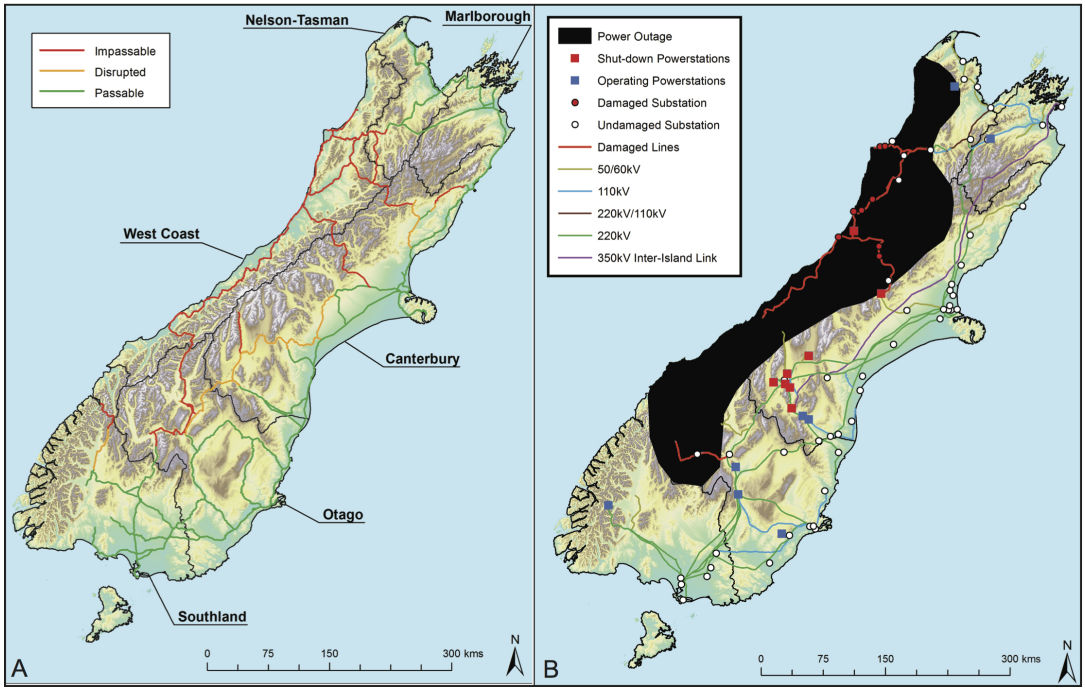

Figure 3.7: Estimated functionality of the a) State Highway and b) Hydroelectric Power networks following an Alpine fault earthquake.

Hydroelectric power

According to Meridian Energy Ltd. all South Island hydro-dams are constructed to withstand MM9 shaking. No dams experience such shaking levels in the present scenario, so none were inferred to be damaged. Any dams experiencing MM7+ shaking were likely to shutdown for

safety inspections (**Fig. 3.7**). The most exposed asset in the HEP network was the transmission network which distributes electricity around the country. Evidence from the Canterbury earthquake sequence was used to determine the likely extent of damage during the Exercise *Te Ripahapa* scenario. Following both the 4 September 2010 and 22 February 2011 earthquakes, substations and steel towers were observed to perform remarkably well despite experiencing shaking intensities >MM8 in several places (Giovinazzi et al., 2011) and it was concluded that significant damage as a result of ground shaking was unlikely. However, transmission lines which distribute power to the West Coast region follow two of the main State Highway routes which were inferred to be completely impassable due to landslides. It was therefore thought likely that the transmission lines would be severely damaged by landslides in these locations (**Fig. 3.7**).

Telecommunications

Telecommunications towers also performed well during the Canterbury earthquake sequence, according to two major telecommunications providers, so damage to these was inferred to only be likely from landslides and rockfalls in the alpine regions. Saturation of the network due to excess use was anticipated to occur in the first 1-2 hours following the event, resulting in telecommunications loss throughout New Zealand. Power loss was inferred as the main long-term vulnerability for telecommunications. The region suffering long-term power loss (**Fig. 3.7**) would therefore also experience communication loss.

3.3.3 Reflection

The disaster scenario developed for Exercise *Te Ripahapa* was, to the best of our knowledge, the first for a regional-scale New Zealand exercise to comprehensively include details of secondary hazards. Consequently, the scenario was substantially different from the previous Exercise Pegasus and Exercise Pandora, which also simulated an Alpine fault earthquake. Notably, Exercise *Te Ripahapa* involved a far larger spatial distribution of effects than either of the previous scenarios. Despite the majority of impacts occurring in the West Coast region, a substantial number of effects, including debris flows, landslide dams, outburst floods and liquefaction (**Fig. 3.5**) also affected areas east of the Southern Alps. Landslide tsunamis were also included for the first-time ever in a New Zealand EM exercise, forcing participants to carefully consider the required response. The differences in temporal affects between Exercise *Te Ripahapa* and Exercises Pegasus and Pandora were also significant. Following the earlier exercises, the primary long-term concern for EM personnel was continued aftershocks, however beyond the emergency response the main focus was on long-term recovery.

Conversely, Exercise *Te Ripahapa* presented the CDEM and their partner agencies with the issue of longer-term continuing hazards in the form of debris flows, surviving landslide dams, increased flooding risks from liquefaction, and aggradation issues from remobilised landslide material. The exercise participants were forced to confront and consider these longer-term issues throughout the exercise, resulting in a more realistic process for an Alpine fault earthquake. The independent reviews from GNS Science, a New Zealand government-funded crown research institute, determined that the proposed disaster scenario was scientifically plausible, realistic, and capable of generating the required processes and behaviours from exercise participants.

There is evidence of subsequent uptake of the disaster scenario, with CDEM Groups offering the same scenario for a joint international Military table-top exercise several months after Exercise *Te Ripahapa*. The disaster scientists involved in the development of the Alpine fault scenario were also involved in this later exercise, building further vital relationships with emergency response personnel and facilitating the further dissemination of realistic hazard information for an Alpine fault earthquake. Exercise *Te Ripahapa* participants who were involved in the response to the Canterbury earthquake sequence have commented on the realism of the disaster scenario. They observed that the required response processes as well as time constraints and flow of information during Exercise *Te Ripahapa* were more representative of real events during the Canterbury earthquakes, compared to previous exercises such as Exercise Pegasus and Exercise Pandora.

3.4 Discussion and conclusions

Despite the success of the Exercise *Te Ripahapa* disaster scenario, a key gap in the current level of knowledge was identified during the IDT discussion groups. It was noted that without an accurate ability to forecast landslide number and, in particular, the spatial distribution of landslides, it was extremely difficult to estimate the subsequent hazards (debris flows, landslide dams, aggradation etc.) and the impacts on critical infrastructure. Whilst the use of empirical models, historic occurrences, and expert elicitation was able to derive a scenario, there remained the potential for significant inaccuracies in the results, which could substantially alter the resulting scenario. Several methods for estimating regional coseismic landslide susceptibility exist, including pseudostatic analysis (Stewart et al., 2003), finite-element modelling (Clough and Chopra, 1966), and Newmark displacement modelling (Newmark, 1965). However, each of these methods requires either a complete historic landslide inventory, or detailed, densely populated geotechnical information; such data do not exist in New Zealand.

Establishing a method to estimate the spatial distribution of landslide susceptibility in locations where no such data exists is therefore a key research gap. In addition, more research is required towards undertaking robust impact assessments for critical infrastructure networks and estimating potential restoration times.

In summary, Exercise *Te Ripahapa* provided an excellent opportunity to directly connect active Hazard and Disaster science research with end-user groups such as emergency managers and critical infrastructure operators. This is a demonstration of the required collaboration between disaster scientists and EM personnel, amongst others, which can be effectively coordinated through the process of developing co-created disaster scenarios. Furthermore, it demonstrates how disaster scenarios can act as effective boundary objects for enabling the sharing and dissemination of vital hazard knowledge between a variety of differently-affected social and other groups. Developing disaster scenarios through the co-production of knowledge is therefore vital for any application for which the disaster scenario is intended.

Finally, Exercise *Te Ripahapa* has generated a substantially increased level of knowledge amongst all participants about the potential affects of a future Alpine fault earthquake - or indeed any major earthquake in mountains. Such knowledge and understanding pre-event may prove critical in the event of the actual disaster as the resulting geomorphic effects should no longer present an unexpected consequence. The uptake of the scenario beyond CDEM suggests that a more widespread understanding of these potential effects is developing, perhaps enabling more extensive and more focussed pre-event mitigation. As well as fostering stronger relationships between disaster researchers and CDEM, it has identified further research needs in identifying the information EM personnel require to understand and manage a future event. The process of developing disaster scenarios is shown to be a vital component of disaster risk reduction, and the conceptual model and methods undertaken herein present a framework for the development of future disaster scenarios, regardless of desired application.

Chapter 4

Regional coseismic landslide susceptibility analysis

4.1 Introduction

The importance of coseismic landsliding in mountainous environments has led to numerous attempts to model its regional-scale effects since the 1950s (Terzhagi, 1950). The complexity of the processes involved has led to the development of many different modelling methods with the most commonly applied being pseudostatic analysis (Bray and Travasarou, 2009; Stewart et al., 2003), finite-element modelling (Clough and Chopra, 1966), Newmark displacement analysis (Jibson et al., 2000; Newmark, 1965) and statistical analysis methods (Lee et al., 2008; Miles and Keefer, 2000). However, each of these methods requires the availability of either densely-populated geotechnical data (i.e. uniaxial compressive strength, soil behaviour, critical acceleration etc.) throughout the study area, or substantially complete historic landslide inventories from the region. For many regions around the world however, such data are not available. The collection of adequate geotechnical data across large areas is extremely expensive and often infeasible in mountainous terrain. Further, the collection of detailed and substantially complete landslide inventories has only been possible since the advent of remote sensing technology in the mid-20th century, yet could not be fully exploited until the development of computer-based geographic information systems (GIS) in the 1990s (Xu, 2014). Consequently, Xu (2014) report just 25 published coseismic landslide inventories globally, of which 13 post-date the advent of GIS and are therefore considered complete and accurate enough for regional analysis.

In the majority of mountainous regions exposed to high seismic hazard, landslide susceptibility modelling relies on basic empirical relationships (see Keefer, 1984; Keefer and

Wilson, 1989; Malamud et al., 2004). Whilst useful to provide first-order estimates of the likely scale of landsliding, such methods have significant margins of error (see Chapter 2). Further, these relationships take no account of the topography of the area affected, relying solely on earthquake magnitude. For instance, the 2010 M_w7.1 Darfield earthquake in Canterbury, New Zealand, is estimated by the empirical relationships defined in Chapter 2, to have produced between 1,200 and 10,500 landslides based on its magnitude. However, this earthquake affected the predominantly flat Canterbury Plains and consequently only a small number of rockfalls occurred in the nearby Port Hills; the majority of damage resulted instead from ground shaking and liquefaction (Cubrinovski et al., 2011a). Clearly there is a need to establish an accurate and detailed method for analysing regional-scale coseismic landslide susceptibility to avoid both over- and under-estimating the potential hazard.

The application of fuzzy logic in GIS provides a viable method for such assessment. Statistical analysis methods have historically accurately modelled specific study areas, yet this method may also be applicable on a more generic basis. The concept of statistical analysis methods assumes that the factors influencing slope failures in previous recorded events in a given area, will similarly influence future slope failures in the same area. However, multiple conditioning factors influence landslide susceptibility and these factors may have similar effects across different regions. If these factors can be identified, recognised and statistically analysed, it may be possible to apply them to model landslide susceptibility in different regions, in the same way that previous methods have modelled susceptibility for specific areas. This chapter approaches this possibility by analysing three historic earthquakes for which substantially complete and accurate landslide inventories are available. The aim is to identify the primary factors that control the spatial distribution of landslides in two of these events, and test if the identified factors can adequately model landslide susceptibility in the third event, from which no data has been included. If this is possible and shown to achieve accurate, meaningful results, those identified factors and their relationships may be applied to other regions for scenario earthquakes in order to establish the consequential landsliding hazard posed.

4.2 Previous methods of predicting coseismic landsliding

4.2.1 Pseudostatic analysis

Pseudostatic analysis considers the seismic stability of a given slope in terms of the horizontal component of seismic shaking in order to determine a factor of safety (Jibson, 2011; Stewart et al., 2003). Typically it provides a rough approximation of slope stability for preliminary

assessments only. If the factor of safety is >1 the site passes and does not require further analysis; however, if the factor of safety is <1 the site fails and requires a more detailed analysis, using different stability assessment methods (Stewart et al., 2003). To calculate the factor of safety a maximum horizontal acceleration likely to occur for the particular rock conditions at the study site is derived. The method has notable drawbacks, particularly that it assumes the applied earthquake force is a constant unidirectional force applied only in the direction that promotes failure (Jibson, 2011; Terzhagi, 1950). To counter this most applications use a pseudostatic coefficient, however these coefficients are primarily calibrated for earth dams and are therefore not necessarily applicable to natural slopes (Blake et al., 2002; Wieczorek et al., 1985). In addition, pseudostatic analysis assumes that the slope fails on the same failure surface on which it would fail aseismically, presenting a possibly non-conservative assumption. Thus despite the simplicity of application, pseudostatic analysis severely over-simplifies the dynamic landslide processes and thus is not applicable for detailed, regional-scale analysis.

4.2.2 Finite-element modelling

Finite-element modelling is a computational assessment of the response of a dense deformable mesh to applied earthquake stresses (Jibson, 2011). This model has the potential to be extremely detailed, representing a slope as a number of different nodes within the mesh, each of which can deform independently of the surrounding nodes. However, these models are computationally intensive and require dense, high-quality geotechnical data and soil models to predict their stress-strain behaviour (Jibson, 2011). As it accounts for the spatial variability of stress-strain properties in a particular slope, this method is recommended for site-specific investigations (often following pseudostatic analysis factor of safety results <1) where detailed soil data are available (usually in engineered slopes); however, it is not appropriate for regional scale analysis or in locations with limited soil data, such as natural slopes (Wasowski et al., 2011).

4.2.3 Newmark analysis

Newmark displacement analysis effectively bridges the gap between overly simplistic pseudostatic analysis and complex finite-element modelling (Newmark, 1965). The method models landslides as a rigid block sliding along an inclined plane when the block's critical acceleration is exceeded. For this, a particular earthquake strong motion record is selected and analysed, with the block being displaced each time the critical acceleration is exceeded and the total cumulative displacement calculated. It is then a task for the user to evaluate

the significance of the cumulative displacement (Jibson, 2011). Newmark analysis has been shown to accurately predict slope displacements but only if slope properties, soil properties, and earthquake ground motions are known (Wartman et al., 2003, 2005; Wilson and Keefer, 1983).

4.2.4 Statistical analysis in GIS

Statistical methods have recently been utilised via GIS for the assessment of aseismic landslides (see Crozier and Glade, 2005; Guzzetti et al., 1999; van Western et al., 1997). The method is based on relationships between known historic landslide locations and various conditioning factors (Remondo et al., 2003b) assuming that future slope failures are likely to occur under similar conditions as those in the past (Varnes et al., 1984; Carrara et al. 1991; Dai and Lee 2002; Guzzetti et al. 1999). This method is generally considered the most appropriate for landslide susceptibility analysis at a regional scale because the results are objective, reproducible, and easy-to-update (He and Beighley, 2008; Naranjo et al., 1994; Soeters and van Western, 1996; van Western et al., 2006). Thus, similar methods have been proposed for modelling coseismic landslide susceptibility in combination with fuzzy logic in GIS (Lee et al., 2008; Miles and Keefer, 2000, 2007, 2009). These methods have been shown to successfully assess the regional landsliding susceptibility for all landslide types without the requirement for detailed geotechnical data required by the methods described above (Lee et al., 2008; Miles and Keefer, 2009). Nevertheless, to perform statistical analysis requires that the area in question has an historic landslide inventory from which statistical data can be collected.

In spite of this, a combination of statistical analysis with fuzzy logic in GIS currently presents the most appropriate method for susceptibility analysis. By expanding these efforts and analysing landslide occurrence across multiple locations it may be possible to derive similarly accurate and meaningful results without being limited to a single location.

4.3 Fuzzy logic

4.3.1 Fuzzy set theory

Landslide susceptibility modelling via statistical analysis, like most other models, requires a number of generalisations and simplifications of the complex processes involved in slope stability. Uncertainties associated with these necessary assumptions can be increased in regional-scale studies leading to unreliable results. Fuzzy logic offers a method for modelling such highly complex systems and effectively deals with uncertainties related to insufficient

knowledge, data limitations, and ambiguous or imprecise input information (Zadeh, 1965). Fuzzy logic derives from classical set theory in which an element has a clearly defined relationship within a set, either belonging (1) or not belonging (0) to that set, therefore achieving a membership value of either 0 or 1.

$$\chi_A(x) = \begin{cases} 1, & x \in A \\ 0, & x \notin A \end{cases} \tag{4.1}$$

where $\chi_A(x)$ is the function of element x representing the membership of x in the set A.

Fuzzy logic adapts this theory by employing the concept of partial membership, where elements can have a varying degree of membership between 0 and 1:

$$\mu_A(x) \in [0,1] \tag{4.2}$$

where $\mu_A(x)$ is the degree of membership of element x to the set A; a value of 1 indicates full membership, 0 indicates no membership, and values between 0 and 1 are possible. Thus fuzzy logic can be thought of as a description of the degree of influence set A has over the occurrence of element x. When undertaken for a variety of different sets, $A, B, C, \ldots$, it becomes possible to accurately model the most susceptible locations for x to occur based on the distributions of various categories within those sets $A, B, C, \ldots$.

Establishing the membership function $\mu_A(x)$, is the fundamental component of fuzzy logic modelling. These functions are defined based on the frequency ratio, Fr, of x with respect to A. The frequency ratio defines the relative frequency of x in various categories of A (e.g. a level of shaking intensity or a particular slope angle etc.) against the relative frequency of x across the entire area.

$$Fr = \frac{N_{xi}/N_{Ai}}{N_x/N_A} \tag{4.3}$$

where N_{xi} is the number of occurrences of x in category i of set A, N_{Ai} is the area of category i in set A, N_x is the total number of occurrences of x, and N_A is the total area of set A. The resulting frequency ratios are then converted to a fraction of the largest observed value in order to scale the values between 0 and 1. Membership functions can then be derived directly from the normalised frequency ratios. Membership functions can be either user-defined (i.e. based on expert judgement) or data-driven (**Fig. 4.1**). Data-driven memberships are most accurate as they ensure the fuzzy membership identically represents the frequency ratio results; however user-defined functions are most common as they allow the user to control input assumptions and account for uncertainties/errors in the data (**Fig. 4.1**). To reduce the subjectivity of user-defined memberships, the coefficient of determination (R^2 value) can be applied.

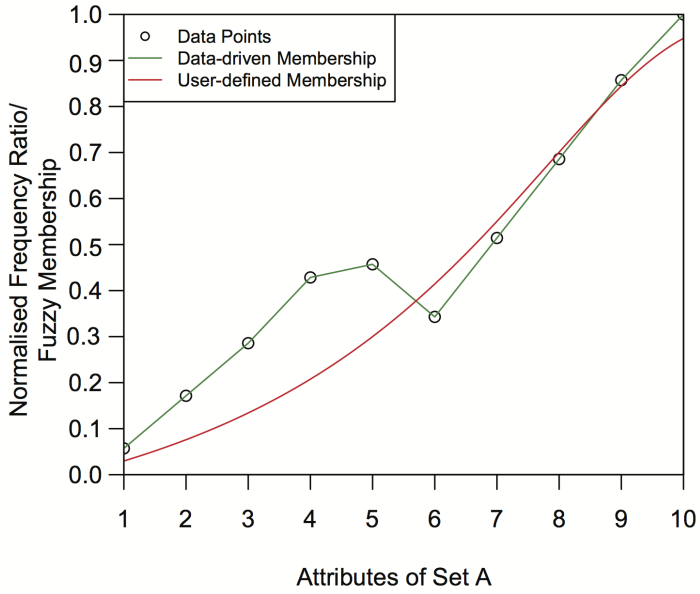

Figure 4.1: Comparison between data-driven and user-defined fuzzy memberships. Data-driven memberships intersect all data points while user-defined memberships have more flexibility and can use expert judgement to account for uncertainties/errors in the data.

Within GIS various membership functions are available which represent the most common distributions (**Fig. 4.2**), however users can define their own functions if necessary. The *fuzzy gaussian* and *fuzzy near* functions define curves which fit a normal distribution, with the user-defined midpoint fully belonging to the set (1) and values on either side of the midpoint decreasing in membership at a rate established by the user-defined spread. The *fuzzy near* membership is most useful for sets with faster-decreasing membership rates and smaller spreads. The *fuzzy linear* function assumes a linear distribution between user-defined minimum and maximum values. The user must also define whether the distribution is increasing or decreasing thus assigning full membership (1) for values above the maximum or below the minimum respectively. *Fuzzy large* defines distributions where larger input values are more likely to be a member of the set. The user-defined midpoint establishes the location of membership value 0.5 (the crossover point) and the user-defined spread establishes the rate of change either side of the midpoint. *Fuzzy MS large* is identical to *fuzzy large* except that the definition of the function is based on a specified mean and standard deviation. *Fuzzy small* and *fuzzy MS small* are the opposite of *fuzzy large* and *fuzzy MS large* respectively.

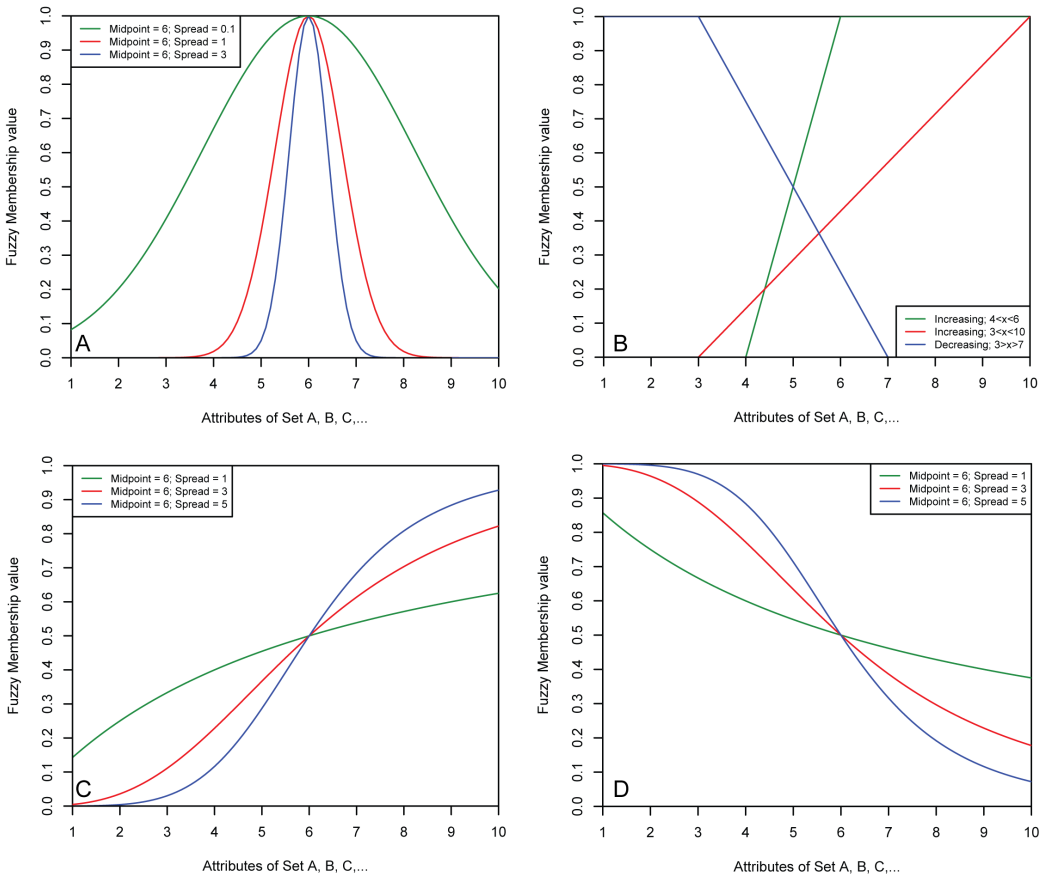

Figure 4.2: Effect of various user-defined values on the shape of a) Gaussian, b) Linear, c) Large, and d) Small fuzzy membership curves

4.3.2 Fuzzy overlay

When presented with a variety of different membership sets, $A, B, C, \ldots$, the occurrence of element x is dependent on how those various membership sets are combined. Fuzzy overlay operators are therefore used to combine membership sets $A, B, C, \ldots$ together on a cell-by-cell basis into a single fuzzy set (Dubois and Prade, 1985; Zimmerman, 1991). This final fuzzy set delineates the susceptibility of a cell to the occurrence of element x; high susceptibility represents cells where the combination of memberships results in a large final membership value (i.e. close to 1), while low susceptibility represents those with small final values (i.e. close to 0). This combining of individual memberships is known as *aggregation* and requires the user to determine how the memberships are combined to produce a meaningful output. Again, different types of fuzzy overlay are available within GIS to accommodate the most common combination styles. These are *fuzzy AND, fuzzy OR, fuzzy Product, fuzzy Sum,* and *fuzzy Gamma* (Bonham-Carter, 1994). *Fuzzy AND* returns the minimum value of all the sets

that the cell belongs to and is useful for identifying the lowest common denominator for the membership of all input data.

$$fuzzyAND = min(A,B,C,\ldots,n) \tag{4.4}$$

Fuzzy OR is the opposite of *fuzzy AND*, returning the maximum value of all the sets the cell belongs to. This is useful for identifying the highest membership value for any of the input criteria.

$$fuzzyOR = max(A,B,C,\ldots,n) \tag{4.5}$$

Fuzzy Product multiplies the fuzzy values for all input criteria in each cell and thus the output value will be less than any of the input values. It effectively assumes that the combination of multiple sets reduces the overall susceptibility of a cell to the occurrence of x and thus is not often used.

$$fuzzyProduct = \prod_{i=A,B,C,\ldots}^{n} (A,B,C,\ldots,n) \tag{4.6}$$

Fuzzy Sum is the opposite of *fuzzy Product* and thus returns output values higher than any of the input values. In this case it assumes that the combination of sets increases the overall susceptibility to the occurrence of x and thus, like *fuzzy Product*, is not often used.

$$fuzzySum = 1 - \prod_{i=A,B,C,\ldots}^{n} (A,B,C,\ldots,n) \tag{4.7}$$

Fuzzy Gamma is the product of the *fuzzy Product* and *fuzzy Sum* both raised to the power of some value, γ, between 0 and 1. It is thus a compromise between *fuzzy Product* and *fuzzy Sum* and effectively establishes the relationship between the various membership sets. *Fuzzy Gamma* is therefore the most appropriate method for analysing susceptibility for natural phenomena.

$$fuzzyGamma = (1 - \prod_{i=A,B,C,\ldots}^{n} (A,B,C,\ldots,n))^{\gamma} \cdot (\prod_{i=A,B,C,\ldots}^{n} (A,B,C,\ldots,n))^{1-\gamma} \tag{4.8}$$

Selection of γ is user-defined with a value of 1 returning the same output as *fuzzy Sum* and a value of 0 returning the same as *fuzzy Product*. Values in-between effectively represent how much relative importance is given to those factors favouring the occurrence of x. Values closer to 1 give a higher importance to favourable memberships while values closer to 0 give higher importance to unfavourable memberships. Appropriate outputs should produce relatively small areas of high susceptibility values corresponding to observed occurrences of x. It is not appropriate to achieve low susceptibility values for known locations of x or areas of high susceptibility very much larger than the area affected by x. Values of $\sim$0.9 are

most typical for γ and Kritikos (2013) showed that such a value provides the best trade-off between ensuring relatively high susceptibilities in locations where x occurs and relatively low susceptibilities where x does not. γ values >0.9 achieve very high susceptibilities in all locations due to the higher weighting of favourable memberships, thus over-predicting the overall susceptibility of the entire area. γ values $<<0.9$ do not produce high values even at known locations of x due to the weighting for unfavourable memberships and therefore under-predict overall susceptibility.

4.4 Coseismic landslide datasets

In order to identify those factors (or sets in fuzzy logic) that influence landsliding across multiple environments, substantially complete landslide inventories from the 1994 Northridge and 2008 Wenchuan earthquake have been statistically analysed in GIS. The resulting fuzzy memberships have then been tested on the 1999 Chi-Chi earthquake in order to test their applicability to other, unrelated environments. Below are brief descriptions of these earthquake events and the associated landslide inventories.

4.4.1 Northridge earthquake

The 1994 M_w6.7 Northridge earthquake occurred 30 km north of the Los Angeles basin beneath the city of Northridge in the San Fernando Valley, Southern California (**Fig. 4.3**). Slip occurred along a 14 km long section of a 42° south dipping blind thrust fault (Wald and Heaton, 1994). The earthquake had a focal depth of 18 km, however little to no slip was detected within 7 km of the surface and consequently no surface rupture occurred. Peak slip was estimated at $\sim$4 m and average slip is thought to have been $\sim$1.2 m. The rate of tectonic deformation in the region is relatively high with shortening rates estimated at 7-10 mm/a within 30 km of the epicentre (Donnellan et al., 1993). Consequently, the region has high seismicity with 15 M$>$4.8 earthquakes occurring in the greater Los Angeles area between 1920 and 1994 including the 1971 M_w7.1 San Fernando earthquake (Hauksson et al., 1995).

Despite being centred in the San Fernando Valley, the earthquake generated strong shaking intensities (up to MM 9) throughout the surrounding Santa Susana Mountains (**Fig. 4.3**). These mountains are bounded by the Santa Ynez fault to the south and the plate boundary San Andreas fault to the north, with many other active faults within the ranges. As a result $>$11,000 landslides were generated across an area of $\sim$10,000 km^2 with the most distant located 70 km from the epicentre (Harp and Jibson, 1996). Nevertheless, a distinct 1,000 km^2 zone north-west of the epicentre represents the region of most concentrated landsliding

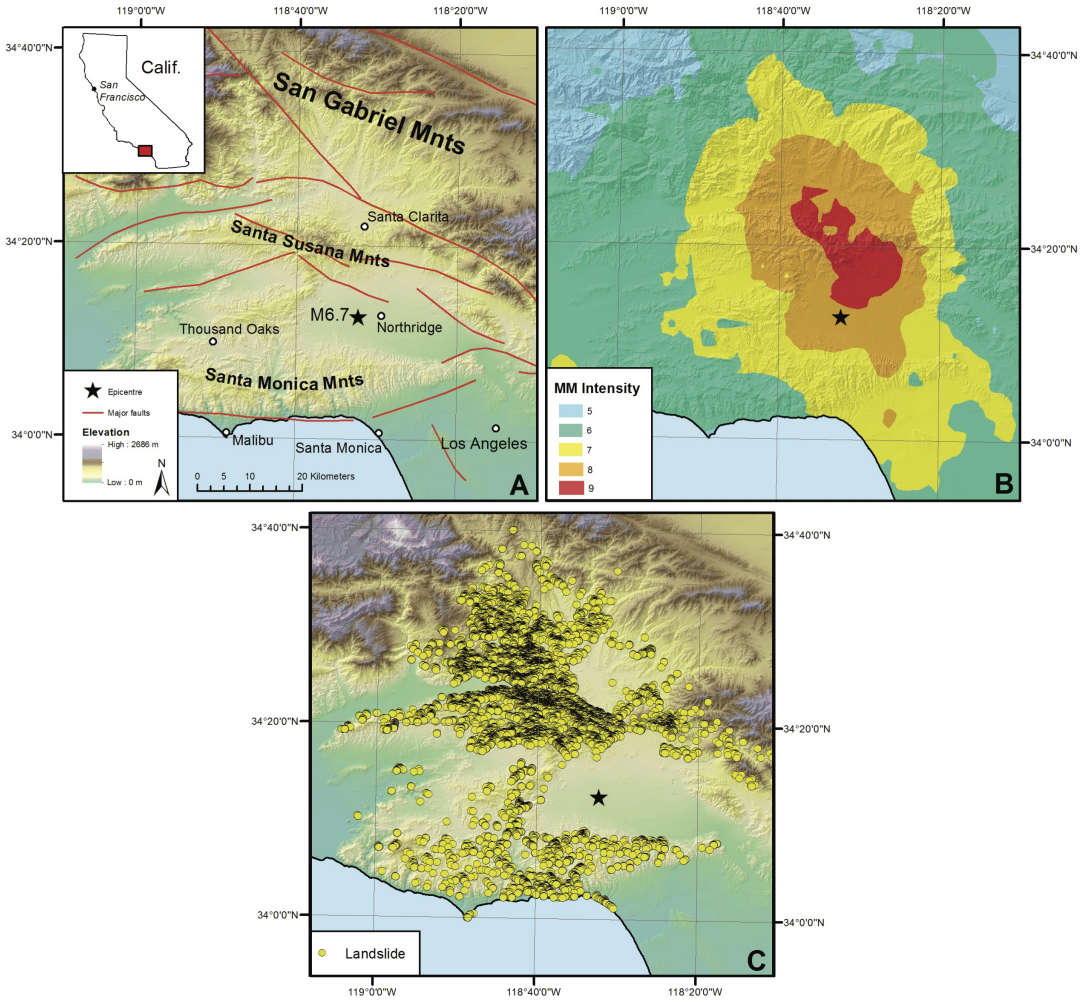

Figure 4.3: The 1994 M_w6.7 Northridge earthquake. a) Location map; b) Shaking intensity and epicentre location; and c) coseismic landslide locations.

(**Fig. 4.3**). Fortunately, landslide-related damage was minor due to a combination of the generally small volume of the landslides and the sparse population of the affected area; however there were some road blockages and disrupted services (Harp and Jibson, 1996).

This event was the first to have a digital landslide inventory compiled using remote sensing imagery and GIS (Xu, 2014). A substantially complete landslide inventory containing 11,111 landslides was compiled immediately after the event and is currently freely available from the USGS. The inventory was compiled via a combination of high-altitude aerial photographs collected within hours of the initial earthquake, and field investigations which lasted several days beginning the day after the event (Harp and Jibson, 1996).

4.4.2 Wenchuan earthquake

The 2008 Wenchuan earthquake occurred in the Longmen Shan mountains of Sichuan Province, eastern China (**Fig. 4.4**). The causative Yingxiu-Beichuan fault is one of three major faults in the Longmen Shan fault zone which accommodate both dip-slip and dextral strike-slip motion (Densmore et al., 2007). As a result, the earthquake involved oblique thrust motion along a >320 km north-west dipping fault (Xu et al., 2009). Rupture originated at a focal depth of 14-19 km and propagated unilaterally towards the north-east, with surface rupture present along the entire fault length. Maximum vertical displacements were measured at 4.5 m while dextral displacements reached 6.2 m (Gorum et al., 2011). The region has a slow slip rate with <1 mm/a dextral slip and an estimated shortening rate of <3 mm/a (Shen et al., 2009). Consequently, prior to 2008, only 66 major earthquakes are known to have occurred in the region since 638 CE, the largest of which was a M_s7.2 in 1976 (Li et al., 2009).

The Longmen Shan mountains are characterised by extreme relief with elevations up to 7,500 m asl. The mountains are bounded on the south-eastern side by a combination of the Yingxiu-Beichuan and Pengguan faults, with the major Wenchuan-Maoxian and Qingchuan faults within the ranges. The earthquake generated MM 9 ground shaking along nearly its entire rupture length with shaking above MM 6 affecting an area of nearly 100,000 km^2 (**Fig. 4.4**). As a result, Xu et al. (2013) suggested up to 200,000 landslides may have formed although several more conservative estimates put this number closer to ∼60,000 (Gorum et al., 2011; Li et al., 2014; Parker et al., 2011). Up to a third of the estimated 88,000 fatalities are thought to have resulted from landsliding (Wang et al., 2009).

Following the event, numerous studies of the landsliding were undertaken and various inventories have been compiled (see Gorum et al., 2011; Li et al., 2014; Parker et al., 2011; Xu et al., 2013). In the present study an inventory of 60,109 landslides identified from high resolution satellite images and air photos was kindly provided by Gorum et al. (2011) (**Fig. 4.4**). The images from which this inventory is derived were flown in the weeks following the event and therefore may include some landslides resulting from strong aftershocks between the mainshock and the image collection. However, these are thought to be few in number.

4.4.3 Chi-Chi earthquake

The 1999 M_w7.7 Chi-Chi earthquake was centred 7.5 km beneath the town of Chi-Chi in central Taiwan (**Fig. 4.5**). The earthquake had a highly complex source, rupturing over 100 km along the Chelungpu fault in a series of jumping dislocations (Shin and Teng, 2001).

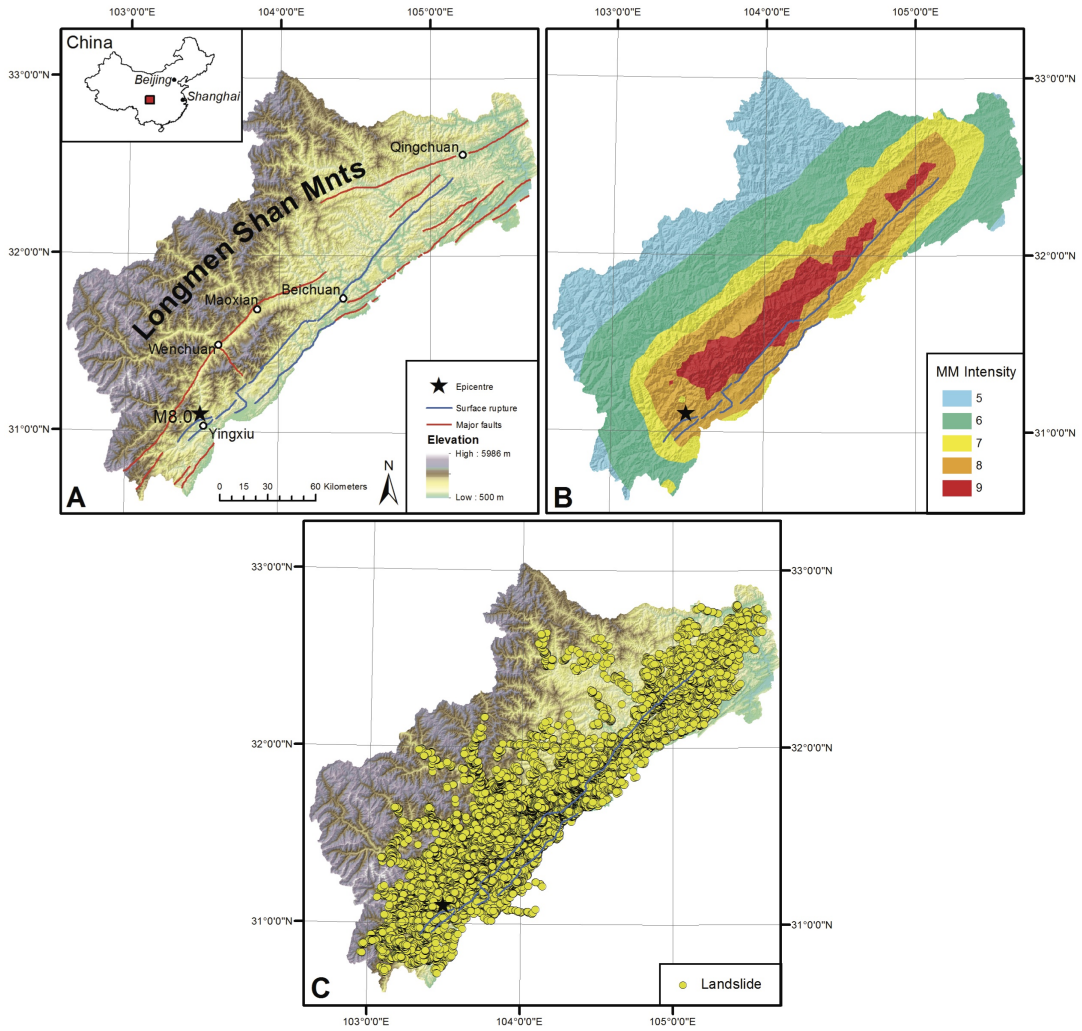

Figure 4.4: The 2008 M_w8.0 Wenchuan earthquake. a) Location map; b) Shaking intensity and epicentre location; and c) coseismic landslide locations.

Furthermore, the rupture surface was non-planar, with numerous changes in strike. Generally the fault had north-south strike and a 30° eastward dip (Chi et al., 2001). Thrust motion predominated with maximum surface displacements of ∼8 m, however the complex fault trace resulted in multiple styles of motion including oblique slip (Chi et al., 2001; Shin and Teng, 2001). The region is tectonically complex, with eastward subduction of the Eurasian plate beneath the Philippine Sea plate in the south-to-southwest, and northward subduction of the Philippine Sea plate beneath the Eurasian plate to the north (Angelier et al., 1986). As a result, the region has an extremely high seismicity rate with ∼80 mm/a shortening (Yu et al., 1997) and at least 17 damaging earthquakes during the 20th century.

The Chelungpu fault marks the boundary between the central mountains of Taiwan and

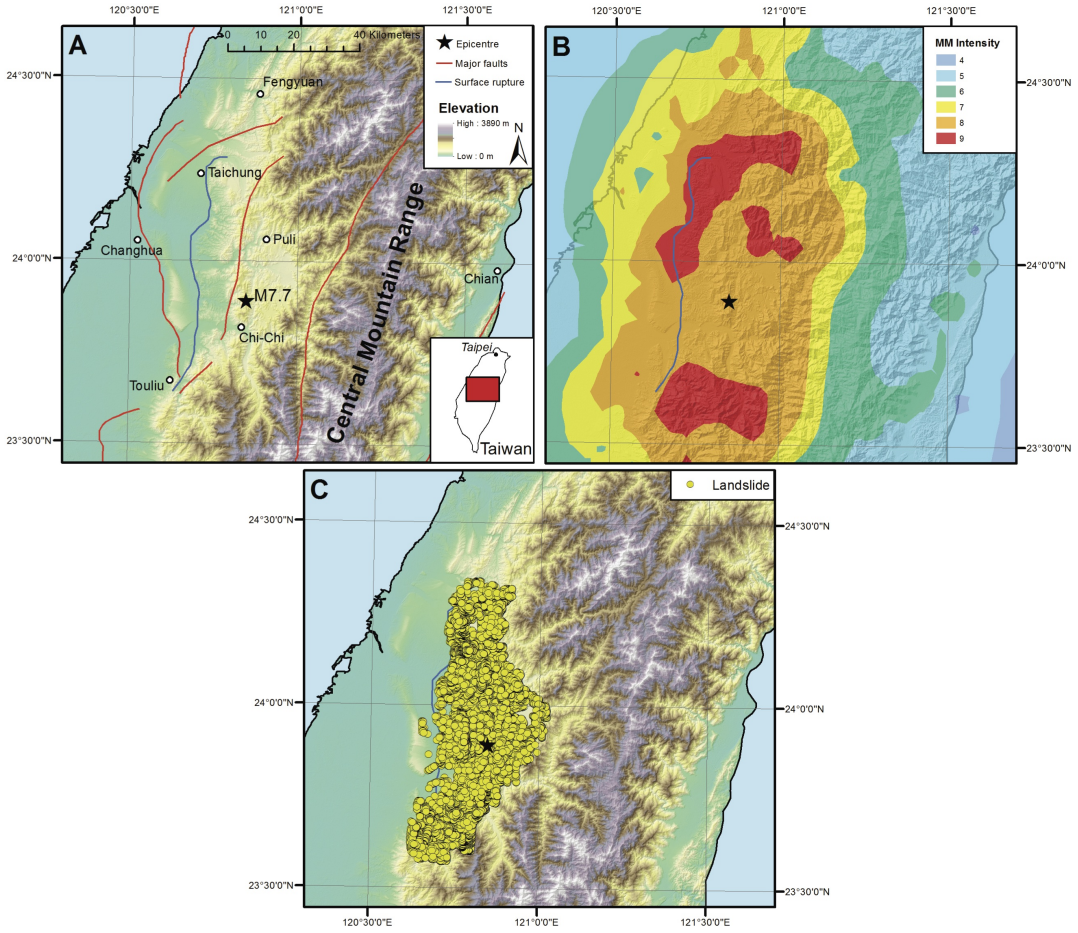

Figure 4.5: The 1999 M_w7.7 Chi-Chi earthquake. a) Location map; b) Shaking intensity and epicentre location; and c) coseismic landslide locations.

the coastal plains (**Fig. 4.5**). The large magnitude of the earthquake resulted in very strong shaking intensities across a large area with MM 8 covering an area >4,000 km^2 and MM 9 occurring at the surface rupture extremities and extending ∼25 km into the Central Mountain Range (**Fig. 4.5**). As a result the earthquake generated >22,000 landslides with the majority occurring across a 3,000 km^2 region (**Fig. 4.5**; Dadson et al. 2004). Most of the landslides were shallow debris slides, and a large amount of landslide debris was subsequently reactivated as devastating debris flows in ensuing typhoons (Lin et al., 2003). There were also at least two very large rock avalanches that occurred and resulted in a total of 78 fatalities (Chigira et al., 2003).

The landslide inventory used herein was kindly provided by Prof. Hongey Chen of the National Taiwan University. It was compiled from comparison of pre- and post-earthquake aerial and satellite images and contains a total of 21,969 landslides. Various other invento-

ries are also available which contain similar numbers (see Lin et al., 2003) suggesting the inventory included in this study is substantially complete.

4.5 Inventory analysis and modelling

The approach taken in this research is based on the hypothesis that those factors which control the regional distribution of coseismic landsliding should be similar for all earthquakes across similar geotectonic environments. In order to identify those factors, this research does not consider local factors such as lithology, vegetation cover/type, soil moisture, etc., as these cannot be applied across multiple locations. Those regionally important factors have been identified using the Northridge and Wenchuan inventories. Fuzzy memberships are then developed for each factor and aggregated using the *fuzzy Gamma* overlay for both earthquakes. The resulting spatial distribution of susceptibility is evaluated to test the model's success. To do this, both inventories in Wenchuan and Northridge are randomly split into two datasets; one acted as a training dataset from which factors are identified, and the other acted as a test dataset on which no statistical analysis has occurred, to evaluate the success of the resulting fuzzy memberships. This provides a test of the model's predictive capability rather than how well it fits the (training) data, known as goodness of fit (Chung et al., 1995; Remondo et al., 2003a). Finally, the derived fuzzy memberships are applied to the Chi-Chi earthquake to establish how applicable they are beyond the Northridge and Wenchuan environments. Below are detailed descriptions of each of these phases.

4.5.1 Factor identification

There are two types of factors which define landslide susceptibility: conditioning (intrinsic) factors which contribute to a location's susceptibility; and triggering (extrinsic) factors which may cause a landslide to occur in a given, already susceptible location. For coseismic landslides, the triggering factor is strong ground motion, measured either quantitatively as, for example, peak ground acceleration (PGA), or qualitatively as, for example, MM intensity. Conditioning factors include slope angle, slope aspect, distance from active faults, and distance from streams, amongst many others. To identify which of these factors control the spatial distribution of landslides in multiple environments, numerous factors are analysed to establish how variations within those factors affect the frequency ratio of landsliding. For example, to establish the effect of slope angle, a slope map is derived and classified into various slope angle classes for which the variation in landslide frequency ratio is then assessed. The results are then compared across both the Northridge and Wenchuan events to identify which

factors show a good degree of correlation. For those which correlate well fuzzy memberships are developed, while those which do no correlate are inferred to have only local effects and are therefore not considered further.

Triggering factor

To test which measure of ground shaking is most appropriate for modelling, both MM intensity and PGA were examined. Interestingly, PGA values did not appear to have a strong influence on the occurrence of landsliding compared to MM intensity, particularly in the Northridge event (**Fig. 4.6**). However, a strong degree of correlation was observed across both the Northridge and Wenchuan events for MM intensity, with stronger intensities resulting in higher landslide occurrences. The lowest shaking intensity inducing landslides was MM 5, in accordance with numerous observations from other historic events (see Keefer, 1984), and as intensity increased the frequency ratio in both events increased almost exponentially (**Fig. 4.6**). Such a result is not unsurprising as ground shaking is the triggering factor and thus it is expected that more landslides will occur with stronger shaking intensities.

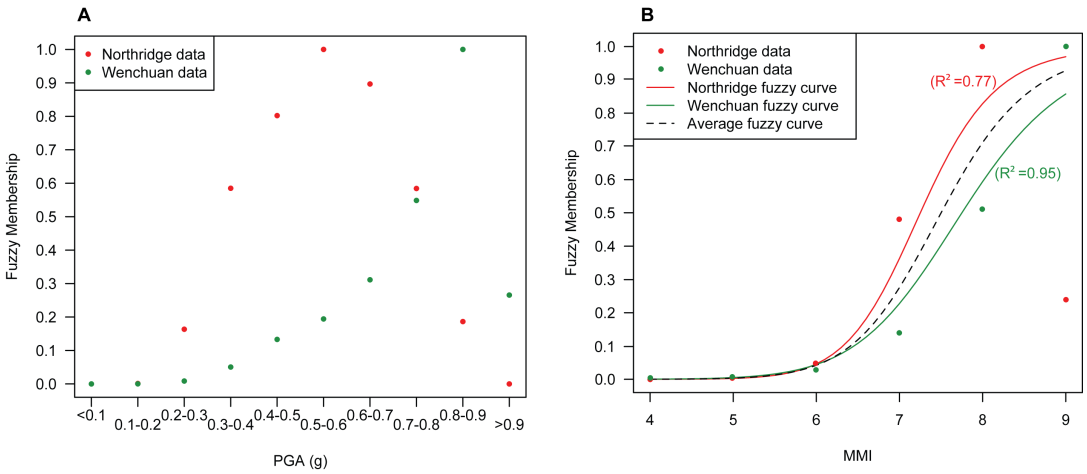

Figure 4.6: Landslide occurrence with respect to ground shaking in Northridge and Wenchuan: a) PGA (g) showing a gaussian distribution in Northridge compared to a large distribution in Wenchuan; and b) MM intensity showing strong correlation with large distribution and the resulting derived best-fit earthquake specific and average fuzzy memberships. Note: for MM 4 and 5 both events have frequency ratios very close to 0.

Conditioning factors

At a regional scale, conditioning factors are generally related to the topography of the region, although other non-topographic factors also play a role (see below). Thus a key component

of identifying various conditioning factors is an accurate DEM. The resolution of the DEMs used should be identical in both study areas to ensure consistency between the factors being analysed. Selecting the resolution of the DEM involves a trade-off between the desired level of detail and computational processing times. In this research 60 m DEMs have been used as these provide a good level of accuracy without involving long processing times. Where the base DEM was of higher resolution it has been re-sampled to 60 m.

Slope angle

Slope gradient is generally considered to be the most critical conditioning factor regardless of triggering mechanism. The greater downslope component of gravity at steeper slopes results in increased gravity-induced shear stress and lower friction because slope-normal stresses are reduced in slope material increasing its susceptibility to failure. This was seen in both events, with frequency ratio increasing at similar rates as slope angle increased (**Fig. 4.7**). Interestingly, a reduction in frequency ratio is observed in Northridge for slopes $>45°$ which is not seen in Wenchuan. This likely does not represent some physical process in Northridge increasing the stability of steeper slopes; instead it is likely a result of only $\sim$6% of slopes $>45°$ occurring in >MM 6 intensity zones. Thus the steepest slopes in Northridge were not exposed to strong enough shaking intensities to trigger significant landsliding; MM 6 corresponds to a membership value of <0.1 therefore making the likelihood of landslides being triggered relatively small.

Active faults

The presence of active faults generally reduces the strength of a rock mass primarily by damage during earthquakes (Brune, 2001; Dramis and Sorriso-Valvo, 1994; Kellogg, 2001); however, other weakening mechanisms such as fault-related gully-slip systems (Korup, 2004a) or groundwater infiltration and geochemical alterations (Warr and Cox, 2001) also play a role. The result is that material close to active faults is strongly primed for future failure (Petley, 2012). Thus, frequency ratio was predictably highest immediately adjacent (<5 km) to active faults in both environments (**Fig. 4.7**). In Northridge a greater density of active faults resulted in no landslides occurring at distances >20 km while in Wenchuan landslides were observed at distances >50 km. Nevertheless, beyond 30 km the frequency ratio in Wenchuan is very close to 0 (**Fig. 4.7**) and thus has virtually no effect on the membership shape.

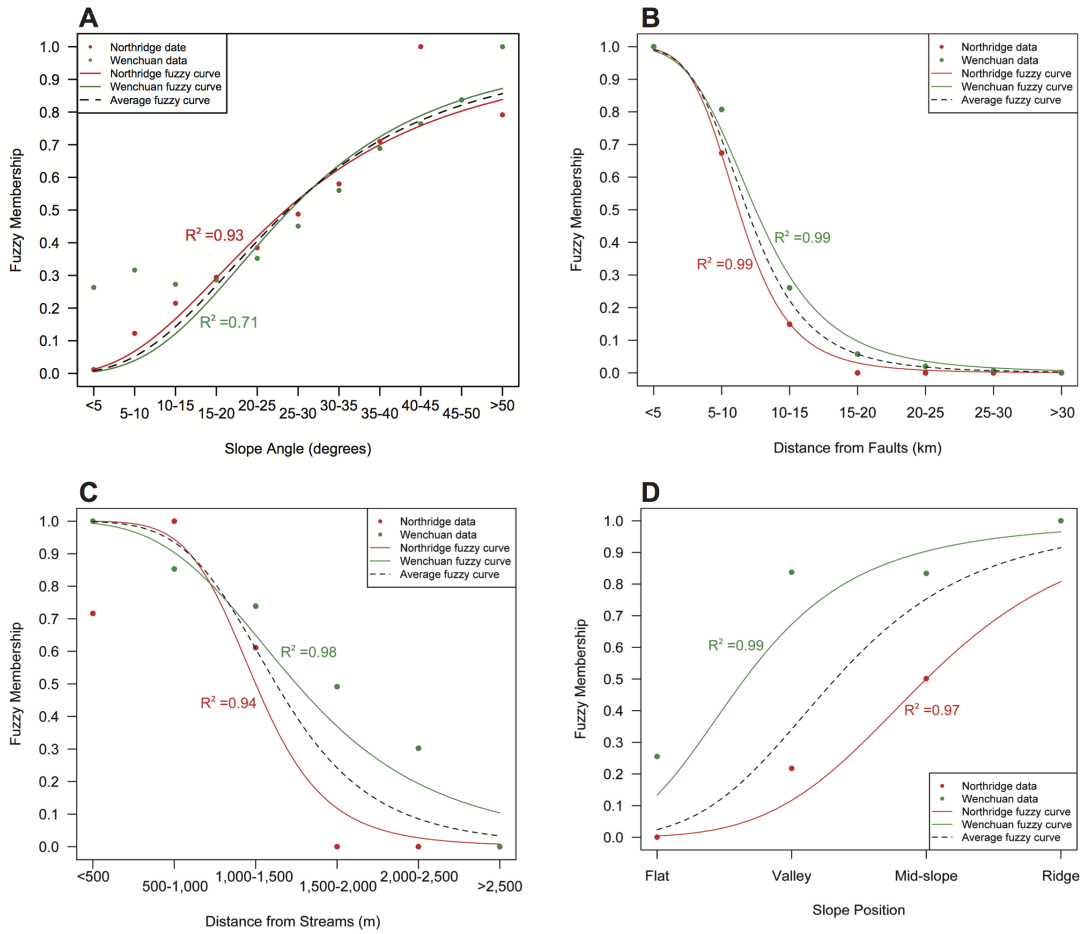

Figure 4.7: Normalised frequency ratio data and associated earthquake specific and averaged fuzzy memberships for a) slope angle, b) distance from faults, c) distance from streams, and d) slope position.

River systems

The role of river channel incision on hillslope processes and landscape evolution has been discussed in numerous studies (see Korup, 2004a; Larsen and Montgomery, 2012; Snyder et al., 2000; Whipple, 2004). Fluvial undercutting, causing high shear stress due to loss of lateral support, has been identified as a key mechanism of slope instability (Korup, 2004a). Therefore, proximity to drainage networks has been used as a factor in many landslide susceptibility studies as a conditioning factor (Akgun and Bulut, 2007; Akgun et al., 2008; Lee and Sambath, 2006; Süzen and Doyuran, 2004). Thus various drainage-related localised processes increasing failure susceptibility (see Dai et al., 2001; Donati and Turrini, 2002; He and Beighley, 2008) are incorporated. This effect is most pronounced in Wenchuan where frequency ratio decreases with distance from stream channels (**Fig. 4.7**). The increase in fre-

quency ratio in Northridge at distances of 500-1,000 m is of note however. The extent of shaking intensity does not explain this difference as it is relatively evenly distributed across each stream distance category. However, >30% of the 500-1,000 m category has slopes >25°, while >80% of the <500 m category has slopes <20° which may explain the increase in frequency ratio. Slopes <20° have a membership value of <0.3 while slopes >25° have values >0.5 thus having a notable effect on the relative likelihood of landslide occurrence.

Slope position

Amplification of seismic waves by topography, known as topographic amplification, is thought to be a key contributor to landslide occurrences (Buech et al., 2010). Thus, identifying different slope positions is potentially a key factor in the spatial distribution of landslides. Buech et al. (2010) showed that ground motions were most notably amplified on mountain ridges, thereby promoting failure at these locations compared to mid-slopes. A few studies have attempted to model the effect of slope position at a regional scale (Lee et al., 2008, 2009). By adapting the Topographic Position Index (TPI) of Weiss (2001) it is possible to establish four distinct slope positions: flat ground, valley, mid-slope, and ridge. As expected, in both the Northridge and Wenchuan events the highest frequency ratios were observed at mountain ridges and the lowest on flat plains, where frequency ratios were virtually 0 (**Fig. 4.7**). Interestingly however, in Wenchuan, valley bottoms had an equal effect to mid-slopes. This is likely a result of many lateral spreads (which occur predominantly at river banks in valleys) being included in the inventory and thus increasing the effect of valley bottoms.

Other factors

Other factors that were investigated included slope aspect, slope curvature, elevation, and distance from epicentre (**Fig. 4.8**). Slope aspect did show definite changes in frequency ratio with different aspect directions, however this could not be correlated across both events. Northridge appeared to show a *fuzzy large* distribution as slope aspect rotated from north facing to approximately southwest-to-west facing slopes; however Wenchuan showed *fuzzy gaussian* distribution around east-to-south facing slopes (**Fig. 4.8a**). A better measure of slope aspect is likely to be slope orientation compared to direction to source, however this requires complex modelling of wave propagation which is beyond the scope of this study. Slope curvature did appear to demonstrate correlation across both events, however there was very little change between concave and convex slopes with both shapes producing similar frequency ratios (**Fig. 4.8b**). Further, curvature is evaluated at a multi-pixel level and thus results for individual pixels may not be representative of the slope as a whole. Thus curvature

is inferred to have little impact on landslide occurrence other than that flat slope faces are less likely to produce landslides than curved slopes. Elevation showed no correlation across either event; Northridge had a *fuzzy small* distribution with highest frequency ratio on slopes 250-500 m asl, while Wenchuan had *fuzzy gaussian* distribution with highest values recorded on slopes 1,500-2,500 m asl (**Fig. 4.8c**). Finally, distance from epicentre did show good correlation and had a very definite *fuzzy small* distribution (**Fig. 4.8d**). However, this is effectively mimicking shaking intensity which on a regional level decreases with distance from epicentre for point source earthquakes, or fault rupture for finite-source earthquakes. Thus including distance from epicentre will regionally have the same effect as MM intensity and is therefore deemed unnecessary.

Thus only MM intensity, slope angle, distance from faults and streams, and slope position are expected to control the regional spatial distribution of landslides with similar effects across multiple environments. These are the factors which will therefore be used to model landsliding in other regions.

4.5.2 Fuzzy memberships and fuzzy overlay

For each of the five identified controlling factors, three different fuzzy memberships have been developed: Northridge specific, Wenchuan specific, and average memberships (**Figs. 4.7**). In order to remove subjectivity from the development of the region-specific fuzzy memberships, these have been fitted using the coefficient of determination (R^2). Due to the strong correlation across both events in each factor, the region-specific memberships, and therefore the resulting averaged memberships, are, as expected, similar. The only noticeable difference is in slope position, perhaps reflecting that this effect is less well-defined than the other factors (**Figs. 4.7**).

Each of the memberships is user-defined, allowing for known errors and inconsistencies within the data. For instance, in Wenchuan there is a notable increase in landslide occurrence on very low slope angles ($<10°$). Gorum et al. (2011) suggest this is a result of specifically mapping lateral spreads on river banks which don't appear to be included in the Northridge inventory. Thus when fitting the fuzzy membership to the Wenchuan data greater weight has been given to those observations on steeper slope angles (i.e. not containing lateral spreads) to better correspond with the Northridge data, resulting in a relatively low R^2 value (0.7). If the two lowest slope angle categories are not included in the best-fit calculations, the R^2 for the Wenchuan specific membership increases to $\sim$0.9, a much more appropriate value.

Two different susceptibility maps are then created for each location: one using the memberships derived specifically for the corresponding location, and one using the averaged mem-

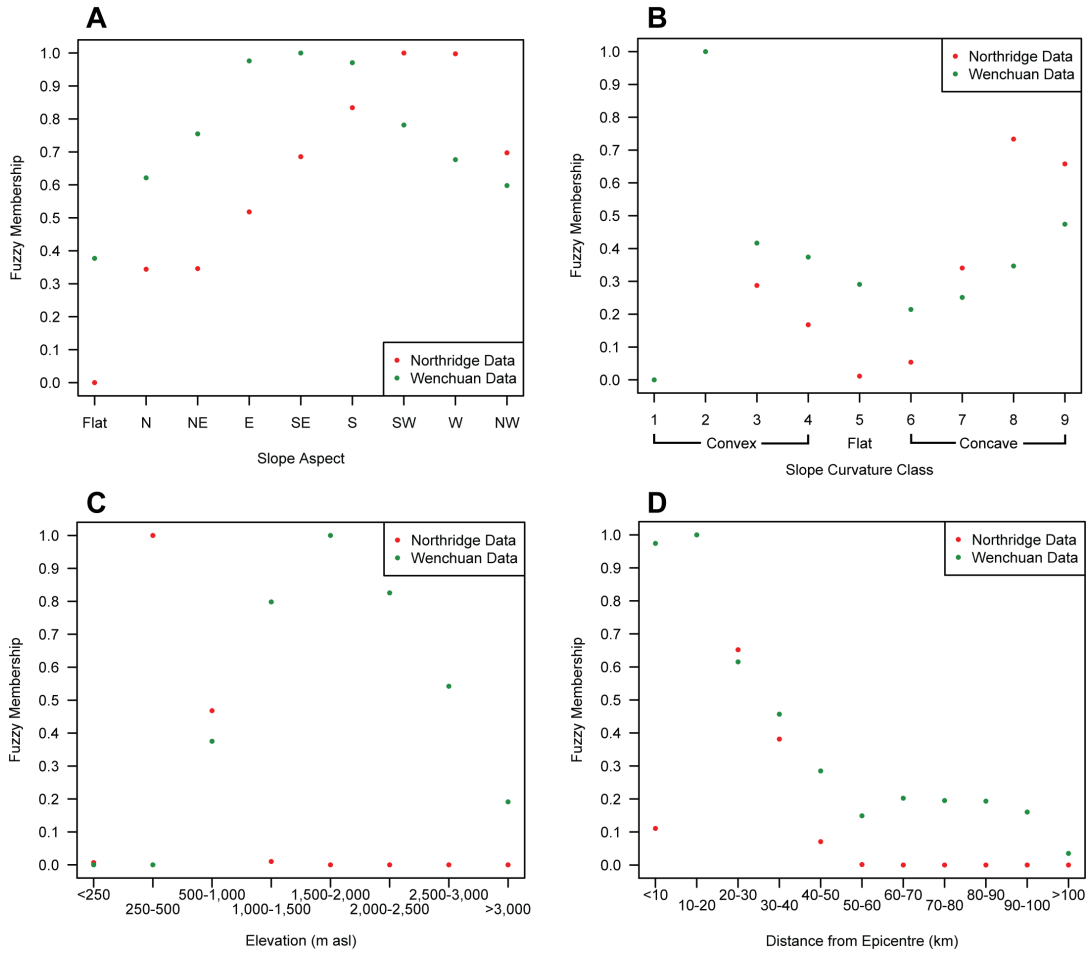

Figure 4.8: Normalised frequency ratio data for a) slope aspect, b) slope curvature, c) elevation and d) distance from epicentre.

berships. To develop these susceptibility maps, each of the fuzzy memberships is aggregated using the *fuzzy Gamma* operator with $\gamma = 0.9$. The results for each event can then be compared to identify any differences between using the specific memberships and the averaged memberships (**Fig. 4.9**). Qualitatively, there appears to be very little difference between either model in both locations. This is expected as there is very little difference between the specific and averaged memberships as a result of the strong correlation across both events. Nevertheless, quantitative evaluation is required to confirm the applicability and success of each set of membership functions.

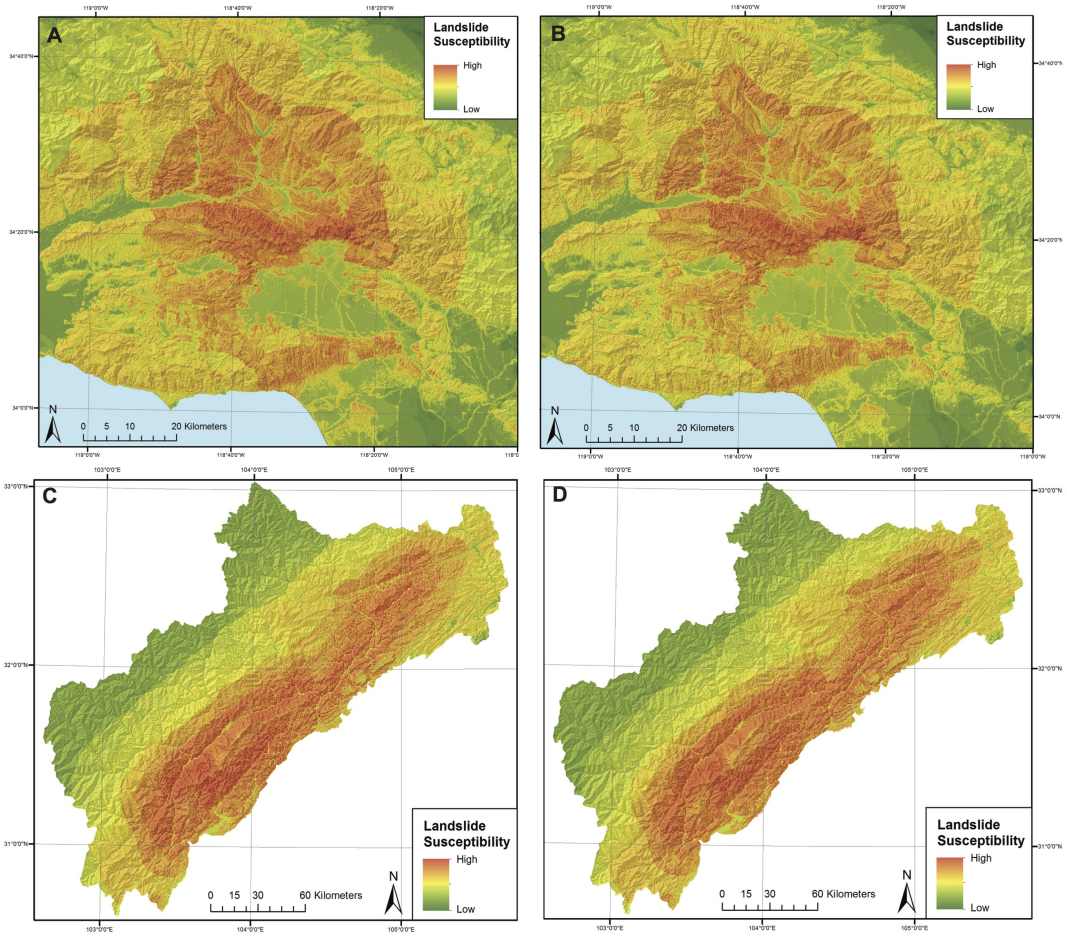

Figure 4.9: Coseismic landslide susceptibility maps for Northridge from a) earthquake specific and b) average memberships, and for Wenchuan from c) earthquake specific and d) averaged memberships.

4.5.3 Model evaluation

The aim of model evaluation is: a) to assess how successfully the fuzzy memberships and aggregation process represent the spatial probability of landslide occurrence; and b) to demonstrate that no meaningful loss in accuracy occurs between the earthquake-specific and average susceptibility maps. The most commonly applied technique for quantitative evaluation is the construction of success rate curves (Chung and Fabbri, 1999; Frattini et al., 2010; Remondo et al., 2003a; van Western et al., 2003). This is based on a comparison between the spatial distribution of landslides and modelled susceptibility. Success rate curves measure the cumulative percentage of landslides against the cumulative percentage of susceptibility area, from highest susceptibility to lowest (Guzzetti et al., 2006; Remondo et al., 2003a). To be successful, the majority of landslides should be modelled by a relatively small area of high susceptibility; a model achieving 100% success would model all landslides in the area represented by the highest 1% of susceptibility. Such a graph would have an area under the curve (AUC) of 1; thus achieving AUC values close to 1 demonstrates a successful model. Generally, AUC values $>$0.7 are considered successful, with values $<$0.7 approaching totally random performance. AUC values $>$0.8 represent good model performance, while values $>$0.9 are considered excellent.

The success rate curves for Northridge and Wenchuan have been developed using the test datasets which were not used in factor identification. This confirms whether the memberships accurately model landslides whose spatial distribution is effectively unknown (predictive ability rather than goodness of fit). In Northridge the earthquake specific memberships result in $\sim$85% of landslides from that event occurring in the area representing the highest 20% of susceptibility, corresponding to an AUC of 0.909 (**Fig. 4.10**). In Wenchuan the earthquake specific memberships result in $\sim$73% of landslides in the highest 20% of susceptibility, giving an AUC of 0.843 (**Fig. 4.10**). Using the averaged memberships the success curves demonstrate AUC values of 0.904 and 0.839 for Northridge and Wenchuan respectively (**Fig. 4.10**). This demonstrates that the method is applicable and highly successful and, furthermore, that the averaged memberships result in no meaningful loss in model accuracy. However, an external, independent assessment is required to confirm these memberships are applicable to other regions.

4.5.4 External analysis

Applying the derived average fuzzy membership curves to another earthquake, for which no data on the factors controlling spatial distribution of landslides have been collected, is in-

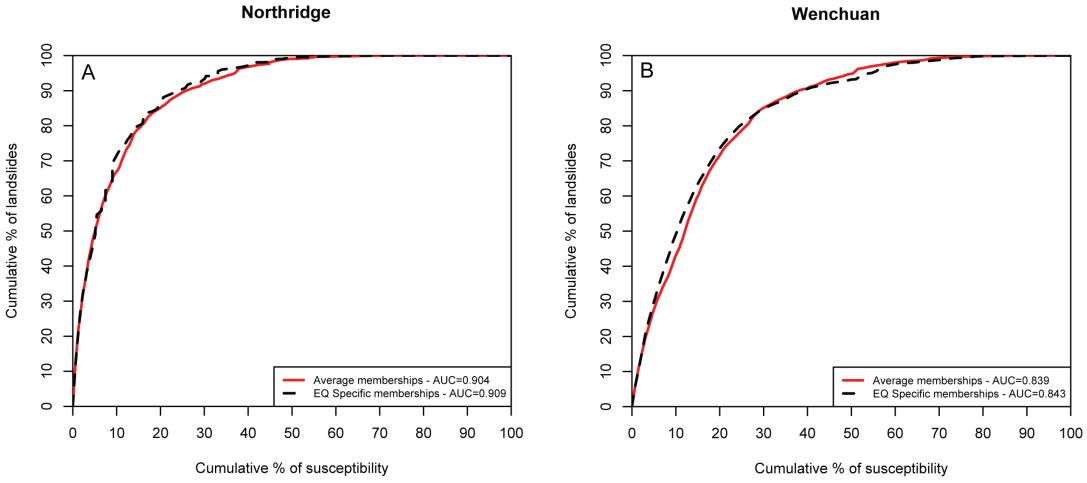

Figure 4.10: Success rate curves of the earthquake specific and average membership functions for the a) Northridge and b) Wenchuan earthquakes.

tended to demonstrate that the five factors established from Northridge and Wenchuan are also applicable to other (similarly geotectonic) environments. To establish this, the average memberships should be able to accurately model the spatial distribution of landslides from another event with a success rate >0.7, and ideally >0.8. This tests whether coseismic landsliding processes are the same globally, and whether the Northridge and Wenchuan earthquakes are representative examples.

To do this, the 1999 Chi-Chi earthquake has been modelled. The distribution of slope angles, streams, and slope positions has been derived from the 60 m ASTER DEM, isoseismals have been digitised from the USGS (USGS, 2014), and active faults are located from Shyu et al. (2005). These factors are subsequently classified into the same-sized categories as Northridge and Wenchuan and modelled using the derived average fuzzy memberships and the *fuzzy Gamma* overlay ($\gamma = 0.9$). The resulting susceptibility map (**Fig. 4.11**) qualitatively appears to be a good match to the observed landslide distributions (**Fig. 4.5c**). As before, plotting success rate curves show that ~90% of landslides occur in the highest 20% of susceptibility, corresponding to an AUC of 0.924 (**Fig. 4.12**). This equates to excellent model performance and is significantly larger than the 0.7 minimum required value and the 0.8 desired value. Furthermore, the success rate for Chi-Chi is higher than that seen for both Northridge and Wenchuan, suggesting the data from Chi-Chi is more accurately fit by the average fuzzy memberships than either of these events.

This confirms that those controlling factors identified from Northridge and Wenchuan appear also to be the dominant control on the spatial distribution of coseismic landslides at Chi-Chi. Thus, identifying these factors and establishing appropriate averaged fuzzy mem-

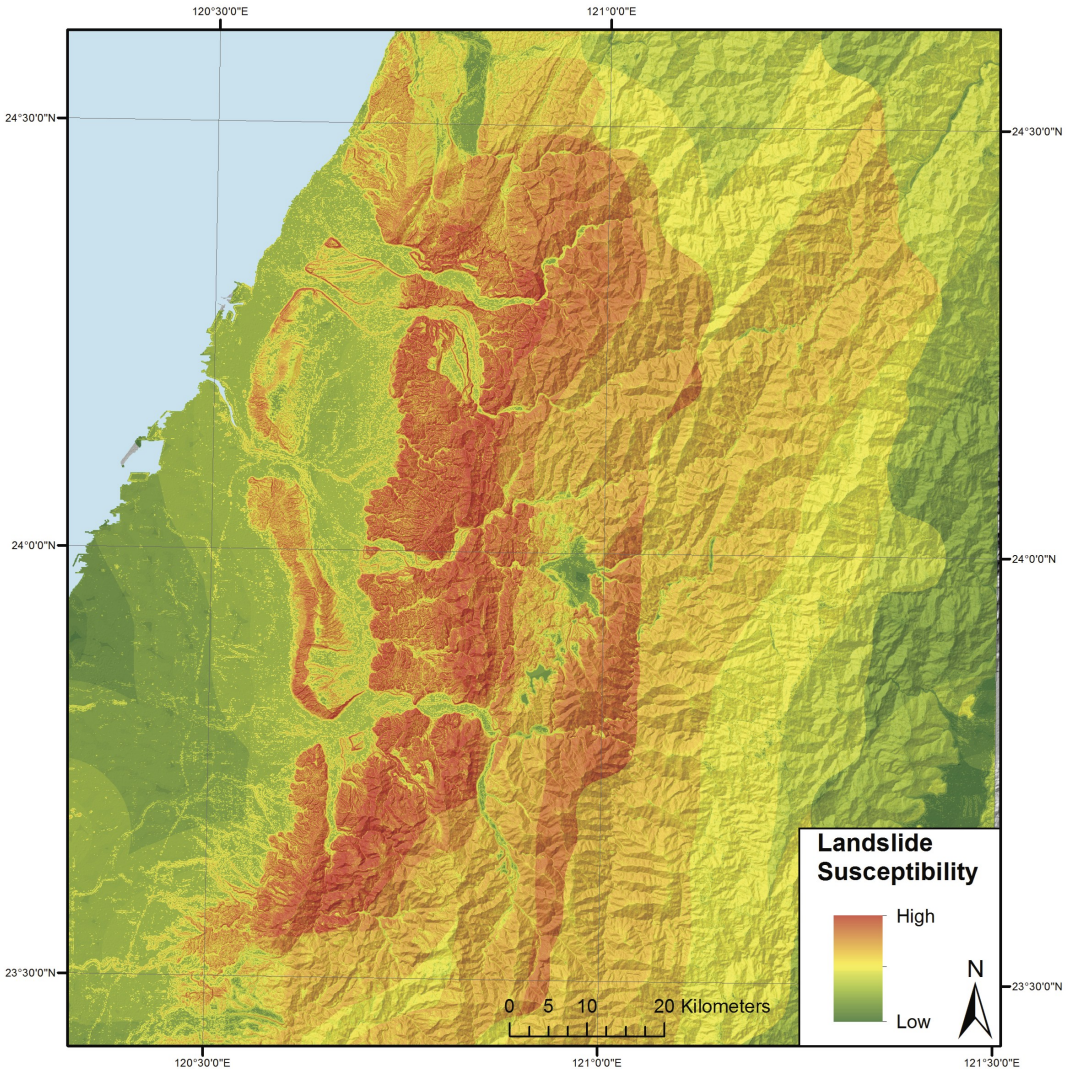

Figure 4.11: Modelled coseismic landslide susceptibility for the 1999 Chi-Chi earthquake.

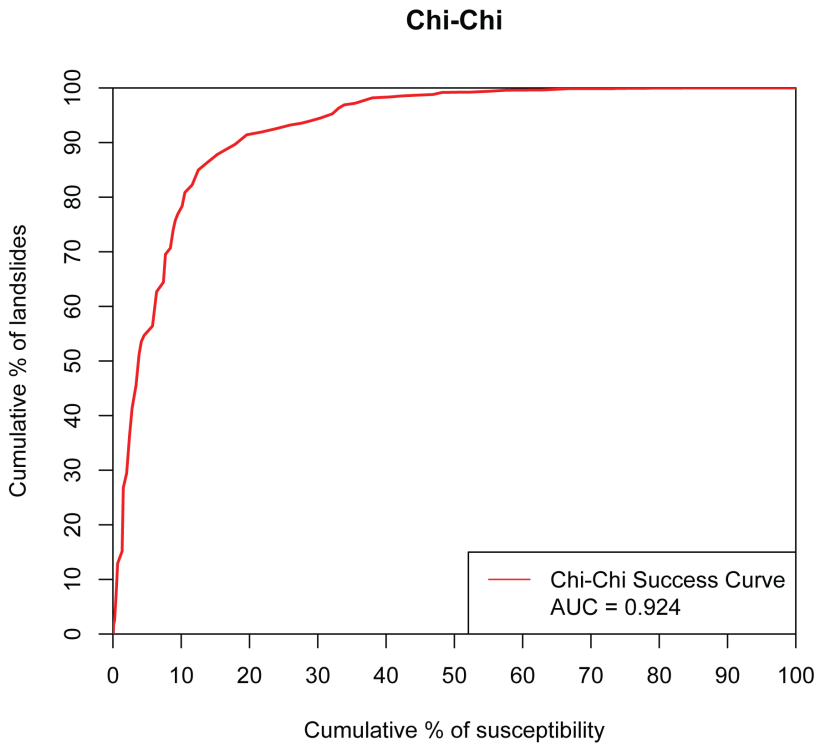

Figure 4.12: Success rate curve for the Chi-Chi earthquake.

berships allows coseismic landslide susceptibility to be modelled for a given earthquake in other geotectonic environments similar to Northridge and Wenchuan.

4.6 Discussion

The spatial distribution of landslides in a given geotectonic environment (i.e. a non-glaciated, fault-bounded mountain system) can be accurately modelled by fuzzy memberships derived from other similar geotectonic environments. This suggests that regional coseismic landslide spatial distribution is dominantly controlled by ground shaking, active tectonics, and topography. Local factors such as lithology, vegetation cover/type, soil moisture etc. appear to have only a minor influence; if such factors played a dominant role it should not be possible to achieve accurate models without their inclusion. This is important for hazard analysis in mountainous regions lacking coseismic landslide data, where previously such detailed modelling was not possible (e.g. the Southern Alps). Demonstrating that it is possible to model susceptibility in a region by using data derived from other regions may allow accurate modelling in those places where it has not previously been possible.

Currently, this model can only be assumed to apply to those geotectonic environments

similar to Wenchuan, Northridge, and Chi-Chi, as it cannot be assumed that spatial distribution in different geotectonic environments is controlled to the same degree by the factors included, or indeed by the same factors themselves. The applicable environment is defined as being a primarily non-glaciated, fault-bounded mountainous region such as the Southern Alps of New Zealand, the Basin and Range in western USA, or the Zagros Mountains in Iran. It is not known how applicable the model is for heavily-glaciated environments such as Alaska or the Karakorum Himalayas. The presence of large glaciers and thick ice accumulation zones may fundamentally alter those factors which control spatial distribution (see McColl et al., 2012). Performing the above analysis on historic coseismic landslide inventories from earthquakes in such regions (e.g. the 2002 Denali earthquake) should therefore be investigated to establish their applicability.

Thus, despite the very high success rate achieved in Chi-Chi, this model needs to be tested and evaluated on a variety of other historic earthquake scenarios. This will conclusively test the model's applicability and also identify if these user-defined memberships are specific to fault-bounded mountainous settings or are in fact more widely applicable. Further analysis of the frequency ratios of other inventories should also be undertaken to fully develop the average fuzzy memberships which currently are derived from just two events. The high success rate for Chi-Chi suggests that the frequency ratios of landslides for each factor in this event must be very close to the average memberships; if there were significant differences the model would not have achieved such a high success rate. This is confirmed by analysing the landslide dataset with respect to each of the five factors. MM intensity, distance from faults, and distance from streams produce expectedly high R^2 values ($>$0.94) while slope position produces reasonable results ($>$0.7).

However, slope angle does not conform to this trend; the highest frequency ratios occur on slopes 20-25° and decrease as slope angle increases. This is in stark contrast to what is expected and to the observations of Khazai and Sitar (2003) who showed that 90% of landslides in Chi-Chi occurred on slopes $>$45°. However, their observations were based on field data while the present data have been analysed from a 60 m DEM. In a 60 m DEM, slopes with angles $>$45° must have a downslope length of $>$60 m to be resolved, otherwise the slope angle will be averaged across the pixel resulting in a smaller angle (**Fig. 4.13**). The area affected by landslides in the Chi-Chi event was generally at low elevation with $\sim$50% of landslides occurring on slopes $<$500 m asl. Local relief in this region was also relatively small with valley bottoms having elevations of $\sim$200 m asl. Thus most of the steep slopes which initiated landslides (Khazai and Sitar, 2003) are unlikely to have downslope lengths sufficient enough to be resolved on a 60 m DEM; field photographs from Khazai and Sitar (2003)

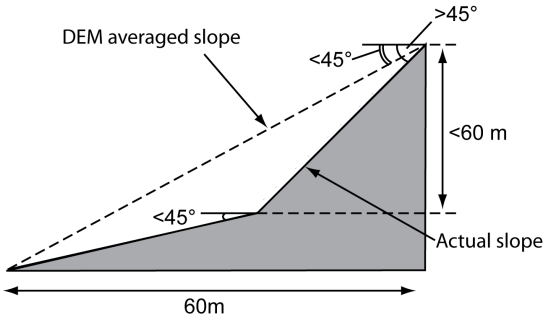

Figure 4.13: Schematic view of the effect of coarse scale (60 m) pixel resolution on slope angles. This effect causes increased frequency ratio of shallow slopes and decreased on steep slopes in Chi-Chi.

appear to confirm this. Thus frequency ratio will be artificially increased on shallow slopes and decreased on steep slopes. Nevertheless, excellent model results were still achieved for Chi-Chi demonstrating that combining multiple factors is able to effectively resolve issues such as this and suggests the method is robust.

As with all GIS-based statistical methods, this model is particularly sensitive to the quality and accuracy of the landslide inventories and the input information layers (i.e. the DEM). The quality of the inventory, which depends on the accuracy of landslide mapping, is crucial to both training and evaluation stages as the spatial correlation between landslides and factor categories is the fundamental component of the modelling approach. For the Wenchuan inventory it is notable that the inventory used herein contains $\sim$60,000 landslides compared to the inventory of Xu et al. (2013) which contains $>$190,000 landslides. Using an inventory which is not substantially complete may result in frequency ratios that are not representative of the complete inventory, thus resulting in incorrect fuzzy memberships. Nevertheless, multiple other inventories compiled for this event agree with Gorum et al. (2011) that the total number of landslides for this event was $\sim$60,000 (see Li et al., 2014; Parker et al., 2011). No other study to-date has found the number of landslides in Wenchuan to be substantially larger than 60,000 and thus this work does not consider the Xu et al. (2013) inventory to be correct.

A final limitation stems from the over-simplification of input data. For instance, the influence of topographic amplification is based on the TPI (Weiss, 2001) to classify the landscape into various slope positions. This is a very simplified method to model an extremely complex process and does not take into account other factors such as resonant frequencies or orientation compared to seismic wave motion, for example. Further, TPI is a scale-dependent parameter, defining slope position based on changes in slope gradient in surrounding pixels. Finer pixel sizes will therefore be able to better resolve slope positions; in some instances in the Northridge and Wenchuan models, ridges are observed adjacent to valleys with no

mid-slope between as the 60 m pixel size is not fine enough to identify constant slope angles (mid-slopes). This may explain why the effect of slope position appears relatively less defined than other factors. However, finer resolution DEMs are not necessarily applicable for regional scale analysis as the computational processing time involved increases dramatically.

4.7 Conclusions

Despite the existence of several methods for the assessment of slope stability during earthquakes, regional-scale coseismic landslide susceptibility analysis remains a top research priority, especially in regions lacking historic landslide inventories and geotechnical data. Herein a new approach for such analysis is presented based upon fuzzy logic in GIS. Statistical analysis of the Northridge and Wenchuan coseismic landslide inventories has shown that five factors (MM intensity, slope angle, distance from faults and streams, and slope position) are dominant in controlling the spatial distribution of landslides. Based on the frequency ratio of landslide occurrence within these factors, user-defined fuzzy memberships are developed and aggregated to produce susceptibility maps for both earthquakes. These models have shown good-to-excellent model performance and have thus been applied to an external event, the Chi-Chi earthquake, for which no statistical analysis of the controlling factors was performed. For this event the model achieved a success rate of 0.924 corresponding to excellent model performance and demonstrating that this method is able to accurately model landslide susceptibility even in regions where no data has been included (i.e. where no data exists). Thus applying this model to areas anticipating future large seismic events with associated landsliding provides a possible method to better quantify the landslide hazard than any currently available. Such applications are likely to yield a greater level of understanding of the entire earthquake-related hazard and thus result in increased societal awareness and, potentially, resilience.

Chapter 5

Coseismic landsliding estimates for an Alpine fault earthquake and the effects on river systems

5.1 Introduction

Landsliding in the Southern Alps is a potential hazard at all times, regardless of cause. Nevertheless, the high seismicity of the region means that large (>M7) earthquakes are common, with 10 recorded since European settlement, most of which have generated widespread landsliding across large areas (**Table 2.1**). The Alpine fault is the longest fault in the South Island, stretching for >400 km along the western edge of the Southern Alps (**Fig. 2.1**) and is thought to be capable of generating M_w8.0+ earthquakes (Adams, 1980b; Berryman et al., 2012a; Cooper and Norris, 1990; De Pascale and Langridge, 2012; De Pascale et al., 2014; Hull and Berryman, 1986; Sutherland et al., 2007; Sutherland and Norris, 1995). Geologic evidence from previous ruptures suggests that earthquakes on this fault have resulted in large-scale landsliding within the Southern Alps, with some suggesting that erosion due to the event exceeds inter-sesimic erosion (Howarth et al., 2012). However, to date, accurately assessing the likely scale of landsliding from a future rupture has been limited to simplistic and imprecise empirical relationships, as outlined in Chapter 2. As current estimates suggest that the Alpine fault is close to its average recurrence interval, and within the error margin (Berryman et al., 2012a), accurately assessing the scale of landsliding likely to result from rupture of the fault is urgent and vital to understanding the true hazard posed by an Alpine fault earthquake.

Previously, estimating coseismic landslide susceptibility has required either detailed geotechnical data or substantially complete historic coseismic landslide inventories for the study

region. No such data exist for the Southern Alps, and consequently detailed regional coseismic landslide assessments have proved elusive. The method established in Chapter 4 however, demonstrates that it is possible to accurately model coseismic landslide susceptibility for a region with no such data by utilising historic landslide inventories in other similar environments. Applying this method to a scenario earthquake on the Alpine fault should enable detailed and accurate modelling of the resulting landslide susceptibility. However, despite the method showing good success in modelling susceptibility in Taiwan, it has yet to be shown to be successful in New Zealand. Thus before it can be applied to an Alpine fault earthquake, it must first be shown to be able to successfully model historic coseismic landslide occurrences in New Zealand.

Coseismic landsliding is an important process in landscape evolution; Li et al. (2014) showed that during the Wenchuan earthquake, the total volume of landslide debris produced was comparable to that of the volume of rock uplifted by the earthquake. Subsequent fluvial remobilisation of this landslide material can have dramatic consequences in the form of aggradation on alluvial fans and floodplains and the infilling of reservoirs as seen in Wenchuan and Chi-Chi. Landsliding in large earthquakes therefore plays an important role in the erosion of active mountain ranges and the evolution of active alluvial fans both within and outside the mountain range. Assessing the potential scale of landsliding likely to occur from an anticipated earthquake is therefore a vital component of pre-disaster hazard assessments and of understanding landscape evolution processes.

This chapter will present strong evidence that landsliding following two earthquakes in Fiordland in 2003 and 2009 can be modelled successfully using the method developed in Chapter 4. The method is then applied to a scenario earthquake on the Alpine fault (see Chapter 2 and 3) to estimate the scale and spatial distribution of landsliding likely to result from this event. The total number and volume of landslides are estimated using observations from the three inventories presented in Chapter 4 and the two Fiordland earthquakes presented herein. Finally, the potential scale of erosion and aggradation likely to result from an Alpine fault earthquake is estimated for some of the South Island's major river systems.

5.2 Background erosion rates in the Southern Alps

As a result of the rapid uplift along the range-bounding Alpine fault, the Southern Alps are some of the fastest-eroding mountains on earth. Regional erosion rates match uplift (up to 12 mm/a; Norris and Cooper 2001), suggesting the Southern Alps are in an overall dynamic equilibrium (Adams, 1980a; Wellman, 1979). Consequently, west-draining river catchments

typically drain far smaller areas than east-draining catchments: the average catchment area for order 6 or higher west-draining rivers is ∼1,300 km^2 compared to ∼4,500 km^2 for east draining catchments (**Fig. 5.1**). Stream order is a measure of a river's branching complexity with larger numbers corresponding to larger, more powerful rivers. Stream order effectively measures the scale of upstream inputs; combining two first-order streams forms a second-order stream, two second-order streams form a third-order stream etc.

In total, using the National Institute for Water and Atmospheric Research (NIWA) River Environment Classification (REC) system, there are 36 river catchments of order 6 or above draining >70% of the South Island, with an almost even split between east-draining and west-draining rivers (**Fig. 5.1**). As a result the Southern Alps form tall, steep mountains with deeply incised river valleys. By contrast, Fiordland to the south has a much lower uplift and erosion (<1 mm/a) and consequently consists of lower mountains with high vertical cliffs and spectacularly-glaciated valley systems.

The NIWA suspended sediment yield (SSY) model (**Fig. 5.1**; NIWA, 2014) shows that erosion is highest in the central Southern Alps where annual rainfall is extremely high (Hicks et al., 1996) and uplift rates are at a maximum. Suspended sediment is estimated to account for ∼50% of total river sediment capacity (Davies and McSaveney, 2006). Thus, the total amount of material removed annually can be estimated by converting SSY, measured in tonnes/a (t/a), into sediment volume S_V:

$$S_V = \frac{2SSY}{\rho} \tag{5.1}$$

where ρ is the density of suspended sediment in t/m^3, inferred to be close to 2.5 t/m^3, corresponding to the densities of schist and greywacke which comprise the majority of the Southern Alps and therefore contribute the majority of suspended sediment.

Total annual denudation in the central Southern Alps is up to 1 cm/a for west-draining catchments. Outside the central Southern Alps, erosion rates are substantially lower, reaching a minimum of <0.01cm/a (**Table 5.1**). Howarth et al. (2012, 2014) showed that these background erosion rates persisted for ∼250 years between earthquakes, with a >40 year 'pulse' of increased sediment yield following each major earthquake, suggesting that substantial erosion occurs in the major river catchments as a result of Alpine fault earthquakes.

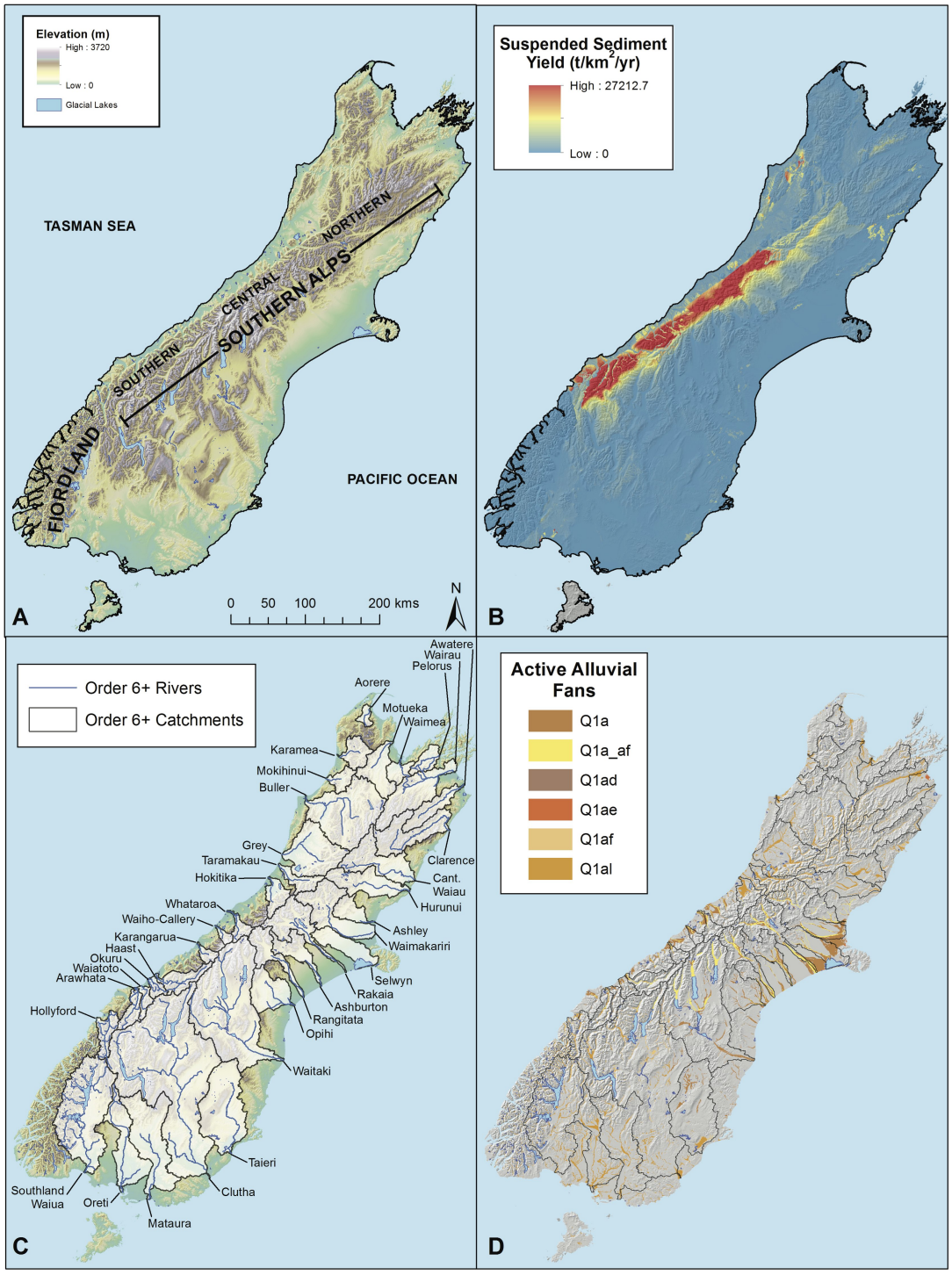

Figure 5.1: a) Overview of the Southern Alps and Fiordland within the South Island; b) erosion rates in the form of suspended sediment yield (from NIWA); c) major (order 6+) river catchments; and d) active alluvial fans of major river systems - see Rattenbury and Isaac (2012) for rock unit descriptions.

Table 5.1: Annual suspended sediment yield (SSY) and resulting denudation for the South Island order 6 or greater river catchments.

Catchment	Catchment Area (km^2)	Alluvial Fan area (km^2)	SSY (Mt/a)	Denudation (cm/a)
Aorere	365.4	14.7	3.6	0.01
Arawhata	930.6	83.2	729.1	0.69
Ashburton	1,600.0	83.2	31.2	0.02
Ashley	1,149.8	93.6	8.4	0.01
Awatere	1,574.5	79.5	20.2	0.01
Buller	6,379.6	378.7	282.5	0.04
Clarence	3,300.7	184.3	64.8	0.02
Clutha	20,608.3	1,240.0	904.5	0.04
Grey	3,948.8	466.6	236.6	0.05
Haast	1,355.6	84.5	595.1	0.37
Hokitika	1,066.6	200.0	632.9	0.58
Hollyford	1,129.9	192.5	199.1	0.17
Hurunui	2,669.4	246.2	105.1	0.03
Karamea	1,211.7	41.9	14.9	0.01
Karangarua	408.2	27.4	249.9	0.53
Mataura	5,357.8	381.9	69.1	0.01
Mokihinui	751.4	22.7	28.5	0.03
Motueka	2,058.0	84.2	34.6	0.01
Okuru	467.9	45.7	312.0	0.59
Opihi	2,375.9	210.0	16.3	0.01
Oreti	3,513.2	516.6	26.0	0.01
Pelorus	891.1	25.4	23.7	0.02
Rakaia	2,830.4	445.1	451.0	0.15
Rangitata	1,816.1	298.6	162.7	0.09
Selwyn	2,027.1	415.4	14.4	0.01
Taieri	5,702.8	366.8	32.6	$<$0.01
Taramakau	1,002.9	186.7	219.4	0.22
Waiatoto	529.1	39.1	428.6	0.70
Waiau (Canterbury)	3,330.7	382.0	280.6	0.08
Waiau (Southland)	8,217.2	814.8	128.8	0.01
Waiho-Callery	290.3	58.4	340.4	1.17

Table 5.1 – continued from previous page

Catchment	Catchment Area (km^2)	Alluvial Fan area (km^2)	SSY (Mt/a)	Denudation (cm/a)
Waimakariri	3,608.9	589.1	314.3	0.08
Waimea	771.1	52.6	10.9	0.01
Wairau	3,582.0	318.6	80.8	0.02
Waitaki	11,887.7	820.3	334.0	0.02
Whataroa	593.5	65.3	483.5	0.73

5.3 Methods

5.3.1 Coseismic landslide modelling

Assuming the processes controlling the spatial distribution of coseismic landsliding in New Zealand are the same as those in Northridge, Wenchuan, and Chi-Chi, the fuzzy memberships and modelling process outlined in Chapter 4 should achieve similarly accurate results when applied to a modelled Alpine fault earthquake. To ensure that these memberships are applicable to New Zealand, they are first applied to two earthquakes in Fiordland in 2003 and 2009 for which landslide inventories are available. These inventories have not been used for traditional statistical analysis (see Lee et al., 2008; Miles and Keefer, 2000) as the number of landslides produced ($\sim$400 and $\sim$200 respectively) are relatively small compared to the tens of thousands included in the inventories in Chapter 4, making statistical analysis of the controlling factors less robust. Nevertheless, they are sufficient for testing the applicability of the fuzzy memberships.

The Fiordland earthquakes

The epicentre of the 2003 M_w7.2 Fiordland earthquake was at the mouth of Thompson Sound near Secretary Island (**Fig. 5.2**) at a depth of $\sim$20 km (Hancox et al., 2003; Power et al., 2005). The earthquake generated a maximum of MM 9 shaking primarily in the uninhabited region west of Lake Te Anau, although MM 6-7 shaking did cause some damage in Te Anau 80 km away (**Fig. 5.2**). As a result, $>$400 landslides were initiated in a region extending 20-30 km from the main fault rupture zone (**Fig. 5.2**; Hancox et al. 2003). Most of these occurred on slopes of 35-60° or more and ranged in volume from a few cubic metres to a maximum of $\sim$700,000 m^3. One landslide fell into Charles Sound and caused a tsunami with maximum wave run-up of 4-5 m above high tide level, damaging a helipad and wharf (Power

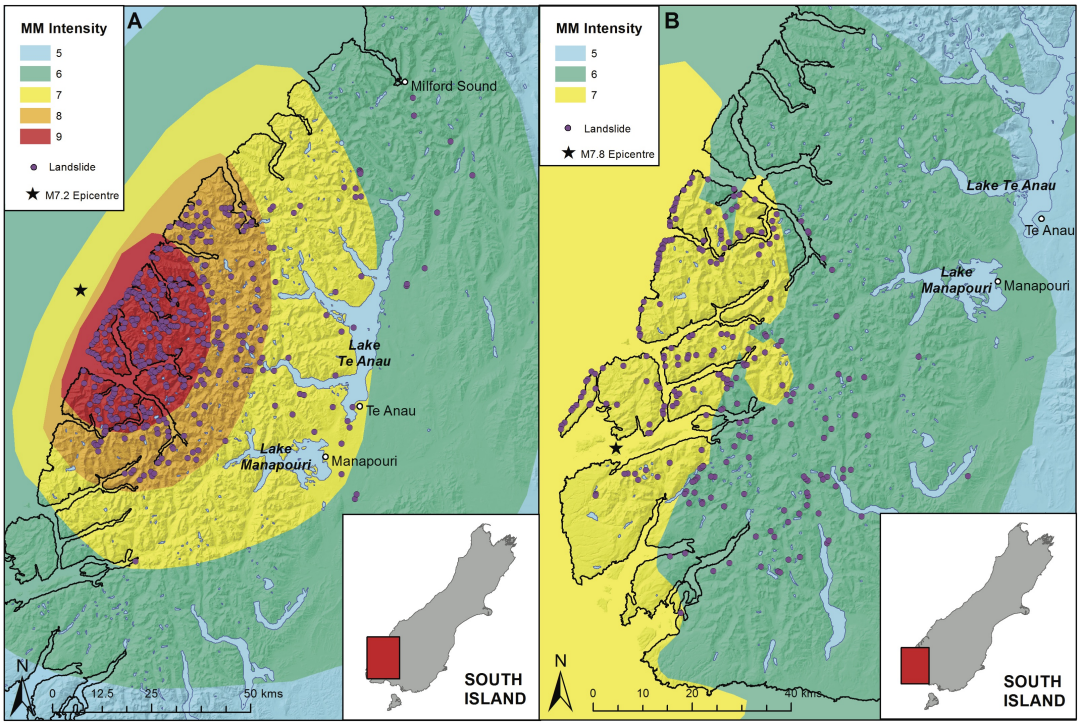

Figure 5.2: Extent of landsliding and shaking intensity from the a) 2003 M_w7.2 Fiordland earthquake and b) 2009 M_w7.8 Fiordland earthquake.

et al., 2005).

The epicentre of the 2009 M_w7.8 Fiordland earthquake was at the mouth of Dusky Sound on the Puysegur subduction zone (**Fig. 5.2**) at a depth of ∼30 km, with rupture propagating up-dip to a depth of ∼15 km (Fry et al., 2010). Despite its large magnitude, the event generated far lower onshore shaking intensities than the smaller 2003 event: MM 7 compared with MM 9 (**Fig. 5.2**). This is thought to have resulted from a combination of the oceanward rupture directivity (i.e. up-dip) and a relatively small amount of radiated seismic energy (Fry et al., 2010). Consequently, the earthquake produced far fewer landslides (∼200) than the 2003 event (**Fig. 5.2**).

Modelling results

Application of the average fuzzy memberships derived in Chapter 4 resulted in the susceptibility maps shown in **Fig. 5.3** for the Fiordland earthquakes. High (≥0.7) susceptibility for the 2003 event covers ∼2,300 km^2 while for the 2009 event it covers an area of ∼1,000 km^2. This confirms the results of other authors (see Keefer, 1984) that shaking intensity is a more relevant indicator of coseismic landslide occurrence than earthquake magnitude. Ac-

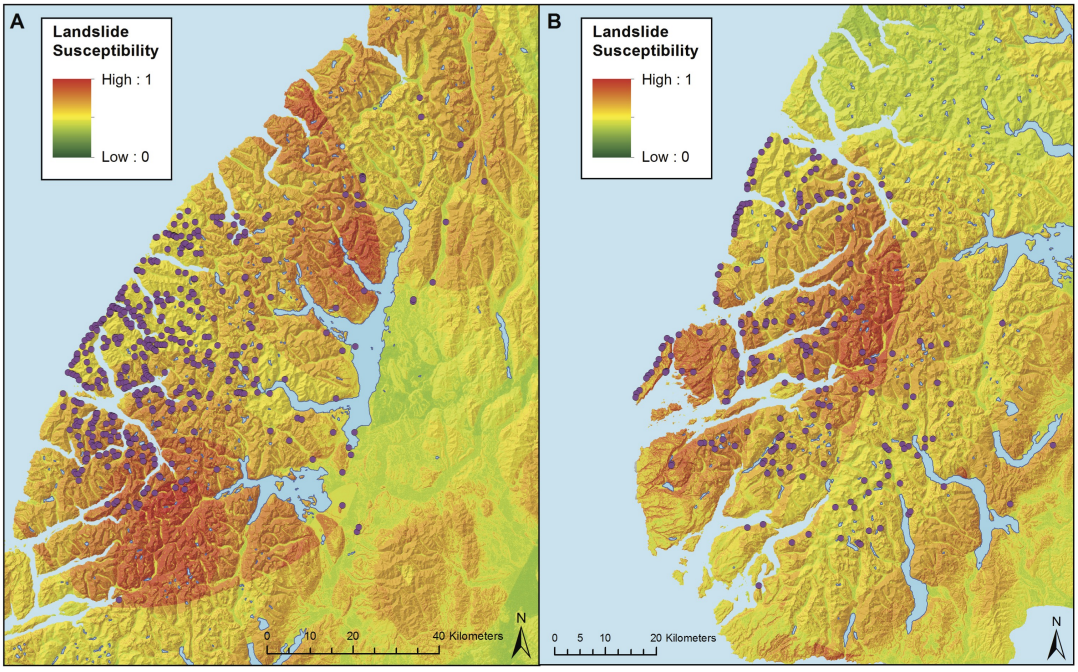

Figure 5.3: Fuzzy logic-derived susceptibility maps for the a) 2003 and b) 2009 Fiordland earthquakes. Mapped landslides indicated as dots.

curate modelling of intensities for future events is therefore essential for useful susceptibility modelling.

Quantitative assessment via success curves for each event confirms that this method is applicable to the New Zealand environment (**Fig. 5.4**). For the 2003 Fiordland earthquake the model estimates 43% of landslides in the 20% highest susceptibility values, corresponding to an acceptable but low AUC of 0.749. The model achieves a much higher success rate for the 2009 event, with 93% of landslides in the highest 20% of susceptibility giving an AUC of 0.912. Thus, each model has exceeded the minimum success rate of 0.7, with the 2009 event achieving excellent model performance. This further establishes the appropriateness of the fuzzy membership models in Chapter 4 and confirms their applicability to the New Zealand environment.

5.3.2 Deriving the scale of landsliding

Total landslide number

Calculating the total number of landslides likely to occur directly from the spatial distribution of susceptibility is difficult, as susceptibility does not determine whether a landslide will occur, only its relative likelihood. Analysing susceptibility maps developed for historic events

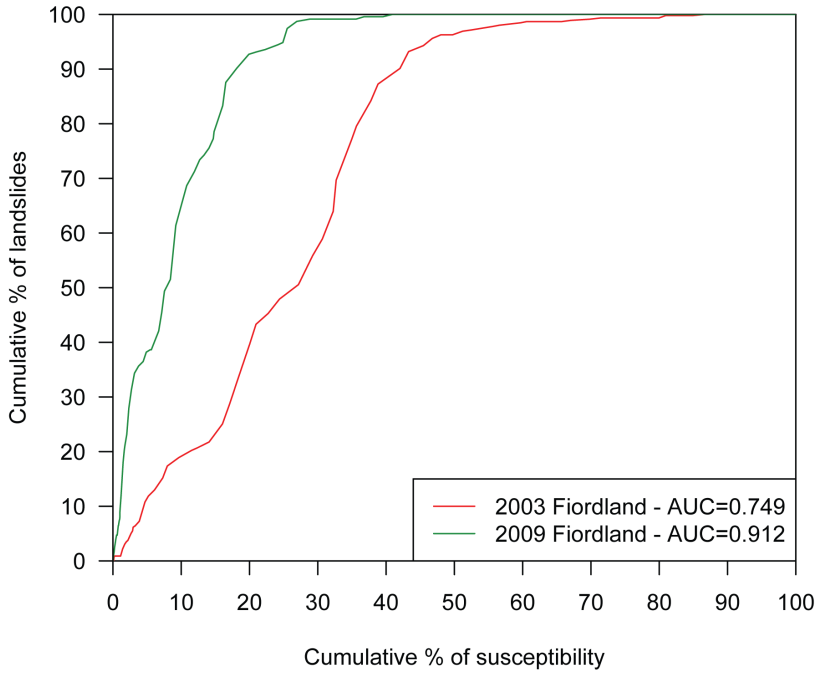

Figure 5.4: Success curves for the 2003 and 2009 Fiordland earthquakes.

however, makes it is possible to relate susceptibility values to observed landslide occurrence and spatial density. This therefore directly links the area of susceptibility to the number of landslides which occur. Combined observations of multiple events thus provide an opportunity to estimate landslide number for a given scenario. Classifying the continuous susceptibility values into discrete classes (0.0-0.1, 0.1-0.2, 0.2-0.3 etc.) is therefore necessary. Using the three events from Chapter 4, as well as the two Fiordland earthquakes described above, shows the large variability in landslide density with respect to susceptibility class (**Table 5.2**). Establishing the most likely landslide densities for each susceptibility class is therefore required. Ideally, probability distributions would be derived, as this would allow likelihoods to be assigned to the total landslide number estimates. However this is not meaningful with such a small sample set. Consequently, the standard error of the mean (SEM) is used instead.

The SEM (**Fig. 5.5**) provides a method for establishing average values from small sample sets. The SEM is the standard deviation of the sample mean's estimate of a population mean. The sample mean is the calculated average value of a given sample of a population; it effectively uses a small sample of a population to estimate the average value for the entire population. However, different samples from the same population can potentially have widely varying sample means. The SEM describes the potential variability in the sample mean for a given sample size, or alternatively, estimates a likely range for a given sample

Table 5.2: Landslide densities (per km^2) observed in five historic inventories whose landslide susceptibility has been modelled herein for each susceptibility class. NA - corresponding susceptibility value not present; a zero value demonstrates that the susceptibility class is present but no observed landslides occur within that class.

Earthquake	Susceptibility class									
	0.0-0.1	0.1-0.2	0.2-0.3	0.3-0.4	0.4-0.5	0.5-0.6	0.6-0.7	0.7-0.8	0.8-0.9	0.9-1.0
Northridge	0	0	0	0.001	0.016	0.134	0.604	2.621	8.144	21.289
Chi-Chi	0	0	0	0.001	0.015	0.054	0.342	2.230	8.154	21.394
Wenchuan	0	0	0.008	0.050	0.195	0.589	0.808	1.885	4.787	8.919
Fiordland (2003)	0	0	0	0.001	0.002	0.033	0.027	0.034	0.028	0
Fiordland (2009)	0	0	0	0	0.002	0.013	0.031	0.083	0.058	NA

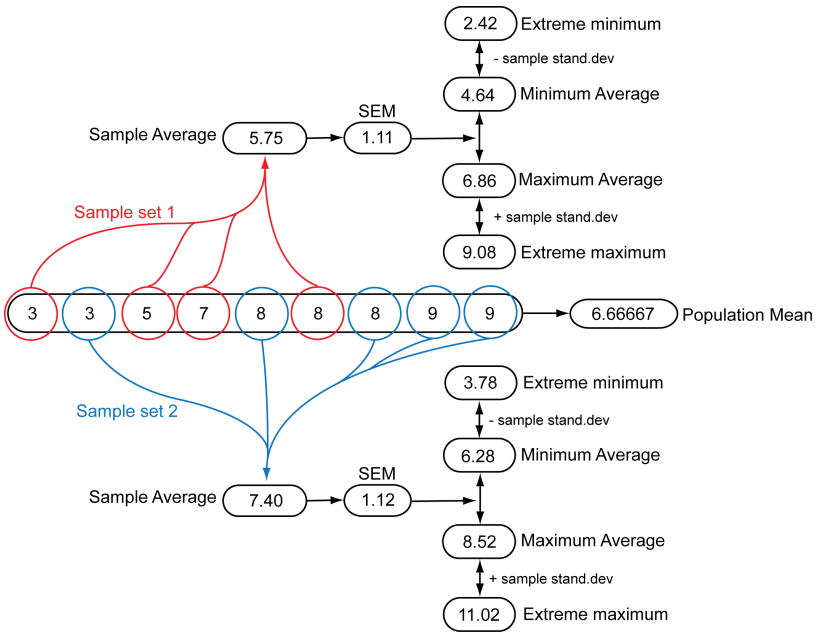

Figure 5.5: Standard error of the mean (SEM) calculates the standard deviation of a sample mean in order to estimate a possible range within which the true population mean exists. For particularly small sample sets compared to the total population, extreme end member values account for the possibility of extreme occurrences.

within which the population mean most likely exists (**Fig. 5.5**). The SEM is calculated from the sample standard deviation, σ_s, and the sample size, n and is thus completely independent of the population size:

$$SEM = \frac{\sigma_s}{\sqrt{n}} \tag{5.2}$$

For natural phenomena, such as landsliding, it is useful to establish extreme values beyond the calculated mean range. This allows for the possibility that the event in question may not represent an average event, instead being more extreme in its nature. It also accounts for the fact that the sample size herein is very small compared to the overall population size. Extending the calculated range by a single sample standard deviation accounts for this and ensures the increased range is not arbitrary. Thus for coseismic landsliding it is possible to identify the most likely range between which average landslide densities exist, as well as some plausibly extreme high and low values. Applying the SEM method to the data in **Table 5.2** establishes such a range of densities for each susceptibility class (**Table 5.3**).

It is immediately apparent that this suggests that under extreme circumstances, an earthquake will not produce any landslides regardless of the corresponding susceptibility values. This is intuitively meaningful because, as stated above, susceptibility does not identify if

Table 5.3: Calculated landslide densities (per km^2) for each susceptibility class using the SEM method. Values calculated represent the Sample Average, the likely range within which the true population mean exists (Minimum Average and Maximum Average), and Extreme Minimum (= Minimum Average - σ_s) and Extreme Maximum (= Maximum Average + σ_s) values.

	Susceptibility class									
	0.0-0.1	0.1-0.2	0.2-0.3	0.3-0.4	0.4-0.5	0.5-0.6	0.6-0.7	0.7-0.8	0.8-0.9	0.9-1.0
σ_s	0	0	0.004	0.022	0.084	0.242	0.342	1.225	4.065	10.405
SEM	0	0	0.002	0.010	0.037	0.108	0.155	0.548	1.818	5.202
Extreme Minimum	0	0	0	0	0	0	0	0	0	0
Minimum Average	0	0	0	0.001	0.008	0.056	0.208	0.822	2.416	7.698
Sample Average	0	0	0.002	0.010	0.046	0.164	0.362	1.369	4.234	12.900
Maximum Average	0	0	0.002	0.011	0.054	0.221	0.570	2.191	6.650	20.598
Extreme Maximum	0	0	0.005	0.033	0.138	0.462	0.916	3.416	10.715	31.003

landslides will occur, only the locations where a combination of factors make occurrence relatively more likely. Thus, for any given earthquake it cannot be guaranteed that any landsliding will occur. However, realistically, if an earthquake is able to produce even medium-to-high susceptibility values it seems extremely unlikely that no landslides will occur. At the other end of the scale landslide densities are extremely high, reaching >31 landslides per km^2 in the very highest susceptibility values. Achieving such extreme densities seems unlikely but cannot be discounted especially since both Northridge and Chi-Chi were able to produce densities of >21 per km^2.

Applied to the five inventories herein, the SEM results are able to successful predict the number of landslides that occurred in each event despite the large range in observed densities (**Table 5.4**). For the Northridge, Wenchuan, and Chi-Chi earthquakes, the extreme scenarios were not required as the potential range of the sample mean is sufficient to predict (or get very close to) the number of landslides observed. For the two Fiordland events, the Extreme Minimum prediction is closer to the observed values suggesting these two events were extreme cases. Nevertheless, the SEM method does show that more landslides would have been expected from the 2003 event compared to the 2009 event, demonstrating that it is more applicable than simple empirical methods. Further, while still having a sizeable error, the SEM method does achieve more accurate results than empirical methods. For instance, for the 2009 Fiordland earthquake empirical methods suggest up to 28,500 landslides would have occurred while the SEM method suggest it would not have exceeded 11,000. Hence, qualitatively these results appear reasonable and able to suggest most likely values as well as plausible extreme scenarios.

Table 5.4: Predicted number of landslides from the SEM method for the five inventories included herein compared to the observed number of landslides.

Inventory	Observed landslides	Ext. Min.	Min. Avg.	Sample Avg.	Max. Avg.	Ext. Max.
Northridge	11,111	0	3,186	5,640	8,826	14,233
Chi-Chi	21,969	0	7,814	13,986	21,800	35,417
Wenchuan	60,109	0	33,301	57,344	90,645	141,889
Fiordland (2003)	455	0	4,554	8,511	13,065	21.882
Fiordland (2009)	233	0	2,035	4,108	6,143	10,780

Total landslide volume

Calculating total landslide volume is important for evaluating sediment yield as a result of the earthquake (see Li et al., 2014) and for establishing the amount of material available for remobilisation and therefore aggradation. Estimating landslide volumes however is a difficult task, particularly when dealing with a large number of individual landslides and especially when attempting to estimate volume prior to an event. Estimating volumes for each individual landslide from site-specific data is impractical when dealing with such large numbers (hundreds-to-tens of thousands) and thus often a more empirical/statistical approach is undertaken (see Guzzetti et al., 2009).

Brunetti et al. (2009) analysed 19 landslide datasets resulting from a variety of different triggers both on Earth (subaerial and submarine) and on other planetary bodies. They showed that the probability of any given landslide having a particular volume followed a negative power law with average component value $\beta \sim -1.3$ (range 1.0-1.9), such that:

$$p(V_L) = kV^{-1.3} \tag{5.3}$$

where $p(V_L)$ is the probability density of landslide volume, V_L, in m^3 and k is constant for a given event. This behaviour was independent of lithology, slope morphology, triggering mechanism, and length of period (e.g. instantaneous (coseismic) or during a prolonged period (sustained rainfall)) and extent of area covered by the dataset. In doing so, this method provides an appropriate means for estimating the total volume of landslide debris likely to result from any given number of landslides. When applying this to a future earthquake scenario, calculating k is crucial to determining the total volumes of landslides produced. Historic inventories for which total landslide volume estimates exist make this possible.

A generated random number, *RAND*, between 0 and 1 can be used to calculate a landslide volume with a corresponding exceedance probability. As *RAND* is randomly generated, there is only a 10% chance that it will exceed 0.9 etc. Thus, if $RAND = 0.9$, V is the volume for which there is a 10% exceedance probability, or alternatively, V is the volume which exceeds that of 90% of all landslides. If *RAND* is therefore considered to represent the probability that V is less than some value V', then *RAND* is effectively equal to 1 minus the integral between V' and ∞ of the probability density function, $p(V_L)$:

$$RAND = 1 - P(|V \geq V'|) \tag{5.4}$$

$$= 1 - \int_{V'}^{\infty} kV^{-1.3}\,\mathrm{d}V \tag{5.5}$$

The range from V' to ∞ is required because the limit on potential individual landslide volume is thought to be very large but remains unknown. However, this is impractical and effectively

makes the equation unsolvable. Setting an upper bound therefore allows V to be calculated but has the negative effect of limiting individual landslide volumes to less than the upper limit. Therefore, the upper limit must be set at a significantly large volume to allow all realistic landslide volumes to occur. This requires identifying the largest realistically plausible individual landslide volume.

Brunetti et al. (2009) noted that because landslides >1 km^3 are so rare (probability density $<10^{-11}$), they could not be certain the established probability distribution accurately represented the occurrence of such landslides. Furthermore, for those inventories studied herein the largest identified landslide is the Daguangbao landslide in Wenchuan whose volume is estimated at $\sim$1 km^3 (Huang et al., 2012). Geologic evidence of previous Alpine fault earthquakes also suggests that the largest landslide to result is the 1 km^3 John O'Groats landslide (see Chapter 2 and Hall et al. (2014) for a discussion of the 27 km^3 Green Lake landslide). Thus, it seems reasonable to expect that in any given landsliding event, the largest likely landslide will have a volume $\leq$ 1 km^3. Of course, larger landslides do exist and are therefore possible (see Appendix A for an example) however, they are inherently extremely unlikely, representing extreme events that cannot realistically be considered for a hazard analysis such as this. Thus, equation 5.5 becomes:

$$RAND = 1 - \int_{V'}^{10^9} kV^{-1.3}\,\mathrm{d}V \tag{5.6}$$

making it possible to solve for V' for each *RAND* value.

Solving for k requires generating the same number of *RAND* values for all landslides in the corresponding inventory (i.e. 11,111 *RAND* values for the Northridge inventory etc.), and calculating their V' initially assuming $k = 1$. Summing for all values of V' gives the total landslide volume estimated for that inventory. k is therefore the ratio between the estimated and observed total volumes. Repeating this method multiple times in a Monte Carlo approach accounts for the use of random numbers and identifies a potential range of k values. The optimum number of trials in Monte Carlo simulation can be derived by applying 'stopping rules'. A standard stopping rule within the SEM method is to stop the trials when the SEM is $<$1% of the sample mean (Buslenko, 1966). The appropriate number of trials, N_t, can be calculated from:

$$N_t = (\frac{\sigma_s}{0.01\sigma_s})^2 \tag{5.7}$$

Thus, for the data used herein, at least 10,000 trials are required.

Of the inventories included herein only the Northridge and Wenchuan earthquakes have published total volume estimates. Harp and Jibson (1996) estimated that total landslide volume from the Northridge earthquake (11,111 landslides) was $\sim$0.12 km^3 while Li et al. (2014)

estimated ~2.8 km^3 for Wenchuan (57,150 landslides, comparable to the estimate of Gorum et al. 2011). Monte Carlo estimates for total landslide volume when $k = 1$ for the Northridge earthquake were 100-1,000 times too large while for Wenchuan they were 10-100 times too large; thus k is inferred to be between 0.001 and 0.1. The large range is likely the result of local factors such as lithology, however without knowledge of the effect of different lithologies on k this cannot be taken into account. Nevertheless, once the number of landslides for an earthquake scenario has been estimated, total landslide volume can also be estimated for this range of k values.

5.4 Results

5.4.1 Coseismic landslide susceptibility for an Alpine fault earthquake

To model the spatial distribution of landslide susceptibility expected from a future Alpine fault earthquake, the distribution of MM intensity shaking is required, and this has been outlined in Chapters 2 and 3 (**Fig. 2.4**). Despite some evidence suggesting the Alpine fault is bimodal and able to produce M_w6.5-7.0 earthquakes (see De Pascale et al., 2014), the general scientific consensus is that the fault is capable of full-length rupture (M_w8.0) events and has regularly produced such events over the last 8,000 years (see Berryman et al., 2012a). Given the fault's potential it is prudent to assess the landslide hazard likely to result from an M_w8.0 earthquake. Distance from active faults was derived from the known active faults map shown in **Fig. 2.1**, while the other factors can be derived directly from the 60 m DEM of the South Island (resampled from the 2002 25 m DEM from Landcare Research to match the resolution of other DEMs used in this research).

The results of the landslide susceptibility modelling for a M_w8.0 Alpine fault earthquake are shown in **Fig. 5.6**. High (>0.7) susceptibility values cover an area >16,300 km^2, affecting almost the entire central Southern Alps. Susceptibility values >0.5 cover an area of ~50,000 km^2 or >⅓ of the South Island, stretching almost the full length and breadth of the Island. It is clear that the highest susceptibility values are heavily focussed on the western range-front, between the Alpine fault and the main divide, and also on the moraines west of the fault (**Fig. 5.7**). These very high susceptibility values stretch the entire length of the fault rupture and correspond to the locations of many identified rock avalanches throughout the South Island (**Fig. 2.7**; Hancox and Perrin 2009; Korup 2005a; Whitehouse 1983). It is also notable that south of the Marlborough fault system high values are generally confined to a relatively narrow zone west of the main divide; however, where the Marlborough faults meet the Alpine fault, this zone widens dramatically, extending for ~40 km east of the fault rupture, compared

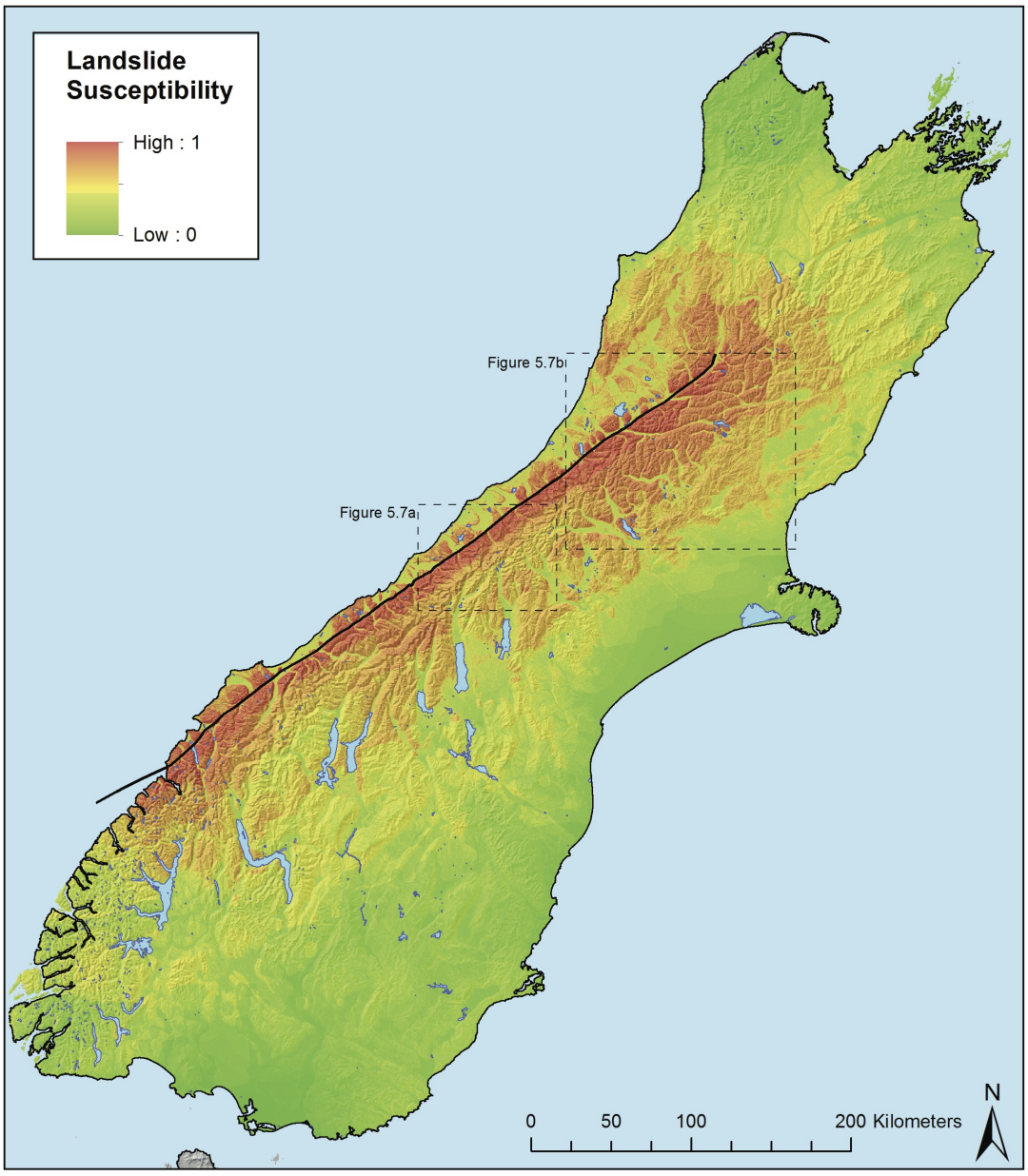

Figure 5.6: Coseismic landslide susceptibility model resulting from a M_w8.0 Alpine fault earthquake. Enlargements of insets in **Fig. 5.7**.

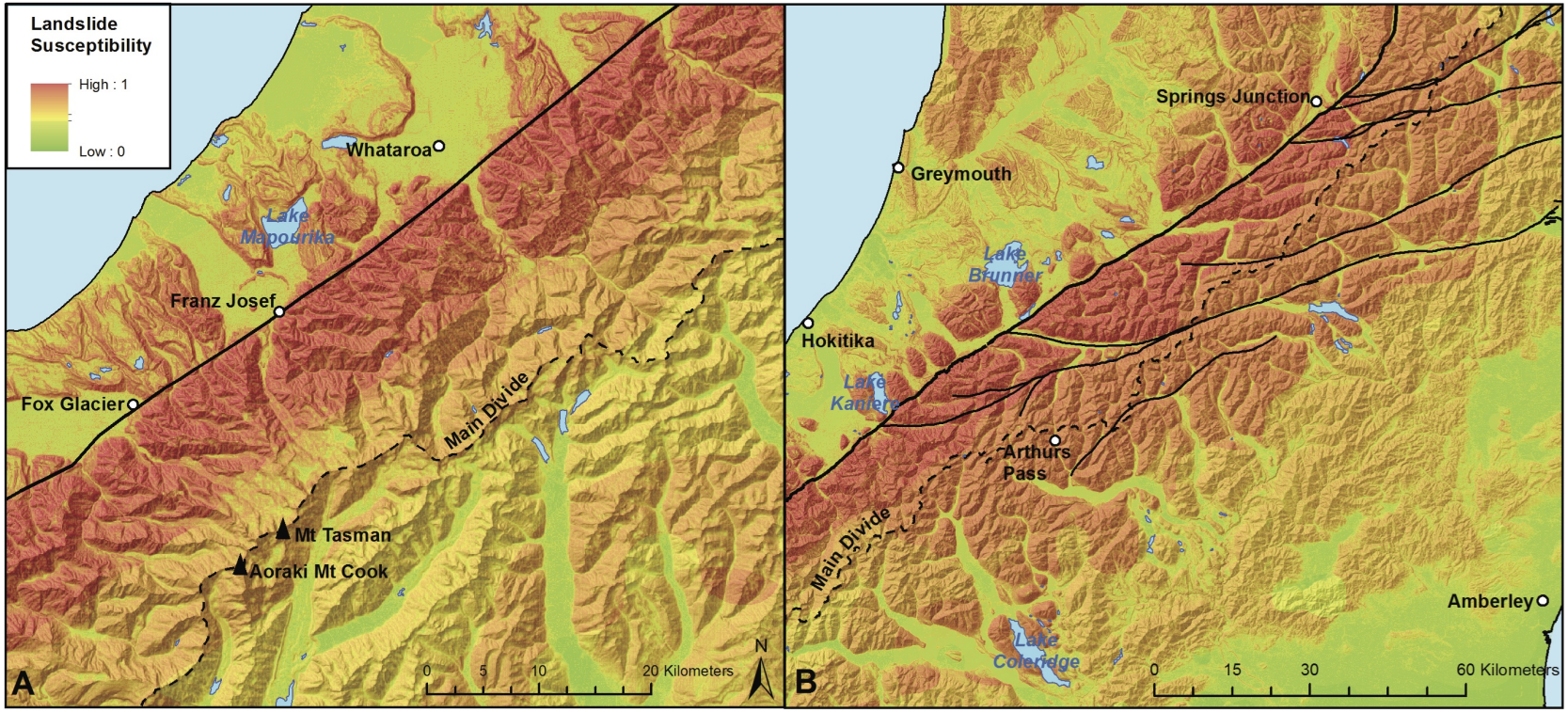

Figure 5.7: Coseismic landslide susceptibility in the a) Aoraki/Mt Cook region, and b) Marlborough fault region of the central Southern Alps.

to <20 km south of the Marlborough system (**Fig. 5.7**). This is likely a direct result of the presence of the Marlborough faults and suggests that this region has the potential for very widespread landsliding, corresponding to the observations of Whitehouse (1983) and Bull (1996).

5.4.2 Total landslide number

Applying the SEM-derived landslide density values to the Alpine fault susceptibility model can establish most likely and extreme scenarios for consequential landsliding (**Table 5.5**). The extreme minimum scenario suggests that no landslides occur; a perhaps feasible, but extremely unlikely, scenario. The extreme maximum scenario suggests that >175,000 landslides could occur. Again, such a number appears feasible, but is considered extremely unlikely. Without direct evidence to suggest an Alpine fault earthquake would be an extreme event, it is more likely that the total number of landslides will be between 40,000 and ∼110,000, with a sample average suggesting around 70,000 landslides (**Table 5.5**). Even these more conservative estimates demonstrate that landsliding from an Alpine fault event is likely to be catastrophic and widespread, with the potential to generate total numbers similar to, or even in excess of, those recorded in Wenchuan.

Table 5.5: Area and number of landslides in each susceptibility class for an Alpine fault earthquake using the five SEM derived cases.

Susceptibility Class	Area (km^2)	Extreme Minimum	Minimum Average	Sample Average	Maximum Average	Extreme Maximum
0.0-0.1	74.1	0	0	0	0	0
0.1-0.2	13,705.2	0	0	0	0	0
0.2-0.3	30,290.9	0	0	49	49	157
0.3-0.4	31,067.4	0	21	325	346	1,028
0.4-0.5	24,963.4	0	209	1,145	1,354	3,447
0.5-0.6	18,010.2	0	1,016	2,962	3,977	8,328
0.6-0.7	16,479.0	0	3,421	5,971	9,392	15,096
0.7-0.8	8,178.2	0	6,719	11,199	17,918	27,934
0.8-0.9	6,427.4	0	15,529	27,213	42,742	68,866
0.9-1.0	1,737.4	0	13,375	22,413	35,788	53,865
Total	**150,933.2**	**0**	**40,289**	**71,277**	**111,566**	**178,722**

Landslide magnitude

The exact number of landslides may not be the best measure for comparing landslide events. Malamud et al. (2004) suggested an appropriate method to compare the scale of landsliding between events was to use a landslide-event magnitude, M_L, rather than the exact number of landslides, N_{LT}, such that

$$M_L = logN_{LT} \tag{5.8}$$

This is because total landslide number has been observed to cover several orders of magnitude and can therefore often be difficult to directly compare. For instance, consider the cases of the Chi-Chi, Northridge, and the 2009 Fiordland event. The difference in absolute landslide number between Fiordland and Northridge is ∼11,000, virtually identical to the difference between Northridge and Chi-Chi (**Table 5.6**). However, comparing M_L demonstrates that Northridge is in fact on a similar scale to Chi-Chi (**Table 5.6**) despite experiencing ∼½ the total number of landslides and despite Chi-Chi and Fiordland having similar earthquake magnitudes. Estimates for the Alpine fault earthquake suggest that it could experience up to M_L5.3, but is more likely to have M_L4.6-5.1 with a sample average of M_L4.9. Thus, despite demonstrating that total landslide number could fall between a large range of values, it is evident that landsliding is likely to be of a similar scale to that which was observed in the Wenchuan earthquake (M_L4.7).

Table 5.6: Comparison of total landslide number (N_{LT}) and landslide magnitude (M_L) for the 1994 Northridge, 1999 Chi-Chi, and 2009 Fiordland earthquakes.

	Northridge	**Chi-Chi**	**Fiordland**
Earthquake magnitude (M_w)	6.7	7.7	7.8
Total Landslide number (N_{LT})	11,111	21,969	240
Landslide magnitude (M_L)	4.0	4.3	2.4

5.4.3 Total landslide volumes

Once the total number of landslides for an Alpine fault earthquake has been estimated, the total landslide volume can also be estimated. To do this, 10,000 trials are undertaken for each of the SEM-derived landslide number scenarios (**Table 5.5**) for 20 different values of k, increasing linearly between 0.001 and 0.01, and 0.01 and 0.1 (∼500 trials per k value).

The results of the Monte Carlo modelling for each of the five landsliding scenarios are shown in **Fig. 5.8**. This shows that the largest total volume observed is ∼8 km^3 when

>175,000 landslides occur, although this number also produces total volumes as low as 0.07 km^3 (70 $\times 10^6$ m^3) depending on the value of k. Taking all 50,000 calculated total volumes, the first (Q1) and third (Q3) quartiles suggest that total volume is likely to be between ~0.05 km^3 and ~1.5 km^3 with a median (Q2) of ~0.3 km^3. However, if the 10,000 scenarios with zero landslides are ignored (Extreme Minimum), then the quartile volume ranges substantially increase to between 0.2 km^3 and 2 km^3 with a median of 0.5 km^3. It should be noted however, that a single very large landslide (i.e. several hundreds of thousands of cubic metres or larger) could substantially increase this volume. For instance, the Daguagbao landslide (see Huang et al., 2012) accounts for nearly half the total volume produced in Wenchuan according to Li et al. (2014). Had this landslide not occurred, total volume in Wenchuan (>2 km^3; Li et al. 2014)would be similar to that estimated for an Alpine fault earthquake, which is estimated to have a similar number of landslides.

The majority of landslides are anticipated to be small in volume (Brunetti et al., 2009), with most of the total volume being contributed by just a few large-volume events (e.g. Daguangbao in Wenchuan). Calculating the precise distribution of volumes allows identification of the number of landslides likely to present a major hazard. Herein this boundary is arbitrarily defined, for the purpose of illustrating the point, as those landslides >10,000 m^3. Calculating the percentage of landslides corresponding to various volumes (**Table 5.7**) demonstrates that nearly 60% of all landslides produced will have volumes <10 m^3, while landslides larger than ~10,000 m^3 account for just ~4% of the total number. Thus, of the total number of landslides estimated (**Table 5.5**) between 1,400 and 4,000 are likely to present a major hazard (i.e. larger than 10,000 m^3), although this could be as high as 6,300 (**Table 5.7**).

Landslides greater than 10,000 m^3 also present a possible landslide dam hazard, particularly if they fall into narrow river valleys or gorges. Smaller volume landslides are unlikely to be sufficiently large to result in any significant blockage. Following the Wenchuan earthquake, >250 landslide dams formed throughout the entire 100,000 km^2 landslide-affected zone (Xu et al., 2009). The largest was the >20 million cubic metre Tangjiashan landslide which blocked the Jiang River to a height of 82 m, impounding a lake of ~316 million cubic metres that stretched up-valley for 20 km submerging several towns and key access routes (Peng and Zhang, 2012). Modelling of the potential outburst flood suggested peak flow rates could reach ~32,000 cumecs (m^3/s) which posed a substantial hazard to >1.2 million people. While the population of the South Island is significantly smaller, and far less people and infrastructure exist in the Southern Alps compared to Wenchuan, given the scale of landsliding estimated from an Alpine fault earthquake, landslide dams will clearly present a major, Island-wide hazard.

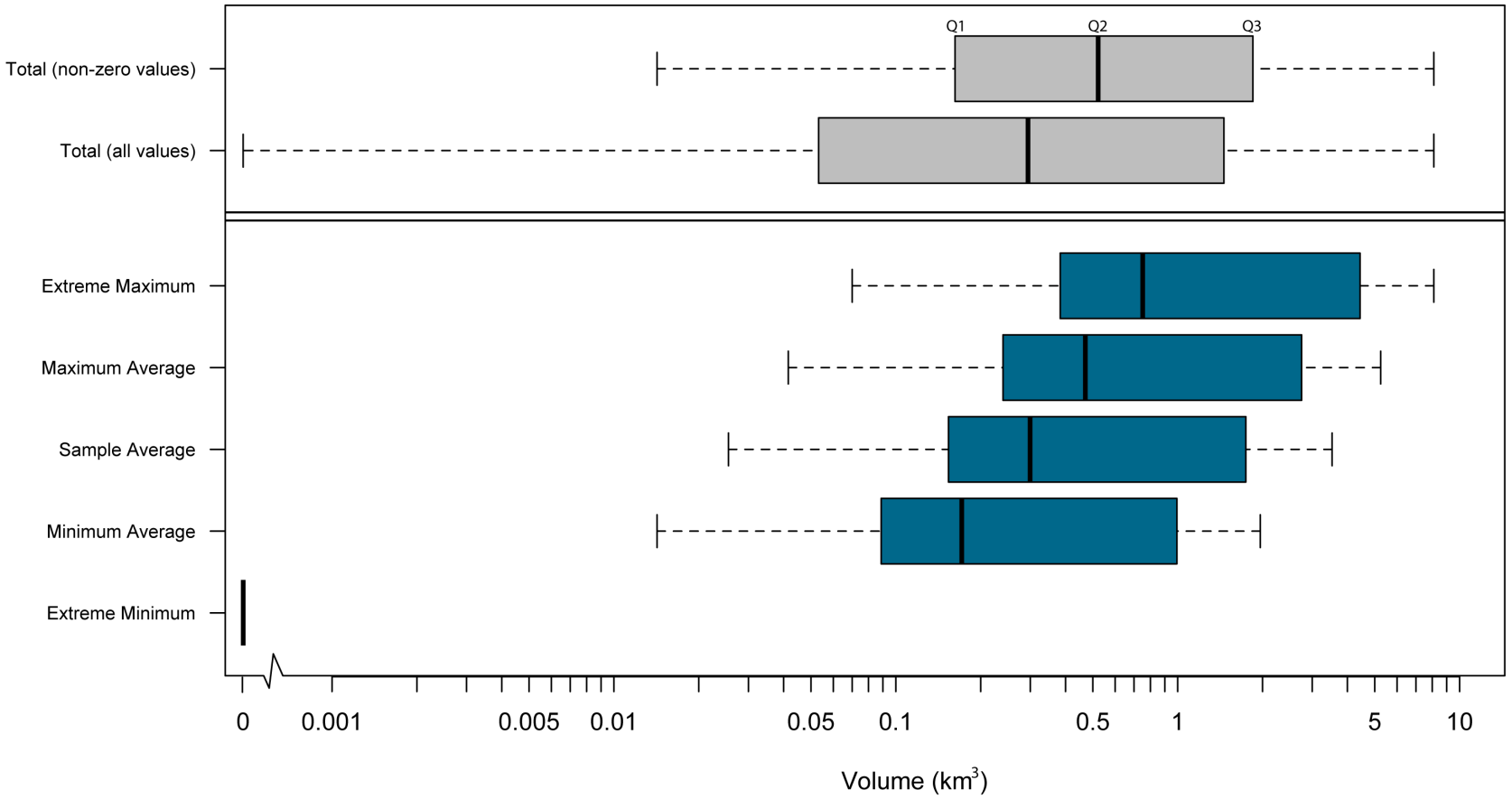

Figure 5.8: Monte Carlo modelling results for total landslide volume for each of the five SEM derived total landslide numbers for an Alpine fault earthquake. Boxes denote limits of Q1 and Q3 quantiles; thick black line shows median (Q2) value.

Table 5.7: Percentage of total landslides corresponding to minor and major landslide hazards for each of the landslide number scenarios considered for an Alpine fault earthquake. The Extreme Minimum scenario is not included as it contains zero landslides.

Volume (m^3)	% total landslides	Minimum Average	Sample Average	Maximum Average	Extreme Maximum
			Minor Hazard		
<10	58.87	23,718	41,960	65,679	105,213
10-99	22.36	9,008	15,937	24,946	39,962
100-999	10.38	4,182	7,398	11,580	18,551
1,000-9,999	4.84	1,950	3,450	5,400	8,650
Subtotal	**96.45**	**38,858**	**68,745**	**107,605**	**172,376**
			Major Hazard		
10,000-99,999	2.27	915	1,618	2,532	4,057
100,000-999,999	0.99	399	705	1,104	1,769
1,000,000-9,999,999	0.29	117	207	323	518
>10,000,000	<0.01	0	2	2	2
Subtotal	**3.55**	**1,431**	**2,532**	**3,961**	**6,346**

5.5 Consequent erosion and aggradation

To understand the environmental impacts of coseismic landsliding, analysing the effects on major river catchments is an especially good measure (Korup, 2005b; Korup et al., 2004). Of particular interest is the amount of erosion and subsequent aggradation that occurs through remobilisation of landslide debris within each catchment. Understanding how much erosion occurs as a result of a particular earthquake is vital to understanding both mountain building processes (Li et al., 2014; Parker et al., 2011) and the medium-to-long-term response of major river systems. Understanding post-seismic aggradation is particularly important in New Zealand, and especially the West Coast region, as farming activities, one of the major economies of the West Coast region, occur primarily on active alluvial fans close to the range-front, because they have fertile soils (formed from historic landsliding and aggradation events) and adequate rainfall. Large-scale and long-term aggradation, as shown to occur post-Alpine fault earthquake (see Chapter 2 and Howarth et al. 2012, 2014), could have potentially devastating effects for the farming community and the West Coast region, and perhaps national, economy.

For a regional-scale study, South Island river catchments of order 6 or larger are investi-

gated. There are 36 river catchments of order 6 or higher in the South Island with an almost even split between east-draining and west-draining rivers (**Fig. 5.1**). To quantify the relative impacts of landsliding between catchments an Impact Factor is calculated. Larger catchments are generally expected to produce more landslides as landslide number is directly related to area. The Impact Factor therefore establishes the relative rate of landsliding across a given catchment area, identifying those catchments with relatively high rates of landsliding for their area:

$$ImpactFactor = \frac{N_C/N_{LT}}{A_C/A_T} \tag{5.9}$$

where N_C is the number of landslides in the catchment, N_{LT} is the total number of landslides, A_C is the area of the catchment, and A_T is the total area. Catchments with Impact Factors >1 are producing more landslides per area than the average, while those <1 produce fewer landslides (**Table 5.8**).

Of the 36 order 6 or larger catchments, 16 have Impact Factors >1, contributing $>65\%$ of the total landslide number despite covering just $\sim 20\%$ of total South Island area (**Table 5.8**). The Taramakau, Waiho-Callery and Hollyford are the worst affected, producing on average more than seven times more landslides than the average for their catchment areas. Further, out of these 16 worst affected catchments, 12 are west-draining (**Table 5.8**). Of the east-draining catchments the Canterbury Waiau is the worst affected, producing nearly twice as many landslides as the average. This demonstrates that while landsliding impacts are anticipated to be greatest west of the main divide, there will still be substantial effects east of the main divide. The other order 6 or greater catchments produce less than half as many landslides as expected and thus, only the 16 worst affected catchments are considered further.

5.5.1 Erosion and denudation

To estimate erosion and denudation resulting from an Alpine fault earthquake, the total volume of landslide debris generated in each catchment is calculated using the same method for estimating total landslide volume for the whole South Island. This shows that in the Buller and Grey catchments, the largest of those considered, total volumes are estimated to be up to >100 million cubic metres, while in the smaller catchments they are unlikely to exceed ~ 10 million cubic metres (**Fig. 5.9**). Nevertheless the Taramakau and Hollyford catchments both have the potential for up to 100 million cubic metres total volume despite being less than a third of the size of the Buller and Grey catchments. This is a result of the large number of landslides anticipated to occur in these catchments and further highlights that these will likely be some of the worst-affected. Notably, each of the east-draining catchments are anticipated to yield >10 million cubic metres, further demonstrating that landsliding impacts will not be

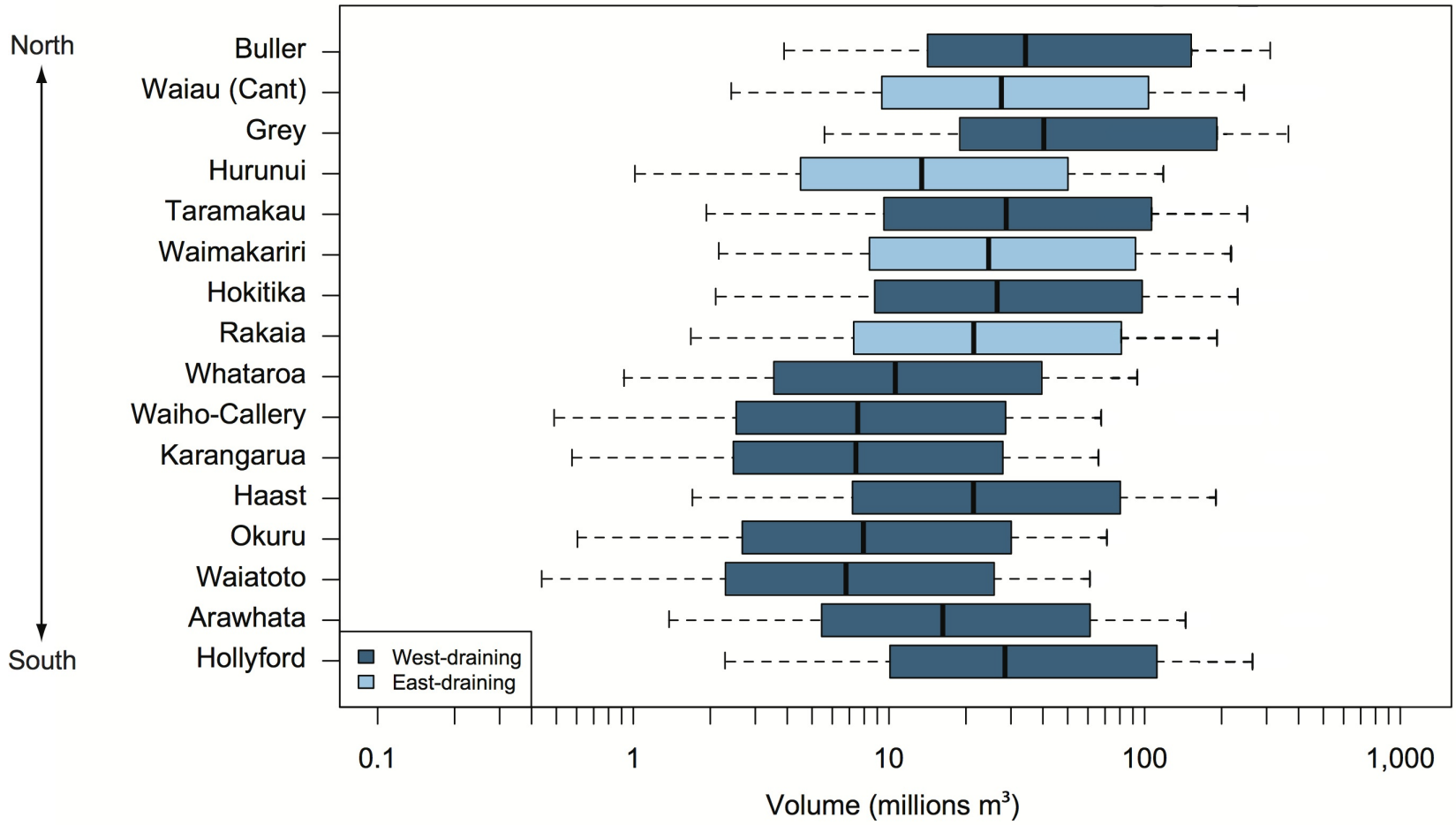

Figure 5.9: Results of Monte Carlo modelling for total volume of landslide debris for the 16 worst affected catchments. The Extreme Minimum SEM values (0) have not been included in modelling.

Table 5.8: Total number of landslides and resultant average Impact Factor for order 6 and above South Island river catchments. Impact Factor is average for all four scenarios.

Catchment	Area (km^2)	% total	Min Avg	Sample Avg	Max Avg	Ext Max	Impact Factor
Taramakau	1,002.9	0.7	2,088	3,570	5,659	8,816	7.56
Waiho-Callery	290.3	0.2	593	1,012	1,605	2,491	7.41
Hollyford	1,129.4	0.7	2,208	3,771	5,979	9,318	7.10
Hokitika	1,066.5	0.7	1,943	3,318	5,261	8,189	6.61
Karangarua	408.1	0.3	556	946	1,502	2,340	4.93
Okuru	467.8	0.3	606	1,034	1,640	2,555	4.70
Whataroa	593.4	0.4	763	1,301	2,063	3,226	4.67
Grey	3,948.8	2.6	4,837	8,278	13,115	20,483	4.45
Arawhata	930.6	0.6	1,129	1,929	3,057	4,796	4.41
Haast	1,355.3	0.9	1,452	2,483	3,935	6,194	3.90
Waiatoto	529.0	0.4	530	905	1,435	2,240	3.64
Waiau (Canterbury)	3,330.6	2.2	1,715	2,983	4,699	7,574	1.90
Rakaia	2,830.6	1.9	1,349	2,329	3,677	5,905	1.75
Buller	6,379.2	4.2	1,793	4,867	7,659	12,355	1.62
Waimakariri	3,608.7	2.4	1,541	2,671	4,212	6,779	1.58
Hurunui	2,669.3	1.8	872	1,528	2,400	3,903	1.22
Subtotal	**30,540.5**	**20.2**	**23,975**	**42,925**	**64,588**	**107,164**	**2.95**
Rangitata	1,816.2	1.2	244	439	683	1,151	0.51
Ashley	1,149.9	0.8	130	235	365	619	0.43

Table 5.8 – continued from previous page

Catchment	Area (km^2)	% total	Min Avg	Sample Avg	Max Avg	Ext Max	Impact Factor
Waitaki	11,887.7	7.9	1,155	2,142	3,297	5,628	0.38
Ashburton	1,600.0	1.1	158	285	443	750	0.38
Clarence	3,299.9	2.2	269	522	791	1,407	0.33
Clutha	20,608.5	13.7	1,089	2,190	3,279	5,628	0.22
Waiau (Southland)	8,217.0	5.4	338	694	1,031	1,891	0.17
Wairau	3,582.0	2.4	119	272	391	763	0.15
Opihi	2,375.9	1.6	70	158	229	444	0.13
Mokihinui	751.4	0.5	15	42	56	121	0.11
Waimea	771.0	0.5	14	42	55	124	0.10
Awatere	1,574.6	1.0	25	74	99	220	0.09
Selwyn	2,027.0	1.3	31	67	98	187	0.07
Motueka	2,057.6	1.4	18	62	81	188	0.06
Oreti	3,513.4	2.3	14	50	64	151	0.03
Mataura	5,357.0	3.5	11	48	59	150	0.02
Pelorus	891.2	0.6	1	8	9	25	0.02
Taieri	5,702.8	3.8	4	28	32	89	0.01
Karamea	1,211.5	0.8	1	5	6	18	0.01
Aorere	365.3	0.2	0	0	0	1	<0.01
Total	**109,300.4**	**72.4**	**28,681**	**50, 287**	**78,976**	**127,016**	**0.97**
South Island Total	**150,933.2**	**100.0**	**40,289**	**71,277**	**111,566**	**178,722**	**1.00**

limited to the West Coast region; there will be substantial impacts east of the main divide also.

Calculating the instantaneous denudation corresponding to each of the defined quartiles (Q1, Q2, and Q3) for total volume demonstrates that substantial amounts of erosion are likely to occur in each of the catchments (**Table 5.9**). Denudation is calculated across the entire catchment area where deposition is not inferred to occur (i.e. the catchment area minus the active alluvial fan area, see **Table 5.1**). Denudation is highest in the Hokitika, Hollyford, Taramakau, and Waiho-Callery catchments were it will most likely be $\sim$1-10 cm. The least affected catchments are the Buller and Hurunui where denudation will most likely be $\sim$0.2-2 cm. Nevertheless, the yearly denudation equivalents are perhaps most important, demonstrating which catchments will experience the most erosion compared to annual background erosion rates.

In those catchments where annual erosion is highest (**Fig. 5.1; Table 5.1**), coseismic denudation is most likely equivalent to $\sim$1-10 years worth of erosion (**Table 5.9**). However, outside of the central Southern Alps where annual erosion rates are far lower (**Fig. 5.1; Table 5.1**), coseismic denudation is equivalent to between $\sim$5 and $>$50 years worth of erosion, and could be as much as $>$100 years of erosion. The worst affected in this respect is the Grey catchment, where denudation is estimated to be between 10 and 100 years worth of average annual erosion. Such levels of erosion occur virtually instantaneously and thus have the potential to be catastrophic for these catchments. This is true even for those catchments in the central Southern Alps where erosion is estimated to be 'only' $<$20 years worth; generating even just several years worth of erosion instantaneously is still a catastrophic event.

This suggests that in the west-draining central Southern Alps catchments, long-term erosion is primarily a function of long-term rainfall processes with Alpine fault earthquakes playing a minor role. However, in the east-draining, northern (Buller, Grey, Taramakau), and southern (Hollyford) catchments, Alpine fault earthquakes appear to play a more dominant role. Nevertheless, the east-draining and northern catchments are also regularly affected by large earthquakes on each of the Marlborough faults as well as minor subsidiary faults, however it is not within the scope of this thesis to establish how Alpine fault-related erosion compares to other earthquakes, although it is possible with this method. Substantial erosion was recorded in the Buller catchment following the 1929 Murchison (Pearce and O'Loughlin, 1985) and 1968 Inangahua (Adams, 1981) earthquakes, while the 1929 Arthurs Pass earthquake resulted in the $>$60 million cubic metre Falling Mountain landslide in the Taramakau catchment (Whitehouse, 1983).

This work shows that Alpine fault earthquakes provide a substantial contribution to the

Table 5.9: Landslide-generated denudation corresponding to the Q1, Q2, and Q3 quartiles of total volume estimates (see **Fig. 5.9**) and corresponding yearly denudation equivalents compared to annual denudation. EQ = Earthquake

Catchment	Annual denudation (cm)	EQ denudation (cm)			Year equivalent (yrs)		
		Q1	Q2	Q3	Q1	Q2	Q3
Grey	0.05	0.54	1.16	5.50	10.0	21.3	101.2
Hollyford	0.17	1.08	3.03	11.91	6.3	17.8	70.1
Buller	0.04	0.24	0.57	2.53	6.3	15.1	67.3
Taramakau	0.22	1.17	3.52	13.03	5.4	16.4	60.6
Hurunui	0.03	0.19	0.55	2.07	5.4	16.0	59.6
Waiau (Cant.)	0.08	0.32	0.93	3.51	4.2	12.3	46.1
Waimakariri	0.08	0.28	0.81	3.05	3.3	9.8	36.6
Rakaia	0.15	0.31	0.90	3.40	2.0	5.9	22.5
Hokitika	0.58	1.01	3.06	11.29	1.7	5.2	19.3
Haast	0.37	0.57	1.68	6.32	1.5	4.5	16.9
Karangarua	0.53	0.65	1.95	7.32	1.2	3.7	13.9
Okuru	0.59	0.63	1.88	7.12	1.1	3.2	12.0
Waiho-Callery	1.17	1.09	3.25	12.33	0.9	2.8	10.5
Arawhata	0.69	0.64	1.92	7.22	0.9	2.8	10.5
Whataroa	0.73	0.67	2.01	7.50	0.9	2.7	10.2
Waiatoto	0.70	0.47	1.39	5.26	0.7	2.0	7.5

long-term erosion of the east-draining and northern Southern Alps catchments and are perhaps the dominant erosion mechanism for the southern Hollyford catchment. As well as this, Alpine fault earthquakes appear to have a large (although not dominant) affect of erosion in the west-draining catchments in the central Southern Alps.

5.5.2 Aggradation

The majority of landslide debris will be remobilised and transported downstream by river processes (Howarth et al., 2012; Korup, 2005b; Korup et al., 2004). Initially, deposition will occur within the river channel; however, given the large amounts of landslide material available in combination with South Island rivers being predominantly shallow ($<$3 m deep), braided systems, the majority of deposition is expected to occur on the rivers' active alluvial fans. Observations of aggradation following the 1999 Poerua outburst flood showed that aggradation predominantly occurred on the active Poerua fan (Davies et al., 2005; Hancox et al., 2005; Oven, 2004). Using the New Zealand 1:250,000 Geologic Maps (QMaps; Rattenbury and Isaac 2012), the youngest quaternary (Holocene) alluvial deposits are inferred to represent the current active fans of the rivers considered (**Fig. 5.1**). Thus the maximum area within each catchment on which aggradation could occur has been calculated (**Table 5.1**).

In the medium-to-long-term, suspended load is presumed to be transported offshore. Therefore, assuming suspended load accounts for half the river carrying capacity (Davies and McSaveney, 2006), $\sim$50% of landslide material has the potential to be mobilised as bedload and deposited on active alluvial fans. Nevertheless, Korup et al. (2004) showed that the amount of landslide material remobilised by rivers varied greatly for three different landslides in the central Southern Alps. Following the Falling Mountain landslide in 1929, the majority of landslide debris has remained *in situ* below the failure scarp. Conversely, 10-30% of the Mt Adams landslide which blocked the Poerua River in 1999 had been reworked and deposited on the active fan within 5 years. The Gaunt Creek landslide periodically produced relatively small slips between 1918 and 1965 with virtually all material being reworked downstream and deposited on the Waitangi-taona River alluvial fan, of which Gaunt Creek is a tributary, causing it to change course (Korup et al., 2004). Thus, herein an estimate of 60% of river bedload, or 30% of total landslide volume, is inferred to be involved in aggradation. It should be noted however, that fine grained sediments found on the Whataroa alluvial fan are inferred to be the result of aggradation from overbank deposits following a large earthquake in the 1600s (Davies and Korup, 2007). Overbank deposits are formed from suspended sediment during flooding and therefore the aggradation values derived herein may be under-estimated.

Spreading the total corresponding volumes for each catchment (**Fig. 5.9**) across the entire

active alluvial fans allows minimum aggradation depths for each catchment to be estimated (**Table 5.10**). This shows that several centimetres to several tens of centimetres of aggradation are expected on the active fans of each catchment; in extreme circumstances several catchments may experience ∼0.5 m or more of aggradation. However, sediment will almost certainly not be deposited equally nor will it affect the entire alluvial fan. Following the Poerua outburst flood, aggradation affected only a ∼5 km length of the active fan proximal to the range-front (Davies et al., 2005; Hancox et al., 2005), despite the whole alluvial fan stretching >20 km from the range-front to the sea. Further, this occurred despite the 10-15 million m^3 of landslide material being deposited upstream in the Poerua gorge, of similar scale to the median estimated total volumes for many of the studied catchments (**Fig. 5.9**).

Table 5.10: Depth of aggradation deposits on active alluvial fans corresponding to the Q1, Q2, and Q3 total volume quartiles for the 16 worst-affected catchments (see **Fig. 5.9**).

Catchment	Active fan area (km^2)	Aggradation (cm)					
		Whole Fan Area			Half Fan Area		
		Q1	Q2	Q3	Q1	Q2	Q3
Grey	466.6	6.8	14.5	69.1	13.6	29.0	138.2
Buller	378.7	5.1	12.3	54.8	10.2	24.6	105.6
Hollyford	192.5	3.6	10.3	40.3	7.2	20.6	80.6
Taramakau	186.7	3.4	10.4	38.4	6.8	20.8	76.8
Waiau (Cant)	382.0	3.4	9.9	37.3	6.8	19.8	74.6
Hokitika	200.0	3.2	9.6	35.3	6.4	19.2	70.6
Waimakariri	589.1	3.0	8.8	33.2	6.0	17.6	66.4
Rakaia	445.1	2.6	7.7	29.2	5.2	15.4	58.4
Haast	84.5	2.6	7.7	29.0	5.2	15.4	58.0
Arawhata	83.2	2.0	5.9	22.1	4.0	11.8	44.2
Hurunui	246.2	1.6	4.8	18.1	3.2	9.6	36.2
Whataroa	65.3	1.3	3.8	14.3	2.6	7.6	28.6
Okuru	45.7	1.0	2.9	10.8	2.0	5.8	21.6
Waiho-Callery	58.4	0.9	2.7	10.3	1.8	5.4	20.6
Karangarua	27.4	0.9	2.7	10.1	1.8	5.4	20.2
Waiatoto	39.1	0.8	2.4	9.3	1.6	4.8	18.6

Consequently, the areas affected by aggradation are likely to be substantially smaller than the whole active alluvial fan systems. Arguably less than half the total areas will be affected suggesting the values can be at least doubled (**Table 5.10**). Thus for several of

the catchments, aggradation depths could reach up to ∼1 m or more. Further, these values are average depths. Davies and Korup (2007) showed that during aggradation events, the maximum depths occurred at the range-front and gradually decreased to zero some distance downstream. Following the Poerua event, maximum aggradation depths at the range-front reached ∼20 m (Davies and Korup, 2007). Further, multiple buried soils at depths of several metres have been identified throughout the central West Coast region, assumed to result from a previous large earthquake (Berryman et al., 2001; Davies and Korup, 2007), suggesting that previous aggradation depths have been on the order of several metres. The results herein are in strong agreement with these observations, suggesting that within the 16 studied catchments *average* aggradation depths are expected to be up to ∼1 m, with substantially larger maximum depths at the range-front likely.

5.6 Discussion

The low (but still acceptable) success rate for susceptibility modelling of the 2003 Fiordland earthquake is likely to result from several factors. Firstly, several landslides appear to have occurred within Lake Te Anau (**Fig. 5.2**), however the landslide data were collected by aerial reconnaissance which would not be able to conclusively identify submarine landslides. It is more likely that these are misplaced subaerial events. The same may be true for the landslides located in the valley bottoms to the northeast of Lake Te Anau, which more likely originated on the steep valley walls that have substantially higher susceptibility. With such a small sample set (∼400), misplacing even a small number of landslides into areas of low susceptibility can have a noticeable effect on the success curves. Simply removing those landslides thought to be misplaced increases the success rate to ∼0.76, while including them using susceptibility values from the inferred true locations increases the success rate to ∼0.78.

Secondly, a large number of landslides in 2003 occurred very close to the epicentre in an area that has only mid-to-high (0.5-0.7) susceptibility values. These values likely result from the lack of a nearby onshore active fault and very few stream systems, as shaking intensities and slope angles in this area are high. It is notable that these landslides cluster to the fiord shoreline. The effect of the shoreline on landslide occurrence has not been incorporated into the fuzzy memberships, however it almost certainly plays a significant role in slope stability, likely being similar to the fluvial undercutting process of river systems. Furthermore, the remote nature of Fiordland makes detailed fault mapping difficult and thus very few active faults have been identified in the region (**Fig. 2.1**). Given the large number of active faults elsewhere throughout the South Island it seems unlikely that no such faults exist in Fiordland.

Thus the susceptibility values observed in this epicentral region likely represent minima; even marginally higher values in this region would substantially increase the success rate.

The results herein have focussed on number of landslides as the inventories included utilise point data. Ideally landslide areas would be derived instead as this is more accurate for deriving total landslide volume (see Li et al., 2014) and can provide a more accurate view of where the largest landslides are likely to occur. However, this requires detailed polygon data for the inventories considered, which is not available, particularly for the Fiordland datasets. The results herein must therefore be considered as order of magnitude estimates, which is suitable for the regional-scale assessment undertaken.

The range in k values is most likely a result of local factors, particularly lithology, which would explain the difference in values between the Northridge and Wenchuan events. Investigating the potential affects of lithology and other local factors on k is therefore likely to yield more accurate and site-specific total volume estimates. It may also provide an appropriate means to include local factors in the fuzzy modelling method. Furthermore, local factors probably play an important role in the number of landslides generated as well. The two Fiordland earthquakes affected a region of strong and only lightly weathered lithologies compared to the Wenchuan, Northridge, and Chi-Chi events. This is potentially the reason for the small number of landslides that formed in these events, as the shaking intensities produced, especially in the 2003 event, were certainly large enough that higher numbers could have been expected. The lithologies and rock strength/weathering in the Southern Alps are more in common with those in Wenchuan, Northridge, and Chi-Chi. Thus including the Fiordland datasets in the SEM method may result in under-estimates for total landslide numbers in the Southern Alps. Nevertheless, given the already small sample set, and no direct evidence to suggest the Fiordland data are inappropriate, including them in the SEM modelling is appropriate.

When estimating total landslide volume, an upper limit has been set for the maximum individual landslide volume possible. Herein this limit has been set at 1 km^3. It is of note that increasing this limit would not alter the results, as the largest landslide observed in any of the 50,000 Monte Carlo trials was $\sim$0.1 km^3. This is because the probability density value for landslides >1 km^3 is $<10^{-11}$, and therefore, even for the large number of landslides considered herein, it is still unlikely that any one will have such a volume. Decreasing this upper limit would affect the total volume estimates however, as this would exclude the largest volume landslides observed, which account for a substantial percentage of the total volume.

Considering the distribution of landslide volumes is also useful for considering the potential for landslide dams. Landslides greater than 10,000 m^3 may have the potential to form

landslide dams if they fall into narrow river valleys or gorges. McCahon et al. (2006a,b,c) identified 15 rivers in seven catchments throughout the Southern Alps that had the potential for landslide dams following an Alpine fault earthquake (**Fig. 2.8**). Five of those catchments (the Buller, Grey, Hokitika, Waiho-Callery, and Haast) are shown herein to be some of the worst affected by landsliding. Further, the Waimakariri catchment, another of those identified herein as being one of the worst-affected catchments, was identified by Yetton and McMorran (2004) as having multiple potential sites for landslide dams to form. In combination with the >250 landslide dams that occurred following the Wenchuan earthquake, as well as the number of landslides likely to be of sufficient size to form landslide dams modelled herein, it is anticipated that numerous dams on multiple rivers and in multiple catchments are likely throughout the entire Southern Alps following an Alpine fault earthquake. These will pose a significant and widespread hazard, and flooding either from the impounded lake or a subsequent outburst flood may result in further damage and/or casualties (see Appendix C). While half of all landslide dams fail within 10 days of formation (Costa and Schuster, 1988), some may potentially survive far longer, presenting a long-term, and continued outburst flood hazard. Managing any landslide dams which form post-earthquake will be vital to the emergency response.

The average aggradation depths estimated herein agree with identified evidence from previous Alpine fault earthquakes. This suggests that both the total volume estimates and the total number estimates are realistic despite the inclusion of the Fiordland earthquakes in the SEM method and the large range in k. The aggradation estimates suggests that the downstream impacts of landsliding from an Alpine fault earthquake are likely to be catastrophic and of long duration. Wells and Goff (2007) identified a series of beach ridges north of the Haast river, which dated to several decades after known ruptures of the Alpine fault. They suggested that these ridges were the result of landslide material from the Haast catchment being mobilised and deposited and re-worked into dune systems once it reached the Tasman Sea. Similarly, Howarth et al. (2012, 2014) found evidence of hyperpycnal deposits in two west coast lakes which lasted for several decades and were preceded by coseismic turbidite deposits. These hyperpycnal deposits were inferred to result from the delivery of coseismic landslide material in the lakes feeder catchment following an Alpine fault earthquake. The implications of these factors for post-earthquake response and recovery are profound, suggesting that these will be hampered by severe and prolonged river aggradation, avulsion, and flooding.

5.7 Conclusions

Estimating the spatial extent and scale of coseismic landsliding expected to occur after a large earthquake is vital to fully understanding the hazard posed by such events. A M_w8.0 earthquake on the Alpine fault is anticipated to produce between ∼40,000 and ∼110,000 landslides, affecting an area >50,000 km^2. This corresponds to M_L4.6-5.1, similar to estimated values for the 2008 Wenchuan earthquake in which catastrophic landsliding presented a hazard as great as, or perhaps greater than, the earthquake shaking itself. Total landslide debris from an Alpine fault earthquake is estimated to be between ∼0.2 km^3 and ∼2 km^3. Landslides with volumes greater than 10,000 m^3 are expected to present the most significant hazard, and between 1,400 and 4,000 of these are expected to occur throughout the South Island. This is likely to result in the formation of numerous landslide dams throughout the Southern Alps.

Landsliding will be most significant along the western range-front, west of the main divide, and throughout the southern Marlborough fault system. In total 16 order 6 or larger catchments are identified as being most severely affected, including all west-draining catchments in the central Southern Alps, and several east-draining catchments. Of these the Taramakau, Waiho-Callery and Hollyford are anticipated to be the worst affected in terms of number of landslides, producing >7 times more landslides than average for their catchment size. Landsliding is expected to result in >5 years worth of erosion in all these catchments, with the Buller, Grey, Hollyford, Taramakau, and Hurunui catchments all potentially experiencing >50 years worth of erosion. Aggradation on active alluvial fans and floodplains is anticipated to be substantial with average depths likely to approach ∼1 m.

Thus, landsliding presents one of the greatest hazards to result from an Alpine fault earthquake, and plays a major role in the erosion of the Southern Alps. In the Hollyford catchment, Alpine fault earthquakes may be the dominant erosion mechanism. The implications for response and recovery following a major earthquake are serious. Investigating the effects of coseismic landsliding from an Alpine fault earthquake to critical infrastructure is therefore vital for planning the emergency response

Chapter 6

Modelling critical infrastructure exposure to coseismic landsliding from an Alpine fault earthquake

6.1 Introduction

Disaster scenarios are a vital aspect of disaster risk reduction and management and have been shown to be a key tool for increasing pre-event awareness and preparedness for future disasters (Chapter 3). The most important feature of any disaster scenario is its description of the resulting impacts on society (Preuss and Godfrey, 2006). Understanding societal exposure to hazards is an important step in the development of scenarios (Chapter 3; **Fig. 3.3**). One of the most vital elements of society to consider in disaster scenarios is critical infrastructure: where disruption of service significantly affects essential facilities, supplies, and/or communication (Church et al., 2004). In the context of disaster resilience and disaster scenarios, it is important to consider the consequent functionality of a critical infrastructure network as a result of its hazard exposure (Whitman et al., 1997). Functionality can be affected by both direct and indirect impacts, and the various interdependencies between networks, both spatially and temporally, must be identified (Preuss and Godfrey, 2006). Disruption to critical infrastructure services can have serious consequences for populations that rely on them. Thus understanding population exposure to direct or indirect effects as a result of critical infrastructure disruption is also important.

Previous attempts to estimate critical infrastructure exposure to earthquakes have primarily focussed on ground shaking (see Azevedo et al., 2010; Chang et al., 1996, 2002; Giovinazzi and King, 2009; O'Rourke, 1996; Pitilakis et al., 2006). Bird and Bommer (2004)

showed that in earthquake disasters, building losses have been mostly attributed to strong ground shaking, while losses to transport and utilities networks are primarily caused by landsliding and liquefaction. Failing to consider the exposure of these networks to coseismic landsliding can therefore result in unrealistic earthquake disaster scenarios. In mountainous environments, difficult topography and excessive road construction and maintenance costs constrain the number of viable network routes (Kohler et al., 2004). Consequently, there is often little redundancy and the networks form long, thin corridor routes through mountainous terrain. A single landslide therefore has the potential to affect multiple densely spaced networks, resulting in serious consequences for downstream populations. For instance, in the Southern Alps of New Zealand, the State Highway and electrical transmission networks primarily follow the same routes through the mountains connecting the east and west coasts (**Fig. 6.1**). A single landslide can therefore affect both the road and the transmission lines simultaneously, exposing downstream populations to isolation and power loss.

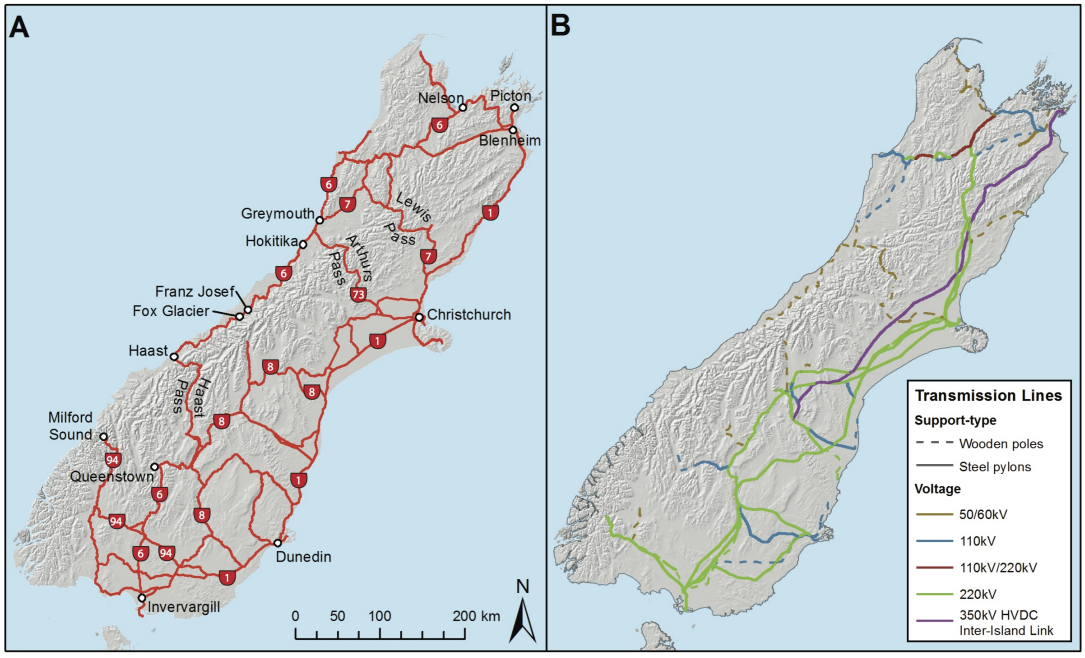

Figure 6.1: The South Island a) State Highway network with locations and b) electrical transmission network showing support-types and transmission voltages.

Coseismic landslide risk assessments are a complex task due to the difficulty in predicting landslide occurrence, runout distance, and landslide magnitude amongst other factors (Pellicani et al., 2013). Developing a method to assess exposure of critical infrastructure to coseismic landsliding is therefore an important research gap. This chapter demonstrates a semi-quantitative method for assessing exposure of critical infrastructure networks to co-

seismic landsliding from susceptibility models. A case study of the Alpine fault earthquake scenario derived in Chapters 2, 3, and 5 of this thesis is presented to demonstrate the applicability of this risk assessment method. The results are used to demonstrate how such risk assessments can be used for basic regional-scale emergency response planning. In addition, the results of this research can be applied to identify critical sections of networks in order to focus pre-event mitigation efforts, and as a planning tool for assessing resource consent applications for constructing new infrastructure links.

6.2 Importance for an Alpine fault earthquake

Large earthquakes within the Southern Alps are relatively common and are known to be capable of producing substantial geomorphic effects (Chapter 2). Modelling of a future Alpine fault earthquake, the largest seismic hazard in the Southern Alps, has suggested between 40,000 and 110,000 landslides could be generated (Chapter 5). Such an event has a significant potential to cause large-scale losses/damage to critical infrastructure throughout the mountains. The transport and electrical transmission networks that traverse these mountains are vital for the local population and for the main regional industries. The West Coast region economy is reliant on the mining, tourism, and agriculture (predominately dairy farming) industries, which account for >NZ$300 million ($\sim$43%) of the region's annual Gross Domestic Product (GDP) (Infometrics 2012; Orchiston 2011; DoC, 2006). For the mining and agriculture industries, the transport network through Arthur's Pass connects the production centres of the West Coast region with Christchurch and Port Lyttleton for domestic and international distribution of goods. For the tourism industry, the alpine passes and State Highway (SH) 6 provide the only access to the West Coast region and its many associated tourist attractions (e.g. the glaciers near Franz Josef and Fox Glacier, Pancake Rocks north of Greymouth etc.). Power is required by mining and agriculture for the production of goods (i.e. operating machinery, milking etc.) as well as providing an essential service for tourists and local populations.

Losses to both these networks therefore has serious implications for economic prosperity, national security, and everyday life in general (Chang and Nojima, 2001; Holmgren, 2006; Shinozuka and Chang, 2004). Road connections between the east and west coasts consist of just three routes across the Southern Alps (Arthur's Pass, Lewis Pass, and Haast Pass; **Fig. 6.1**) each of which cross the Alpine fault and several other large active faults as well as traversing steep, landslide prone terrain (**Fig. 6.2**). Only one highway (SH6) provides access for the small, isolated communities in the West Coast region, and this also crosses the Alpine

fault multiple times and traverses several steep moraines (**Fig. 6.2**). The electrical power transmission network has similar problems, with only two links transmitting energy from the east, where the majority of electrical power is generated, to the communities west of the Southern Alps (**Fig. 6.1**). Thus, assessing the exposure of both these networks to landsliding from an Alpine fault earthquake is vital.

Figure 6.2: Sections of the South Island State Highway network. a) Otira Viaduct on SH73 in Arthur's Pass between Otira and Arthur's Pass townships; b) SH6 crossing the Waikukupa River and the Alpine fault (dashed red line) between Franz Josef and Fox Glacier; and c) SH6 in Haast Pass between Haast township and Wanaka (Photo by Andrew Walsh).

6.3 Exposure analysis method

Exposure is generally defined as the monetary value of the assets at risk (including human life) (Catani et al., 2005; Pellicani et al., 2013). This definition is important for risk assessments for insurance or land-use, but less relevant for emergency response, where information on network functionality is required. Thus, for the purposes of this discussion, exposure is defined simply as the likelihood of a network being affected by a hazard. High exposure

describes a network with high likelihood of being affected, and low exposure corresponds to low likelihood. Hazard exposure is therefore a function of the spatial distribution of the network(s) in relation to the various hazards modelled (see Chapter 3; **Fig. 3.3**). When undertaken for a single specific scenario it is simply a process of identifying locations where one or more hazards coincide within the network(s). For multiple scenarios (or probabilistic models), exposure is a function of the frequency with which a network coincides with a hazard (Peduzzi et al., 2009):

$$E = \sum_{i}^{n} FN_i \tag{6.1}$$

where E is exposure, F is frequency of a given hazard, N_i is a point on the network, and n is the number of hazards being considered. Exposure modelling is therefore intrinsically linked to the hazard scenario(s)/model(s) being used.

Precise landslide scenarios are difficult to produce as the exact locations and runout of any given landslide cannot be predicted with complete certainty. Pellicani et al. (2013) and Catani et al. (2005) therefore attempted to evaluate critical infrastructure exposure as a function of landslide susceptibility. Pellicani et al. (2013) evaluated this qualitatively at a municipal scale with composite weighted asset maps overlain on a susceptibility index (very high, high, medium, low, very low etc.) map to evaluate exposure. Exposure is therefore a function of the composite asset value for each municipality combined with its susceptibility index score (Pellicani et al., 2013). The result is a map with each municipality rated (none, low, medium, high, very high) for its overall landslide exposure. For emergency response however, such a method is not sufficiently quantitative and does not provide enough detail. Alternatively, Catani et al. (2005) considered exposure quantitatively on an individual pixel-scale, estimating total loss (in Euros) per pixel for a variety of different timescales. Any pixel which does not contain a network will therefore automatically have zero exposure. This method requires estimating potential landslide runout paths and distances as the finer resolution requires an understanding of precisely which pixels are likely to be affected by landslide paths (Catani et al., 2005).

Herein, a method adapted from Catani et al. (2005) and Pellicani et al. (2013) has been developed, using the susceptibility map for coseismic landsliding derived in Chapter 5 (**Fig. 5.6**). Instead of estimating the potential monetary loss for each individual pixel, this method focusses on identifying the likelihood of pixels on the State Highway or electrical transmission networks being affected by one or more landslides. This requires estimating the potential runout distance and direction of any coseismic landslides. Establishing these factors defines a region surrounding a point on the network from which the landslide susceptibility contributing to exposure is considered (**Fig. 6.3**). Rather than classifying this surrounding area into a

susceptibility index like Pellicani et al. (2013), four corresponding landslide densities are calculated directly from the susceptibility values present using the four landslide scenarios from Chapter 5 (**Table 5.3**; the scenario with zero landslides is not considered). Using landslide densities instead of a qualitative index value provides a more quantitative method for comparing relative exposure across the entire network. Hazard thresholds are then selected which establish whether the point on the network is likely to be affected by landsliding or not; density values above the threshold result in the pixel being considered likely to be affected. The exposure of any network pixel is therefore the frequency with which its surrounding density exceeds the hazard threshold (i.e. the likelihood of being affected).

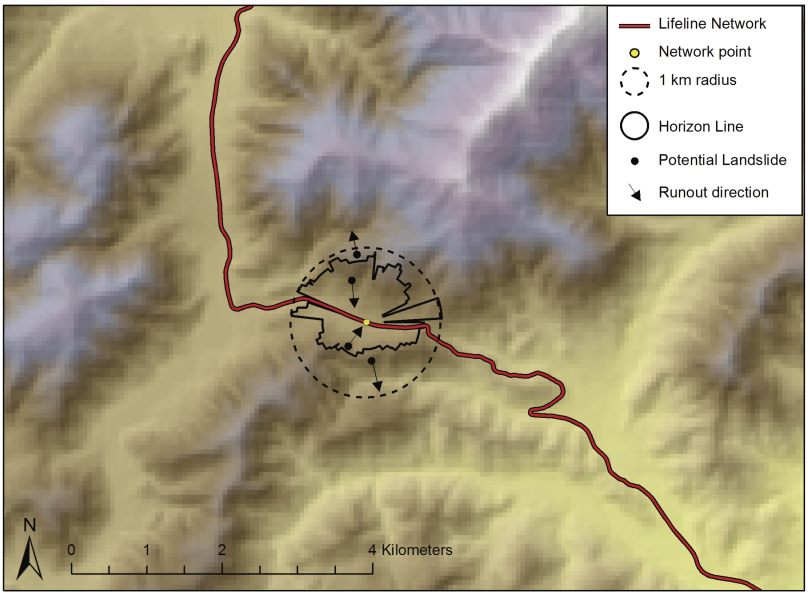

Figure 6.3: Schematic diagram for defining the area contributing landslide susceptibility for a point on a network (area within the horizon line). Landslides which occur within the maximum runout distance but with a runout direction away from the network will not affect the network.

6.3.1 Estimating surrounding regions

Defining the area surrounding a point on the network that contributes the landslide susceptibility used to derive exposure is vital to the assessment. The area must define the region within which any landslides have potential to affect the network. Establishing maximum potential runout distance is therefore key as this describes the maximum distance a landslide can affect the network. Runout direction is also important. A landslide with maximum runout distance away from the network will cause no damage to infrastructure (**Fig. 6.3**). The surrounding region must therefore define the area within the maximum runout distance and with

a runout direction towards the network.

To do this, horizon lines (also known as ridgelines) are established along the network using a GIS (**Fig. 6.3**). Horizon lines identify the visible horizon for an observer positioned at a defined point on the network and can be limited to show the horizon at any desired distance. This identifies those slopes visible to an observer at the given point on the network, and these constitute the slopes with landslide potential around that point (**Fig. 6.3**). This assumes that any landslide runout is in the steepest downhill direction from its source point.

The maximum runout distance to be considered can be defined by analysing the maximum landslide volume likely to affect the network. Landslide volume has been empirically linked to maximum runout distance by numerous studies (e.g. Davies, 1982; Hungr et al., 2005; Kilburn and Sørensen, 1998; Legros, 2002; Nicoletti and Sorriso-Valvo, 1991; Scheidegger, 1973), and therefore can provide an approximate, first-order estimate of the runout distance to be considered. From Chapter 5, >99% of all landslides are anticipated to be ≤1 million m^3 (**Table 5.7**). The potential for a network to be affected by a landslide >1 million m^3 is therefore considered negligible. From the various different available empirical models, maximum runout distance for a 1 million m^3 landslide equates to ∼1 km. The surrounding region for any point on a network is therefore considered herein to be the horizon line within 1 km of the corresponding pixel (**Fig. 6.3**).

6.3.2 Hazard thresholds

Hazard thresholds are defined as the method of deriving landslide density from susceptibility, which is only truly meaningful for sufficiently large areas, such as an entire river catchment (see Chapter 5). This is because for small areas, the pixel size/area (60 m × 60 m) is somewhat comparable to the total area and therefore inclusion or exclusion of a single pixel can have a dramatic effect. In very large areas (>1,000 pixels) this is not the case as a single pixel is negligible compared to the total area. Considering the relative exposure for the network effectively negates this issue as the absolute value is considered in relation to all other points, rather than judged individually. Hazard thresholds therefore provide a more appropriate means to evaluate the data.

Hazard thresholds are user-defined and are selected based upon the densities deemed likely to result across a network. Selecting large density values assumes that networks are only likely to be affected when surrounded by very large landslide densities. To decrease the subjectivity and increase the robustness in this selection process, multiple thresholds are selected. Given the large range in landslide densities for the four scenarios considered (0/km^2 to >30/km^2, **Table 5.3**), two thresholds corresponding to densities observed in <50% and

<25% of the total South Island area are selected. This corresponds to 1/km^2 and 3/km^2 respectively. Consequently, exposure values are scored out of eight (four landslide scenarios × two threshold values); values of 8 represent points with densities >3/km^2 in all four scenarios, while scores of 0 represent points with <1/km^2 in all scenarios.

6.3.3 Network analysis

For scenarios developed for emergency response purposes, it is important to understand what the effects of the network exposure will mean for local populations. Network analyses provide a method to establish the connectivity of a critical infrastructure network and can therefore demonstrate the population exposed as a result of network exposure. For instance, high exposure on a road network will mean that populations dependent on that road link are highly exposed to isolation in the event of the hazard scenario occurring. Network analyses establish the linkages between nodes along various pathways (**Fig. 6.4**) and are regularly used to assess connectivity of critical infrastructure networks (e.g. Holmgren, 2006; Song and Ok, 2010). Herein network analyses are performed at a meshblock level using population data from the 2006 New Zealand Census.

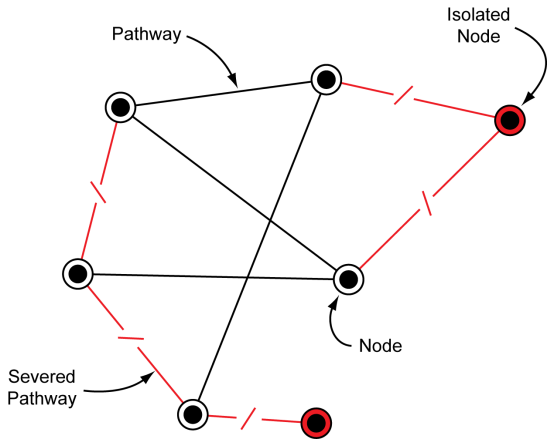

Figure 6.4: A schematic network analysis with accessible and severed pathways resulting in connected and isolated nodes.

6.4 Critical infrastructure exposure results

6.4.1 State Highway network

Applying this method to the State Highway network establishes the exposure map shown in **Fig. 6.5**. This shows that the majority of the network (∼4,760km or ∼90%) scores 0 for exposure, demonstrating the landslide densities surrounding these sections of the network never exceed 1/km^2. The total length of road with high exposure scores (>4) is ∼240 km (∼5%): approximately the same as the distance between Christchurch and Greymouth by road. Of the highly exposed sections of road, ∼115 km (∼48%) is on SH6 between Hokitika and Haast. In fact, >98% of the total length of road highly exposed to landslides is found on just three highways: SH6 in the central West Coast region; SH73 through Arthur's Pass; and SH7 through Lewis Pass (**Fig. 6.5**). These roads provide the only access between the east and west coasts and to the central West Coast region, suggesting the alpine and West Coast regions are highly exposed to isolation by road. The only other sections of highway with high exposure scores are short (<5 km) sections of SH6 north of Greymouth and SH94 near Milford Sound, which have scores of 5 and 6 respectively (**Fig. 6.5**).

Analysis of the along-route changes in density for SH6, SH7, and SH73 further demonstrates the exposure of these roads, with all three having long, continuous sections that have densities substantially larger than the assigned threshold values (**Fig. 6.6**). The maximum landslide density observed is ∼14/km^2 between Franz Josef and Fox Glacier, and all three routes have multiple locations where observed landslide densities exceed 8/km^2. The variability in observed densities is high, with densities either very much larger or very much smaller than the assigned threshold values, suggesting different thresholds would not produce substantially different results. The longest continuous section of road with high exposure is on SH7, stretching for ∼30 km along the road immediately east of Springs Junction (**Figs. 6.5 & 6.6b**). In terms of exposed length compared to total length, SH7 and SH73 have the largest proportion, with ∼23% of the total length highly exposed. In comparison, only ∼10% of SH6 is highly exposed, however this road is substantially longer than SH7 and SH73 and its highly exposed sections provide the only access route to the central West Coast region. While exposure does not directly translate to impact severity, these results suggest SH6, SH7, and SH73 are likely to be the worst affected roads following an Alpine fault earthquake, with the section of SH6 between Franz Josef and Fox Glacier likely to be especially badly affected.

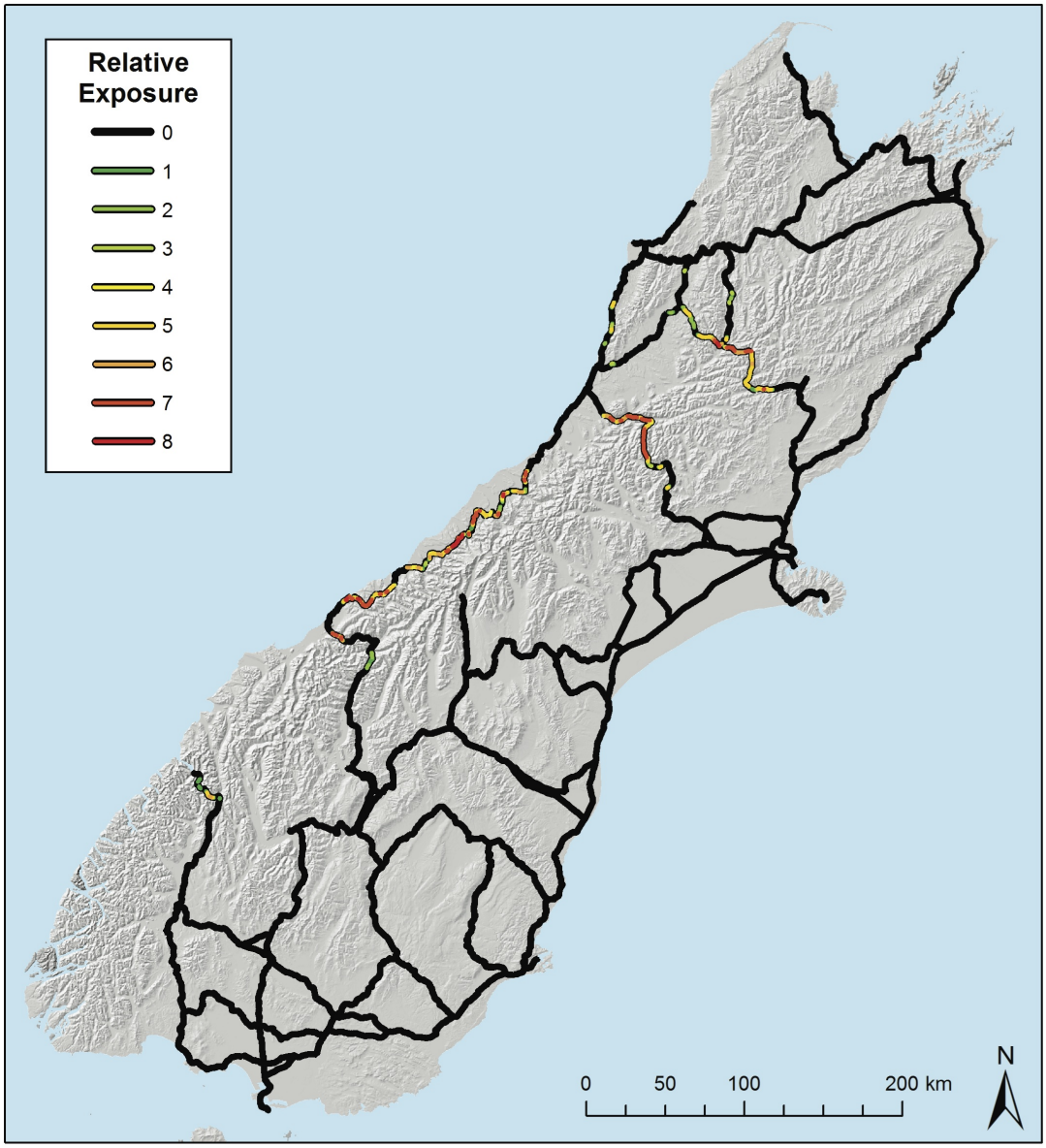

Figure 6.5: Relative exposure scores for the South Island State Highway network to coseismic landsliding from an Alpine fault earthquake.

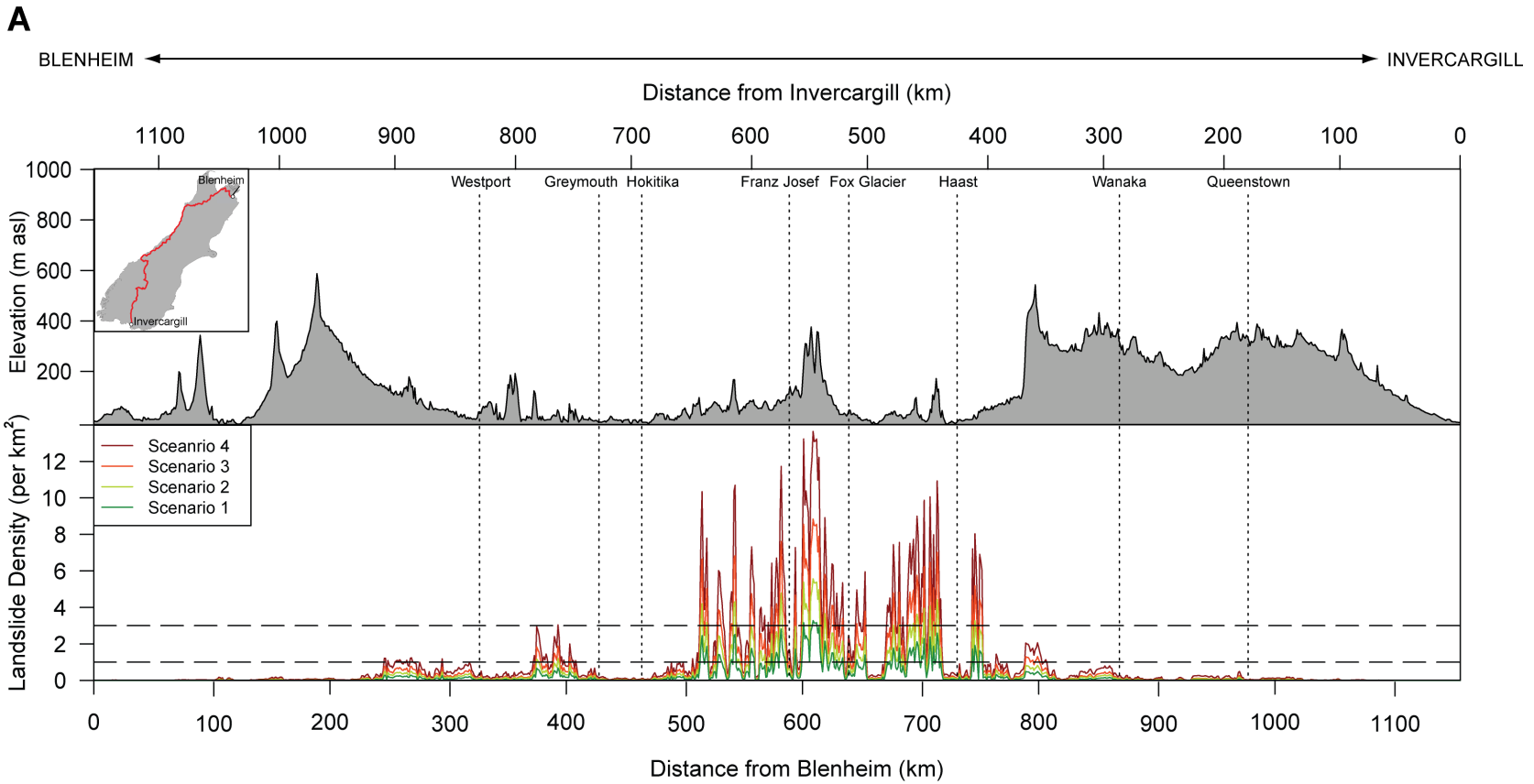
A
BLENHEIM
INVERCARGILL
Distance from Invercargill (km)
1100
1000
900
800
700
600
500
400
300
200
100
0
Westport
Greymouth
Hokitika
Franz Josef
Fox Glacier
Haast
Wanaka
Queenstown
Blenheim
Invercargill
Elevation (m asl)
1000
800
600
400
200
Landslide Density (per km^2)
Sceanrio 4
Scenario 3
Scenario 2
Scenario 1
12
10
8
6
4
2
0
0
100
200
300
400
500
600
700
800
900
1000
1100
Distance from Blenheim (km)

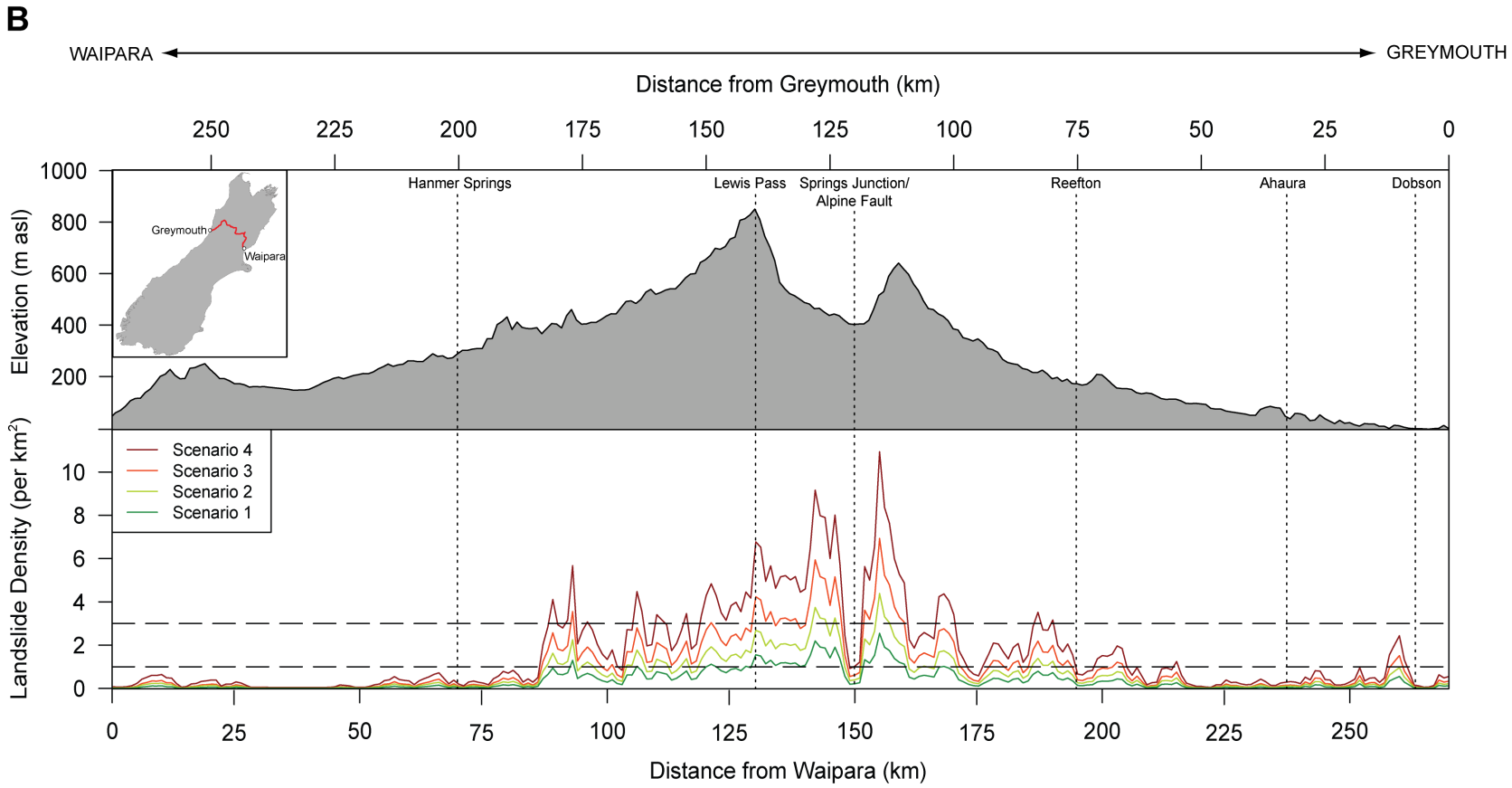
B
WAIPARA
GREYMOUTH
Distance from Greymouth (km)
250
225
200
175
150
125
100
75
50
25
0
Hanmer Springs
Lewis Pass
Springs Junction/
Alpine Fault
Reefton
Ahaura
Dobson
Greymouth
Waipara
Elevation (m asl)
1000
800
600
400
200
Landslide Density (per km2)
Scenario 4
Scenario 3
Scenario 2
Scenario 1
10
8
6
4
2
0
0
25
50
75
100
125
150
175
200
225
250
Distance from Waipara (km)

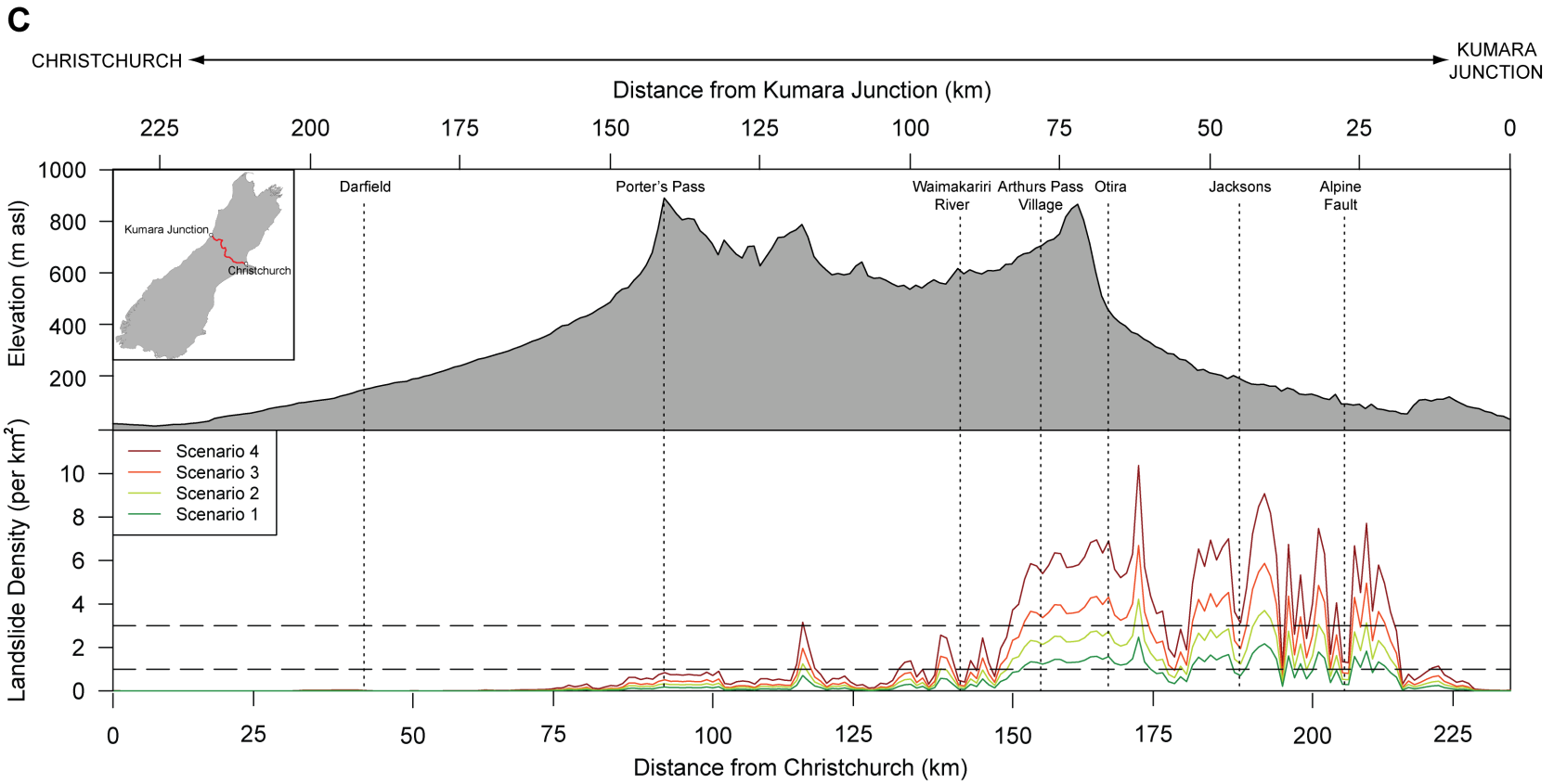

Figure 6.6: Continued from previous pages - Along-road profiles showing change in road elevation (top) and estimated landslide density values (bottom) for a) SH6; b) SH7; and c) SH73. Dashed lines show hazard thresholds; Scenario numbers refer to landsliding scenarios from Chapter 5: 1 = Minimum Average; 2 = Sample Average; 3 = Maximum Average; 4 = Extreme Maximum (see **Table 5.5**).

6.4.2 Electrical transmission network

The most important factor in the transmission network is the support structures which hold the high-voltage transmission cables (Alexander, 2005). These structures are generally resistant to strong ground shaking during earthquakes, as demonstrated by the performance of these structures during the 2010-11 Canterbury earthquake sequence (Giovinazzi et al., 2011). Nevertheless, like all built infrastructure, their survivability when impacted by coseismic landslides is low (see Lekkas, 2000). Two types of structures support the transmission network in the South Island: steel pylons and wooden poles (**Fig. 6.1**). The precise positions of all steel pylons are known and thus only pixels corresponding to the location of pylons are used, opposed to all pixels for the network which represent the cables strung between pylons. The locations of pole supports however are not known, and thus all pixels for these sections of the network are investigated.

Of the >10,500 steel pylons within the South Island, just 32 are highly exposed to coseismic landsliding from an Alpine fault earthquake (**Fig. 6.7**). Of these 30 are located in the Arthur's Pass region where the transmission network follows SH73. In total, just 119 pylons ($\sim$1%) have exposure scores >0. Importantly, the High Voltage Direct Current (HVDC) Inter-Island transmission link, which allows power sharing between the North and South Islands, has only four pylons with scores of 1 while the remaining 1,760 pylons have scores of 0 (**Fig. 6.7**). The pylon supported section of the transmission network therefore has, in general, low exposure to coseismic landsliding from an Alpine fault earthquake, with the only pylons likely to be affected being those in Arthur's Pass. Nevertheless, repairing or replacing a single steel pylon is estimated to take approximately two days once safe and secure access has been established (Adam Henderson, Transpower Ltd., pers. comm., 2012). Reinstating those pylons in Arthur's Pass could therefore take several weeks once access has been gained, although this is not accounting for continued aftershocks, landslides, debris flows etc.

The majority of wooden pole supports are located in the alpine regions and west of the Southern Alps, where the terrain and limited road links make construction and maintenance of steel pylons difficult (**Fig. 6.1**). Consequently, they are exposed to very strong ground motions (MM8+) as well as high landslide susceptibilities. There are $\sim$98 km of wooden pole-supported transmission cables with high exposure to landsliding, and >50 km with extremely high (>6) exposure (**Fig. 6.7**). Assuming average distances between poles of $\sim$50 m, this equates to $\sim$2,000 wooden poles with high exposure, and 1,000 with extremely high exposure. The most exposed sections are through Arthur's Pass and around Franz Josef and Fox Glacier, although small sections of the network north of Greymouth are also highly exposed. Despite repairing or replacing wooden poles likely requiring significantly less time than steel

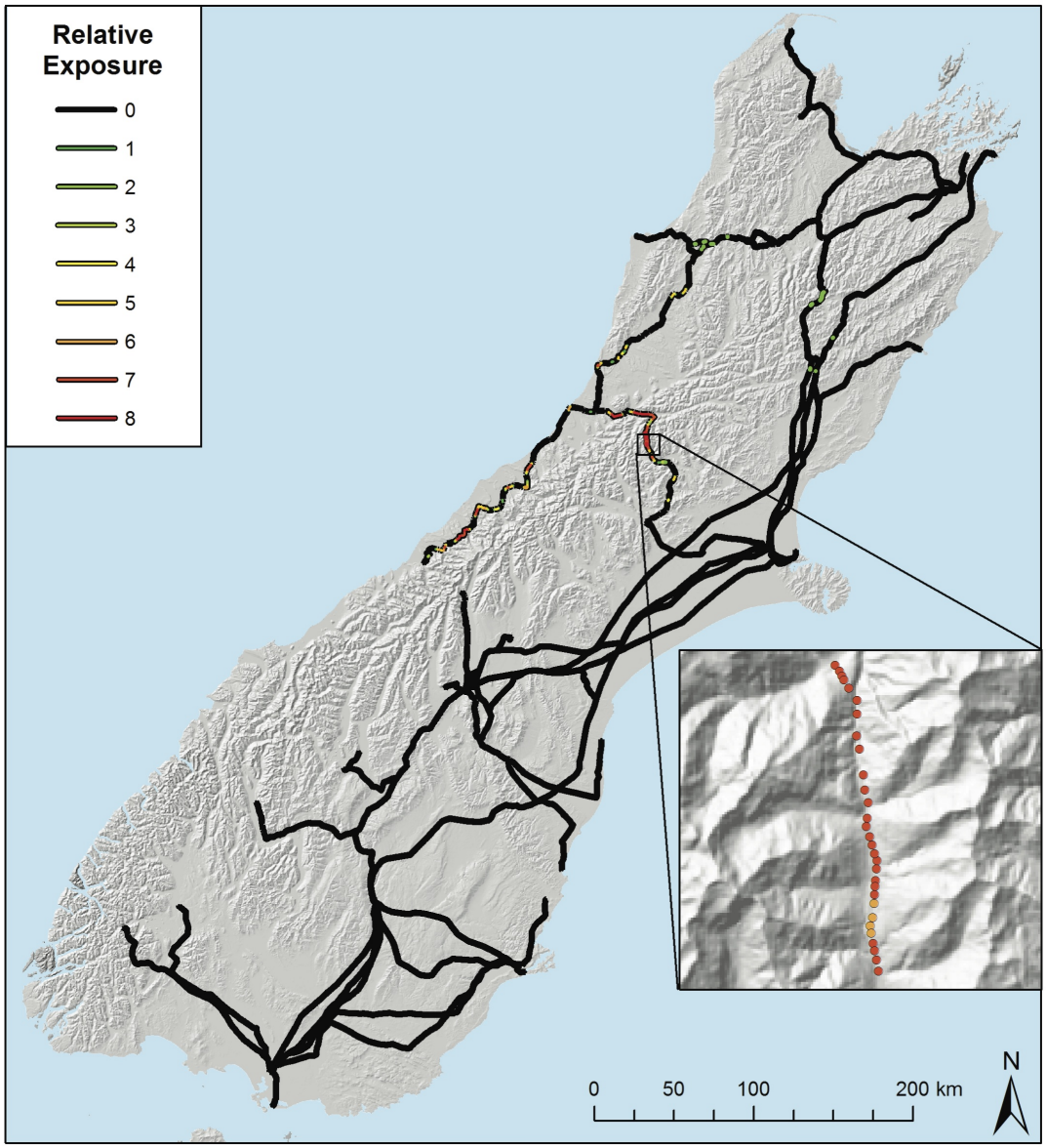

Figure 6.7: Relative exposure scores for the electrical transmission network to coseismic landsliding from an Alpine fault earthquake. Inset: steel pylons in the Arthur's Pass area with high exposure to landsliding.

pylons (see above), this still likely equates to several thousand person-hours, again not accounting for further hazards. Repairing/replacing wooden pole supports post-earthquake is therefore likely to present a major restoration effort.

6.5 Network analysis results

Undertaking network analyses using these exposure maps (**Figs. 6.5 & 6.7**) allows the total number and spatial distribution of the population at risk of isolation and power loss to be assessed. This is important for basic emergency response planning as it can identify the population which is most likely to be severely affected and in need of emergency services. Using data from the 2006 New Zealand Census, the State Highway and electrical transmission connectivity is assessed at a meshblock scale. Each meshblock is scored out 8 corresponding to the number of landslide scenarios in which it remains connected; a score of 8 corresponds to a meshblock whose connected pathways have at least one exposure score of 8 (i.e. landslide densities >3/km^2 in all four landslide scenarios), a score of 0 corresponds to a meshblock whose connections have no score >0 (i.e. landslide densities <1/km^2 for all scenarios).

6.5.1 Isolation

Meshblock isolation exposure scores as a result of the State Highway exposure to landsliding are shown in **Fig. 6.8**. Scores >4 represent meshblocks that are highly exposed to isolation as a result of coseismic landsliding from an Alpine fault earthquake. In terms of area, $\sim$14,500 km^2 ($\sim$10%) of the South Island has a high exposure to isolation, $>$11,200 km^2 ($>$75%) of which is in the West Coast region, accounting for $\sim$48% of its total area. Within the West Coast region, Westland district, which comprises the area south of the Taramakau River (see **Fig. 3.1**), is the most exposed, with $>$8,500 km^2 scoring >4, which accounts for $>$70% of the total district area.

However, the West Coast region is sparsely populated with a total of just 30,825 residents giving an average population density of 1.3 people/km^2. South of Fox Glacier this sparsity is even more apparent with only 690 permanent residents inhabiting an area of $>$6,000 km^2 at a density of $\sim$0.1 people/km^2. Thus, the total population with high exposure to isolation is estimated to be 2,748, of which 1,830 live in Westland district, south of Hokitika. The remaining population live in the alpine regions around Arthur's Pass and Lewis Pass, however this figure does not include visitors to the region. The total permanent population of Franz Josef and Fox Glacier combined is $\sim$400, but during the tourism high season between September and March several thousand visitors could be staying in these towns, placing a significant burden

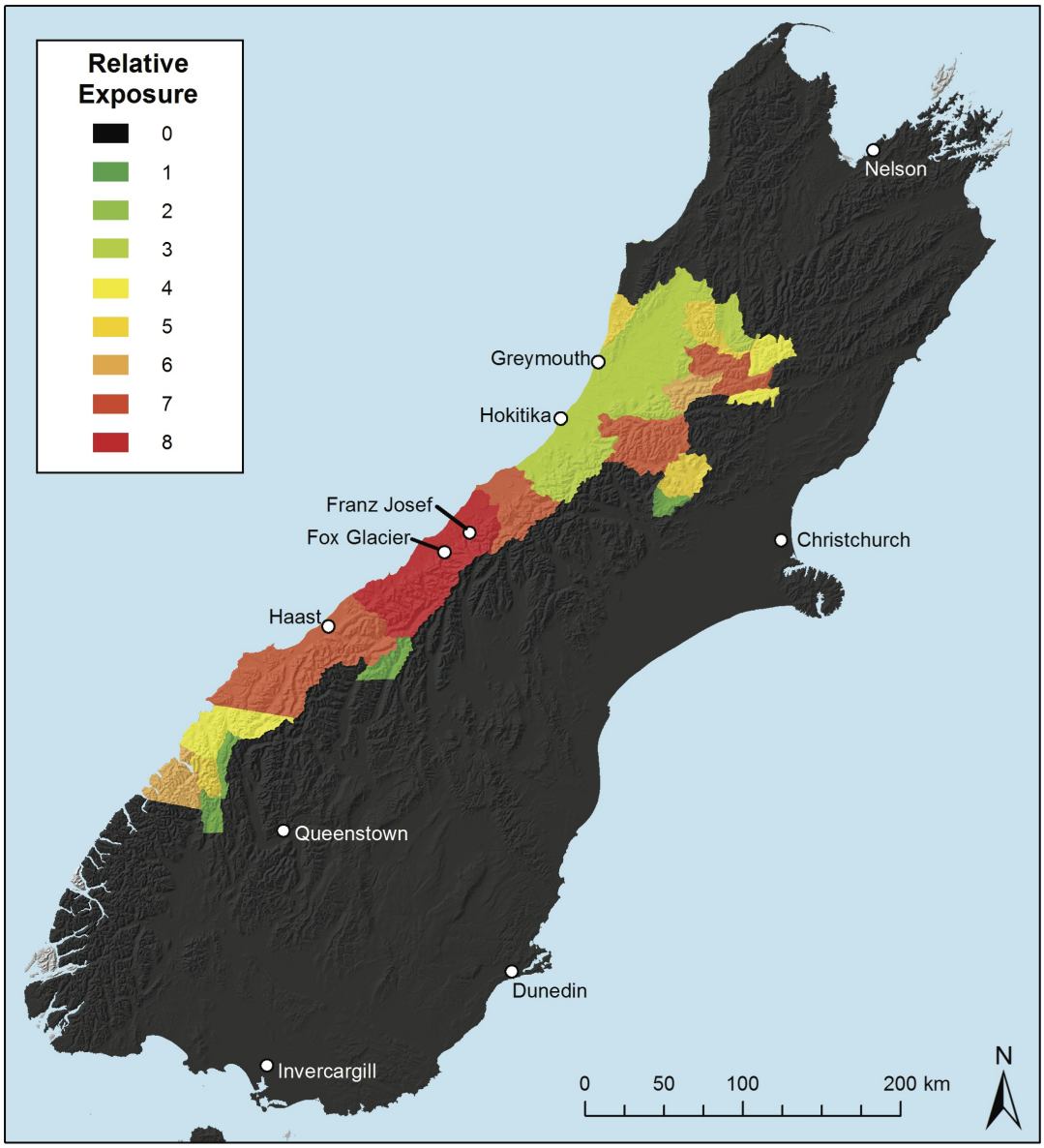

Figure 6.8: Relative exposure to isolation scores across the South Island as a result of coseismic landsliding exposure of the State Highway network to an Alpine fault earthquake.

on local emergency resources (Orchiston, 2011). Of further note, ∼24,000 people have an isolation exposure score of 3 primarily in Greymouth, Hokitika, and the surrounding regions (**Fig. 6.8**). Despite this being considered low-to-medium exposure, there is clearly the potential for coseismic landsliding in an Alpine fault earthquake to cause large numbers of local people to become isolated from the rest of the South Island.

6.5.2 Power loss

Results for meshblock exposure to power loss as a result of the electrical transmission network exposure to coseismic landsliding are shown in **Fig. 6.9**. This suggests that a far larger area of the South Island is highly exposed to power loss compared to isolation. In total, >20,000 km^2 is estimated to have power loss scores >4, more than 5,000 km^2 larger than the area with corresponding scores for isolation. The majority (>85%) of the area highly exposed to power loss is in the West Coast region, accounting for >60% of the total region. In total, ∼16,000 km^2 has exposure scores >6, which includes the entire Westland district and the Arthur's Pass area. This equates to a total of >23,000 people exposed to power loss, of which the vast majority are in the West Coast region.

6.5.3 Combined isolation and power loss

Combining **Figs. 6.8 & 6.9** demonstrates a meshblocks combined exposure to both isolation and power loss simultaneously. Meshblocks with high combined exposure scores are likely to be the worst affected by the earthquake scenario and therefore the primary focus of the emergency response. In this instance, meshblocks which have combined exposure scores ≤5 are considered to have low exposure, while those with combined scores ≥11 are considered to have high exposure. The combined isolation and power loss exposure results are shown in **Fig. 6.10**.

The most exposed area (combined score ≥11) covers ∼13,000 km^2 and contains >2,300 people. As expected, this predominately affects Westland district south of Hokitika and the alpine regions in the Arthur's Pass and Lewis Pass regions (**Fig. 6.10**). In total, >21,000 people across >7,000 km^2 have medium combined exposures, the majority of which are in Greymouth, Hokitika, and the surrounding areas. These results highlight that in the event of an Alpine fault earthquake, central and southern Westland district and the Arthur's Pass area are expected to be the worst affected, with high combined exposure scores.

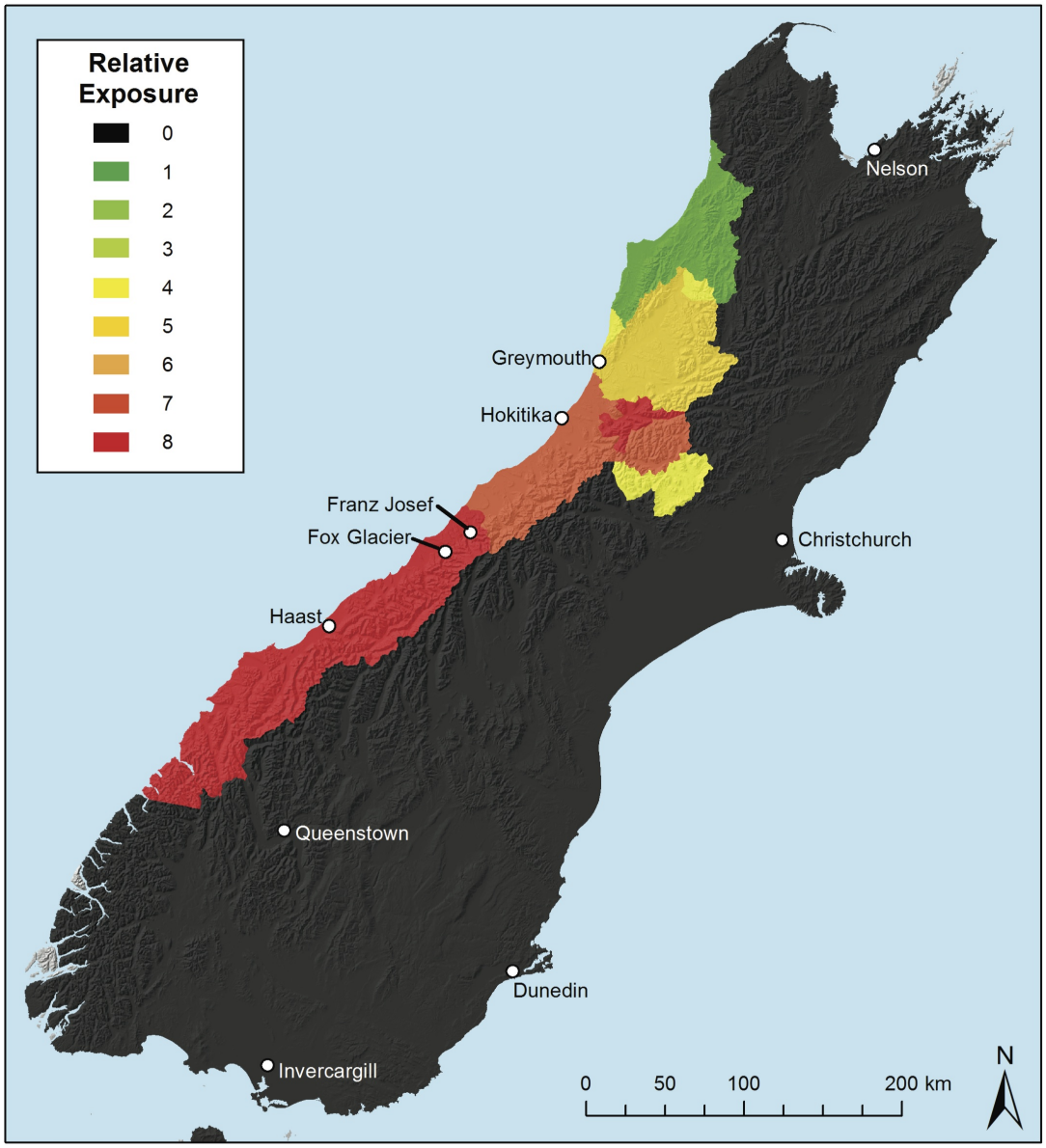

Figure 6.9: Relative exposure to power loss scores across the South Island as a result of coseismic landsliding exposure of the electrical transmission network to an Alpine fault earthquake.

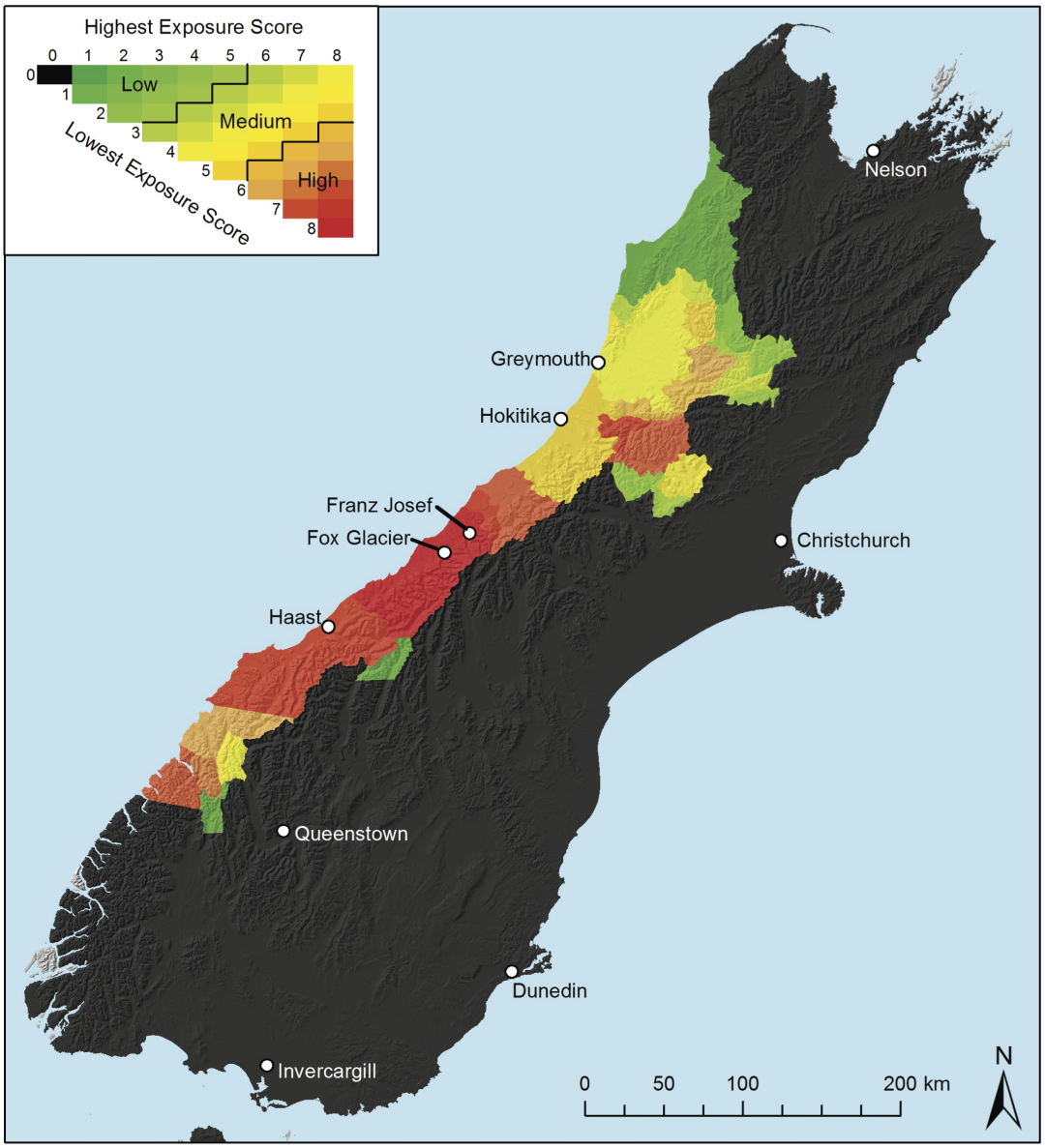

Figure 6.10: Relative exposure to combined isolation and power loss as a result of coseismic landsliding exposure of the State Highway and electrical transmission networks.

6.6 Emergency response planning

Areas most exposed to combined isolation and power loss were found to correspond to locations where >75% of fatalities are expected to occur (see Chapter 3 and Appendix C) and where large numbers of visitors will put a significant burden on local resources (Orchiston, 2011). These regions and communities should, therefore, be targeted for rapid emergency response immediately after a large Alpine fault earthquake. Planning potential emergency response routes to facilitate a rapid emergency response is vital. Using the State Highway exposure map (**Fig. 6.5**), it is possible to plan potential emergency response routes and identify any critical sections of the network whose functionality post-earthquake is vital to the emergency response.

Emergency response following the earthquake will need to originate from relatively unaffected large towns or cities with emergency operations centres (EOCs) as these will have the greatest emergency response capacity. EOCs have been shown to be critical to any emergency response (Drabek, 1985) and thus establishing which EOCs are physically connected to the worst-affected regions is vital. The South Island's primary EOCs are located in:

- Nelson (Nelson-Tasman CDEM);
- Blenheim (Marlborough CDEM);
- Greymouth (West Coast CDEM);
- Christchurch (Canterbury CDEM);
- Dunedin (Otago CDEM); and
- Invercargill (Southland CDEM)

Emergency response routes herein are planned to originate from the three largest EOCs: Christchurch, Dunedin, and Nelson. Routes from these EOCs are planned for four key nodes in the West Coast region as this is where the majority of the emergency response will be required. These nodes are: Greymouth, Franz Josef, Fox Glacier, and Haast.

Scaled route diagrams (**Fig. 6.11**) between each of the selected locations demonstrate the vulnerability of a particular route by schematically displaying the length of the route as a function of its relative exposure to landsliding. Several conclusions can be drawn from these. Firstly, access to Franz Josef and Fox Glacier, which can only be gained along SH6 from the north or south, is likely to be impossible as all access routes pass through long areas of high exposure (**Fig. 6.11**). Both townships are located on one of the most exposed sections

of road (**Fig. 6.5**), with multiple sections of high exposure north of Franz Josef and south of Fox Glacier, as well as between both townships. Emergency access by road post-earthquake to, and between these townships is therefore considered highly unlikely.

All access to the West Coast region directly from Christchurch requires travelling through either Arthur's, Lewis, or Haast Passes. Both Arthur's Pass and Lewis Pass have high exposure to landsliding and Haast Pass also has sections of high exposure, although these are much shorter in length (**Fig. 6.11**). Gaining access to any of the considered nodes directly from Christchurch is therefore infeasible. The same is also the case for Dunedin as routes from here to the West Coast region also travel through the three alpine passes. While the exposed section of Haast Pass is substantially shorter than those in Arthur's and Lewis Pass, the exposure score is the same. Gaining emergency access through Haast Pass is therefore considered unlikely.

In contrast, **Fig. 6.11** demonstrates that a route with low exposure exists between Greymouth and Nelson, via SH69 and SH7 west of Reefton (**Fig. 6.12**). None of the exposed sections of this route have exposure scores >3 and the exposed lengths are just $\sim$1 km. The likelihood of this route being affected by landsliding is therefore considered low. As this route can provide direct access to Greymouth, Hokitika, and the surrounding rural regions, these meshblocks all have low-to-medium exposure (=3) to isolation (**Fig. 6.8**). The population within these meshblocks is $\sim$21,000, which represents $>$85% of the total population with exposure scores >0. If this route remains functional post-earthquake, the total isolated population is estimated to be $\sim$2,700, most of whom live south of Hokitika; however if it is compromised in any way, this number will increase almost ten-fold to $\sim$24,000 people. It therefore constitutes the most critical section of highway following an Alpine fault earthquake.

This section of the network is anticipated to experience MM7-8 shaking (**Fig. 2.4**) and thus it is vital that it is able to withstand such shaking intensities. During the 22 February 2011 Christchurch earthquake, road bridges experiencing similar shaking intensities performed poorly, with five out of the six bridges across the Avon River closed due to damage and many others requiring reduced weight limits (Giovinazzi et al., 2011). It is therefore vital that the bridges on SH69 and SH7 between Reefton and Greymouth are able to withstand the shaking intensities they will be exposed to, as this will further increase the likelihood of this section of highway remaining functional post-earthquake. Further consideration must also be given to liquefaction and lateral spreading which was identified by McCahon et al. (2006b) as being likely to occur in the Grey River valley where these sections are located. Liquefaction and lateral spreading greatly damaged the roads during the Christchurch earthquake (Giov-

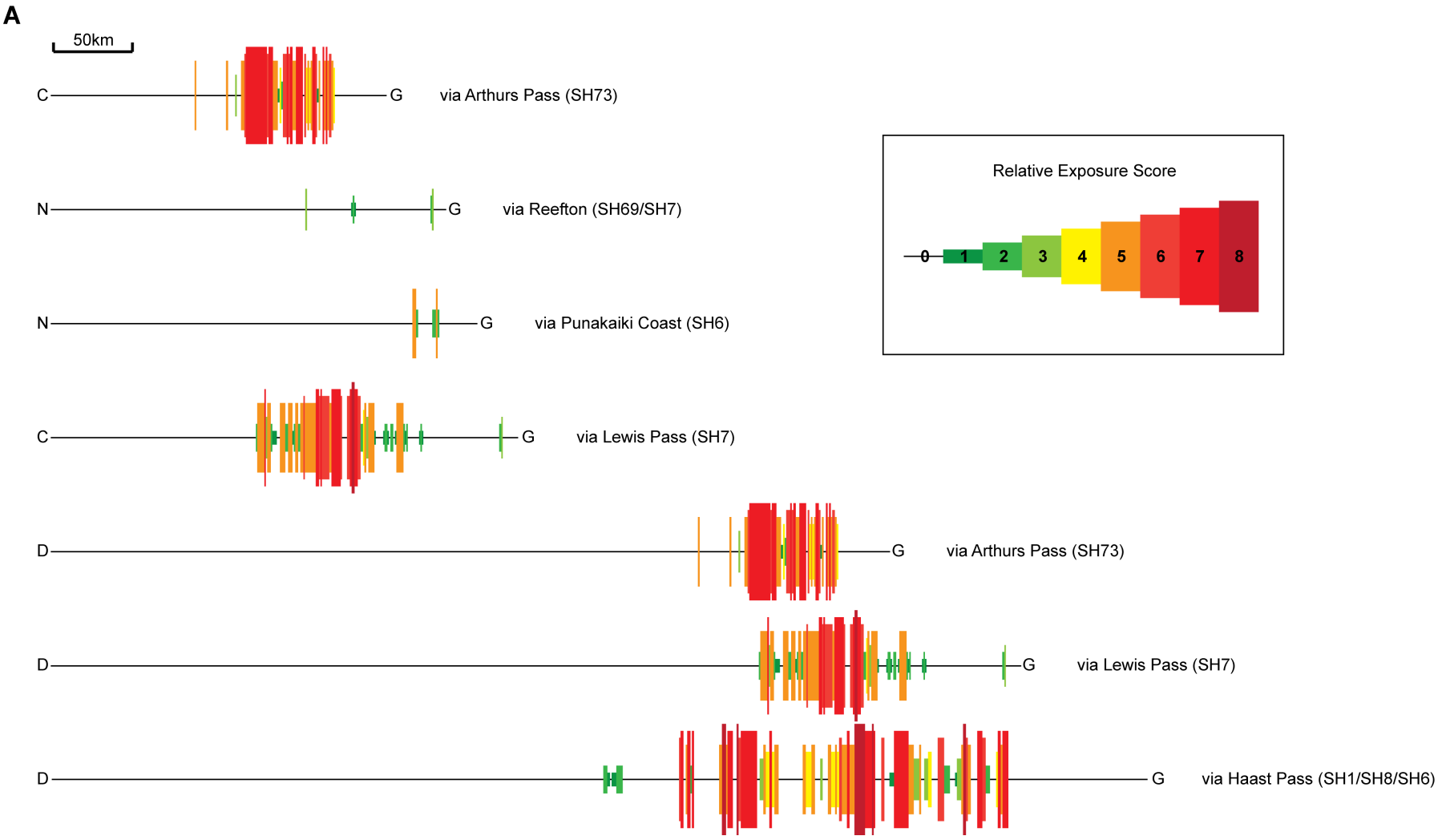
A
50km
C
G
via Arthurs Pass (SH73)
N
G
via Reefton (SH69/SH7)
N
G
via Punakaiki Coast (SH6)
C
G
via Lewis Pass (SH7)
D
G
via Arthurs Pass (SH73)
D
G
via Lewis Pass (SH7)
D
G
via Haast Pass (SH1/SH8/SH6)
Relative Exposure Score
0
1
2
3
4
5
6
7
8

B

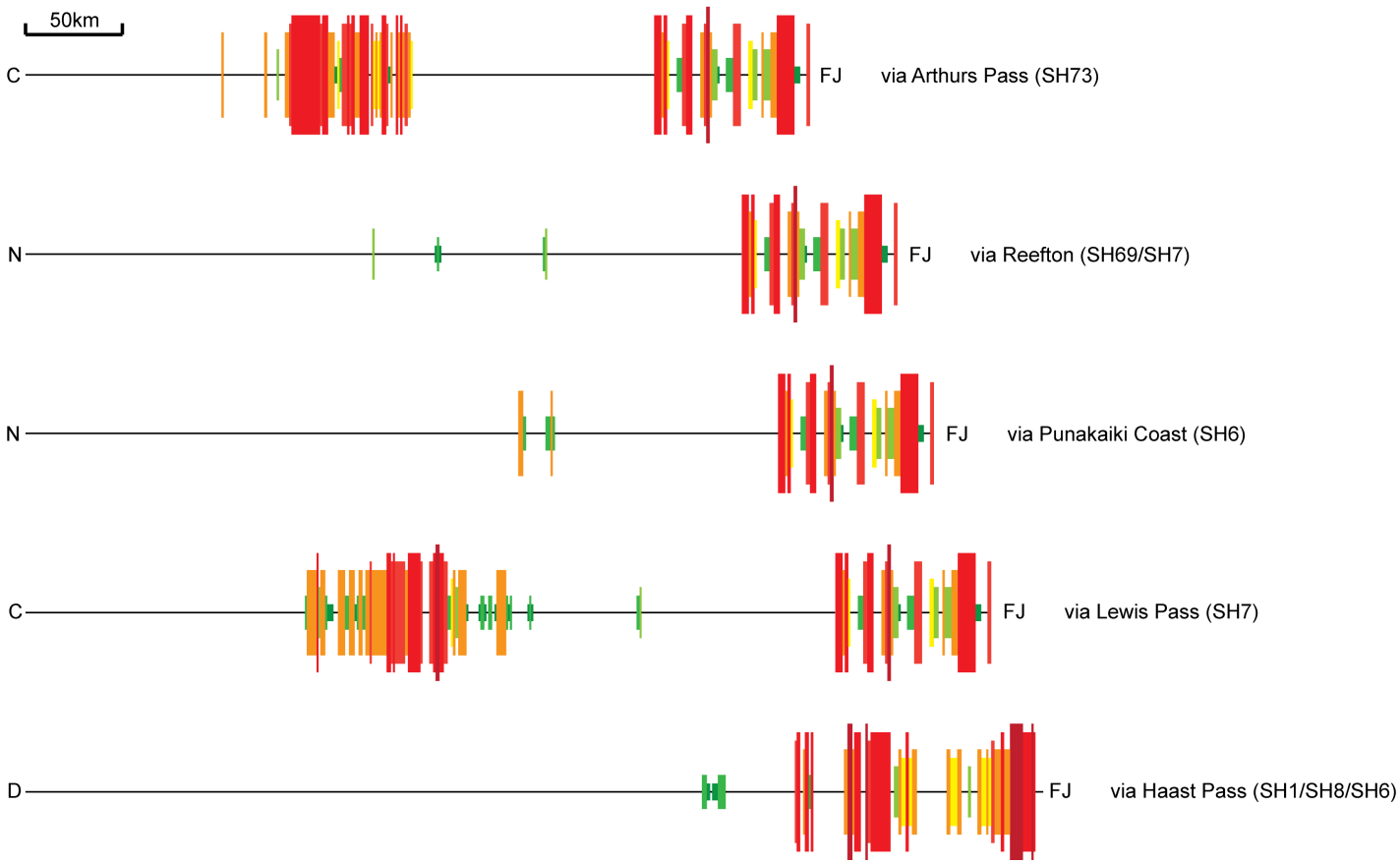
50km
C
FJ
via Arthurs Pass (SH73)
N
FJ
via Reefton (SH69/SH7)
N
FJ
via Punakaiki Coast (SH6)
C
FJ
via Lewis Pass (SH7)
D
FJ
via Haast Pass (SH1/SH8/SH6)

C

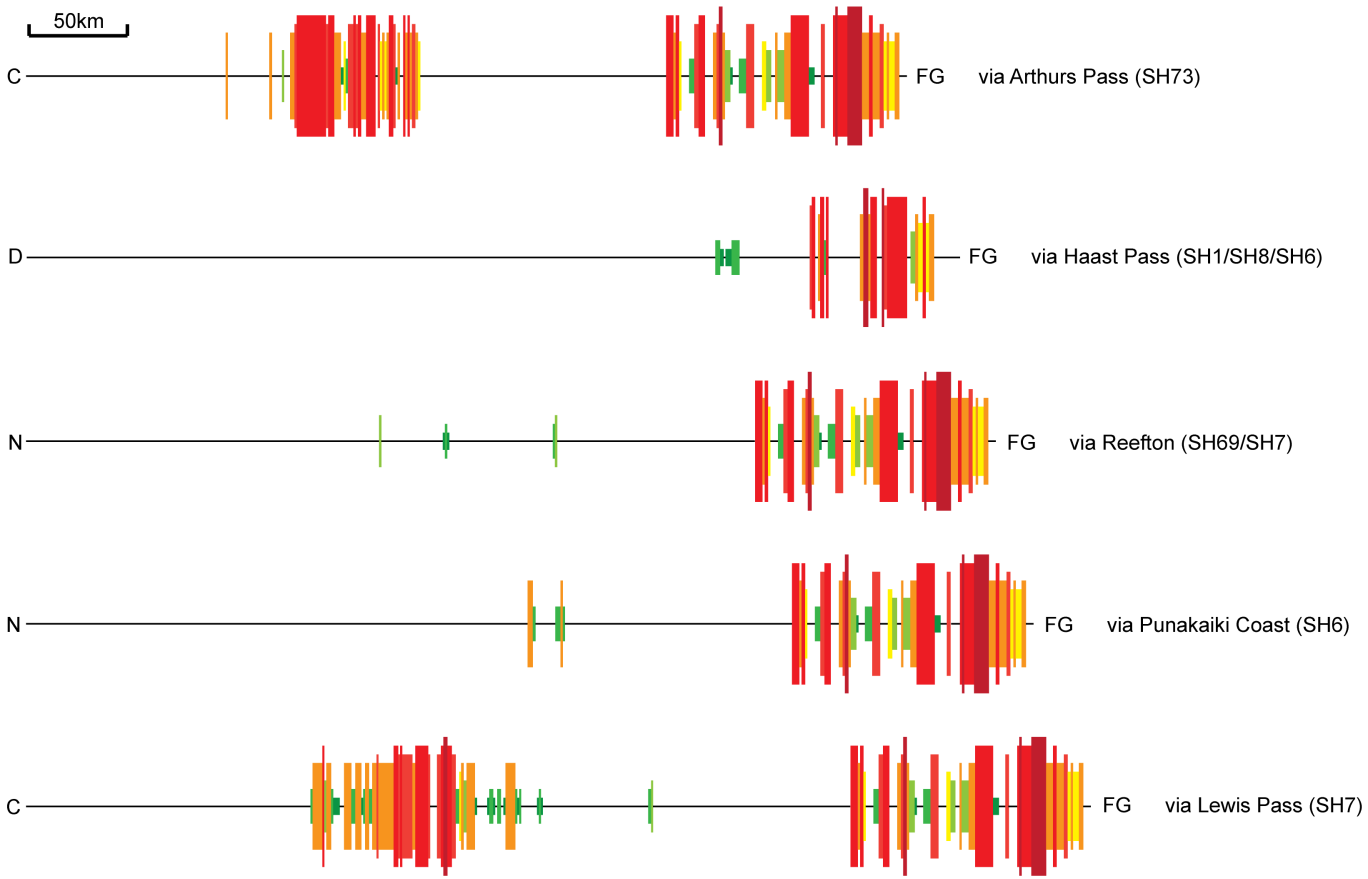
50km
C
FG
via Arthurs Pass (SH73)
D
FG
via Haast Pass (SH1/SH8/SH6)
N
FG
via Reefton (SH69/SH7)
N
FG
via Punakaiki Coast (SH6)
C
FG
via Lewis Pass (SH7)

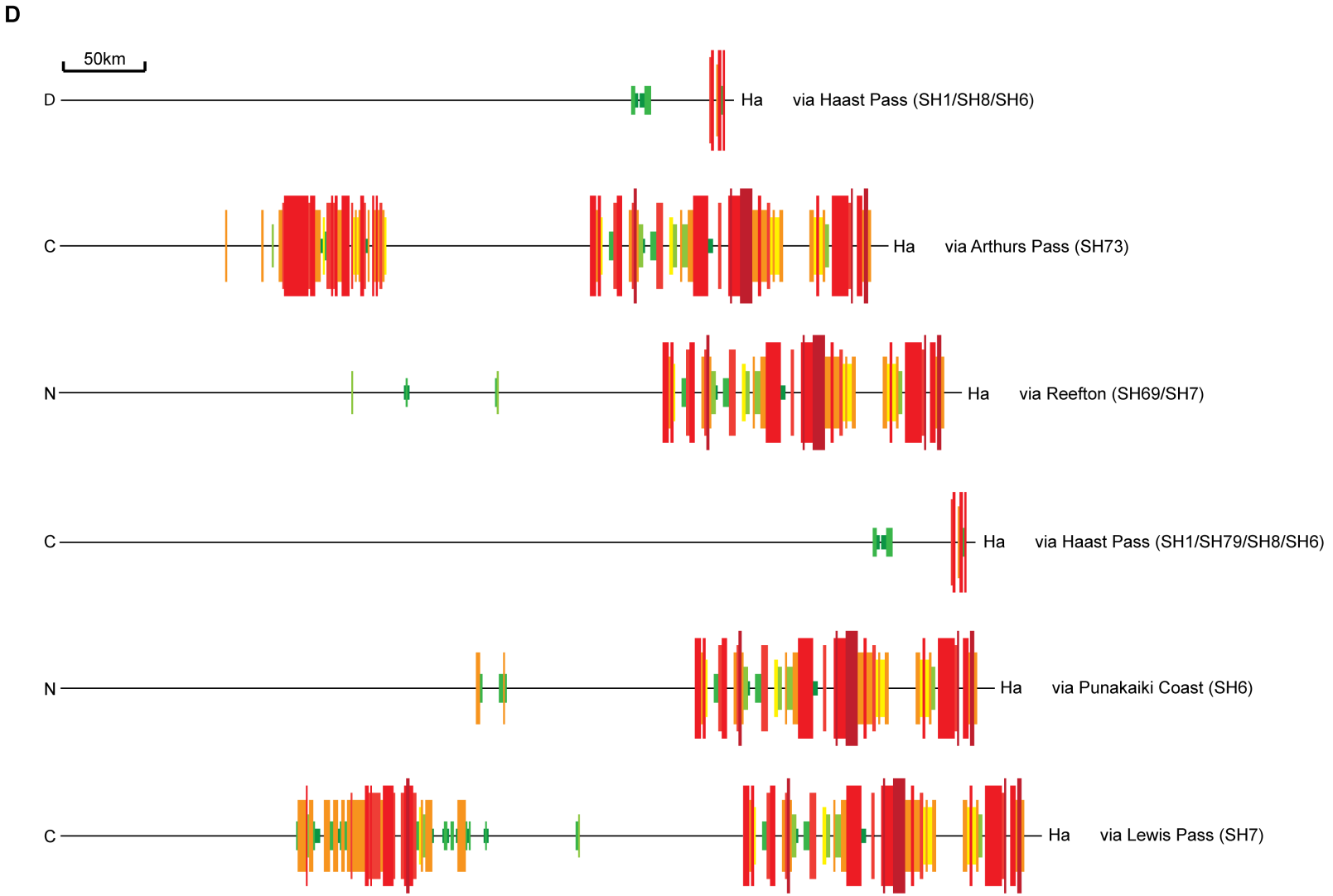

Figure 6.11: Continued from previous pages - Schematic route diagrams showing the relative length and exposure (bar width) to coseismic landsliding for various routes between: Christchurch (C), Dunedin (D), Nelson (N) and a) Greymouth (G); b) Franz Josef (FJ); c) Fox Glacier (FG); and d) Haast (H).

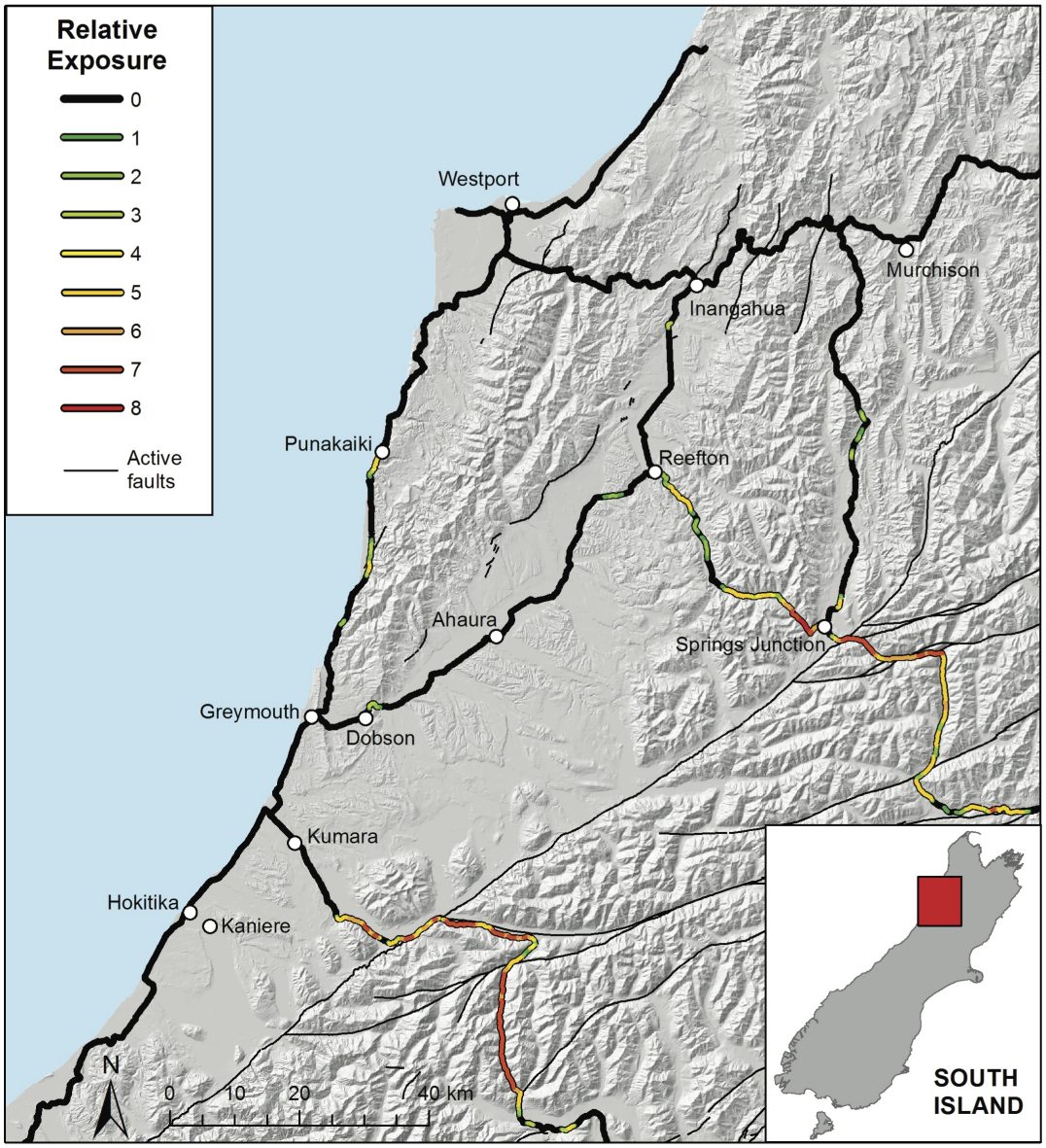

Figure 6.12: Relative exposure to coseismic landsliding of the State Highway network in the Grey River Valley region. SH69 (Inangahua to Reefton) and SH7 (Reefton to Greymouth) have a maximum exposure scores of just 3 and thus represent the most critical section of the network with regard to an Alpine fault earthquake.

inazzi et al., 2011), and while most remained traversable this was only to four-wheel drive vehicles and at greatly reduced speeds.

Assuming the functionality of the State Highway network through the Grey River valley can be retained post-earthquake has important consequences for potential emergency response operations. Emergency response to the worst affected regions from Christchurch and Dunedin has been shown to be infeasible given the extremely high exposures that exist on all potential access routes. However access may be gained from Nelson via the Grey River valley. Nelson is the South Island's third-largest city (population ∼46,000) and therefore has some capacity to respond to such an emergency, having a major port and long-runway airport. In addition, Nelson is within a one hour drive of Woodbourne military airbase and the Picton ferry terminal (along highways with exposure scores of 0), from which ferries directly connect the South Island to Wellington and the rest of the North Island. Thus Nelson is well-connected to Wellington, New Zealand's capital and second-largest city, with total sea-and-land journey times between Wellington and Nelson lasting four hours, compared to six-to-seven hours between Christchurch and Nelson via Kaikoura. Wellington hosts New Zealand's Parliament, the National Crisis Management Centre (NCMC), and Ministry for Civil Defence and Emergency Management (MCDEM) headquarters, as well as containing a major port, airport, and rail terminal connected to the rest of the North Island. Utilising this link between Wellington and Nelson will therefore likely prove vital in responding to an Alpine fault earthquake. Basing the emergency response to an Alpine fault earthquake out of Wellington and using Nelson as a forward operating base, utilising the land, air, and sea connections between the two, therefore likely presents the best response option.

6.7 Hazard assessment of proposed future highway project

As well as being useful for emergency response assessments, the method described herein can also be applied as a planning tool to assess the landsliding exposure of potential future network projects from an Alpine fault earthquake. Currently, a proposal is being drafted to gain resource consent for a new highway connecting Haast with Milford Sound via the Hollyford and Cascade River valleys (The Press, 2014; Wilderness Magazine, 2014). The road is intended to provide easier access between the West Coast region, Queenstown, and Milford Sound, some of New Zealand's most popular tourist destinations. The proposed route (**Fig. 6.13**) follows an *unformed legal road* (ULR), a parcel of land that has legally been designated as a road but has not actually been formed. Legally in New Zealand, a ULR has the same status as any fully formed road. Known as the Haast-Hollyford road, it would

reduce the trip between Haast and Milford Sound by ∼355 km and four-to-five hours (The Press, 2014). Construction analysis has already been undertaken and the road is expected to cost <NZ$230 million to build and is anticipated to be used by >800,000 people in its first year, with an expected growth rate of 6% annually (The Press, 2014; Wilderness Magazine, 2014). At the time of writing, proponents of the road are contemplating legal action over whether a 38 km section of road was illegally removed from ULR status in the 1970s. If the action goes to court and is successful, resource consent for the road will be sought. As a potentially relevant example of the use of the present technique in planning, an assessment of the exposure of the proposed road to coseismic landsliding from an Alpine fault earthquake is undertaken.

Firstly, the proposed route crosses the known trace of the Alpine fault at least four times, following the fault trace for ∼10 km between the Arawhata and Cascade Rivers (**Fig. 6.13**). Furthermore, the route passes across the deposits of at least three known rock avalanches and is in close proximity to the headscarps of two others (**Fig. 6.13**). The Cascade rock avalanche deposit transects the proposed highway, and has the potential to generate a failure involving ∼0.25 km^3 towards the road, with a *sackung* located behind the previous headscarp (Barth, 2014).

High coseismic landslide exposures are expected along ∼100 km of the 159 km route (**Fig. 6.14**). Between the Cascade and Pyke Rivers, modelled landslide densities exceed the previous highest observed density for the current network (∼14/km^2) for an almost continuous 20 km section (**Fig. 6.15**). Consequently, ∼90 km (∼56%) of the route has high exposure to landsliding, and ∼60 km (∼38%) has extremely high (>6) exposure (**Fig. 6.14**). Given the potential numbers of people using the road annually, its construction would clearly present a significant risk to road users, as well as any consequent infrastructure (fuel stations, townships etc.) which may subsequently develop along the road. From a planning point of the view this analysis has clearly demonstrated that such a road would be extremely exposed to landsliding in an Alpine fault earthquake, and this should be considered when assessing whether or not to grant resource consent. A further point for consideration is that the risk of landslide tsunami affecting tourists staying overnight in Milford Sound has been shown to be unacceptable with current tourist numbers (Dykstra, 2012). The Haast-Hollyford road is intended to increase tourist numbers to Milford Sound, further exacerbating this already unacceptable risk.

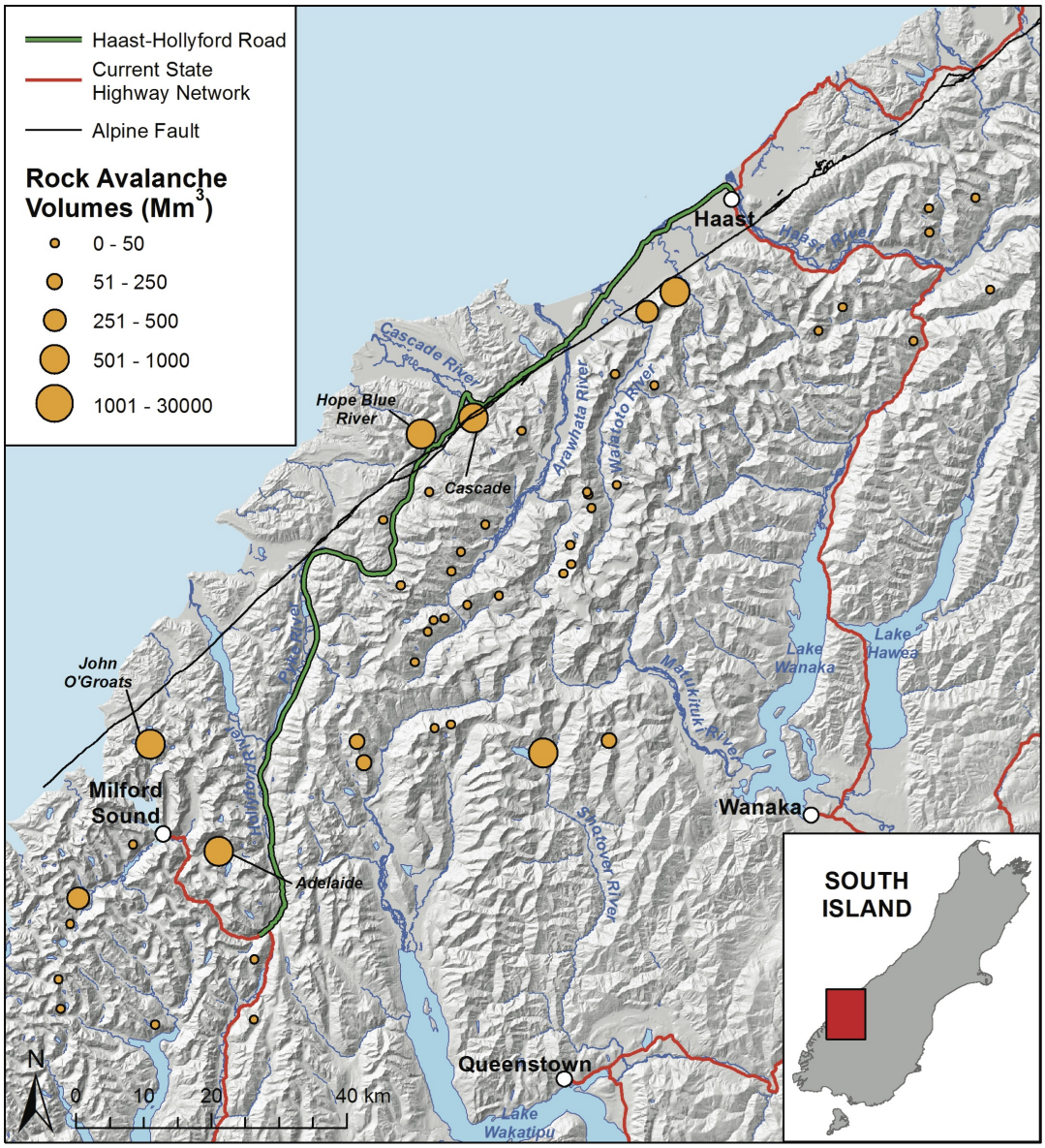

Figure 6.13: Existing route of the Haast-Hollyford unformed legal road (from The Press 2014) in relation to the existing State Highway network and known locations of large rock avalanches and the Alpine fault.

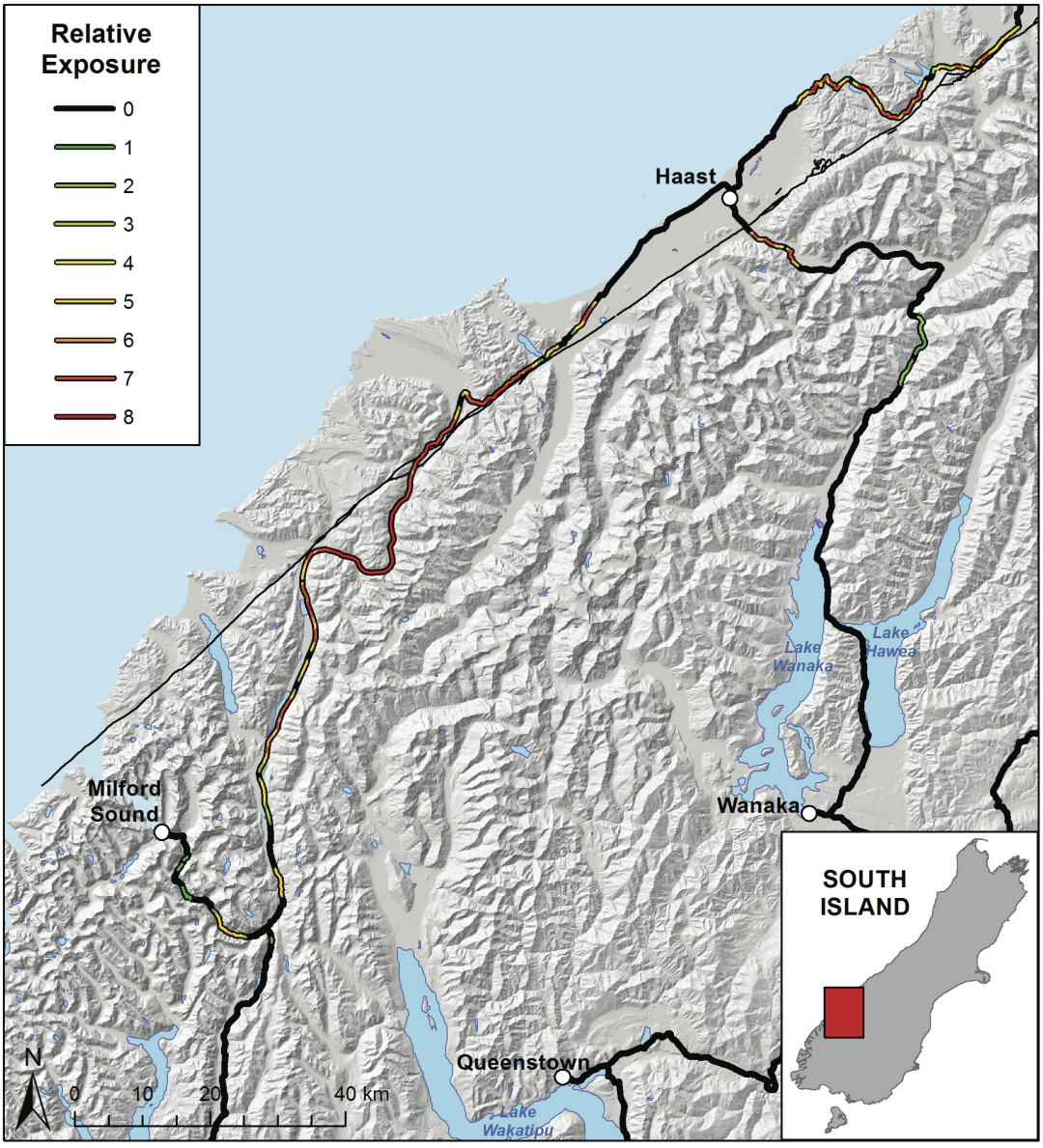

Figure 6.14: Relative exposure to coseismic landsliding for the proposed Haast-Hollyford road.

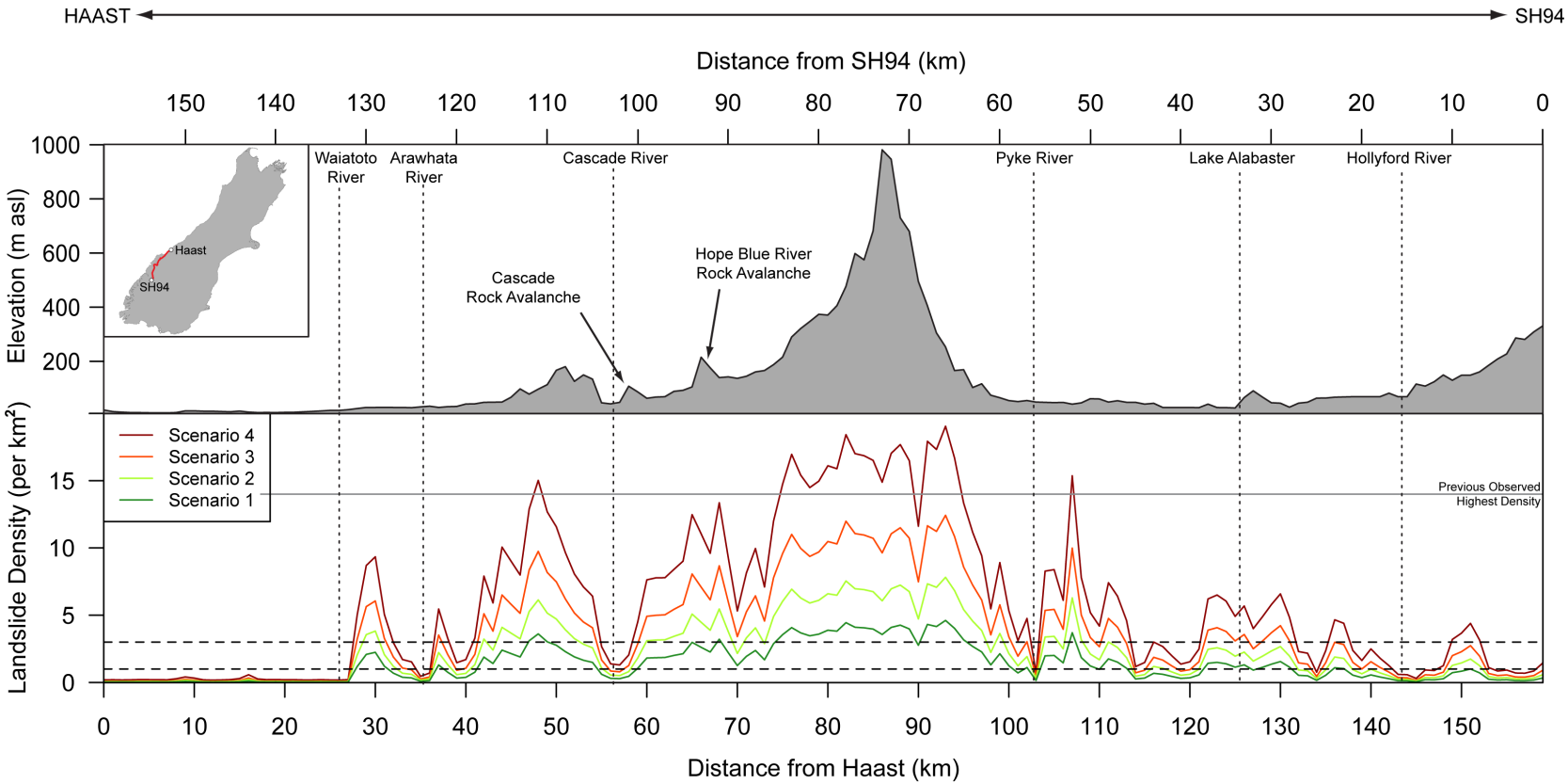

Figure 6.15: Along-road profile of the proposed Haast-Hollyford road showing the change in road elevation (top) and estimated landslide density values (bottom). Dashed lines show impact thresholds; solid grey line shows the highest observed landslide density on the current network.

6.8 Discussion

Understanding the exposure of critical infrastructure such as transport and utilities networks as a result of coseismic landsliding is vital to understanding the potential losses from an earthquake as a whole (Bird and Bommer, 2004). Given the complexities in predicting landslide occurrence, runout, and magnitude amongst other factors, measuring the exposure of critical infrastructure networks to coseismic landsliding has proved difficult (Pellicani et al., 2013). This chapter has therefore established a method for analysing the exposure of critical infrastructure to coseismic landsliding utilising a susceptibility map and associated landslide scenarios. This method is applicable to any critical infrastructure network (water supplies, telecommunications, fuel supply, buildings etc.) and can also be applied to aseismic landsliding as long as a susceptibility map can be produced. Nevertheless, several limitations should be considered.

Firstly, in order to determine the region surrounding a network from which susceptibility is analysed, landslide runout is assumed to be in the steepest downhill direction. In some instances however, landslides can become channelised within narrow valley systems (see Okada et al., 2008) and can thus have complex runout paths. A network may therefore still be exposed to landslides occurring outside the surrounding area. Further, during heavy rainfall, increased water content can result in landslides becoming fluidised and consequently runout distances typically increase (Legros, 2002). Other factors can also affect mobility resulting in extremely mobile landslides which can travel several tens of kilometres (see Appendix A). Further still, some very large landslides have been observed to travel over opposing ridgelines and into adjacent valleys (see Huang et al., 2012). This should be taken into account when considering the exposure results as clearly there is the potential for landslides outside the surrounding areas to affect a network. To fully incorporate these effects however requires modelling of individual landslide runout which is currently complex, particularly from a susceptibility model, and beyond the scope of this study.

Consideration must also be given to the fact that not all landslides occurring within the surrounding area will pose a threat to the network. This is particularly true for small volume landslides that typically have very short (several tens-to-hundreds of metres) runout distances. If such landslides occur at the very edge of the surrounding region (i.e. $\sim$1 km from the network) it is unlikely that their total runout distance will result in any damage to the network, regardless of the density of landslides in the area. Nevertheless, this is true for all surrounding areas and therefore all pixels along the network. Considering exposure relatively compared to the rest of the network effectively negates this effect. However, this should be considered when evaluating the absolute density values.

Exposure has been defined as a function of the landslide density resulting from the susceptibility values observed in the various surrounding regions. This assumes that larger landslide densities are more likely to affect a network than smaller densities. However only a single landslide is required to impact a point on a network, regardless of density. Thus, any surrounding region within which one or more landslides occurs exposes the network to landslide hazard. Intuitively however, points experiencing larger densities are more likely to be impacted (and therefore more exposed) than those experiencing smaller densities, as there is a greater likelihood of any single landslide intersecting the network. Thus, any section of the network which achieves low (or no) exposure may still have landslides occurring nearby, but at a sufficiently low density that the likelihood of them affecting the network is considered negligible. Again, considering the exposure relative to the rest of the network allows this to be considered as it describes the locations that are relatively more or less exposed.

Finally, the present results have been obtained using hazard threshold landslide densities of 1 and 3 landslides/km^2 and it is appropriate to consider the sensitivity of the results to these thresholds. From the along-route changes in landslide density graphs presented, it is evident that altering the thresholds would alter these results very little, as the observed densities across both networks are either substantially larger or smaller than the threshold densities. Nevertheless, applied elsewhere or to different networks, these thresholds may not be applicable. They have been selected under the assumption that only the highest 50% and 25% of landslide densities are likely to affect the network. Selecting these thresholds is primarily a function of the desired application, for instance one could use the thresholds to identify the sections of network exposed to the highest 1% of landslide densities in order to establish the worst-affected locations. Such a threshold is not applicable for emergency response planning however, as it will substantially underestimate the sections likely to be affected. Yet again, considering the relative exposure overcomes any potential bias in the hazard thresholds as it simply acts as a cutoff value for establishing relatively high and low exposed sections.

This work has shown the potential of both the method described herein as well as the coseismic landslide susceptibility analysis undertaken throughout this research for estimating critical infrastructure exposure to landsliding. Such analysis forms the basis for developing impact scenarios for specific disaster scenarios as established in Chapter 3 (**Fig. 3.3**). The analysis has the capability to be extended to other earthquakes on different faults, to a much wider range of infrastructure, or indeed to aseismic landsliding assuming a susceptibility map can be developed. This method may therefore prove useful for a wide range of different potential applications, including exposure and vulnerability analysis for the development of disaster scenarios.

6.9 Conclusions

Exposure mapping is a key component of disaster scenario development and can be utilised for effective emergency management planning. During earthquakes, building damage is mostly attributed to strong ground shaking, however damage to transport and utility networks is primarily a function of landsliding and liquefaction. Landslide exposure assessments however are a complex task due to the difficulty in predicting various landslide factors including landslide occurrence, runout distance, and magnitude. A method for the evaluation of landslide exposure for critical infrastructure networks using a landslide susceptibility model has been established. This method considers the landslide density calculated from the susceptibility values surrounding a network and establishes relative exposure scores based upon various hazard thresholds. Its applicability has been demonstrated for a case study of coseismic landsliding from an Alpine fault earthquake, determining the exposure of the South Island State Highway and electrical transmission networks for emergency response assessments. The method has also been demonstrated as being applicable for planning purposes when considering the potential construction of new network links to establish exposure to landslides from a scenario earthquake. This method is not limited to road and transmission networks however, and can be applied to any desired network for which the spatial distribution is known. Furthermore, the method is not limited to coseismic landsliding as it can be applied to any landsliding scenario for which a susceptibility map can be derived.

The application of this method to the Alpine fault earthquake case study has generated a series of key findings and recommendations that are important for both emergency response assessment and construction planning.

Exposure

- Approximately 240 km of highway are highly exposed to landsliding, primarily along SH6 between Hokitika and Haast, SH7 through Lewis Pass, and SH73 through Arthur's Pass. Arthur's Pass and Lewis Pass are the most exposed by length, however SH6 has the highest observed density values, with a maximum of 14 landslides/km^2 estimated to occur on the section between Franz Josef and Fox Glacier.

- Thirty steel pylons supporting the electrical transmission network in Arthur's Pass are identified as having high exposure to landsliding. The alternate power transmission route into the West Coast region following the Buller River is identified as having low exposure and thus impacts from the loss of the Arthur's Pass route will be localised. Nevertheless, repair/reinstallation of these pylons is likely to require several weeks

assuming safe and reliable access can be established.

- Up to 2,000 wooden pole supports are highly exposed to landsliding mainly in the West Coast region and Arthur's Pass. No alternate transmission routes exist for these sections of the network. A major restoration effort of several thousand person-hours will be required to repair/reinstall the large number of exposed poles.

- The vital HVDC Inter-Island electricity link is inferred to have low-to-extremely low exposure to coseismic landsliding from an Alpine fault event. Power sharing between the North and South Island's is therefore unlikely to be affected by damage to the transmission network. Exposure of generation sites (hydro dams) and substations (grid exit points) have not been considered in this analysis and should be investigated to fully understand the exposure of the Inter-Island link.

- A total of $\sim$14,500 km^2 of the South Island is exposed to isolation following an Alpine fault earthquake, $>$75% of which is in the West Coast region. Consequently $\sim$2,750 permanent residents primarily south of Hokitika are highly exposed to isolation. Tourists visit this region year round, with the largest numbers occurring between September and March, and their isolation in small communities will add a significant burden to local resources.

- More than 20,000 km^2 of the South Island is highly exposed to power loss as a result of landslide damage to transmission line supports. In total $>$60% of the West Coast region is included in this area. Consequently $>$23,000 people are exposed to power loss, the majority residing in Greymouth, Hokitika, and the surrounding areas.

Emergency response

- The Grey River valley region presents the most critical section of the State Highway network. Landslide exposures in this region are considered low and thus it is vital that bridges are able to withstand long-duration MM7-8 shaking intensity as well as likely liquefaction and lateral spreading. If SH69 and SH7 between Reefton and Greymouth can remain functional post-earthquake, direct access to $>$20,000 isolated people will be possible.

- Nelson is recommended as the most suitable emergency forward operating base in conjunction with basing the emergency response out of Wellington. Emergency response to the worst-affected areas from Christchurch and Dunedin appears infeasible due to

the extremely high landslide exposures on all routes from these locations. Maintaining a functional access route through the Grey River valley will allow the emergency response to be based out of Wellington in the North Island, using land, sea, and air connections with Nelson which could act as a forward operating base.

- Pre-event long-term recovery planning for the current critical infrastructure networks is vital to ensuring the long-term continuity of key mining, agriculture, and tourism industries in the West Coast region. Developing plans to re-establish safe road access and reliable power supply to the region before the event occurs is strongly recommended.

Resource consents

- A proposed highway linking Haast and Hollyford has extremely high exposure to landsliding along the majority of its route. Landslide densities at multiple locations along the route significantly exceed the largest densities anticipated on the current network. Given the anticipated number of annual road users (>800,000), building the highway presents a substantial risk to life. This should be considered in any decision-making process with regards to granting resource consent.

Chapter 7

Discussion, conclusions, recommendations, and future work

7.1 Thesis overview

Secondary natural hazards are experienced in virtually all environmental disasters (see Xu et al., 2014), yet quantitative assessments of their nature and spatial distribution are generally lacking from current disaster risk management (Chapter 3). Understanding secondary hazards is important as they have the potential to greatly exacerbate the scale and duration of an initial hazard (Hewitt et al. 2008; Chapter 2). In some instances, the secondary hazards can be as catastrophic as, or more catastrophic than, the initial hazard. Inclusion of secondary natural hazards in quantitative risk assessments can increase the complexity of the modelling scope and methodology, introducing additional sources of error and uncertainty. This is a result of the complex interlinkages between various cascading hazards, which therefore require a variety of assumptions and simplifications (see Chapter 2). One area of research which has seen recent advances in secondary hazards is that of seismogenic tsunami modelling. The 2004 Indonesian and 2011 Japanese earthquake and tsunami disasters have demonstrated the need to identify and understand the hazard and risk associated with subduction zone earthquakes and consequential tsunamis. As a result, a substantial amount of work has been undertaken globally to better understand the threat of mega-earthquakes (>M9) on subduction zones and the implications for near- and far-field tsunami (e.g. Okal and Synolakis, 2008; Okal et al., 2011; Villianatos and Sammonds, 2013). Yet for large earthquakes in mountainous terrain, very limited research has attempted to address the issue of secondary hazards *pre-event*, despite these events being more prolific than large-scale tsunami (Chapter 1).

This thesis addresses the issue of secondary hazards resulting from mountainous earth-

quakes from a disaster risk management perspective. To achieve this, first the relevant hazards and impacts were identified and collaboration with an EM group, who have the responsibility of managing these hazards, was undertaken to co-identify the relevant scientific knowledge required to manage/reduce the associated risks (Chapters 1-3). Subsequently, this required the development of risk assessment methodologies for coseismic landsliding for scenarios and other planning tools, which identified some valuable science knowledge and methodology gaps (Chapter 4-6). More specifically, this included:

- Identifying and compiling first-order quantitative estimates of the secondary, cascading geomorphic hazards that result from large mountainous earthquakes (Chapter 2);
- Establishing the need for the inclusion of secondary hazards in disaster scenarios regardless of their application (Chapter 3);
- Developing a conceptual model for the inclusion of secondary hazards in emergency planning exercises (Chapter 3);
- Establishing a method to quantify the spatial distribution of coseismic landslide susceptibility resulting from scenario earthquakes (Chapter 4);
- Applying this method to an Alpine fault earthquake scenario to estimate the scale and spatial distribution of coseismic landsliding and consequent erosion and aggradation (Chapter 5);
- Establishing a method to assess exposure of critical infrastructure from coseismic landsliding susceptibility models (Chapter 6); and
- Estimating the exposure of State Highway and electrical transmission networks to coseismic landsliding from an Alpine fault earthquake scenario to inform emergency response planning (Chapter 6)

As a result, this thesis is a contribution to both the understanding and modelling of coseismic landslides and earthquake disaster risk management in mountainous environments in general. Key findings from this research will contribute directly to pre-event planning and readiness for an anticipated large Alpine fault earthquake, as well as enabling similar studies of other mountainous environments where large earthquakes and associated landsliding are possible. The establishment and application of a coseismic landslide susceptibility analysis method for fault-bounded mountainous terrain has enabled a greater understanding of the hazard and risk posed by future Alpine fault earthquakes. It has also enabled critical sections

of the State Highway and electrical transmission networks to be identified, and informed pre-event mitigation to reduce the impacts of a future earthquake. Applying this methodology to other earthquake scenarios, both in New Zealand and globally, for which coseismic landsliding analysis has not previously been possible, could yield similar results, leading to greater awareness and resilience to coseismic landsliding and large earthquakes in general. This thesis is of direct benefit to vulnerable communities, EM, and relevant industries and institutions both in the South Island of New Zealand and globally.

This chapter builds on the discussion and conclusions presented in Chapters 2-6. First, this chapter addresses the Exercise *Te Ripahapa* disaster scenario, the coseismic landslide modelling process, and its results and their implications for past and future events; second, the key conclusions and recommendations derived throughout this research are summarised and contextualised; and finally, the chapter finishes with suggestions of future avenues of research which will strengthen and advance the methods and results found herein.

7.2 Discussion

7.2.1 Exercise *Te Ripahapa*

A maximum-credible scenario?

Following the devastating secondary consequences that resulted from the 2008 Wenchuan and the 2010-11 Canterbury earthquakes, the South Island CDEM Groups realised the need to better understand the full complement of hazards likely to result from a future Alpine fault earthquake. Consequently, Exercise *Te Ripahapa* was developed to provide a realistic scenario for a maximum-credible rupture of the Alpine fault in order that they could appropriately and effectively plan for, mitigate against, and respond to such an event. While the resulting scenario did represent a maximum-credible event, a number of caveats exist.

Firstly, it was noted in the independent review of the disaster scenario that different weather conditions at the time of the earthquake could substantially increase the scale of secondary hazards. The weather scenario involved generally fine conditions with some occasional light rainfall in the far south of the Island; typical conditions for late May (when the exercise took place) in the South Island (see Appendix B). Had the weather scenario included heavy rainstorms and low cloud, which are not uncommon for the alpine and West Coast regions, the impacts would have been substantially worse. Landslide dams would have filled faster as a result of greater river flow rates potentially leading to more rapid outburst floods, and larger amounts of landslide material remobilised as debris flows. In addition saturated

soils may have led to landslides with longer runout lengths as a result of higher water content (see Appendix A). In terms of human welfare, affected populations would have required shelter from the weather, while low cloud cover would have prevented flying over the Southern Alps, placing a major strain on reconnaissance and supply distribution.

Further, a maximum-credible event for an Alpine fault earthquake should account for tourist numbers, which Exercise *Te Ripahapa* did. However, during May tourist numbers are substantially lower than between September and March (Orchiston, 2011). A scenario representing an earthquake during the tourist season would involved a substantially larger number of exposed people. For instance, the combined population of Franz Josef and Fox Glacier during Exercise *Te Ripahapa* was ∼400; between September and March this could be as many as 4,000. Further, Milford Sound has an average ∼1,750 visitors each day throughout the year (Department of Conservation, 2006; Dykstra, 2012), yet Environment Southland estimated just 95 people were likely to be there during the scenario. A scenario representing an Alpine fault earthquake during the tourist season could therefore involve a far larger number of injuries or fatalities than used during Exercise *Te Ripahapa* (see Appendix C).

A further point of note is the hill slope 400 m east of Franz Josef township, which has been identified by Barth (2014) as having the potential to cause a rock avalanche with a ∼2 km^2 deposit that would devastate the town (**Fig. 7.1**). While it is not currently possible to ascertain whether this slope will fail in the next Alpine fault earthquake, or indeed if it will fail at all, it appears to be a credible event and thus could feasibly be included in a maximum-credible Alpine fault earthquake. Exercise *Te Ripahapa* is therefore an excellent example of the challenges in establishing the intended scenario scale, and demonstrates the fact that multiple maximum-credible events may exist for a variety of different scenario requirements (e.g. time of year). It is vital that all participants are aware of this during the scenario development phase.

Nevertheless, as discussed in Chapter 3 and shown by Holling (2004) and Park et al. (2013), establishing the processes and behaviours required to respond to an emergency are far more important than the precise scenario used. While the specifics of any emergency response may differ as a result of different weather or larger tourist numbers, the processes established during Exercise *Te Ripahapa* for responding to an Alpine fault earthquake are unlikely to be substantially different. Thus the scenario has, hopefully, contributed to increased awareness and resilience to such a disaster, as well as enabling the development of appropriate and effective response processes and behaviours.

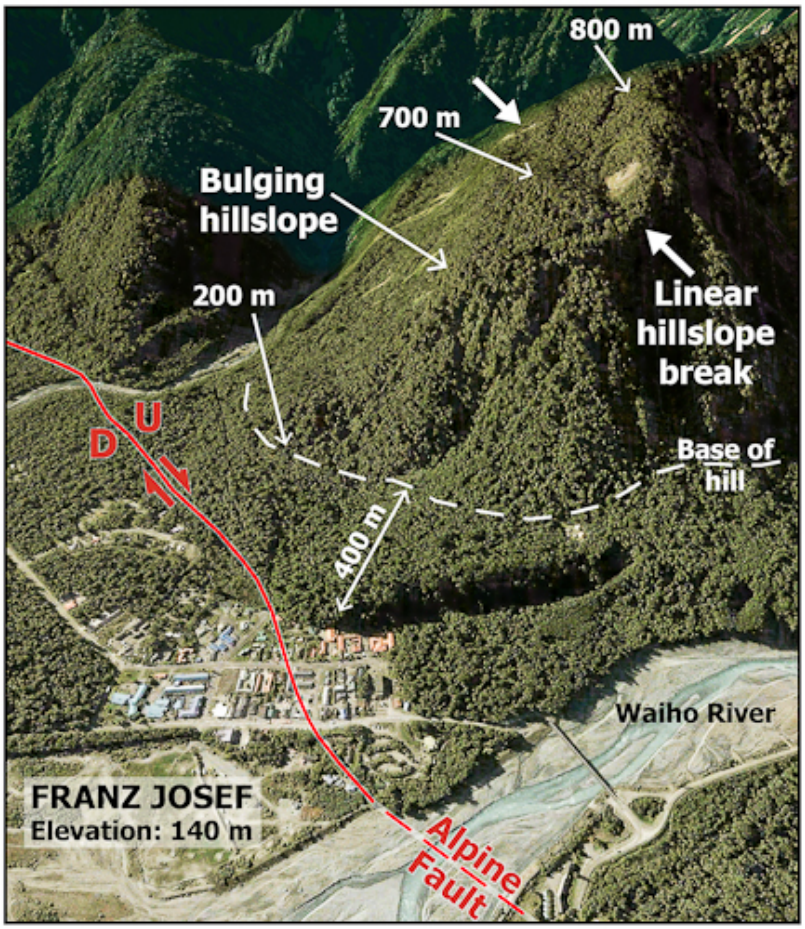

Figure 7.1: Franz Josef township and the potential rock avalanche source above the town. From Barth (2014)

Differences with later modelling

One of the primary issues experienced during the development of the Exercise *Te Ripahapa* disaster scenario, was establishing the scale and spatial distribution of landsliding from empirical observations and expert elicitation. It was these difficulties that led to the development of a method to model coseismic landsliding for an Alpine fault earthquake. It is therefore logical to compare the Exercise *Te Ripahapa* scenario to the results from the fuzzy logic coseismic landslide modelling to identify any differences.

Firstly, the general scale of landsliding is similar in both scenarios, with empirical methods suggesting ~50,000 landslides over ~35,000 km^2 (**Table 2.2**; Chapters 2 & 3), compared to ~40,000 landslides over ~50,000 km^2 (Chapter 5) from fuzzy logic modelling. Further, the spatial distribution was broadly similar, with both scenarios suggesting the landsliding

would be concentrated along the western range-front of the Southern Alps, although fuzzy logic also identified the southern Marlborough faults region as being similarly affected. Of the nine river catchments identified as having the potential for landslide dams during Exercise *Te Ripahapa* (**Fig. 3.5**), it is notable that seven of these are also found to be some of the worst affected from fuzzy logic modelling. The two catchments not included are the Karamea and Mokihinui, which were found in fuzzy logic modelling to have Impact Factors of just 0.01 and 0.11 respectively (**Table 5.8**; Chapter 5). In fact, the Karamea catchment is inferred to have $<$20 landslides throughout the entire catchment and the Mokihinui will likely have $<$100. Landslide dams in these catchments therefore appear unlikely. The small population in these areas of the South Island means that the inclusion of landslide dams here during Exercise *Te Ripahapa* is unlikely to have substantial affected the response.

Two landslide-generated tsunamis were also included in Exercise *Te Ripahapa*; in Milford Sound and Lake Brunner. While the possibility of landslide-generated tsunami has not been examined following the fuzzy logic modelling, visual analysis of the landslide susceptibility map (**Fig. 5.6**) confirms that such events may be possible at these locations. Milford Sound has previously been shown to be highly susceptible to such events (see Dykstra, 2012) and **Fig. 5.6** shows that very high susceptibility values are present along the entire coastline of the fiord, confirming that landsliding into the fiord should be expected. The hillslopes surrounding Lake Brunner are also shown to have very high susceptibility (**Fig. 5.7**) and thus landsliding into the lake is also possible. While not conclusive, this does suggest that landslide-generated tsunami in these location is plausible. Other lakes which are surrounded by high susceptibility include: Lakes Sumner, Coleridge, Kaniere, Paringa, and McKerrow (**Fig. 7.2**). Of these, Lake Coleridge has a hydroelectric dam, Lake Kaniere has several campgrounds and holiday homes, and Lake Paringa is near to SH6. Some areas of medium-to-high susceptibility are also present near Lakes Te Anau, Wakatipu, Wanaka, and Hawea (**Fig. 7.2**), all of which have relatively large populations and State Highway routes on their shoreline. Investigating whether previous landslide-generated tsunami have occurred in any of these lakes is therefore strongly recommended.

Finally, Exercise *Te Ripahapa* involved landslides blocking the State Highways and damaging the electrical transmission links into Queenstown (**Fig. 3.7**). These sections were not identified as having high relative exposure from the fuzzy logic modelling (**Figs. 6.5 & 6.7**; Chapter 6). This suggests that the impacts from landsliding to Queenstown suggested in Exercise *Te Ripahapa* may be over-estimated, as the town is not exposed to isolation or power loss according to the fuzzy logic modelling (**Figs. 6.8 & 6.9**). Furthermore, SH69 and SH7 through the Grey Valley were also anticipated to be impassable for Exercise *Te Ripahapa*.

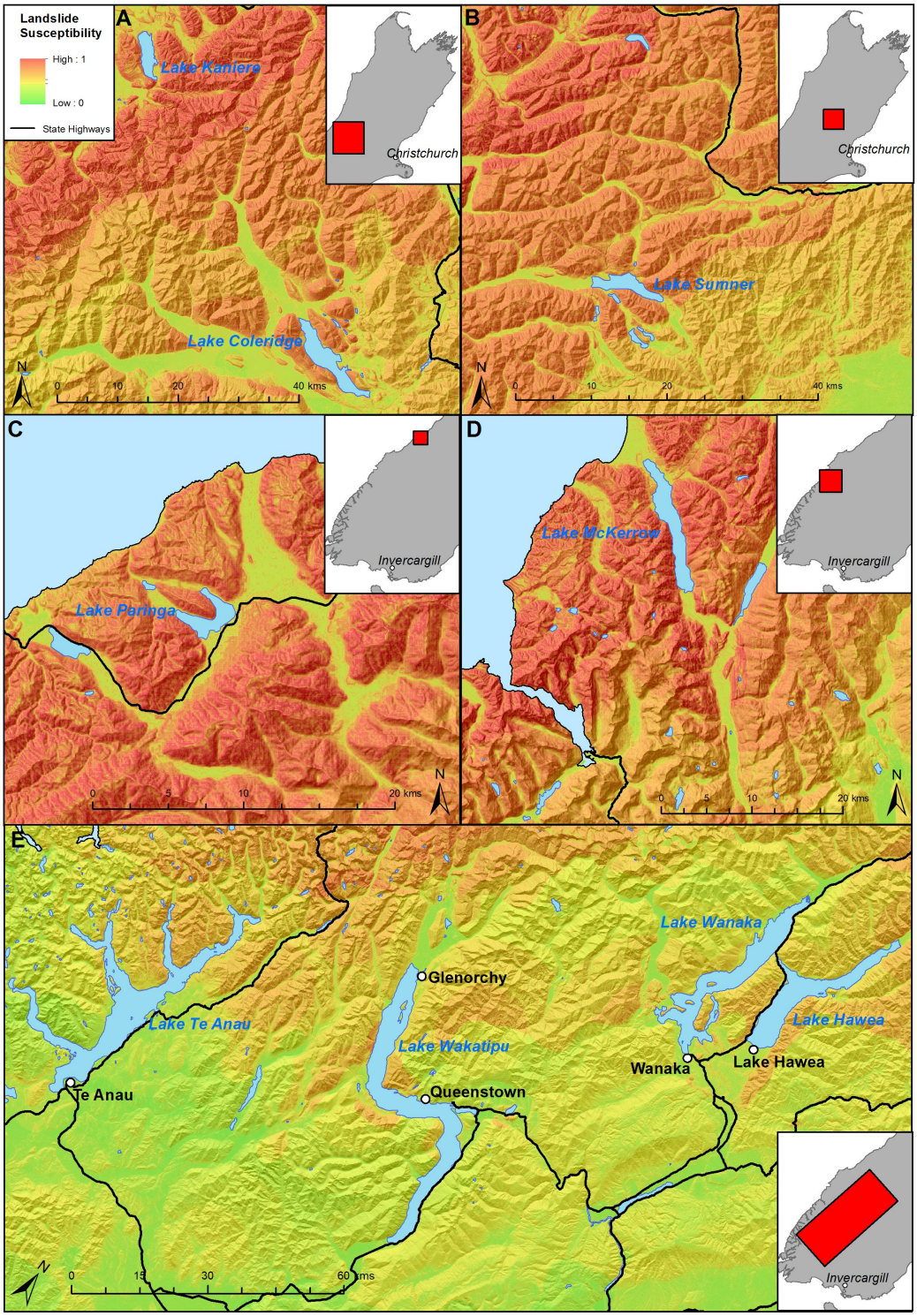

Figure 7.2: Landslide susceptibility values surrounding a) Lakes Coleridge and Kaniere; b) Lake Sumner; c) Lake Paringa; d) Lake McKerrow; and e) Lakes Te Anau, Wakatipu, Wanaka, and Hawea with nearby towns and State Highways. High susceptibility along the shorelines of the these lakes suggest they have the potential for landslide-generated tsunami during an Alpine fault earthquake.

Fuzzy logic modelling has shown this section to be the most critical section for an Alpine fault earthquake as landsliding exposure here is considered low. Nevertheless, the area is thought to be highly susceptible to liquefaction (see McCahon et al., 2006a,b,c) and thus without any mitigation to this hazard, the likelihood of this section of road becoming impassable must be considered likely. The other sections of the State Highway and electrical transmission networks badly affected in Exercise *Te Ripahapa* correspond to those sections found to be highly exposed from the fuzzy logic modelling.

Thus, while there are notable differences between the Exercise *Te Ripahapa* scenario and the fuzzy logic scenario, generally the results are similar, with the only major difference being the isolation and power loss in Queenstown. Including the fuzzy logic coseismic landslide modelling into Exercise *Te Ripahapa* would have very little affect on its overall scenario. This further demonstrates that detailed and realistic scenarios can be effectively developed via the co-production of knowledge, adding further weight to such a method being utilised in future local- and regional-scale exercises.

7.2.2 Coseismic landslide modelling

Landslide inventories

The coseismic landslide modelling undertaken herein has relied heavily on available landslide inventories for statistical analysis. It is therefore dependent on the accuracy and quality of the datasets utilised for identifying and locating landslides. Any errors or inaccuracies within the data are carried forward into the modelling phase. For this reason, it is only feasible to use datasets digitised using GIS, as non-digital datasets are likely to contain a larger error. Further, digitising non-digital inventories increases the associated error as any original mapping errors are compounded during the digitising process (**Fig. 7.3**). If the associated error is larger than the DEM resolution this can have dramatic effects on the statistical analysis by placing a landslide in an incorrect pixel and thus attributing incorrect factor values to the landslide point (**Fig. 7.3**).

The model also relies on a consistent mapping approach being undertaken. For instance with point data, two different mapping techniques exist: centroid (the centre of the landslide source zone) and top point (the highest elevation of the headscarp). Ensuring that the inventories employ the same technique is vital, particularly when considering slope position. It is also important that the inventories include the same types of landslides (i.e. rotated blocks, slumps, flows etc.). The inventories included herein contain all landslide types, however an inventory for the 2011 M9.0 Tohoku earthquake could not be utilised as it was specific to dis-

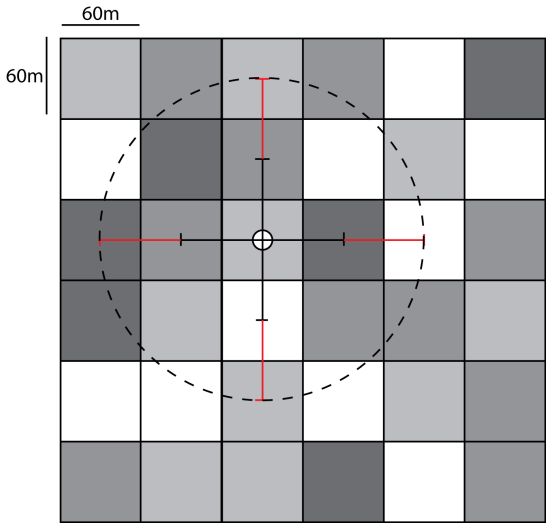

Figure 7.3: Schematic diagram showing the effect of mapping errors (black bars) combined with digitising errors (red bars) for locating a landslide point within a 60m DEM. Grey shading represents different pixel values. This landslide point could belong to any of 20 pixels within the total error margins (black dotted line).

rupted landslides and therefore did not correlate to the other inventories. The Wenchuan inventory included lateral spreads which are not thought to have been included in the Northridge and Chi-Chi datasets. This could explain the increased frequency ratio values seen for small slope angles in Wenchuan (**Fig. 4.7**) compared to Northridge and Chi-Chi. For this reason, the user-defined membership curves for Wenchuan were selected to produce smaller fuzzy membership values for low slope angles in accordance with observations from Northridge. The landslide susceptibility map produced for the Alpine fault (**Fig. 5.6**) therefore represents all landslide types but does not include lateral spreads.

Local factors

Despite local factors such as lithology, vegetation, soil cover etc. being excluded from the modelling, they will have an effect on the production of coseismic landslides. While this effect is inferred to be minimal in determining the spatial distribution because regional factors alone produced highly successful results, local effects may play an important role in the total number and volume of landslides produced. This is particularly notable when comparing the 1929 M7.3 Murchison and 2003 M7.3 Fiordland earthquakes. Both events were the same magnitude, produced the same level of shaking across similar sized areas (see Dowrick, 1994), and involved similar faulting mechanisms (reverse motion). Nevertheless, the 1929

earthquake resulted in >5 times as many landslides as the 2003 event. The primary difference between the two events is their location within the South Island. The 1929 earthquake primarily affected an area of highly weathered mixed lithologies (intrusive igneous and sedimentary rocks) west of the Marlborough fault system, while the 2003 earthquake affected comparatively less weathered metamorphic and igneous rocks of southern Fiordland (**Fig. 7.4**). As a result, the 2003 Fiordland earthquake resulted in just ∼400 generally shallow-seated, small-volume landslides, compared to >2,000 landslides many of which were large-volume and deep-seated during the 1929 Murchison earthquake (Hancox et al., 1997; Pearce and O'Loughlin, 1985). The Alpine fault will predominantly affect the Southern Alps, although parts of Fiordland will also be affected, and thus the values derived herein (Chapter 5) are considered credible for the local factors.

Area versus number

Landslide inventories used in this thesis consist of point data used to derive the number of landslides likely to result from an Alpine fault earthquake. Other inventories are available which contain polygon data that would be useful for deriving total landslide area. Polygon data would be preferred because it would enable individual landslide area to be estimated, and thus specific volumes to be derived (see Hovius et al., 2011; Li et al., 2014). The specific area and volume of an individual landslide are important for local hazard and risk analysis as they can be used to predict potential landslide runout. The current model identifies locations where landslide densities are likely to be highest. While this is useful, establishing where the largest area/volume landslides are likely to occur would be preferred. A town or critical infrastructure in a high density location is clearly highly exposed, however if each of those landslides is of small volume, a different location with low density but high volume could be considered more exposed.

Nevertheless, in its current form this model would be difficult to apply to polygon data as these cover multiple pixels making a statistical analysis of the contributing factors difficult to ascertain. Furthermore, there appears to be no general consensus in the mapping technique for polygon inventories; for instance some combine source zone and runout zone into a single polygon while others classify source and runout zones into distinct groups. Another common difference is that some inventories include multiple densely-spaced small area/volume landslides into a single large landslide complex, while others map each individual slope failure. Again, for this method to be applicable, all the inventories used would need to employ the same mapping technique.

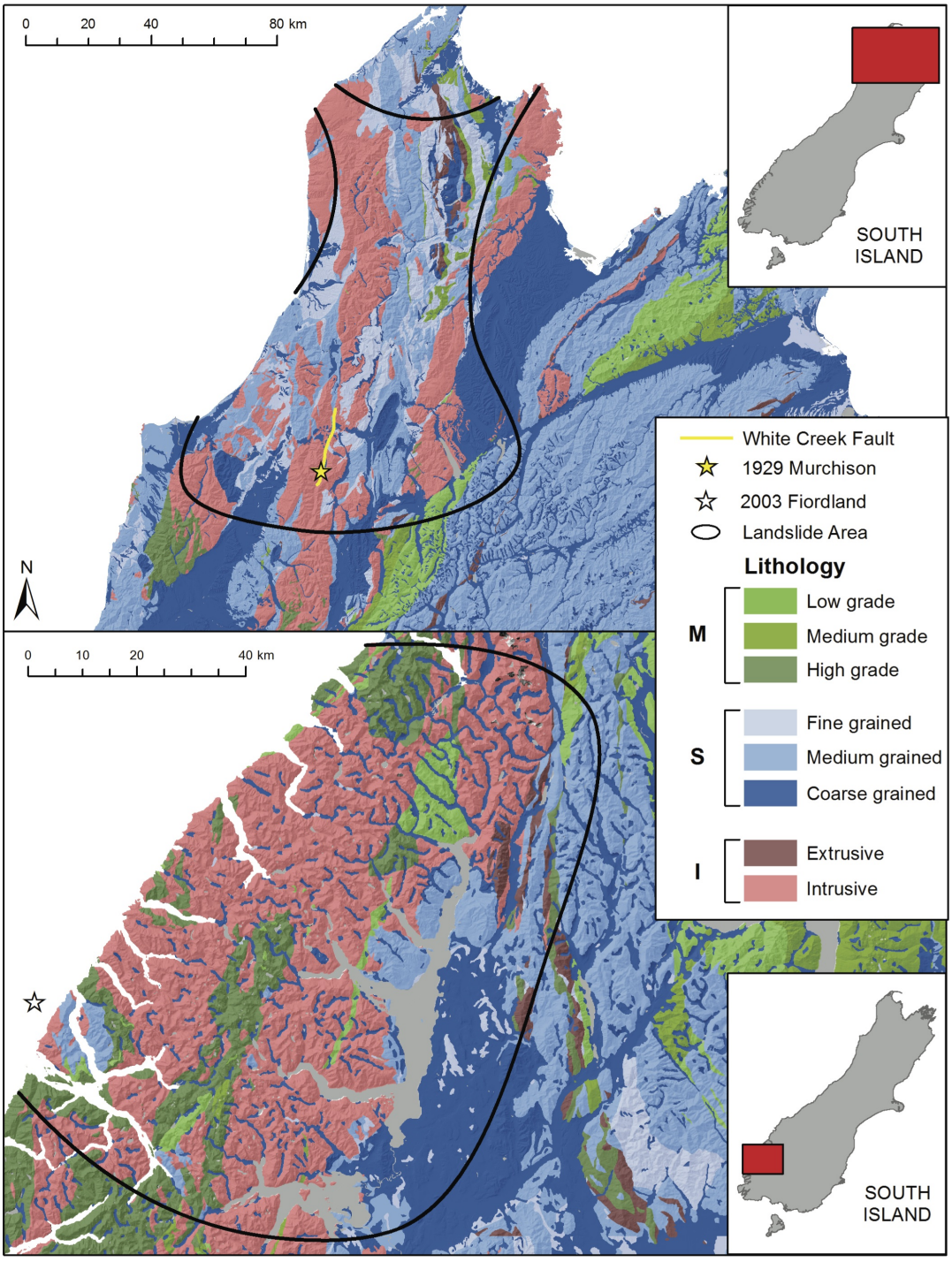

Figure 7.4: Extent of landsliding in relation to lithology for the 1929 Murchison (top) and 2003 Fiordland (bottom) earthquakes. M - metamorphic; S - sedimentary; I - igneous rocks.

Small sample datasets

As a result of the small number of digital landslide inventories available with corresponding mapping techniques and resolution, only a small sample of datasets has been used. This is particularly important for the statistical analysis for the fuzzy membership functions and for the standard error of the mean (SEM) method to derive landslide number. In the case of the fuzzy memberships this means that the resulting susceptibility maps are weighted towards those factors which influenced landsliding in Northridge, Wenchuan, and Chi-Chi. While the results have achieved good-to-excellent model performance, including more datasets will develop more robust memberships giving the results a higher degree of credibility. Nevertheless, three different earthquake events occurring in three different environments showing strongly correlated distributions for those factors described (Chapter 4) seems unlikely to be coincidental, and thus these factors are likely to be the main contributors to regional landsliding. Including more datasets however may identify further factors which correlate between the majority of events but that do not correlate between the Northridge, Wenchuan, and Chi-Chi inventories.

With regard to the SEM method to derive landslide number, more datasets would allow probability distributions to be defined which correlate landslide density to modelled susceptibility class. This would enable landslide number to be derived with an associated likelihood, rather than simply a potential range between which it may occur. Currently, defining a probability distribution from the five modelled inventories (Northridge, Wenchuan, Chi-Chi, 2003 Fiordland, and 2009 Fiordland) is not possible as there is no meaningful way to determine which probability distribution best fits the data or even how the data are distributed. Evaluating more inventories will better define how these densities are distributed and thus provide a more robust answer for total landslide number.

7.2.3 Coseismic landsliding results

Aggradation from 1717 Alpine fault earthquake

Coseismic landsliding has been modelled for a full-length rupture of the Alpine fault, similar to the last known rupture in 1717 CE. The landslide volumes derived from such an event have been used to estimate aggradation in some of the major river catchments throughout the South Island. In the central Southern Alps this has suggested that post-event aggradation could average $\sim$1 m. However no evidence of major aggradation from the 1717 earthquake exists on any of the alluvial fans in central Westland studied by Davies and Korup (2007). Evidence of substantial aggradation was identified for the c. 1600 CE Alpine fault earthquake. This

may suggest that either substantial landsliding did not occur during the 1717 earthquake, or evidence of subsequent aggradation was not preserved. The former appears unlikely as Howarth et al. (2012, 2014) identified large coseismic and post-seismic sediment inputs into Lakes Paringa and Mapourika following the 1717 event. This post-seismic sediment input has a duration of ∼80 years and must have formed as a result of remobilised landslide material in the (small) drainage catchments for these lakes. It therefore appears more likely that evidence of aggradation from the 1717 earthquake was not preserved, although explaining the lack of evidence is challenging given evidence from the earlier c. 1600 earthquake is preserved.

Despite evidence of aggradation from the c. 1600 earthquake on alluvial fans (Davies and Korup, 2007), no post-seismic sediment deposits were identified corresponding to this event in either Lake Paringa or Lake Mapourika (Howarth et al., 2014). This suggests that rupture during this earthquake only occurred on the section of the Alpine fault north of about the Waitaha River (Howarth et al., 2014), in accordance with fault trench data (De Pascale and Langridge 2012; De Pascale et al. 2014; **Fig. 7.5**). Yet aggradation from this event has been identified as far south as Fox Glacier township, >75 km south of the fault rupture. Furthermore, De Pascale et al. (2014) demonstrated evidence of substantial landsliding as far south as the Haast River, >200 km south of the fault rupture. It seems unlikely that major landsliding would occur at such large distances from the fault rupture.

Cox et al. (2012) identified a large number of faults east of the main divide in the Aoraki/Mt Cook area, many of which have the potential for earthquakes $>M_w6.5$, although the potential activity of most of these remains unknown (**Fig. 7.5**). Rupture of one of these faults may explain the discord between evidence of landsliding and observed Alpine fault rupture in c. 1600. This would require two large ($\sim M_w7.0$) earthquakes to have occurred relative close in time around 1600 CE. Such events have been witnessed historically in New Zealand during 1929, when the $\sim M_w7.0$ Arthurs Pass earthquake preceded the $M_w7.3$ Murchison earthquake by just four months. This does not explain the lack of post-seismic deposits in Lakes Paringa and Mapourika, although it could be a result of only minor landsliding in the small river catchments that feed the lakes. Rupture of one of the southern Aoraki/Mt Cook faults may be sufficient to generate the observed landslide effects at the Haast River mouth, while also being at a large enough distance from Lakes Paringa and Mapourika to explain the lack of substantial post-seismic sediment inputs. Using the methods described herein to model landsliding from a number of different earthquakes on the identified faults of Cox et al. (2012) may indicate whether such events are capable of producing substantial landsliding, and if so, the spatial distribution throughout the central Southern Alps.

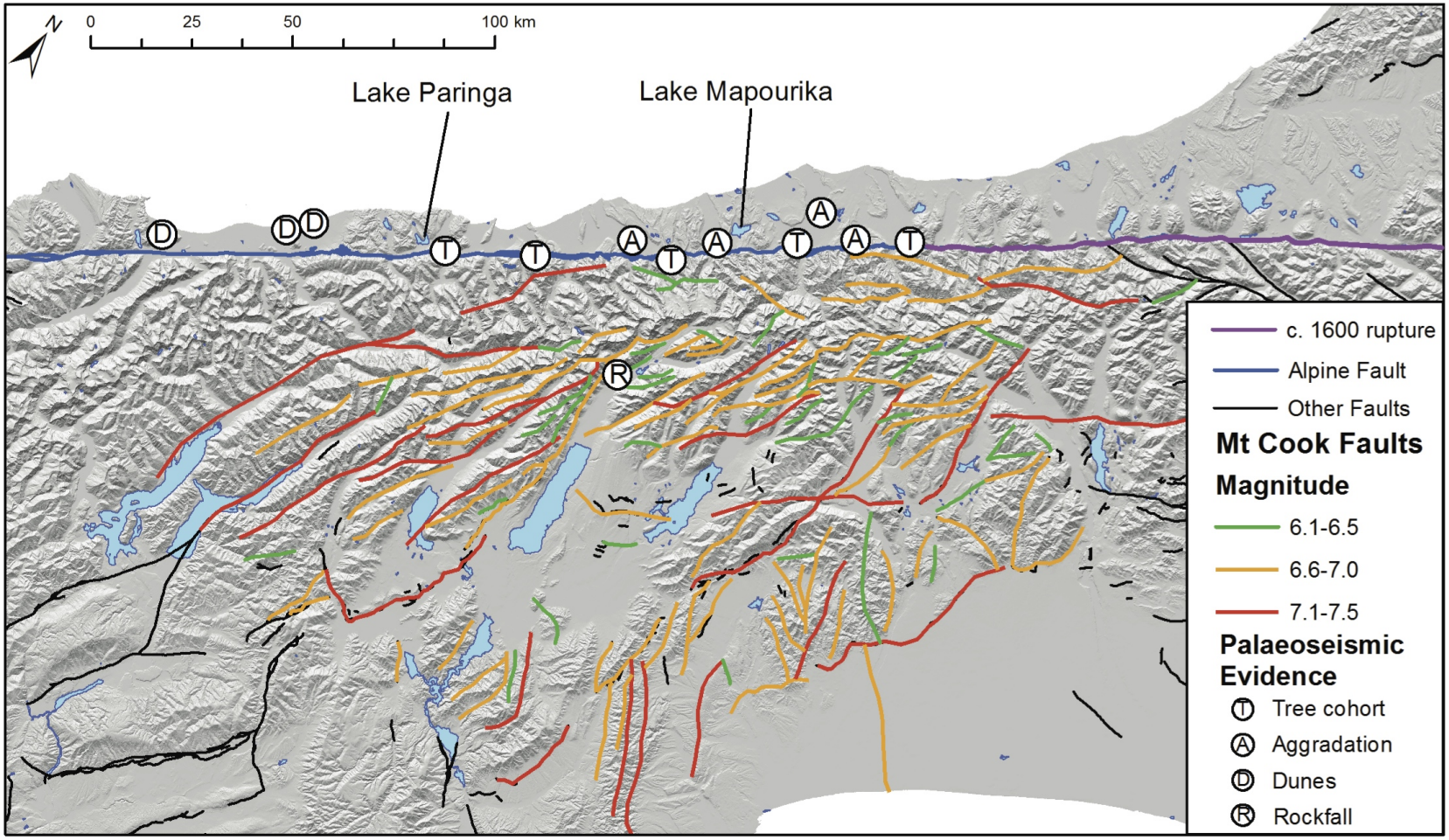

Figure 7.5: Extent of fault rupture during the c. 1600 Alpine fault event in relation to palaeoseismic evidence for the earthquake, Lakes Paringa and Mapourika, and recently identified faults and their magnitude potential in the Aoraki Mt Cook region. Palaeoseismic evidence from Davies and Korup (2007) and De Pascale et al. (2014); Aorkai/Mt Cook faults from Cox et al. (2012)

2002 M_w7.9 Denali, Alaska earthquake

This thesis has looked at several examples of catastrophic coseismic landsliding to compare with a potential Alpine fault earthquake, most notably the 2008 M_w8.0 Wenchuan earthquake. However, the 2002 M_w7.9 Denali earthquake presents an alternative example in that it only resulted in ~1,500 landslides (Gorum et al., 2014), compared to the ~60,000 in Wenchuan. The primary difference between these two events is that the Denali earthquake occurred in a heavily glaciated environment, which is thought to have the potential to reduce seismic shaking and consequently coseismic landsliding (McColl et al., 2012). However Gorum et al. (2014) showed that fault type, geometry, and rupture process played a more dominant role in reducing the number of landslides than glaciated terrain. The Wenchuan earthquake had a similar dynamic rupture to the Denali earthquake but occurred on less steeply dipping faults involving a combination of reverse and strike-slip motion, with fewer landslides observed along the strike-slip section compared to the reverse section (**Fig. 7.6**). In comparison the faults involved in the Denali earthquake were near vertical dipping and sustained purely strike-slip motion (**Fig. 7.6**).

Gorum et al. (2014) therefore suggested that steeply dipping, dominantly strike-dip faults are likely to produce fewer landslides for the same magnitude earthquake as less steeply dipping reverse and oblique faults. They provided evidence from 15 further events which appear to confirm this suggestion (numbers 1-15 in **Fig. 7.6**). While the 1929 Murchison earthquake appears to fit with this trend, the 2003 and 2009 Fiordland earthquakes do not, occurring on a very shallowly dipping subduction zone (reverse motion) but resulting in very few landslides. Further, the 1976 Guatemala earthquake occurred on a vertical strike-slip fault and resulted in ~50,000 landslides (Kanamori and Stewart 1978; **Fig. 7.6**). The Alpine fault is segmented at a scale of several kilometres into near vertical strike-slip and 40-45° dipping reverse segments (**Fig. 2.2**). If fault dip and motion do control landslide number, the presence of shallow dipping reverse segments throughout the northern and central segment of the fault will likely result in large numbers of landslides, and the estimates herein correlate well with the observations from Wenchuan (**Fig. 7.6**). The 1976 Guatemala earthquake also demonstrates that vertical strike-slip faults can generate large numbers of coseismic landslides, and thus the numbers estimated for an Alpine fault earthquake are considered plausible.

7.3 Conclusions and recommendations

This thesis has made a substantial contribution to the disaster risk management of a future Alpine fault earthquake, as well as of large earthquakes in mountainous environments in

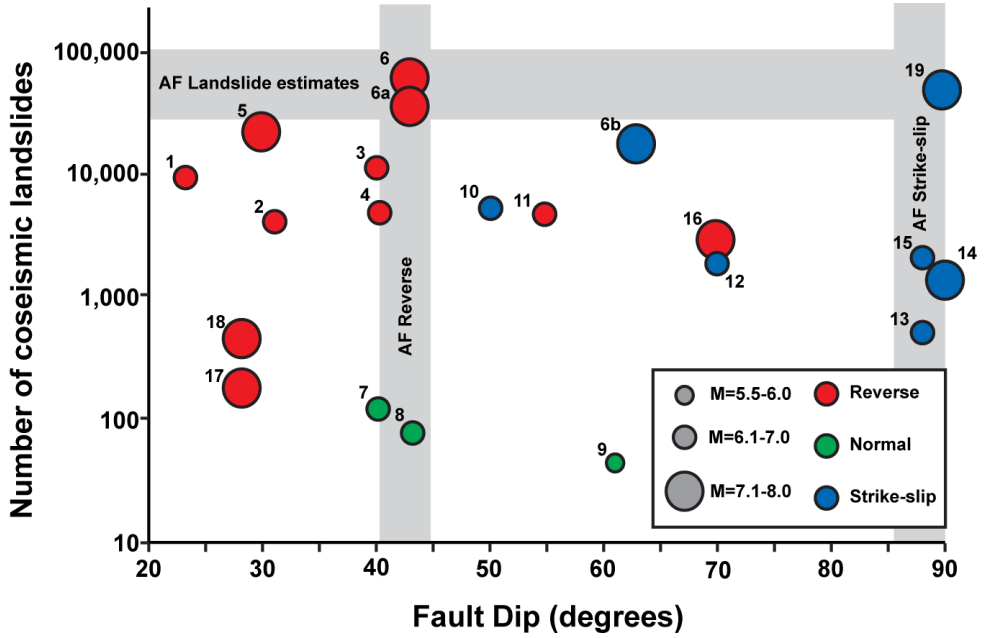

Figure 7.6: Total number of coseismic landslides in relation to fault dip and faulting mechanism on reverse and strike-slip segments of the Alpine fault, and the range of coseismic landslides estimated herein. 1 - M6.5 Coalinga, USA (1983); 2 - M6.9 Iwate-Miyagi, Japan (2008); 3 - M6.7 Northridge, USA (1994); 4 - M7.0 Haiti (2010); 5 - M7.6 Chi-Chi, Taiwan (1999); 6 - M8.0 Wenchuan, China (2008), 6a - reverse slip segment and 6b - strike slip segment; 7 - M6.0 Umbria Marcha, Italy (1997); 8 - M6.3 L'Aquila, Italy (2009); 9 - M5.6 Rotoehu, New Zealand (2004); 10 - M6.2 Mammoth Lakes, USA (1980); 11 - M6.7 Niigata, Japan (2009); 12 - M6.9 Loma Prieta, USA (1989); 13 - M6.2 Aysén, Chile (2007); 14 - M7.9 Denali, USA (2002); 15 - M6.8 Yushu, China (2010); 16 - M7.3 Murchison, New Zealand (1929); 17 - M7.8 Fiordland, New Zealand (2009); 18 - M7.3 Fiordland, New Zealand (2003); 19 - M7.6 Guatemala (1976). Adapted from Gorum et al. (2014); events 16-19 added herein.

general. A number of significant conclusions and potential recommendations have been developed throughout the thesis and these are summarised and contextualised below.

1. Establishing disaster scenarios provides an effective method to develop preparedness and resilience to anticipated disasters such as an Alpine fault earthquake. Regardless of potential application these disaster scenarios should be as realistic as possible, and should invoke the processes and behaviours required to respond to a future emergency. Thus they require the detailed inclusion of secondary effects, which are typical of all natural hazards, along with the exposure and vulnerability of those social elements included in the scenario. The development of disaster scenarios which are realistic and meet the priorities and information needs of all users, can be improved through the

co-production of knowledge between disaster scientists and all potential users, such as emergency management personnel, local communities, and critical infrastructure operators.

2. The hazard from Alpine fault earthquakes is not simply a function of strong ground shaking. A series of complex interlinked secondary geomorphic effects including landsliding, landslide dams, outburst floods, landslide tsunami, and aggradation will exacerbate the impacts from the primary hazard event. Evidence of some or all of these effects has been observed in the majority of historic South Island earthquakes, and geologic evidence of pre-historic Alpine fault earthquakes suggests they affect the entire Southern Alps, both east and west of the main divide. Without complete historic landslide inventories or detailed geotechnical information however, modelling the potential extent of coseismic landsliding was not previously possible.

3. Statistical observation of the spatial distribution of coseismic landslides in the Northridge, Chi-Chi, and Wenchuan earthquakes has identified five common factors which appear to control the spatial distribution of coseismic landslides despite differences in local environment and seismic and tectonic processes. These factors are: shaking intensity, slope angle, slope position, and distance from active faults and streams. Utilising fuzzy logic in GIS, membership functions for each of these factors derived from two events are able to successfully model the spatial distribution in a third event in a different environment with excellent model performance. These membership functions can therefore be applied to other environments for which coseismic landslide modelling has not previously been possible under the assumption that the factors controlling coseismic landslide distribution are the same for all fault-bounded mountainous environments.

4. Applying these memberships to the 2003 and 2009 Fiordland earthquakes has achieved similarly successful results demonstrating the robustness of the memberships and their applicability to the New Zealand environment. Applied to an Alpine fault earthquake scenario, this demonstrates that coseismic landsliding is likely to affect an area $>$50,000 km^2, predominantly along the western range-front of the Southern Alps and throughout the southern Marlborough faults region. Consequently, between 40,000 and 110,000 landslides are anticipated to occur resulting in between 0.2 and 2 km^3 of landslide debris. In total, up to $\sim$4,000 landslides $>$10,000 m^3 could occur, suggesting potential large numbers of landslide dams could form on multiple rivers.

5. Coseismic landsliding from an Alpine fault event will most severely affect 16 major

river catchments, which include all west-draining order 6 or larger catchments between the Buller and Hollyford rivers as well as the east-draining Canterbury Waiau, Hurunui, Waimakariri, and Rakaia rivers. The Taramakau, Waiho-Callery and Hollyford catchments are likely to be the worst affected producing >7 times more landslides per unit area than the average for the entire South Island. Erosion as a result of landsliding will likely correspond to >5 years of normal erosion in the central Southern Alps, and to >50 years of normal erosion in the Buller, Grey, Hollyford, Taramakau, and Hurunui catchments. Consequent aggradation is likely to average up to 1 m or more in all 16 river catchments, presenting a major long-term hazard for all societal activities on the alluvial fans and floodplains of these rivers. Such aggradation has the potential to last for up to several decades and therefore also present a substantial issue to long-term recovery, particularly with respect to re-establishing critical infrastructure such as road bridges.

6. Losses to critical infrastructure such as transport and utilities networks are predominantly a function of landsliding. Estimating exposure to landsliding is complex however, due to the challenges in predicting landslide occurrence, runout, and magnitude. A method for estimating exposure of critical infrastructure networks from a landslide susceptibility model has therefore been developed. This is a semi-quantitative method which utilises susceptibility values surrounding a network point to calculate landslide densities. These are then considered in relation to a hazard threshold which establishes the relative likelihood of any point on a network being affected. The method is applicable to any network whose spatial distribution is known and can be applied to aseismic landslide scenarios as well as coseismic scenarios as long as a landslide susceptibility map is available.

7. The South Island State Highway and electrical transmission networks are particularly exposed to coseismic landsliding during an Alpine fault earthquake. Up to 240 km of road, particularly SH6 between Hokitika and Haast, and Arthurs and Lewis Passes, are highly exposed to landsliding. Consequently a permanent population of ∼2,750 people are exposed to isolation. This number could more than double during peak tourist season between September and March. In the electrical transmission network up to 2,000 wooden poles and 30 steel pylons are exposed to landsliding and consequently >23,000 people are exposed to power loss.

8. Exposure analysis for the State Highway and electrical transmission network resulted in a series of key findings and recommendations:

(a) The Grey River valley region, between Inangahua and Greymouth, is the most critical section of the State Highway network. In this region the network has low-to-very low exposure to landsliding and it is therefore vital that the road and its bridges can withstand MM7-8 shaking as well as liquefaction and lateral spreading. Retaining functional access through this route will ensure emergency response access to 20,000 people who would otherwise be isolated by road.

(b) Following an Alpine fault earthquake, the emergency response will likely be most successful if based out of Wellington using Nelson as a forward operating base. Road access between Christchurch and Dunedin and the West Coast region will be severely damaged by landsliding. In addition, some damage is expected in Christchurch and Dunedin and their surrounding areas from strong ground shaking, which will require require local-to-regional-scale responses. As a result, basing the primary emergency response in Wellington will alleviate some of the stress on the emergency response in Christchurch and Dunedin, and also provide a direct link to some of the worst-affected areas in the West Coast region. Wellington is also the location for any National-level response, as central government, the NCMC, and MCDEM are all located here. An Alpine fault earthquake is likely to require a National-level CDEM response.

(c) Damage from landsliding to 2,000 wooden poles supporting the electrical transmission network is likely to require several thousand person-hours to repair. Further damage from ground shaking, liquefaction, and other geomorphic hazards could greatly exacerbate the total number affected and thus increase the repair time. Considering repairs cannot begin until safe and reliable access can be gained, affected populations (i.e. those south of Hokitika) should anticipate power loss for a considerable amount of time. Establishing alternative, less exposed power sources, or reducing reliance on power from the main network is recommended.

(d) The currently proposed Haast-Hollyford highway would be extremely exposed to landsliding and if constructed would be the worst-affected road on the State Highway network in an Alpine fault earthquake. With $>$800,000 people anticipated to use the road per annum as well as the inevitable service stations and population centres that will form along the route, its construction would present a substantially increased risk to life for users and inhabitants. Any planning process for the road should consider this.

7.4 Future work

This research has identified and enabled a number of avenues, both practical and theoretical, for future work. In general, continued efforts should be invested in identifying and modelling secondary hazards resulting from mountainous earthquakes globally. This will enable a greater understanding of the complex interlinkages between the various hazards (see Chapter 2) and may lead to greater resilience towards mountainous hazards in general. In addition, further efforts should also be given to disaster science-practitioner collaboration as this provides an effective means to reduce and manage disaster risk in general. More specific details of potential future work are explored below.

Disaster risk management of earthquakes in mountains

- Continuing engagement between disaster scientists and emergency managers throughout New Zealand should be undertaken for the development of realistic disaster scenarios. New Zealand has a large number of potential earthquake sources, particularly in the Southern Alps, and any large earthquake within the mountains presents a substantial hazard. Development of further disaster scenarios for other earthquake hazards, for instance a large Hope fault event, is likely to yield further increases in preparedness and resilience within the emergency management sector for large mountainous earthquakes.

- A focus on more effective methods for developing long-term disaster science-stakeholder partnerships for inclusion in CDEM planning, decision making, resource management planning etc. is also required. A specific focus should be given to increasing stakeholder knowledge and understanding of secondary hazards both for earthquakes in mountains and in general. Such a process will enable greater understanding of these effects and potential identify feasible mitigation efforts for implementation.

- This work has focussed primarily on impacts to critical infrastructure and the effects for the immediate emergency response. Developing and evaluating methods to estimate potential recovery times for critical infrastructure will also be vital for long-term recovery planning. Achieving resilience to large earthquakes in mountains requires the development of plans for fast and effective recovery as well as emergency response. Estimating potential down times for critical networks post-earthquake will enable a greater understanding of the long-term economic effects an Alpine fault earthquake is likely to have, both regionally and nationally.

- Following from this, developing ways to enable at risk industries and economies to become more resilient to critical infrastructure losses is also recommended. For instance, developing alternative means for the mining industry to distribute products without being solely reliant on the transport links in Arthur's Pass may allow faster post-event recovery leading to smaller economic effects. Establishing pre-event the priorities required for each industry to recover as well as establishing plans for their continuation is likely to be vital for recovery post-earthquake.

- Applying the current model on a probabilistic basis will likely establish the level of hazard coseismic landsliding presents from all potential earthquake sources. This will allow the identification of the most likely critical infrastructure losses from coseismic landsliding in general rather than from specific events. Such a process has the potential to identify the most at risk locations from all earthquake sources that could be targeted for mitigation. For instance the HVDC Inter-Island link is found to have low exposure to landsliding in an Alpine fault event, however it could be at risk from an earthquake on one of the Marlborough faults.

Coseismic landslide modelling

- Generating and analysing further coseismic landslide inventories will improve and increase the robustness of the memberships derived herein as well as potentially identifying further regional-factors which control the spatial distribution of landslides. Utilising inventories from a variety of different geotectonic environments may establish whether the factors identified in this research are ubiquitous or unique to fault-bounded mountainous environments. Inventories from different environments will increase the applicability of the fuzzy logic model by establishing robust membership curves for a wide range of environments with the potential for coseismic landsliding.

- Analysing further inventories will also provide more insight into the distribution of landslide densities with regard to susceptibility values. Including more inventories will significantly increase the robustness of the SEM method by reducing the absolute SEM value as well as the standard deviation. Substantial increases in the number of inventories used should enable the method to move from the SEM to a more probabilistic approach that will enable likelihoods to be assigned to total number estimates.

- Utilising landslide area will more effectively establish the total and individual volumes of landslides likely to occur. An extension of the method described herein to statistically analyse polygon inventories would therefore provide a substantial step forward in

coseismic landslide modelling. This could potentially enable the identification of specific areas where large coseismic landslides are anticipated rather than areas where the largest densities of landslides are expected. This will be critical for local-scale hazard assessments and for better establishing the vulnerability of critical infrastructure.

- Evaluating the effect of local factors on the number and volume of landslides will add a significant component to the current fuzzy logic model. While spatial distribution appears to be suitably modelled without considering local factors, these do appear to control the number and volume of landslides which result. Establishing the effect these factors have on landslide production may prove critical. For instance, what effect does lithology have on the k value when estimating total volume?

- Analysing the effects of previous coseismic landsliding occurrences on critical infrastructure networks may identify threshold landslide densities for which networks are most likely to be affected, increasing the robustness of the exposure model described in Chapter 6. Using past events to identify potential threshold values compared to user-defined values may allow absolute values to be considered rather than relative values. This may also enable exposure and susceptibility to be directly translated to impact severity, which is important for long-term recovery planning.

Specific research opportunities

- Undertaking field studies to search for evidence of previous landslide-generated tsunami in many of the South Island lakes is strongly recommended. The potential for tsunami in some of these lakes from an Alpine fault scenario cannot be overlooked as the Lituya Bay example demonstrates how catastrophic these events can be. With such a large population living in Queenstown ($\sim$30,000) on the shoreline of Lake Wakatipu, this lake is specifically suggested for future work. Adapting the current method to incorporate landslide areas may also provide further information on the potential hazard for South Island lakes.

- On-going palaeoseismic investigations, particularly for evidence of aggradation following the 1717 Alpine fault earthquake is recommended as this will allow better understanding of the potential issues that long-term aggradation presents. A suggested location to begin work is Potters Creek which drains into Lake Mapourika where Howarth et al. (2014) unequivocally identified evidence of long-term post-seismic sediment inputs following the 1717 earthquake. Potters Creek is an isolated catchment and the

only input to Lake Mapourika; it therefore presents an excellent opportunity to identify previous aggradation from landsliding within the catchment.

- Understanding how sediment is remobilised and transported post-earthquake is also a vital question which needs further investigation. The subsequent long-term sediment mobilisation presents a substantial issue to the recovery process as well as industries such as farming which rely on the fertile soils on alluvial fans. The 2008 Wenchuan earthquake presents an opportunity to study and understand such effects as sediment continues to be reworked and removed. Studying sediment remobilisation following volcanic eruptions in places such as Mt Pinatubo may also be a useful research option as this process should not differ substantially from remobilisation of landslide debris.

- Continued work into the activity and seismic potential of faults in the Aoraki/Mt Cook area is also recommended. One or more of these faults may be responsible for the palaeoseismic evidence of a c. 1600 earthquake in the far south of the West Coast region which is unlikely to be derived from the Alpine fault earthquake farther north at a similar time. An earthquake on one of these faults today would present a substantial issue for the inland highways, the large number of communities in the area (including Queenstown and Wanaka), and the hydroelectric dams on the Waitaki River. Further, being within the ranges these faults may present a greater landslide potential than the range-front Alpine fault.

- Further research into the formation, failure, and runout of large coseismic rock avalanches is also currently required. These catastrophic events present a substantial hazard yet they remain relatively poorly understood. In general, large volume events are most likely to arise from strong ground shaking, however New Zealand has recently had several large volume events with no apparent trigger (e.g. the 1999 Mt Adams landslide). Understanding the formation and failure of these events is essential for hazard and risk analysis. Similarly the identification of large runout events (e.g. Round Top and Komansu; see Appendix A) suggest a need for greater understanding of these processes. Communities situated several kilometres from potential source zones may still be exposed if such runout lengths are possible under certain conditions.

- The Green Lake rock avalanche in southern Fiordland presents an interesting research opportunity. At 27 times larger than the next largest rock avalanche in the South Island it is anomalously large, yet its location does not conform to that expected for such a massive failure. Unlike the other extremely large failures, which cluster to the Milford Sound/Hollyford River area (**Fig. 2.7**), Green Lake is relatively isolated with only

three other large landslides nearby, although the largest of these is >100 times smaller. Further, Hall et al. (2014) demonstrated that it cannot be Alpine fault-derived and suggested the nearby Hauroko fault as an alternative earthquake source. This may have important consequences for seismic hazard in the southern South Island. It may also suggest that M∼7 earthquakes in the ranges are capable of producing significant rock avalanches.

Bibliography

Abrahamson, N. A. (2000). State of the practice of seismic hazard evaluation. In: *International Society for Rock Mechanics International Symposium*, **1**, 659–685, Australia.

Adams, J. (1980a). Contemporary uplift and erosion of the Southern Alps, New Zealand: Summary. *Geological Society of America Bulletin*, **91**:2–4.

Adams, J. (1980b). Paleoseismicity of the Alpine Fault seismic gap, New Zealand. *Geology*, **8**:72–76.

Adams, J. (1981). Earthquake-dammed lakes in New Zealand. *Geology*, **9**:215–219.

Akgun, A. and Bulut, F. (2007). GIS-based landslide susceptibility for Arsin-Yomra (Trabzon, North Turkey) region. *Environmental Geology*, **51(8)**:1377–1387.

Akgun, A., Dag, S., and Bulut, F. (2008). Landslide susceptibility mapping for a landslide-prone area (Findikli, NE of Turkey) by likelihood-frequency ratio and weighted linear combination models. *Environmental Geology*, **54(6)**:1127–1143.

Alexander, D. E. (1995). A survey of the field of natural hazards and disaster studies. In: *Geographical Information Systems in Assessing Natural Hazards*, 1–19. Springer, Amsterdam.

Alexander, D. E. (2000). Scenario methodology for teaching principles of emergency management. *Disaster Prevention and Management*, **9(2)**:89–97.

Alexander, D. E. (2005). Vulnerability to landslides. *Landslide Hazard and Risk*, 175–198.

Andersen, T. (2001). Managing economic exposures of natural disasters: exploring alternative financial risk management opportunities and instruments. Internal Report, Islamic Development Bank.

Anderson, H., Beanland, S., Blick, G., Darby, D., Downes, G., Haines, J., Jackson, J., Robinson, R., and Webb, T. H. (1994). The 1968 May 23 Inangahua, New Zealand, earthquake: an integrated geological, geodetic, and seismological source model. *New Zealand Journal of Geology and Geophysics*, **37**:59–86.

Angelier, J., Barrier, E., and Chu, H. (1986). Plate collision and paleostress trajectories in a fold-thrus belt: the foothills of Taiwan. *Tectonophysics*, **125(1)**:161–178.

Annaka, T., Satake, K., Sakakiyama, T., Yanagisawa, K., and Shuto, N. (2007). Logic-tree approaches for probabilisitic tsunami hazard analysis and its applications to the Japanese coasts. In: *Tsunami and its hazards in the Indian and Pacific Oceans*, 577–592. Birkhäuser Basel.

Ansal, A., Akinci, A., Cultrera, G., Erdik, M., Pessina, V., Tönük, G., and Ameri, G. (2009). Loss estimation in Istanbul based on deterministic earthquake scenarios of the Marmara Sea region (Turkey). *Soil Dynamics and Earthquake Engineering*, **29(4)**:699–709.

Arshad, A. W., Doscher, C., and Davies, T. R. (2004). Landslide dambreak hazard analysis in Westland, New Zealand - a GIS approach. In: *Proceedings of the 6th International Conference of Hydroinformatics*, **21**, 730–737. World Scientific Pulblishing.

Azevedo, J., Guerreiro, L., Bento, R., Lopes, M., and Proença, J. (2010). Seismic vulnerability of lifelines in the greater Lisbon area. *Bulletin of Earthquake Engineering*, **8(1)**:157–180.

Bannister, S. and Gledhill, K. (2012). Evolution of the 2010-2012 Canterbury earthquake sequence. *New Zealand Journal of Geology and Geophysics*, **55(3)**:295–304.

Barth, N. C. (2014). The Cascade rock avalanche: implications of a very large Alpine Fault-triggered failure, New Zealand. *Landslides*, **11(3)**:327–341, doi:10.1007/s10346-013-0389-1.

Bearnson, C. S. and Wiker, K. M. (2005). Human patient simulators: A new face in baccalaureate nursing education at Brigham Young University. *Journal of Nursing Education*, **44**:421–425.

Beavan, J., Denys, P., Denham, M., Hager, B., Herring, T., and Molnar, P. (2010a). Distribution of present-day vertical deformation across the Southern Alps, New Zealand, from 10 years of GPS data. *Geophysical Research Letters*, **37**:7–11.

Beavan, J., Fielding, E., Motagh, M., Samsonov, S., and Donnelly, N. (2011). Fault location and slip distribution of the 22 February 2011 Mw 6.2 Christchurch, New Zealand, earthquake from geodetic data. *Seismological Research Letters*, **82(6)**:789–799.

Beavan, J., Moore, M., Pearson, C., Henderson, M., Parsons, B., Bourne, S., England, P., Walcott, D., Blick, G., Darby, D., and Hodgkinson, K. (1999). Crustal deformation during 1994-1998 due to oblique continental collision in the central Southern Alps, New Zealand, and implications for seismic potential of the Alpine fault. *Journal of Geophysical Research*, **104(B11)**:25233–25255.

Beavan, J., Samsonov, S., Denys, P., Sutherland, R., Palmer, N., and Denham, M. (2010b). Oblique slip on the Puysegur subduction interface in the 2009 July MW 7.8 Dusky Sound earthquake from GPS and InSAR observations: implications for the tectonics of southwestern New Zealand. *Geophysical Journal International*, **183**:1265–1286.

Becker, J. S., Johnston, D. M., Paton, D., Hancox, G. T., Davies, T. R., McSaveney, M., and Manville, V. R. (2007). Response to landslide dam failure rmergencies: Issues resulting from the October 1999 Mount Adams landslide and dam-break flood in the Poerua River, Westland, New Zealand. *Natural Hazards Review*, **8(2)**:35–42.

Berkes, F., Colding, J., and Folke, C. (2003). *Navigating social-ecological systems: building resilience for complexity and change*. Cambridge University Press.

Berkes, F. and Folke, C. (1998). *Management practices and social mechanisms for building resilience*, Chapter: Linking social and ecological systems. Cambridge University Press.

Berril, J. B., Mulqueen, P. C., and Ooi, E. T. C. (1994). Liquefaction of Kaiapoi in the 1901 Cheviot, New Zealand, earthquake. *Bulletin of the New Zealand National Society of Earthquake Engineering*, **27**:178–189.

Berryman, K., Alloway, B. S., Almond, P. C., Barrell, D. J. A., Duncan, R. P., McSaveney, M., Read, S., and Tonkin, P. (2001). Alpine fault rupture and landscape evolution in Westland. In: *Proceedings of the 5th International Conference of Geomorphology*, Tokyo.

Berryman, K., Beanland, S., Cooper, A., Cutten, H. N., Norris, R., and Wood, P. R. (1992). The Alpine Fault, New Zealand: variation in Quaternary tectonic style and geomorphic expression. *Annales Tectonicae*, **VI**:126–163.

Berryman, K., Cochran, U. A., Clark, K. J., Biasi, G., Langridge, R. M., and Villamor, P. (2012a). Major earthquakes occur regularly on an isolated plate boundary fault. *Science*, **336**:1690–1693.

Berryman, K., Cooper, A., Norris, R., Villamor, P., Sutherland, R., Wright, T., Schermer, E., Langridge, R. M., and Biasi, G. (2012b). Late holocene rupture history of the Alpine Fault in South Westland, New Zealand. *Bulletin of the Seismological Society of America*, **102(2)**:620–638.

Berryman, K. and Villamor, P. (2004). Surface rupture of the Poulter Fault in the 1929 March 9 Arthur's Pass earthquake, and redifinition of the Kakapo Fault, New Zealand. *New Zealand Journal of Geology and Geophysics*, **47**:341–351.

Bhattacharya, S., Hyodo, M., Goda, K., Tazoh, T., and Taylor, C. (2011). Liquefaction of soil in the Tokyo Bay area from the 2011 Tohoku (Japan) earthquake. *Soil Dynamics and Earthquake Engineering*, **31**:1618–1628.

Bielak, J., Graves, R. W., Olsen, K. B., Taborda, R., Ramírez-Guzmán, L., Day, S. M., Ely, G. P., Roten, D., Jordan, T. H., Maechling, P. J., Urbanic, J., Cui, Y., and Juve, G. (2010). The ShakeOut earthquake scenario: Verification of three simulation sets. *Geophysical Journal International*, **180**:375–404.

Bird, J. F. and Bommer, J. J. (2004). Earthquake losses due to ground failure. *Engineering Geology*, **75**:147–179.

Blake, T. F., Hollingsworth, R. A., and Stewart, J. P. (2002). Recommended procedures for implementation of DMG special publication 117 - guidelines for analyzing and mitigating landslide hazards in California. Technical Report, Southern California Earthquake Center, Los Angeles, CA.

Blanchard, B. W. (2008). Guide to emergency management and related terms, definitions, concepts, acronyms, organizations, programs, guidance, executive orders, and legislation. Retrieved 5 August 2014, from: www.training.fema.gov/EMIWeb/edu/docs/-terms%20and%20definitions/Terms%20and%20Definitions.pdf.

Bommer, J. J. (2002). Deterministic vs. Probabilistic seismic hazard assessment: An exaggerated and obstructive dichotomy. *Journal of Earthquake Engineering*, **6(1)**:43–73.

Bommer, J. J. and Martínez-Pereira, A. (1999). The effective duration of earthquake strong motion. *Journal of Earthquake Engineering*, **3(2)**:127–172.

Bonham-Carter, G. F. (1994). *Geographic information systems for geoscientists*. Pergamon, Ottawa.

Borodzicz, E. and van Haperen, K. (2002). Individual and group learning in crisis simulation. *Journal of Contingencies and Crisis Management*, **10(3)**:139–148.

Bouchon, M. and Vallèe, M. (2003). Observation of Long Supershear Rupture During the Magnitude 8.1 Kunlunshan Earthquake. *Science*, **301**:824–826.

Bray, J. D. and Travasarou, T. (2009). Pseudostatic coefficient for use in simplified seismic slope stability evaluation. *Journal of Geotechnical Engineering*, **135**:1336–1340.

Brown, L. J., Beetham, R. D., Paterson, B. R., and Weeber, J. H. (1995). Geology of Christchurch, New Zealand. *Environmental and Engineering Geoscience*, **1(4)**:427–488.

Brune, J. N. (2001). Shattered rock and precarious rock evidence for strong asymmetry in ground motions during thrust faulting. *Seismological Society of America Bulletin*, **91**:441–447.

Brunetti, M. T., Guzzetti, F., and Rossi, M. (2009). Probability distributions of landslide volumes. *Nonlinear Processes in Geophysics*, **16**:179–188.

Buech, F., Davies, T. R., and Pettinga, J. R. (2010). The Little Red Hill Seismic Experimental Study: Topographic Effects on Ground Motion at a Bedrock-Dominated Mountain Edifice. *Bulletin of the Seismological Society of America*, **100(5A)**:2219–2229, doi:10.1785/0120090345.

Bull, W. B. (1996). Prehistorical earthquakes on the Alpine Fault, New Zealand. *Journal of Geophysical Research*, **101(B3)**:6037–6050.

Bull, W. B. (2003). Lichenometry dating of coseismic changes to a New Zealand landslide complex. *Annals of Geophysics*, **46(5)**:1155–1167.

Burton, I. and Hewitt, K. (1974). Ecological dimensions of environmental hazards. In: Sargent, F. (Ed.), *Human Ecology*, 253–284, New York. American Elsevier.

Buslenko, N. P. (1966). *The Monte Carlo method: the method of statistical trials*, **87**. Pergamon.

Byerlee, J. (1978). Friction of rocks. *Pure and Applied Geophysics*, **116(4-5)**:615–626.

Carlile, P. R. (2002). A pragmatic view of knowledge and boundaries: Boundary objects in new product development. *Organization science*, **13(4)**:442–455.

Carrara, A., Cardinali, M., Detti, R., Guzzetti, F., Pasqui, V., and Reichenbach, P. (1991). GIS techniques and statistical models in evaluating landslide hazard. *Earth Surface Processes and Landforms*, **16**:427–445.

Catani, F., Casagli, N., Ermini, L., Righini, G., and Menduni, G. (2005). Landslide hazard and risk mapping at catchment scale in the Arno River basin. *Landslides*, **2(4)**:329–342, doi:10.1007/s10346-005-0021-0.

Centre for Research on the Epidemiology of Disasters (2013). Retrieved 9 May 2014, from: http://www.emdat.be/database.

Chang, S. E. and Nojima, N. (2001). Measuring post-disaster transportation system performance: the 1995 Kobe earthquake in comparative perspective. *Transportation Research Part A: Policy and Practice*, **35(6)**:475–494.

Chang, S. E., Seligson, H., and Eguchi, R. (1996). Estimation of the economic impact of multiple lifeline disruption: Memphis Light, Gas and Water Division case study. Technical Report NCEER-96-0011, National Center for Earthquake Engineering Research.

Chang, S. E., Svekla, W. D., and Shinozuka, M. (2002). Linking infrastructure and urban economy: simulation of water-disruption impacts in earthquakes. *Environment and Planning B*, **29(2)**:281–302.

Chi, W., Dreger, D., and Kaverina, A. (2001). Finite-source modeling of the 1999 Taiwan (Chi-Chi) earthquake derived from a dense strong-motion network. *Bulletin of the Seismological Society of America*, **91(5)**:1144–1157.

Chigira, M., Wang, W.-N., Furuya, T., and Kamaia, T. (2003). Geological causes and geomorphological precursors of the Tsaoling landslide triggered by the 1999 Chi-Chi earthquake, Taiwan. *Engineering Geology*, **68**:259–273.

Chinn, T. J. (1989). Glaciers of New Zealand. Professional Paper 131386-H2, United States Geological Survey, Washington D.C.

Chinn, T. J. (2001). Distribution of the glacial water resources of New Zealand. *Journal of Hydrology*, **40(2)**:139–187.

Chung, C. F. and Fabbri, A. (1999). Probabilistic prediction models for landslide hazard mapping. *Photogrammetric Engineering and Remote Sensing*, **65(12)**:1389–1399.

Chung, C. F., Fabbri, A., and van Western, C. J. (1995). Multivariate regression analysis for landslide hazard zonation. In: Carrara, A. and Guzzetti, F. (Eds.), *Geographical Infromation Systems in Assessing Natural Hazards*, 107–133, Netherlands. Kluwer Academic Publishers.

Church, R. L., Scaparra, M. P., and Middleton, R. S. (2004). Identifying critical infrastructure: the median and covering facility interdiction problems. *Annals of the Association of American Geographers*, **94(3)**:491–502.

Clough, B. R. (2006). Liquefaction in Christchurch City. In: *Earthquakes and Urban development: New Zealand Geotechnical Society 2006 Symposium, Nelson*, Wellington, New Zealand. Institution of Professional Engineers New Zealand.

Clough, R. W. and Chopra, A. K. (1966). Earthquake stress analysis in earth dams. *ASCE Journal of the Engineering Mechanics Division*, **92**:197–211.

Cooke, R. M. and Goosens, L. H. J. (2004). Expert judgement elicitation for risk assessments of critical infrastructures. *Journal of Risk Research*, **7(6)**:643–656.

Cooper, A. (1990). Retrograde alteration of Chrimian Kyanite in Metachert and Amphibolite Whiteschist from the Southern Alps, New Zealand, with implications for uplift of the Alpine Fault. *Mineralogy and Petrology*, **75**:153–164.

Cooper, A. and Norris, R. (1990). Estimates for the timing of the last coseismic displacement on the Alpine fault, northern Fiordland, New Zealand. *New Zealand Journal of Geology and Geophysics*, **40**:303–307.

Cooper, A. and Norris, R. (1994). Anatomy, structural evolution, and slip rate of a plate-boundary thrust: The Alpine fault at Gaunt Creek, Westland, New Zealand. *Geological Society of America Bulletin*, **106**:627–633.

Costa, J. E. and Schuster, R. L. (1988). The formation and failure of natural dams. *Geological Society of America Bulletin*, **100**:1054–1068.

Cowan, H. A. (1990). Late Quaternary displacements in the Hope Fault at Glynn Wye, North Canterbury. *New Zealand Journal of Geology and Geophysics*, **33**:285–293.

Cox, S., Stirling, M., Herman, F., Gerstenberger, M., and Ristau, J. (2012). Potentially active faults in the rapidly eroding landscape adjacent to the Alpine Fault, central Southern Alps, New Zealand. *Tectonics*, **31(TC2011)**, doi:10.1029/2011TC003038.

Crozier, M. J. and Glade, T. (2005). Landslide hazard and risk: issues, concepts and approach. In: Glade, T., Anderson, M. G., and Crozier, M. J. (Eds.), *Landslide risk assessment*, 1–40. John Wiley.

Cubrinovski, M., Bradley, B., Wotherspoon, L., Green, R., Bray, J. D., Wood, C., Pender, M., Allen, J., Bradshaw, A., Rix, G., Taylor, M., Robinson, K., Henderson, D., Giorgini, S., Ma, K., Winkley, A., Zupan, J., O'Rourke, T., De Pascale, G., and Wells, D. (2011a). Geotechnical aspects of the 22 February 2011 Christchurch earthquake. *Bulletin of the New Zealand Society for Earthquake Engineering*, **44(4)**:205–226.

Cubrinovski, M., Bray, J. D., Taylor, M., Giorgini, S., Bradley, B., Wotherspoon, L., and Zupan, J. (2011b). Soil liquefaction effects in the Central business district during the February 2011 Christchurch earthquake. *Seismological Research Letters*, **82(6)**:893–904.

Dadson, S. J., Hovius, N., Chen, H., Dade, W. B., Lin, J.-C., Hsu, M.-L., Lin, C.-W., Horng, M.-J., Chen, T.-C., Milliman, J., and Stark, C. P. (2004). Earthquake-triggered increase in sediment delivery from an active mountain belt. *Geology*, **32(8)**:733–736, doi:10.1130/G20639.1.

Dai, F. C. and Lee, C. F. (2002). Landslide characteristics and slope instability modeling using GIS, Lantau Island, Hong Kong. *Geomorphology*, **42(3-4)**:213–228.

Dai, F. C., Lee, C. F., Li, J., and Xu, Z. W. (2001). Assessment of landslide susceptibility on the natural terrain of Lantau Island, Hong Kong. *Environmental Geology*, **40(3)**:381–391.

Davey, F., Henyey, T., Kleffmann, S., and Melhuish, A. (1995). Crustal reflections from the Alpine Fault Zone, South Island, New Zealand. *New Zealand Journal of Geology and Geophysics*, **38**:37–41.

Davies, T. R. (1982). Spreading of Rock Avalanche Debris by Mechanical Fluidization. *Rock Mechanics*, **15(1)**:9–24.

Davies, T. R. (2002). Landslide-dambreak floods at Franz Josef Glacier township, Westland, New Zealand: a risk assessment. *Journal of Hydrology*, **41(1)**:1–17.

Davies, T. R. and Korup, O. (2007). Persistent alluvial fanhead trenching resulting from large, infrequent sediment inputs. *Earth Surface Processes and Landforms*, **32**:725–742.

Davies, T. R., Manville, V. R., Kunz, M., and Donadini, L. (2007). Modelling landslide dambreak flood magnitudes: a case study. *Journal of Hydrological Engineering*, **133(7)**:713–720.

Davies, T. R. and McSaveney, M. (2006). Runout of rock avalanches and volcanic debris avalanches (Invited Keynote Lecture). In: Piceralli, L. (Ed.), *Proceedings of the international conference on fast slope movements: prediction and prevention for risk mitigation*, Pàtron, Naples.

Davies, T. R., McSaveney, M., and Doscher, C. (2005). Monitoring and effects of landslide-induced aggradation in the Poerua Valley, Westland. Technical Report, The Earthquake Commision, Wellington.

De Pascale, G. and Langridge, R. M. (2012). New on-fault evidence for a great earthquake in A.D. 1717, central Alpine fault, New Zealand. *Geology*, **40(9)**:791–794, doi:10.1130/G33363.1.

De Pascale, G., Quigley, M., and Davies, T. R. (2014). Lidar reveals uniform Alpine fault offsets and bimodal plate boundary rupture behavior, New Zealand. *Geology*, **42(5)**:411–414, doi:10.1130/G35100.1.

DeMets, C., Gordon, R. G., Argus, D. F., and Stein, S. (1994). Effect of recent revisions to the geomagnetic reversal timescale on estimates of current plate motions. *Geophysical Research Letters*, **21**:2191–2194, doi:10.1029/94GL02118.

Densmore, A. L., Ellis, M., Li, Y., Zhou, R., Hancock, G., and Richardson, N. (2007). Active tectonics of the Beichuan and Pengguan faults at the eastern margin of the Tibetan Plateau. *Tectonics*, **26(TC4005)**, doi:10.1029/2006TC001987.

Department of Conservation (2006). The value of conservation: what does conservation contribute to the economy? Retrieved 5 August 2014, from: http://www.doc.govt.nz/-documents/conservation/value-of-conservation.pdf.

Department of Homeland Security (2007). *DHS Lexicon: Terms and Definitions*. Department of Homeland Security, Washington D.C.

Department of the Prime Minister and Cabinet (2011). New Zealand's National Security System. Technical Report, Department of the Prime Minister and Cabinet.

Donati, L. and Turrini, M. C. (2002). An objective method to rank the importance of the factors predisposing to landslide with GIS methodology: application to an area of the Apennines (Valnerine, Perugia, Italy). *Engineering Geology*, **63(3-4)**:277–289.

Donnellan, A., Hager, B., King, R., and Herring, T. (1993). Geodetic measurement of deformation in the Ventura Basin region, southern California. *Journal of Geophysical Research: Solid Earth*, **98(B12)**:21727–21739.

Downes, G. (2005). The 1855 January 23 M8+ Wairarapa earthquake - what contemporary accounts tell us about it. In: *The 1855 Wairarapa Earthquake Symposium*, 1–11, Wellington, New Zealand.

Dowrick, D. J. (1994). Damage and intensities in the M7.8 1929 Murchison, New Zealand, earthquake. *Bulletin of the New Zealand National Society of Earthquake Engineering*, **27**:190–204.

Drabek, T. E. (1985). Managing the emergency response. *Public Administration Review*, **45**:85–92.

Dramis, F. and Sorriso-Valvo, M. (1994). Deep-seated gravitational slope deformation, related landslides and tectonics. *Engineering Geology*, **38**:231–243.

Dubois, D. and Prade, H. (1985). A review of fuzzy set aggregation connectives. *Information Sciences*, **36**:85–121.

Dufresne, A., Davies, T. R., and McSaveney, M. (2009). Influence of runout-path material on emplacement of the Round Top rock avalanche, New Zealand. *Earth Surface Processes and Landforms*, **35(2)**:190–201, doi:10.1002/esp.1900.

Dykstra, J. L. (2012). *The role of mass wasting and ice retreat in the post-LGM evolution of Milford Sound, Fiordland, New Zealand*. PhD thesis, University of Canterbury.

Eisbacher, G. H. (1979). Cliff collapse and rock avalanches (sturzstroms) in the Mackenzie Mountains, northwestern Canada. *Canadian Geotechnical Journal*, **16**:309–334.

Evans, S. G. and Clague, J. J. (1988). Catastrophic rock avalanches in glacial environments. In: *Proceedings of the 5th International Symposium on Landslides*, **2**, 1153–1158.

Faccioli, E. (2006). Seismic hazard assessment for derivation of earthquake scenarios in Risk-UE. *Bulletin of Earthquake Engineering*, **4**:341–364.

Fäh, D., Kind, F., Lang, K., and Giardini, D. (2001). Earthquake scenarios for the city of Basel. *Soil Dynamics and Earthquake Engineering*, **21(5)**:405–413.

Federal Emergency Management Agency (2004). Hurricane Pam Exercise concludes. Retrieved 20 August 2013, from: http://www.fema.gov/news-release/2004/07/23/-hurricane-pam-exercise-concludes.

Field, E. H., Jordan, T. H., and Cornell, C. A. (2003). OpenSHA: A Developing Community-Modeling Environment for Seismic Hazard Analysis. *Seismological Research Letters*, **74(4)**:406–419.

Folke, C., Hahn, T., Olsson, P., and Norberg, N. (2005). Adaptive governance of social-ecological systems. *Annual Review of Environmental Resources*, **30**:441–473.

Frattini, P., Crosta, G., and Carrara, A. (2010). Techniques for evaluating the performance of landslide susceptibility models. *Engineering Geology*, **111(1-4)**:62–72.

Freeman, P. K. and Kunreuther, H. (1997). *Managing environmental risk through insurance*. AEI Press (soft back), Kluwer Academic Publishers (hardback).

Freeman, P. K., Martin, L. A., Linnerooth-Bayer, J., Mechler, R., Pflug, G., and Warner, K. (2003). Disaster risk management: national systems for the comprehensive management of disaster financial strategies for natural disaster reconstruction. Regional Policy Dialogue, Inter-American Development Bank, Washington D.C.

Fritz, C. E. (1961). Disaster. In: Merton, R. K. and Nisbet, R. A. (Eds.), *Contemporary Social Problems*, New York, NY. Harcourt, Brace and World.

Fritz, H. M., Mohammed, F., and Yoo, J. (2009). Lituya Bay Landslide Impact Generated Mega-Tsunami 50th Anniversary. *Pure and Applied Geophysics*, **166**:153–175.

Fry, B., Bannister, S., Beavan, J., Bland, L., Bradley, B., Cox, S., Cousins, J., Gale, N., Hancox, G. T., Holden, C., Jongens, R., Power, W., Prasetya, G., Reyners, M., Ristau, J., Robinson, R., Samsonov, S., Wilson, K., and The GeoNet Team (2010). The Mw 7.6 Dusky Sound earthquake of 2009: Preliminary report. *Bulletin of the New Zealand National Society of Earthquake Engineering*, **43(1)**:24–40.

Giovinazzi, S. and King, A. (2009). Estimating seismic impacts of lifelines: an international review for RiskScape. In: *New Zealand Society of Earthquake Engineering Annual Conference (NZSEE)*, Christchurch, New Zealand.

Giovinazzi, S., Wilson, T., Davis, C., Bristow, D., Gallagher, M., Schofield, A., Villemure, M., Eidinger, J., and Tang, A. (2011). Lifelines performance and management following the 22 February 2011 Christchurch earthquake, New Zealand: Highlights of resilience. *Bulletin of the New Zealand Society for Earthquake Engineering*, **44(4)**:402–417.

Gledhill, K., Ristau, J., Reyners, M., Fry, B., and Holden, C. (2011). The Darfield (Canterbury, New Zealand) Mw 7.1 Earthquake of September 2010: A Preliminary Seismological Report. *Seismological Research Letters*, **82**:378–386, doi:10.1785/gssrl.82.3.378.

GNS Science (2014). New Zealand Active Faults Database. Retrieved 29 May 2014, from: data.gns.cri.nz/af/.

Gorum, T., Fan, X., van Western, C. J., Huang, R. Q., Xu, Q., Tang, C., and Wang, G. (2011). Distribution pattern of earthquake-induced landslides triggered by the 12 May 2008 Wenchuan earthquake. *Geomorphology*, **133**:152–167.

Gorum, T., Korup, O., van Western, C. J., van der Meijde, M., Xu, C., and van der Meer, F. D. (2014). Why so few? Landslides triggered by the 2002 Denali earthquake, Alaska. *Quaternary Science Reviews*, **95**:80–94.

Grapes, R. (1988). Geology and revegetation of an 1855 landslide, Ruamahanga River, Kopuaranga, Wairarapa. In: *Tuatara*, **30**, 77–83, Wellington.

Grapes, R. and Downes, G. (1997). The 1855 Wairarapa, New Zealand, earthquake: analysis of historical data. *Bulletin of the New Zealand Society for Earthquake Engineering*, **30**:271–368.

Grapes, R., Little, T. A., and Downes, G. (1998). Rupturing of the Awatere fault during the 1848 October 16 Marlborough earthquake, New Zealand: historical and present day evidence. *New Zealand Journal of Geology and Geophysics*, **41**:387–399.

Griffiths, G. A. (1979). High sediment yields from major rivers of the Western Southern Alps, New Zealand. *Nature*, **282**:61–63.

Guzzetti, F., Ardizzone, F., Cardinali, M., Rossi, M., and Valigi, D. (2009). Landslide volumes and landslide mobilization rates in Umbria, central Italy. *Earth and Planetary Science Letters*, **279(3)**:222–229.

Guzzetti, F., Carrarra, A., Cardinali, M., and Reichenbach, P. (1999). Landslide hazard evaluation: a review of current techniques and the application in a multiscale study. *Geomorphology*, **31**:181–216.

Guzzetti, F., Reichenbach, P., Ardizzone, F., Cardinali, M., and Galli, M. (2006). Estimating the quality of landslide susceptibility models. *Geomorphology*, **81(1-2)**:166–184.

Hainzl, S., Zöller, G., and Kurths, J. (2000). Self-organization of spatio-temporal earthquake clusters. *Nonlinear Processes in Geophysics*, **7**:21–29.

Hall, L., Robinson, T. R., Duffy, B., Borella, M., Gravley, D., and Hampton, S. (2014). Using landslide susceptibility modelling to investigate potential earthquake triggers for the anomalously large Green Lake rock avalanche, New Zealand. In: *Geologic Society of America Conference Abstracts, October 2014*, Vancouver, Canada. Geological Society of America.

Hancox, G. T. (2005). Landslides and liquefaction effects caused by the 1855 Wairarapa earthquake: then and now. In: *The 1855 Wairarapa Earthquake Symposium*, 84–95, Wellington, New Zealand.

Hancox, G. T., Cox, S., Turnbull, I. M., and Crozier, M. J. (2003). Reconnaissance studies of landslides and other ground damage caused by the Mw 7.2 Fiordland earthquake of 22 August 2003. Technical Report, GNS Sciences, GNS Science Limited, Lower Hutt, New Zealand.

Hancox, G. T., McSaveney, M., Manville, V. R., and Davies, T. R. (2005). The October 1999 Mt Adams rock avalanche and subsequent landslide dam-break flood and effects in Poerua River, Westland, New Zealand. *New Zealand Journal of Geology and Geophysics*, **48**:683–705.

Hancox, G. T. and Perrin, N. (1994). Green Lake Landslide: A very large ancient rock slide in glaciated terrain, Fiordland, New Zealand. Technical Report Report 93/18, GNS Sciences.

Hancox, G. T. and Perrin, N. (2009). Green Lake Landslide and other giant and very large postglacial landslides in Fiordland, New Zealand. *Quaternary Science Reviews*, **28(11-12)**:1020–1036.

Hancox, G. T., Perrin, N., and Dellow, G. (1997). Earthquake-induced landsliding in New Zealand and implications for MM intensity and seismic hazard assessment. Client Report 43601B, GNS Sciences.

Harder, B. N. (2010). Use of Simulation in Teaching and Learning in Health Sciences: A Systematic Review. *Journal of Nursing Education*, **49(1)**:23–28.

Harp, E. L. and Jibson, R. W. (1996). Landslides triggered by the 1994 Northridge, California, earthquake. *Bulletin of the Seismological Society of America*, **86(1B)**:S319–S332.

Harpp, K. S. and Sweeney, W. J. (2002). Simulating a Volcanic Crisis in the classroom. *Journal of Geoscience Education*, **50(4)**:410–418.

Hauksson, E., Jones, L., and Hutton, K. (1995). The 1994 Northridge earthquake sequence in California: Seismological and tectonic aspects. *Journal of Geophysical Research: Solid Earth*, **100(B7)**:12335–12355.

He, Y. P. and Beighley, R. E. (2008). GIS-based regional landslide susceptibility mapping: a case study in southern California. *Earth Surface Processes and Landforms*, **33(3)**:380–393.

Hewitt, K. (2009). Rock avalanches that travel onto glaciers and related developments, Karakoram Himalaya, Inner Asia. *Geomorphology*, **103**:66–79.

Hewitt, K., Clague, J. J., and Orwin, J. F. (2008). Legacies of catastrophic rock slope failures in mountain landscapes. *Earth Science Reviews*, **87**:1–38.

Hicks, D. M., Hill, J., and Shankar, U. (1996). Variation of suspended sediment yields around New Zealand: the relative importance of rainfall and geology. In: *Erosion and Sediment Yield: Global and Regional Perspectives*, number 236, 149–156. IAHS Publishing.

Hok, S., Fukuyama, E., and Hashimoto, C. (2011). Dynamic rupture scenarios of anticipated Nankai-Tonankai earthquakes, southwest Japan. *Journal of Geophysical Research*, **116(B12319)**, doi:10.1029/2011JB008492.

Holden, C. (2011). Kinematic source Model of the 22 February 2011 Mw 6.2 Christchurch earthquake using strong motion data. *Seismological Research Letters*, **82(6)**:783–788.

Holling, C. S. (2004). From complex regions to complex worlds. *Ecology and Society*, **9(1)**:11.

Holmgren, A. J. (2006). Using graph models to analyze the vulnerability of electric power networks. *Risk Analysis*, **26(4)**:955–969, doi:10.1111/j.1539-6924.2006.00791.x.

Hovius, N., Meunier, P., Lin, C. W., Chen, H., Chen, Y., Dadson, S. J., Horng, M. J., and Lines, M. (2011). Prolonged seismically induced erosion and the volume balance of a large earthquake. *Earth and Planetary Science Letters*, **279(3-4)**:222–229, doi:10.1016/j.epsl.2009.01.005.

Howarth, J. D., Fitzsimons, S. J., Norris, R., and Jacobsen, G. E. (2012). Lake sediments record cycles of sediment flux driven by large earthquakes on the Alpine fault, New Zealand. *Geology*, **40(12)**:1091–1094.

Howarth, J. D., Fitzsimons, S. J., Norris, R., and Jacobsen, G. E. (2014). Lake sediments record high shaking that provides insights into the location and rupture length of large earthquakes on the Alpine fault, New Zealand. *Earth and Planetary Science Letters*, **403**:340–351.

Hsü, K. J. (1975). Catastrophic Debris Streams (Sturzstroms) Generated by Rockfalls. *Geological Society of America Bulletin*, **86**:129–140.

Huang, R., Li, W., Xu, Q., and Tang, C. (2010). Large landslides triggered by the M 8.0 Wenchuan Earthquake of 12 May 2008, China. *Geophysical Research Abstracts*, **12**:15031.

Huang, R., Pei, X., Fan, X., Zhang, W., Li, S., and Li, B. (2012). The characteristics and failure mechanism of the largest landslide triggered by the Wenchuan earthquake, May 12, 2008, China. *Landslides*, **9**:131–142, doi:10.1007/s10346-011-0276-6.

Hull, A. G. and Berryman, K. (1986). Holocene tectonism in the region of the Alpine fault at Lake McKerrow, Fiordland, New Zealand. *Royal Society of New Zealand Bulletin*, **24**:317–331.

Hung, J. (2000). Chi-Chi earthquake induced landslides in Taiwan. In: *International Workshop on Annual Commemoration of Chi-Chi Earthquake*, **3**, 23–36, Taipei. National Centre for Research on Earthquake Engineering.

Hungr, O., Corominas, J., and Eberhardt, E. (2005). Estimating landslide motion mechanism, travel distance and velocity. In: *Landslide Risk Management*, 99–128. Taylor & Francis Group, London.

Infometrics (2012). West Coast labour market and economic profile. Retrieved 27 July 2014, from: http://www.infometrics.co.nz/reports/regional/TEC/WestCoastRevised-Jun2012.pdf.

Irikura, K. and Miyake, H. (2011). Recipe for predicting strong ground motion from crustal earthquake scenarios. *Pure and Applied Geophysics*, **168(1-2)**:85–104.

Jibson, R. W. (2011). Methods for assessing the stability of slopes during earthquakes - A retrospective. *The next generation of research on earthquake-induced landslides*, **122(1-2)**:43–50.

Jibson, R. W., Harp, E. L., and Michael, J. A. (2000). A method for producing digital probabilistic seismic landslide hazard maps. *Engineering Geology*, **58**:271–289.

Jones, L. M., Bernknopf, R., Cox, D., Goltz, J., Hudnut, K., Mileti, D., Perry, S., Ponti, D., Porter, K., Reichle, M., Seligson, H., Shoaf, K., Treiman, J., and Wein, A. (2008). The ShakeOut Scenario. Open-File Report 2008-1150, United States Geological Survey.

Kaiser, A., Holden, C., Beavan, J., Beetham, D., Benites, R., Celentano, A., Collett, D., Cousins, J., Cubrinovski, M., Dellow, G., Denys, P., Fielding, E., Fry, B., Gerstenberger, M., Langridge, R. M., Massey, C., Motagh, M., Pondard, N., McVerry, G., Ristau, J., Stirling, M., Thomas, J., Uma, S. R., and Zhao, J. (2012). The Mw 6.2 Christchurch earthquake of February 2011: preliminary report. *New Zealand Journal of Geology and Geophysics*, **55(1)**:67–90.

Kameda, H. (2000). Engineering management of lifeline systems under earthquake risk. *Bulletin of the New Zealand Society for Earthquake Engineering*, **33(3)**:248–264.

Kamp, P. J. J., Green, P. F., and White, S. H. (1989). Fission track analysis reveals character of collisional tectonics in New Zealand. *Tectonics*, **8**:169–195.

Kamp, P. J. J. and Tippett, J. M. (1993). Dynamics of Pacific Plate Crust in the South Island (New Zealand) Zone of Oblique Continent-Continent Convergence. *Journal of Geophysical Research*, **98**:16105–126118, doi:10.1029/93JB01091.

Kanamori, H. and Stewart, G. S. (1978). Seismological aspects of the Guatemala earthquake of February 4, 1976. *Journal of Geophysical Research: Solid Earth*, **83(B7)**:3427–3434.

Kapucu, N. (2008). Collaborative emergency management: better community organising, better public preparedness and response. *Disasters*, **32(2)**:239–262.

Keefer, D. K. (1984). Landslides caused by earthquakes. *Geological Society of America Bulletin*, **95**:406–421.

Keefer, D. K. and Wilson, R. C. (1989). Predicting earthquake-induced landslides with emphasis on arid and semi-arid environments. In: Sadler, P. M. and Morton, D. M. (Eds.), *Landslides in a Semi-Arid Environment with emphasis on the inland valleys of Southern*

California, **2**, 118–149, Riverside, CA. Inland Geological Society of Southern California Publications.

Kellogg, K. S. (2001). Tectonic controls on a large landslide complex: Williams Fork Mountains near Dillion, Colorado. *Geomorphology*, **41**:355–368.

Khajavi, N., Quigley, M., McColl, S. T., and Rezanejad, A. (2012). Seismically induced boulder displacement in the Port Hills, New Zealand during the 2010 Darfield (Canterbury) earthquake. *New Zealand Journal of Geology and Geophysics*, **55(3)**:271–278.

Khazai, B. and Sitar, N. (2003). Evaluation of factors controlling earthquake-induced landslides caused by the Chi-Chi earthquake and comparison with the Northridge and Loma Prieta events. *Engineering Geology*, **71**:79–95.

Kilburn, C. R. J. and Sørensen, S.-A. (1998). Runout lengths of sturzstroms: The control of initial conditions and of fragment dynamics. *Journal of Geophysical Research*, **103(B8)**:17877–17884.

Kohler, T., Hurni, H., Wiesmann, U., and Kläy, A. (2004). *Key Issues for Mountain Areas*, Chapter: Mountain Infrastructure: Access, communications, and energy. United Nations University Press.

Korup, O. (2004a). Geomorphic implications of fault zone weakening: slope instability along the Alpine Fault, South Westland to Fiordland. *New Zealand Journal of Geology and Geophysics*, **47**:257–267.

Korup, O. (2004b). Geomorphometric characteristics of New Zealand landslide dams. *Engineering Geology*, **73**:13–35.

Korup, O. (2005a). Distribution of landslides in southwest New Zealand. *Landslides*, **2**:43–51, doi:10.1007/s10346-004-0042-0.

Korup, O. (2005b). Large landslides and their effect on sediment flux in South Westland, New Zealand. *Earth Surface Processes and Landforms*, **30**:305–323.

Korup, O., McSaveney, M., and Davies, T. R. (2004). Sediment generation and delivery from large historic landslides in the Southern Alps, New Zealand. *Geomorphology*, **61**:189–207.

Kramer, S. L. (1996). *Geotechnical earthquake engineering*. Prentice Hall.

Kritikos, T. (2013). *Geomorphic hazard analyses on tectonically-active mountains: application to the western Southern Alps, New Zealand*. PhD thesis, University of Canterbury.

Kroll-Smith, J. S. and Couch, S. R. (1991). What is a disaster? An ecological-symbolic approach to resolving the definitional debate. *International Journal of Mass Emergencies and Disasters*, **9(3)**:355–366.

Larsen, I. J. and Montgomery, D. R. (2012). Landslide erosion coupled to tectonics and river incision. *Nature Geoscience*, **5**:468–473.

Lee, C. T., Huang, C. C., Lee, J. F., Pan, K. L., Lin, M. L., and Dong, J. J. (2008). Statistical approach to earthquake-induced landslide susceptibility. *Engineering Geology*, **100**:43–58.

Lee, J., Davies, T. R., and Bell, D. (2009). Successive Holocene rock avalanches at Lake Coleridge, Canterbury, New Zealand. *Landslides*, **6**:287–297.

Lee, S. and Sambath, T. (2006). Landslide susceptibility mapping in the Damrei Romel area, Cambodia using frequency ratio and logistic regression models. *Environmental Geology*, **50(6)**:847–855.

Legros, F. (2002). The mobility of long-runout landslides. *Engineering Geology*, **63(3)**:301–331.

Leitner, B., Eberhart-Phillips, D., Anderson, H., and Nabelek, J. L. (2001). A focused look at the Alpine fault, New Zealand: Seismicity, focal mechanisms, and stress observations. *Journal of Geophysical Research*, **106(B2)**:2193–2220.

Lekkas, E. (2000). Analysis of damage parameters of the Chi-Chi Taiwan earthquake. *Risk Analysis*, **3**:419–432.

Leone, F. and Gaillard, J. C. (1999). Analysis of the institutional and social responses to the eruption and the lahars of Mount Pinatubo volcano from 1991 to 1998 (Central Luzon, Philippines). *GeoJournal*, **49**:223–238.

Li, G., West, J., Densmore, A. L., Jin, Z., Parker, R. N., and Hilton, R. G. (2014). Seismic mountain building: Landslides associated with the 2008 Wenchuan earthquake in the context of a generalized model for earthquake volume balance. *Geochemistry, Geophysics, Geosystems*, **15(4)**:833–844.

Li, Y., Huang, R. Q., Zhou, R. J., Densmore, A. L., Ellis, M., Yan, L., Dong, S., Richardson, N., Zhang, Y., He, Y., Chen, H., Qiao, B., and Ma, B. (2009). Geological background of Longmen Shan seismic belt and surface ruptures in Wenchuan earthquake. *Journal of Engineering Geology*, **17(1)**:3–18.

Lichterman, J. D. (2000). A "community as resource" strategy for disaster response. *Public Health Reports*, **115(2-3)**:262–265.

Lin, C.-W., Shieh, C.-L., Yuan, B.-D., Shieh, Y.-C., Liu, S.-H., and Lee, S.-Y. (2003). Impact of Chi-Chi earthquake on the occurrence of landslides and debris flows: example from the Chenyulan River watershed, Nantou, Taiwan. *Engineering Geology*, **71**:49–61.

Little, T. A. and Rodgers, D. W. (2004). 1855 Wairarapa Fault earthquake: world record strike-slip displacment now even bigger. In: *Geoscience Society of New Zealand Miscellaneous Publications*, **117A**, 64–65.

Malamud, B. D., Turcotte, D. L., Guzzetti, F., and Reichenbach, P. (2004). Landslides, earthquakes, and erosion. *Earth and Planetary Science Letters*, **229**:45–59.

McCahon, I., Dewhirst, R., and Elms, D. (2006a). Alpine Fault Earthquake Scenario. Technical Report, Buller District Council.

McCahon, I., Dewhirst, R., Mackenzie, J., and Elms, D. (2006b). Alpine Fault Earthquake Scenario. Technical Report, Grey District Council.

McCahon, I., Elms, D., and Dewhirst, R. (2006c). Alpine Fault Earthquake Scenario. Technical Report, West Coast Engineering Lifelines Group.

McColl, S. T., Davies, T. R., and McSaveney, M. (2012). The effect of glaciation on the intensity of seismic ground motion. *Earth Surface Processes and Landforms*, **37**:1290–1301.

McLean, I., Oughton, D., Ellis, S., Wakelin, B., and Rubin, C. B. (2012). Review of the Civil Defence Emergency Management response to the 22 February Christchurch earthquake. Technical Report, Director of the Civil Defence and Emergency Management.

McSaveney, M. (1975). *The Sherman Glacier Rock Avalanche of 1964: Its emplacement and subsequent effects on the glacier beneath it*. PhD thesis, Ohio State University.

McSaveney, M. (1978). Sherman glacier rock avalanche, Alaska, USA. *Rockslides and Avalanches*, **1**:197–258.

Miles, S. B. and Keefer, D. K. (2000). Evaluation of seismic slope-performance models using a regional case study. *Environmental and Engineering Geoscience*, **6**:25–39.

Miles, S. B. and Keefer, D. K. (2007). Comprehensive areal model of earthquake-induced landslides: technical specification and user guide. Open-File Report 2007-1072, US Geological Survey.

Miles, S. B. and Keefer, D. K. (2009). Evaluation of CAMEL - Comprehensive Areal Model of Earthquake-Induced Landslides. *Engineering Geology*, **104**:1–15.

Miller, D. J. (1960). The Alaska earthquake of July 10, 1958: Giant wave in Lituya Bay. *Bulletin of the Seismological Society of America*, **50(2)**:253–266.

Ministry of Business, Innovation and Employment (2013). Building Amendment Act 2013: Changes that come into effect immediately. Goverment Act, Ministry of Business, Innovation and Employment.

Minstry of Civil Defence and Emergency Management (MCDEM) (2002). Civil Defence Emergency Management Act 2002. Goverment Act, Ministy of Civil Defence and Emergency Management.

Mullin, T. M. (1989). Experts' estimation of uncertain quantities and its implications for knowledge acquisition. *IEEE Transactions on Systems, Man, and Cybernetics*, **19(3)**:616–625.

Naranjo, J. L., van Western, C. J., and Soeters, R. (1994). Evaluating the use of training areas in bivariate statistical landslide hazard analysis: a case study in Colombia. *ITC Journal*, **3**:292–300.

Nash, T., Bell, D., Davies, T. R., and Nathan, S. (2008). Analysis of the formation and failure of Ram Creek landslide dam, South Island, New Zealand. *New Zealand Journal of Geology and Geophysics*, **51**:187–193.

National Institute for Water and Atmospheric Research (2014). Suspended-sediment yield estimator. Retrieved 23 June 2014, from: http://www.niwa.co.nz/freshwater/management-tools/sediment-tools/suspended-sediment-yield-estimator.

Newmark, N. M. (1965). Effects of earthquakes on dams and embankments. *Geotechnique*, **15**:139–159.

Ng, M. K.-F., Leblond, P. H., and Murty, T. S. (1990). Simulation of tsunamis from Great earthquakes on the Cascadia Subduction Zone. *Science*, **250(4985)**:1248–1251, doi:10.1126/science.250.4985.1248.

Nichol, S. L., Goff, J. R., Devoy, R. J. N., Chagué-Goff, C., Hayward, B., and James, I. (2007). Lagoon subsidence and tsunami on the West Coast of New Zealand. *Sedimentary Geology*, **200**:248–262.

Nicoletti, P. G. and Sorriso-Valvo, M. (1991). Geomorphic controls of the shape and mobility of rock avalanches. *Geological Society of America Bulletin*, **103**:1365–1373.

Nirupama, N. (2013). Disaster risk management. *Encyclopedia of Natural Hazards*, **D**:164–170.

Norris, R. and Cooper, A. (1995). Origin of small-scale segmentation and transpressional thrusting along the Alpine fault, New Zealand. *Geological Society of America Bulletin*, **107(2)**:231–240.

Norris, R. and Cooper, A. (2001). Late Quaternary slip rates and slip partitioning on the Alpine Fault, New Zealand. *Journal of Structural Geology*, **23**:507–520.

Okada, Y., Ochiai, H., Kurokawa, U., Ogawa, Y., and Asano, S. (2008). A channelised long run-out debris slide triggered by the Noto Hanto Earthquake in 2007, Japan. *Landslides*, **5(2)**:235–239.

Okal, E. A. and Synolakis, C. E. (2008). Far-field tsunami hazard from mega-thrust earthquakes in the Indian Ocean. *Geophysical Journal International*, **172(3)**:995–1015.

Okal, E. A., Synolakis, C. E., and Kalligeris, N. (2011). Tsunami simulations for regional sources in the South China and adjoining seas. *Pure and Applied Geophysics*, **168(6-7)**:1153–1173.

Ongley, M. (1943). Surface trace of the 1855 earthquake. *Transactions of the Royal Society of New Zealand*, **73**:84–89.

Orchiston, C. (2011). Seismic risk scenario planning and sustainable tourism management: Christchurch and the Alpine Fault zone, South Island, New Zealand. *Journal of Sustainable Tourism*, **20(1)**:59–79, doi:10.1080/09669582.2011.617827.

O'Rourke, T. D. (1996). Lessons learned for lifeline engineering from major urban earthquakes. In: *Eleventh World Conference on Earthquake Engineering*.

Oven, K. (2004). The hydraulic modelling of sedimentation and erosion caused by large scale valley landslides: Investigating the downstream impacts of the Poerua River flood event. Master's thesis, Durham University.

Owen, L. A., Kamp, U., Khattak, G. A., Harp, E. L., Keefer, D. K., and Bauer, M. A. (2008). Landslides triggered by the 8 October 2005 Kashmir earthquake. *Geomorphology*, **94(1-2)**:1–9.

Park, J., Seager, T. P., Rao, P. S. C., Convertino, M., and Linkov, I. (2013). Integrating risk and resilience approaches to catastrophe management in engineering systems. *Risk Analysis*, **33(3)**:356–367, doi:10.1111/j.1539-6924.2012.01885.x.

Parker, R. N., Densmore, A. L., Rosser, N. J., de Michele, M., Li, Y., Huang, R., Whadcoat, S., and Petley, D. N. (2011). Mass wasting triggered by the 2008 Wenchuan earthquake is greater than orogenic growth. *Nature Geoscience*, **4**:449–452, doi:10.1038/ngeo1154.

Paton, D. and Johnston, D. (2001). Disasters and communities: vulnerability, resilience and preparedness. *Disaster Prevention and Management*, **10(4)**:270–277.

Pearce, A. J. and O'Loughlin, C. L. (1985). Landsliding during a M7.7 earthquake: influence of geology and topography. *Geology*, **13(12)**:855–858.

Peduzzi, P., Dao, H., Herold, C., and Mouton, F. (2009). Assessing global exposure and vulnerability towards natural hazards: the Disaster Risk Index. *Natural Hazards and Earth System Sciences*, **9**:1149–1159.

Pellicani, R., van Western, C. J., and Spilotro, G. (2013). Assessing landslide exposure in areas with limited landslide information. *Landslides*, **11(3)**:463–480, doi:10.1007/s10346-013-0386-4.

Peng, M. and Zhang, L. M. (2012). Analysis of human risks due to dam break floods - part1: application to Tangjiashan landslide dam failure. *Natural Hazards*, **64(2)**:1899–1923, doi:10.1007/s11069-012-0336-9.

Peterson, T., Ristau, J., Beavan, J., Denys, P., Denham, M., Field, B., François-Holden, C., McCaffrey, R., Palmer, N., Reyners, M., Samsonov, S., and The GeoNet Team (2009). The Mw 6.7 George Sound earthquake of October 15 2007: response and preliminary results. *Bulletin of the New Zealand Society for Earthquake Engineering*, **42**:192–141.

Petley, D. (2012). Global patterns of loss of life from landslides. *Geology*, **40(10)**:927–930.

Pettinga, J. R., Yetton, M. D., Van Dissen, R. J., and Downes, G. (2001). Earthquake source identification and characterisation for the Canterbury region, South Island, New Zealand. *Bulletin of the New Zealand Society for Earthquake Engineering*, **34**:282–317.

Pitilakis, K., Alexoudi, M., Argyroudis, S., Monge, O., and Martin, C. (2006). Earthquake risk assessment of lifelines. *Bulletin of Earthquake Engineering*, **4**:365–390, doi:10.1007/s10518-006-9022-1.

Power, W., Downes, G., McSaveney, M., Beavan, J., and Hancox, G. T. (2005). The Fiordland earthquake and tsunami, New Zealand, 21 August 2003. In: Satake, K. (Ed.), *Tsunamis: Case Studies and Recent Developments*, 31–42.

Power, W., Downes, G., and Stirling, M. (2007). *Tsunami and its hazards in the Indian and Pacific Oceans*, Chapter: Estimation of tsunami hazard in New Zealand due to South American earthquakes. Pageoph Topical Volumes. Birkhäuser Basel.

Preuss, J. and Godfrey, J. (2006). *Guidelines for developing an earthquake scenario*. Earthquake Engineering Research Institute, Oakland, CA.

Quarantelli, E. L. (1985). What is Disaster: The need for clarification in definition and conceptualization in research. In: Sowder, B. J. (Ed.), *Disasters and Mental Health*, 41–73, Washington D.C. National Institute of Mental Health, U.S. Department of Health and Human Services.

Quarantelli, E. L. (1987). What should we study? Questions and suggestions for researchers about the concept of disasters. *International Journal of Mass Emergencies and Disasters*, **5**:7–32.

Quarantelli, E. L. (1998). *Defining Disasters*. Routledge, London.

Quigley, M., Van Dissen, R. J., Villamor, P., Litchfield, N., Barrell, D. J. A., Furlong, K., Stahl, T., Duffy, B., Bilderback, E., Noble, D., Townsend, D., Begg, J., Jongens, R., Ries, W., Claridge, J., Klahn, A., Mackenzie, H., Smith, A., Hornblow, S., Nichol, R., Cox, S., Langridge, R. M., and Pedley, K. (2010). Surface rupture of the Greendale Fault during the Mw 7.1 Darfield (Canterbury) earthquake, New Zealand: initial findings. *Bulletin of the New Zealand Society for Earthquake Engineering*, **43**:236–242.

Rattenbury, M. S. and Isaac, M. J. (2012). The QMAP 1:250 000 Geological Map of New Zealand Project. *New Zealand Journal of Geology and Geophysics*, **55(4)**:393–405.

Read, S. A. L., Beetham, R. D., and Riley, P. B. (1992). Lake Waikaremoana barrier: a large landslide dam in New Zealand. In: Bell, D. H. (Ed.), *Proceedings of the 6th International Symposium*, 1481–1488, Christchurch.

Reichle, M. (1991). Earthquake planning scenario for the San Diego-Tijuana area. *California Geology*, **44(9)**:204–211.

Reiter, L. (1990). *Earthquake hazard analysis: Issues and insights*. Columbia University Press.

Reitman, W. (1989). Intergrated Design Teams: Knowledge Engineering for Large Scale Commercial Expert System Development. *IEEE Transactions on Systems, Man, and Cybernetics*, **19(3)**:443–447.

Remondo, J., Gonzalez, A., Diaz De Terán, J. R., Cendrero, A., Fabbri, A., and Chung, C. F. (2003a). Validation of landslide susceptibility maps; Examples and applications from a case study in northern Spain. *Natural Hazards*, **30(3)**:437–449.

Remondo, J., González-Diaz, A., Diaz De Terán, J. R., and Cendrero, A. (2003b). Landslide susceptibility models utilising spatial data analysis techniques. A case study from the Lower Deba Valley, Guipúzcoa (Spain). *Natural Hazards*, **30(3)**:267–279.

Reyners, M., Gledhill, K., and Waters, D. (1991). Tearing of the subducted Australian Plate during the Te Anau, New Zealand, earthquake of 1988 June 3. *Geophysical Journal International*, **104**:105–115.

Reyners, M. and Webb, T. H. (2002). Large earthquakes near Doubtful Sound, New Zealand 1989-1993. *New Zealand Journal of Geology and Geophysics*, **45**:109–120.

Reznichenko, N. V., Davies, T. R., and Alexander, D. J. (2011). Effects of rock avalanches on glacier behaviour and moraine formation. *Geomorphology*, **132**:327.

Rhoades, D. A. and Van Dissen, R. J. (2003). Estimates of the time-varying hazard of rupture of the Alpine Fault, New Zealand, allowing for uncertainties. *New Zealand Journal of Geology and Geophysics*, **46**:479–488.

Robinson, D. P., Brough, C., and Das, S. (2006). The Mw 7.8, 2001 Kunlunshan earthquake: Extreme rupture speed variability and effect of fault geometry. *Journal of Geophysical Research*, **111(B08303)**, doi:10.1029/2005JB004137.

Robinson, R., Reyners, M., Webb, T. H., Arnadottir, T., Beavan, J., Cousins, J., Van Dissen, R. J., and Pearson, C. (1995). The Mw 6.7 Arthur's Pass Earthquake in the Southern Alps, New Zealand, June 18, 1994. *Seismological Research Letters*, **66**:11–14.

Rogers, N., Williams, K., Jacka, M., Wallace, S., and Leeves, J. (2014). Geotechnical aspects of disaster recovery planning in residential Christchurch and surrounding districts affected by liquefaction. *Earthquake Spectra*, **30(1)**:493–512.

Scheidegger, A. E. (1973). On the prediction of the reach and velocity of catastrophic landslides. *Rock Mechanics*, **5**:231–236.

Scherer, Y. K., Bruce, S. A., and Runkawatt, V. (2007). A comparison of clinical simulation and case study presentation on nurse practitioner students' knowledge and confidence in managing cardiac events. *International Journal of Nursing Education Scholarship*, **4(1)**:1–14, doi:10.2202/1548-923X.1502.

Selvarajah, C. T. (1993). Training system effectiveness in Australia. *Human Systems Management*, **13(3)**:295–302.

Shen, Z., Sun, J., Zhang, P., Wan, Y., Wang, M., Bürgmann, R., Zend, Y., Gan, W., Liau, H., and Wang, Q. (2009). Slip maxima at fault junctions and rupturing of barriers during the 2008 Wenchuan earthquake. *Nature Geoscience*, **2(10)**:718–724.

Shin, T. and Teng, T. (2001). An overview of the 1999 Chi-Chi, Taiwan, earthquake. *Bulletin of the Seismological Society of America*, **91(5)**:895–913.

Shinozuka, M. and Chang, S. E. (2004). Evaluating the disaster resilience of power networks and grids. In: Okuyama, Y. and Chang, S. E. (Eds.), *Modelling spatial and economic impacts of disasters*, Advances in Spatial Science, 289–310.

Shulmeister, J., Davies, T. R., Evans, D. J. A., Hyatt, O. M., and Tovar, D. S. (2009). Catastrophic landslides, glacier behaviour and moraine formation – A view from an active plate margin. *Quaternary Science Reviews*, **28**:1085–1096.

Shyu, J., Sieh, K., Chen, Y., and Liu, C. (2005). Neotectonic architecture of Taiwan and its implications for future large earthquakes. *Journal of Geophysical Research: Solid Earth*, **110(B8)**, doi:10.1029/2004JB003251.

Slavov, S., Paskaleva, I., Kouteva, M., Vaccari, F., and Panza, G. (2004). Deterministic earthquake scenarios for the city of Sofia. In: *Seismic Ground Motion in Large Urban Areas*, 1221–1237. Springer.

Smith, W. and Berryman, K. (1986). Earthquake hazard in New Zealand: Inferences from seismology and geology. *Royal Society of New Zealand Bulletin*, **24**:223–243.

Snyder, N. P., Whipple, K. X., Tucker, G. E., and Merritts, D. J. (2000). Landscape response to tectonic forcing: Digital elevation model analysis of stream profiles in Mendocino triple junction region, northern California. *Geological Society of America Bulletin*, **112**:1250–1263.

Soeters, R. and van Western, C. J. (1996). Slope stability: recognition, analysis and zonation. In: Turner, A. K. and Schuster, R. L. (Eds.), *Landslides: Investigations and mitigation*, 129–177. Transportation Research Board.

Song, J. and Ok, S.-Y. (2010). Multi-scale system reliability analysis of lifeline networks under earthquake hazards. *Earthquake Engineering and Structural Dynamics*, **39**:259–279.

Star, S. L. and Griesemer, J. R. (1989). Institutional ecology, translations' and boundary objects: Amateurs and professionals in Berkeley's Museum of Vertebrate Zoology, 1907-39. *Social Studies of Science*, **19(3)**:387–420.

Stewart, J. P., Blake, T. F., and Hollingsworth, R. A. (2003). A screen analysis procedure for seismic slope stability. *Earthquake Spectra*, **19**:697–712.

Stirling, M., McVerry, G., and Berryman, K. (2002). A new seismic hazard model for New Zealand. *Bulletin of the Seismological Society of America*, **92(5)**:1878–1903.

Sutherland, R., Eberhart-Phillips, D., Harris, R. A., Stern, T., Beavan, J., Ellis, S., Henrys, S., Cox, S., Norris, R., Berryman, K., Townend, J., Bannister, S., Pettinga, J. R., Leitner, B., Wallace, L. M., Little, T. A., Cooper, A., Yetton, M. D., and Stirling, M. (2007). Do Great earthquakes occur on the Alpine fault in central South Island, New Zealand? *Geophysical Monologue Series*, **175**:235–251.

Sutherland, R. and Norris, R. (1995). Late Quaternary displacement rate, paleoseismicity, and geomorphic evolution of the Alpine Fault: evidence from Hokuri Creek, South Westland, New Zealand. *New Zealand Journal of Geology and Geophysics*, **38**:419–430.

Süzen, M. L. and Doyuran, V. (2004). A comparison of the GIS based landslide susceptibility assessment methods: multivariate versus bivariate. *Environmental Geology*, **45(5)**:665–679.

Tang, C., Zhu, J., Ding, J., Cui, X., and Zhang, J. (2011). Catastrophic debris flows triggered by a 14 August 2010 rainfall at the epicenter of the Wenchuan earthquake. *Landslides*, **8**:485–497.

Tarr, R. S. and Martin, L. (1912). The earthquakes of Yakutat Bay, Alaska in September 1899. Professional Paper 69, United States Geological Survey.

Terzhagi, K. (1950). Mechanism of landslides. In: Paige, S. (Ed.), *Application of Geology to Engineering Practice*, **Berkley Volume**, 83–123, New York, NY. Geological Society of America.

The Press (2014). $230 m Haast-Hollyford road mooted. Retrieved 20 August 2014, from: www.stuff.co.nz/the-press/news/west-coast/9872211/230m-Haast-Hollyford-road-mooted.

Tocher, D. (1960). The Alaska earthquake of July 10, 1958: Introduction. *Bulletin of the Seismological Society of America*, **50(2)**:217–322.

Toda, S., Lin, J., Meghraoui, M., and Stein, R. S. (2008). 12 May 2008 M=7.9 Wenchuan, China, earthquake calculated to increase failure stress and seismicity rate on three major fault systems. *Geophysical Research Letters*, **35(17)**, doi:10.1029/2008GL034903.

Tovar, D., Shulmeister, J., and Davies, T. R. (2008). Evidence for a landslide origin of New Zealand's Waiho Loop moraine. *Nature Geoscience*, **1(8)**:524–526.

United States Geological Survey (2014). Retrieved 11 May 2014, from: www.earthquake.usgs.gov.

Utsu, T. (1970). Aftershocks and earthquake statistics (1): Some parameters which characterize an aftershock sequence and their interrelations. *Journal of the Faculty of Science, Hokkaido Univeristy*, **3(3)**:129–195.

Utsu, T., Ogata, Y., and Matsu'ura, R. S. (1995). The centenary of the Omori formula for a decay law of aftershock activity. *Journal of Physics of the Earth*, **43**:1–33.

van Western, C. J., Rengers, N., and Soeters, R. (2003). Use of geomorphological information in indirect landslide susceptibility assessment. *Natural Hazards*, **30(3)**:399–419.

van Western, C. J., Rengers, N., Terlien, M. T. J., and Soeters, R. (1997). Prediction of the occurrence of slope instability phenomena through GIS-based hazard zonation. *Geologische Rundschau*, **86**:404–414.

van Western, C. J., van Asch, T. W. J., and Soeters, R. (2006). Landslide hazard and risk zonation: why is it still so difficult. *Bulletin of Engineering Geology and the Environment*, **65**:167–184.

Varnes, D. J. and IAEG Commission of Landslide and other Mass-Movements (1984). *Landslide hazard zonation: a review of principles and practice*. UNESCO Press.

Villianatos, F. and Sammonds, P. (2013). Evidence of non-extensive statistical physics of the lithospheric instability approaching the 2004 Sumatran-Andaman and 2011 Honshu mega-earthquakes. *Tectonophysics*, **590**:52–58.

Wald, D. J. and Heaton, T. (1994). A dislocation model of the 1994 Northridge, California, earthquake determined from strong ground motions. Open-File Report, US Geological Survey.

Wang, W. D., Xie, C. M., and Du, X. G. (2009). Landslide susceptibility mapping based on geographical information systems, GuiZhou, south-west China. *Environmental Geology*, **58**:33–43.

Warr, L. N. and Cox, S. (2001). Clay mineral transformations and weakening mechansims along the Alpine fault, New Zealand. In: Holdsworth, R. E., Strachan, R. A., Magloughlin, J. F., and Knipe, R. J. (Eds.), *The nature and tectonic significance of fault zone weakening*, **186**, 85–101. Geological Society, London.

Wartman, J., Bray, J. D., and Seed, R. B. (2003). Inclined plane studies of the Newmark sliding block procedure. *Journal of Geotechnical and Geoenvironmental Engineering*, **129**:673–684.

Wartman, J., Seed, R. B., and Bray, J. D. (2005). Shaking talble modeling of seismically induced deformations in slopes. *Journal of Geotechnical and Geoenvironmental Engineering*, **131**:610–622.

Wasowski, J., Keefer, D. K., and Lee, C.-T. (2011). Toward the next generation of research on earthquake-induced landslides: Current issues and future challenges. *Engineering Geology*, **122**:1–8.

Weiss, A. D. (2001). Topographic Position and Landforms analysis. In: *ESRI User Conference*, San Diego, CA.

Wellman, H. W. (1955). New Zealand Quaternary tectonics. *Geologische Rundshau*, **43**:248–257.

Wellman, H. W. (1979). An uplift map for the South Island of New Zealand, and a model for uplift of the Southern Alps. *Royal Society of New Zealand Bulletin*, **18**:13–20.

Wellman, H. W. and Willett, R. W. (1942). The Geology of the West Coast from Abut Head to Milford Sound - Part 1. *Transactions of the Royal Society of New Zealand*, **71(4)**:282–306.

Wells, A. and Goff, J. (2007). Coastal dunes in Westland, New Zealand, provide a record of paleoseismic activity on the Alpine fault. *Geology*, **35(8)**:731–734, doi:10.1130/G23554A.1.

Wells, A., Yetton, M. D., Duncan, R. P., and Stewart, G. H. (1999). Prehistoric dates of the most recent Alpine fault earthquakes, New Zealand. *Geology*, **27(11)**:995–998.

Welsh, A. and Davies, T. R. (2011). Identification of alluvial fans susceptible to debris-flow hazards. *Landslides*, **8**:183–194.

Whipple, K. X. (2004). Bedrock rivers and the geomorphology of active orogens. *Annual Review of Earth and Planetary Sciences*, **32**:85–151.

Whitehouse, I. E. (1983). Distribution of large rock avalanche deposits in the central Southern Alps, New Zealand. *New Zealand Journal of Geology and Geophysics*, **26**:271–279.

Whitehouse, I. E. and Griffiths, G. A. (1983). Frequency and hazard of large rock avalanches in th central Southern Alps, New Zealand. *Geology*, **11**:331–334.

Whitman, R. V., Anagnos, T., Kircher, C. A., Lagorio, H. J., Lawson, R. S., and Schneider, P. (1997). Development of a national earthquake loss estimation methodology. *Earthquake Spectra*, **13(4)**:643–661.

Wieczorek, G. F., Wilson, R. C., and Harp, E. L. (1985). Map showing slope stability during earthquakes in San Mateo County, California. Miscellaneous Investigations Map I-1257-E, US Geological Survey.

Wilderness Magazine (2014). Haast Hollyford Road could go to court. Retrieved 20 August 2014, from: www.wildernessmag.co.nz/view/page/articles/read/haast-hollyford-road-could-go-to-court/.

Wilson, R. C. and Keefer, D. K. (1983). Dynamic analysis of a slope failure from the 6 August 1979 Coyote Lake, California, earthquake. *Bulletin of the Seismological Society of America*, **73**:863–877.

Wright, C. A. (1998). The AD 930 long-runout Round Top debris avalanche, Westland, New Zealand. *New Zealand Journal of Geology and Geophysics*, **41**:493–497.

Xu, C. (2014). Preparation of earthquake-triggered landslide inventory maps using remote sensing and GIS technologies: Principles and case studies. *Geoscience Frontiers*, doi:10.1016/j.gsf.2014.03.004.

Xu, C., Xu, X., Yao, X., and Dai, F. (2013). Three (nearly) complete inventories of landslides triggered by the May 12, 2008 Wenchuan Mw 7.9 earthquake of China and their spatial distribution statistical analysis. *Landslides*, **11(3)**:441–461, doi:10.1007/s10346-013-0404-6.

Xu, L., Meng, X., and Xu, X. (2014). Natural hazard chain research in China: A review. *Natural Hazards*, **70(2)**:1631–1659.

Xu, Q., Fan, X.-M., Huang, R.-Q., and Westen, C. V. (2009). Landslide dams triggered by the Wenchuan Earthquake, Sichuan Province, south west China. *Bulletin of Engineering Geology and the Environment*, **68(3)**:373–386.

Xu, Q., Zhang, S., Li, W. L., and van Asch, T. W. J. (2012). The 13 August 2010 catastrophic debris flows after the 2008 Wenchuan earthquake, China. *Natural Hazards and Earth System Sciences*, **12**:201–216.

Yetton, M. D. (1998). Progress in understanding the paleoseismicity of the central and northern Alpine Fault, Westland, New Zealand. *New Zealand Journal of Geology and Geophysics*, **41**:475–483.

Yetton, M. D. and McMorran, T. (2004). Landslide dam hazard assessment: Waimakariri River gorge study - Part 2a. Technical Report, Environment Canterbury.

Yin, Y., Wang, F., and Sun, P. (2009). Landslide hazards triggered by the 2008 Wenchuan earthquake, Sichuan, China. *Landslides*, **6(2)**:139–152.

Yu, S., Chen, H., and Kuo, L. (1997). Velocity field of GPS stations in the Taiwan area. *Tectonophysics*, **274(1)**:41–59.

Zadeh, L. A. (1965). Fuzzy sets. *Information and control*, **8(3)**:338–353.

Zimmerman, H. J. (1991). *Fuzzy Set theory and its applications*. Kluwer Academic Publishers, Boston, MA.